ISSN 0975 – 2595

PRAJÑĀ

Volume 17, 2009

Journal of Pure and Applied Sciences

SARDAR PATEL UNIVERSITY
VALLABH VIDYANAGAR
Gujarat – 388 120, INDIA
www.spuvvn.edu

PRAJÑĀ - Journal of Pure and Applied Sciences

(Abbreviation: *PRAJÑĀ - J. Pure & Appl. Sci.*)

Since 1991 Sardar Patel University has been regularly publishing the ***PRAJÑĀ* - Journal of Pure and Applied Sciences** with an aim of providing a platform to Academicians, Researchers and Scientists for the rapid dissemination of original scientific work carried out in the University departments, Affiliated Colleges and Research Laboratories located in Gujarat. All articles published in PRAJNA are deemed to reflect the individual views of the authors and not the official points of view of the Sardar Patel University.

A Peer Reviewed Journal

Indexed in Indian Science Abstracts

Published by the Registrar, Sardar Patel University, Vallabh Vidyanagar, Gujarat – 388 120

Printed at Sardar Patel University Press, Vallabh Vidyanagar, Gujarat – 388 120

PRAJÑĀ - Journal of Pure and Applied Sciences

Volume 17, December 2009

An Official Publication of

Sardar Patel University

Vallabh Vidyanagar, Gujarat – 388 120, INDIA

www.spuvvn.edu **E-mail: spu.prajna@gmail.com**

Sardar Patel University

is grateful to

Prof. Vithalbhai A. Patel,

Humboldt State University, Arcata, Califonia, USA,

whose generous donation to organize academic activities

in the name of Shri Ishwarbhai Ambalal Patel (Shertha) helped

to meet a part of the publication cost of PRAJÑĀ Journal.

* * * * * * * * * * * *

The Editorial Board of PRAJÑĀ is grateful to all those experts who rendered their valuable services as referees for reviewing the papers received for this volume of the Journal.

* * * * * * * * * * * *

The computational assistance received from Mr. Prakash R. Patel, a Doctoral Research Student of Biosciences Department, for making of this volume of PRAJÑĀ Journal is also gratefully acknowledged.

PRAJÑĀ- Journal of Pure and Applied Sciences
Vol. 17: 001-006, 2009 ISSN 0975 - 2595

AVIFAUNAL DIVERSITY IN AND AROUND VALLABH VIDYANAGAR - A SHORT TERM SURVEY

Mukesh H. Koladiya [1] and Narasimhacharya A. V. R. L [*]

Department of Biosciences, Sardar Patel University, Vallabh Vidyanagar, Gujarat – 388 120
[1]Gujarat Institute of Desert Ecology, Post Box-83, Mundra Road, Bhuj, Gujarat – 370 001

ABSTRACT

In view of increasing population and urbanization of Vallabh Vidyanagar, a time bound short-term survey was conducted in Vallabh Vidyanagar and its environs to study the avifaunal diversity. Several sites- approach roads to four major villages near Vallabh Vidyanagar i.e., Lambhvel, Vadtal, Bakrol and Karamsad and Shastri Maidan within Vallabh Vidyanagar were selected. The study sites except Shastri Maidan, included both residential and commercial areas, besides the open areas. A total of 210 visits were made during the morning and evening hours comprising of 105 rounds between Dec 23, 2007 and April 12, 2008. In this study period 44 species of birds belonging to 24 families were encountered. Our observations indicate that 15 species of birds are abundant in frequency while 10 common, 7 frequent and 5 rare. These observations indicate that despite the rapid urbanization of Vallabh Vidyanagar, it is still rich in avian biodiversity.

***Keywords*: avifauna, diversity, density, evenness, vallabh vidyanagar, species richness.**

INTRODUCTION

Presence of large numbers of birds and their variety indicate the health of an ecosystem. Vallabh Vidyanagar, an educational township in Anand district in the State of Gujarat (22° 5′ to 23° 5′ N and 72° 5′ to 73° 5′E) is famous for its educational institutions, is also aptly called "Vrikshanagar" as it is endowed with rich vegetation in spite of an ever increasing population as well as concrete constructions. As the vegetation is rich, a large number of birds are found in and around Vallabh Vidyanagar throughout the year. However, there is no specific document referring to the distribution or population of bird species in this township and its environs. Therefore the present work was undertaken to investigate and measure the population of birds in Vallabh Vidyanagar and its surroundings for approximately four months (from December 2007 to April 2008). The objectives of the study are (1) to find out various bird species in and around Vallabh Vidyanagar and (2) to measure the Density, Diversity Index (H′) and Evenness Index (EI or J′) of different bird species in and around Vallabh Vidyanagar.

MATERIALS AND METHODS

Selection of sites

For the present study five main sites were selected for counting the bird populations in surroundings of Vallabh Vidyanagar. The sites are Lambhvel Road, Vadtal Road, Bakrol Road, Shastri Maidan and Karamsad Road. Bird counts were carried out from 23 December 2007 to 12 April 2008, approximately for four months, routinely in the mornings (0600-0900 h) and evenings (1700-1900 h). For counting birds at each of the sites, three rounds were decided each with seven consecutive days. Each site has been divided into seven different sub-study areas with each covering 70 meter area. The data on sunrise and sunset timings, minimum and maximum temperatures for the study period were obtained from Sardar Patel Renewable Energy Resources Institute (SPRERI), Vallabh Vidyanagar.

(1) Lambhvel Road (LR)

This area was selected with the following sub-study areas: (a) Opposite to Munshi Nature Cure Hospital; (b) Near Vaishnav Township; (c) Opposite and near Siddharth Kutir; (d) Anand-Nadiad Road; (e) Near Indian Gas Agency; (f) Near Khodiyar Temple and (g) Behind S. K. Cinema.

(2) Vadtal Road (VR)

On this site the bird counts were carried out in the following sub-study areas: (a) Behind Vaibhav Cinema; (b) Near Astha Bunglow; (c) Shantikunj Society; (d) Near Sewage canal; (e) On the way to Rampura area; (f) Back side of the B. R. Doshi School of Biosciences and (g) Bakrol Colony area.

* Corresponding author – narasimhacharya@yahoo.com

(3) Bakrol Road (BR)

This site was demarcated into the following sub-study areas: (a) Bakrol gate area; (b) Opposite Pramukhswami Computer Institute; (c) Behind Tirth Bunglow; (d) Area near Madhav Gurukul; (e) Bakrol Village; (f) Left side area of canal and (g) Area behind Bakrol village.

(4) Shastri Maidan (SM)

For counting the birds in this site the following were the sub-study areas: (a) Area near main gate; (b) Area near and opposite to Apna bazaar; (c) Area near basket ball court; (d) Area near B. V. M. College; (e) Area adjacent to Polytechnique College; (f) Area near V. P. Science College and (g) Area adjacent to Bus stand.

(5) Karamsad Road (KR)

In Karamsad Road, the following sub-study areas were selected: (a) H. S. Buildcon Ground; (b) Right side of the Railway track ; (c) Left side of the Railway track ; (d) Area behind Shivdham Tenement; (e) Area opposite to Hindustan petrol pump; (f) Area behind Hindustan petrol pump and (g) Ground near Ganesh Bunglow.

Quadrate method was adopted in order to observe the birds during the study period. This method was used to count; measure the density, diversity and frequency of species.

Data Analysis

From the collected data, density, species diversity and species evenness were calculated using the following formulae:

1. Density [1]: n/ Πr2 where n= total number of birds; r = radius

2. Diversity Index [1]: (H′) H′ = Σ Pi x ln (Pi), where Pi = the v Proportion of ith species; ln= natural log.

3. Evenness Index EI or J′ [2]: J' = H'/ ln (S), where ln= natural log; S=total number of species.

The numerical data generated out of the bird counts at various sites has been subjected to logarithmic transformation [3].

RESULTS

Bird counts

As mentioned in methodology, the bird counts were recorded on regular basis and tabulated. Table 1 shows the habitats of the study areas in Vallabh Vidyanagar. All these areas could be seen teeming with a variety of birds. When the species of birds were counted during 105 rounds (210 visits) over a period of time (Dec 23, 2007 to April 12, 2008) for their numbers in different localities, out of total of 44 species, 15 were found to be abundant, 7 frequent, 10 common and 5 rare (Table 2). The total counts for three rounds (R 1-3) / visits (both during morning and evening hours) for each site are recorded, average number of each species was calculated and species status was ranked for respective sites. Additionally, total counts of birds for each study site during each visit were also calculated and tabulated. The data from all sites was finally pooled, total number of birds and average were calculated and ranking status was given to species for all sites and tabulated. Among the species Rose-ringed parakeet occupies first rank as its number was the highest and Pea fowl, 44th rank as its number was the lowest (Table 3). Based on this data, species richness, density, diversity and evenness were computed and recorded for all the sites. While the Vadtal road area was found to be species rich, highest species density was found in Shastri maidan, maximum diversity species evenness in Karamsad road area (Table 4).

Table 1: Habitat of the selected sites.

Sr. No.	Area/ Site	LR	VR	BR	KR	SM
1	Residential area	✓	✓	✓	✓	X
2	Road area	✓	✓	✓	✓	X
3	Large Trees	✓	✓	✓	✓	✓
4	Water bodies	X	✓	✓	X	X
5	Scrub area	✓	✓	✓	✓	X
6	Commercial/ Industrial area	✓	✓	✓	✓	X
7	Open area and trees	✓	✓	✓	✓	✓
8	Residential area and water source	✓	✓	✓	✓	X

LR - Lambhvel Road, VR - Vadtal Road, BR - Bakrol Road, KR - Karamsad Road , SM - Shastri Maidan

Table 2: **Frequency of Species and Birds found in study areas.**

Frequency No. of species	Birds
Abundant (15)	Blue rock pigeon, Eurasian Collared Dove, Common Hoopoe, Greater Coucal, House crow, Black Drongo, Common babbler, Indian Robin, Purple Sun-bird, Red-vented Bulbul, Common Myna, Rose-Ringed Parakeet, Red-wattled Lapwing, Cattle Egret and Black Ibis
Frequent (07)	Red Collared Dove, Spotted Dove, Small green bee- eater, Jungle crow, House Sparrow, Bank Myna and White Ibis
Common (10)	White breasted Kingfisher, Asian Koel, Common Swallow, Red rumped Swallow, Wire tailed Swallow, Rosy Starling, Indian pond Heron, Median Egret, Little Egret and White breasted Waterhen
Uncommon (07)	Indian Treepie, Common tailor bird, Oriental Magpie-Robin, Brahminy Starling, Black Kite, Yellow wattled Lapwing and Black Winged Stilt
Rare (05)	Indian Pea fowl, Red backed Shrike, White wagtail, White throated Fantail flycatcher and Eurasian Golden oriole
Families of Birds observed	Columbidae, Alcedinidae, Meropidae, Upupidae, Cuculidae, Phasianidae, Corvidae, Dicruidae (Corvidae), Hirundinidae, Lanidae, Motacillidae, Muscicapidae, Nectariniidae, Oriolidae (Corvidae), Ploceidae, Pycononotidae, Sturnidae, Psittacidae, Accipitridae (Falconidae), Charadriidae, Recurvirostridae, Ardeidae, Threskiornithidae and Rallidae

Weather Data

The average day lengths during the study period were recorded and found to be 11.27 h (23-12-2007 to 02-02-2008), 11.34 h (03-02-2008 to 01-03-2008) and 12.11 h (02-03-2008 to 12-04-2008). Thus from the onset of the study to the completion, the day lengths increased by 44 minutes (Fig. 1). The average minimum temperature recorded for the study period was 12.36º C (specifically during the first half of February, lowest temperatures ranging from 8 and 9.57º C were recorded) while the average highest temperature was 35.94º C. However, during the study period, minimum temperature range was between 8ºC and 21.87ºC and maximum temperature range was between 24.2ºC and 38ºC (Fig. 2).

DISCUSSION

The Indian avifauna is noted for its remarkable variations in features and numbers. The sub-continent's avifauna is rich in variety and numbers accounting for about 14% of the world's total number of 8600 species of birds. Of these about 1750 are resident species, rest being seasonal and extra limital emigrants [4]. It is a common misconception that bird study can be done by ringing the birds. Although ringing is an accepted and well practiced method for bird movement especially with regard to migratory paths, it is always not feasible for field studies concerning the population studies. In modern industrialized societies people have the habit of observing birds for different reasons-just for pleasure or detailed habitat study of birds. Sharp increases in numbers of birds can often be related to unusually favourable conditions, especially when the food supply is unusually abundant. Many birds depend on seed crops during the winter and when these are plentiful, birds will feed on them in large numbers [5].

In the present work, we have selected five major sites of Vallabh Vidyanagar as representative sites of the town. The survey of birds has been divided into three phases - pre winter, winter and post winter (early summer). In brief, it became apparent that on Lambhvel Road, the populations of birds like House Crow, Dove, Rosy Starling, Wire-tailed Swallow, Red- rumped and Barn Swallows decreased as winter progressed to early summer (Table 3, Fig. 2). However, populations of Bulbul and Purple Sunbird showed a continuous increase in their numbers through out the study period. On Vadtal Road, populations of Black Ibis and Bulbul showed a marginal increase during the entire study period. The Cattle Egret and Kingfisher populations were found to be less in number in this study site possibly due to lack of wet areas/water bodies. Data collected from Bakrol Road showed that the Common Myna population is smaller as compared to other sites and birds such as Black Ibis, Bulbul and Cattle Egret were found to be higher in number. In Shastri Maidan area, although the total number of Common Myna and Black Ibis was higher during early part of the study period, their number decreased during the later part of the study period. Observations on Karamsad Road area showed that while the number of Bulbul, Dove, House

Table 3: Total, average and ranking of birds in study sites.*

Sr. No.	Name of the bird	LR	VR	BR	SM	KR	Total	Rank
1	Blue Rock Pigeon, *Columba livia*	3.75	3.64	3.92	3.80	3.76	4.48	02
2	Ring Dove, *Streptopelia decaocto*	3.33	3.31	3.35	3.36	3.34	4.04	05
3	Turtle Dove, *Streptopelia tranquebarica*	NF	NF	NF	NF	2.95	2.95	29
4	Spotted Dove, *Streptopelia chinensis*	2.81	NF	NF	NF	3.14	2.60	22
5	White breasted Kingfisher, *Halycon smymensis*	2.22	2.26	2.30	NF	2.24	2.16	31
6	Small green bee-eater, *Merops orientalis*	3.11	3.10	3.13	NF	3.03	3.00	14
7	Common Hoopoe, *Upupa epops*	2.32	2.59	2.30	NF	2.34	2.31	28
8	Koel, *Eudynamys scolopacea*	1.88	2.23	NF	1.86	2.51	2.11	34
9	Coucal, *Centropus sinensis*	2.42	2.45	NF	NF	2.46	2.22	30
10	Pea fowl, *Pavo cristatus*	NF	NF	1.69	NF	NF	1.00	44
11	Treepie, *Dendrocitta vagabunda*	NF	NF	NF	NF	2.47	1.77	41
12	House crow, *Corvus splendens*	3.30	3.09	3.26	3.10	3.38	3.24	07
13	Jungle crow, *Corvus macrorhynchos*	3.16	2.78	2.91	2.93	3.22	3.03	13
14	Black Drongo, *Dicrurus macrocercus*	3.27	3.04	3.18	2.05	3.11	3.07	10
15	Common Swallow, *Hirundo rustica*	2.78	NF	NF	NF	NF	2.08	35
16	Red rumped Swallow, *Hirundo daurica*	2.34	3.19	3.14	NF	NF	2.80	18
17	Wire tailed Swallow, *Hirundo smithii*	2.42	3.17	2.94	NF	NF	2.72	20
18	Red backed Shrike, *Lanius collurio*	NF	2.59	NF	NF	NF	1.89	40
19	White wagtail, *Motaacilla alba*	NF	2.84	NF	NF	NF	2.14	33
20	Babbler, *Turdoides caudatus*	3.52	3.51	3.68	3.65	3.71	3.62	03
21	White throated Fantail flycatcher, *Rhipidura albicollis*	NF	NF	NF	NF	2.08	1.38	43
22	Tailor bird, *Orthotomus sutorius*	2.92	NF	NF	NF	2.85	2.49	25
23	MagpieRobin, *Copsychus saularis*	NF	NF	NF	NF	2.77	2.07	36
24	Indian Robin, *Saxicoloides fulicata*	3.13	3.08	2.83	NF	2.99	2.92	17
25	Purple Sunbird, *Nectarinia asiatica*	3.05	2.76	3.21	NF	3.00	2.94	16
26	Golden oriole, *Oriolus oriolus*	NF	NF	NF	NF	2.12	1.42	42
27	House Sparrow, *Passer domesticus*	2.97	3.04	3.29	NF	3.17	3.04	12
28	Red-vented Bulbul, *Pycnonotus cafer*	3.29	3.14	3.27	NF	3.37	3.18	08
29	Common Myna, *Acridotheres tristis*	3.60	3.36	3.66	3.73	3.48	4.28	04
30	Brahminy Myna, *Sturnus pagodarum*	3.13	NF	NF	NF	2.56	3.23	23
31	Bank Myna, *Acridotheres ginginianus*	3.23	3.12	3.16	NF	3.08	3.75	11
32	Rosy Pastor, *Starnus roseus*	3.47	3.20	2.51	NF	NF	3.69	15
33	Rose-Ringed Parakeet, *Psittacula krameri*	3.26	2.97	3.25	5.89	3.36	5.86	01
34	Black Kite, *Milvus migrans*	2.18	NF	1.86	1.88	3.14	3.22	24
35	Red-wattled Lapwing, *Vanellus indicus*	2.96	3.01	3.06	1.63	3.52	3.81	09
36	Yellow wattled Lapwing, *Vanellus malabaricus*	NF	2.62	NF	NF	NF	2.62	39
37	Black Winged Stilt, *Himantopus himantopus*	2.93	2.75	3.15	NF	NF	3.45	19
38	Pond Heron, *Ardeola grayii*	2.53	2.82	2.73	NF	NF	3.19	26
39	Cattle Egret, *Bulbulcus ibis*	3.40	3.50	3.37	1.66	2.92	3.95	06
40	Median Egret, *Mesophoyx intermedia*	NF	2.70	NF	NF	NF	2.70	38
41	Little Egret, *Egretta garzetta*	NF	2.84	NF	NF	NF	2.84	32
42	Black Ibis, *Pseudibis papillosa*	2.48	2.88	2.75	1.99	2.92	3.41	27
43	White Ibis, *Threskiornis melanocephalus*	NF	2.58	2.27	NF	NF	2.75	37
44	White breasted Waterhen, *Amaurornis phoenicurus*	NF	2.63	2.96	NF	NF	3.13	27

*Data represented in logarithmic value; Taxonomic names of the birds as cited in Ali and Ripley [6]. NF – not found.

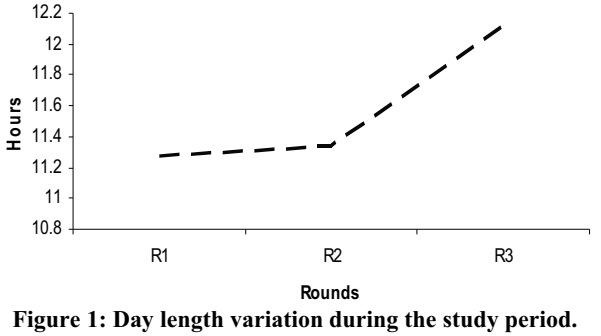

Figure 1: Day length variation during the study period.

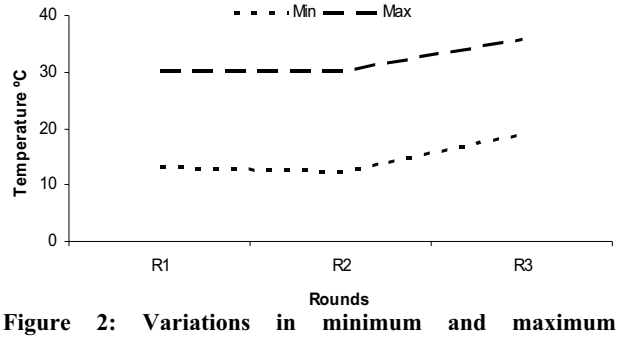

Figure 2: Variations in minimum and maximum temperatures during the study period

Table 4: Species richness (S), Density (D*), Diversity (H') and Evenness (J') of all selected sites.

Round	Site / Parameter	LR	VR	BR	SM	KR
R1	S	27	28	25	10	29
	D	3.94 ± 3.64	3.86 ± 3.70	3.97 ± 3.63	5.22 ± 4.75	3.94 ± 3.39
	H'	2.41 ± 0.15	2.21 ± 0.24	2.39 ± 0.38	0.18 ± 0.07	2.57 ± 0.24
	J'	0.88 ± 0.05	0.81 ± 0.09	0.85 ± 0.08	0.09 ± 0.03	0.89 ± 0.05
R2	S	27	32	28	11	28
	D	3.99 ± 3.53	3.99 ± 3.64	4.03 ± 3.72	5.24 ± 4.71	4.00 ± 3.35
	H'	2.64 ± 0.21	2.64 ± 0.30	2.64 ± 0.32	0.17 ± 0.07	2.74 ± 0.16
	J'	0.89 ± 0.06	0.86 ± 0.08	0.89 ± 0.06	0.09 ± 0.03	0.91 ± 0.03
R3	S	28	29	23	10	24
	D	4.00 ± 3.53	3.95 ± 3.32	4.01 ± 3.72	5.27 ± 4.78	4.01 ± 3.26
	H'	2.71 ± 0.24	2.73 ± 0.17	2.59 ± 0.27	0.17 ± 0.05	2.72 ± 0.13
	J'	0.90 ± 0.07	0.90 ± 0.02	0.90 ± 0.05	0.08 ± 0.02	0.93 ± 0.02
Average	S	27.33	29.66	25.33	10.33	27
	D	3.98 ± 3.57	3.93 ± 3.58	4.01 ± 3.69	5.24 ± 4.75	3.98 ± 3.34
	H'	2.58 ± 0.2	2.52 ± 0.23	2.54 ± 0.32	0.17 ± 0.06	2.68 ± 0.18
	J'	0.89 ± 0.06	0.85 ± 0.06	0.88 ± 0.06	0.08 ± 0.03	0.91 ± 0.03

R1 = Round one (winter), R2 = Round two (winter/early summer), R3 = Round three (summer), D* = Density (* in logarithmic values)

Sparrow and Green Bee-eater increased over time, the population of House Crow showed a decrease in the later part of the observation period. All three types of Swallows were found only during the winter in all sites. Although Koels were found in Karamsad area through out the study period, Bakrol area did not register their presence at any time during the study period. The Vadtal and Lambhvel areas showed the presence of Koels in both late-winter and early summer periods respectively.

There are several birds which are found to be higher in population in all the sites irrespective of the changes in the weather conditions. These included Blue rock pigeon, Common Myna, Bulbul, House Sparrow, Rose-ringed Parakeet and Common Babbler. There are some birds which were found only on specific sites, for example, Spotted Dove in Karamsad area during the entire period of observation, whereas in Lambvel area only in the later part of the observation. In Bakrol, Shastri Maidan and Vadtal area, turtle and spotted doves were not found at all during the study period. Similarly Red-collared dove was found throughout the study period, while White-throated Fantail Flycatcher was seen only during the first part of the observation period on Karamsad Road. While Yellow-wattled Lapwings were found through out the study period only in Vadtal area, Wagtails were seen during winter period and Red-backed Shrike during winter and late-winter periods.

Variation in the number of birds found in particular area during the study period might be because of variation in diurnal temperatures which might affect the available resources in terms of food, water and shelter. Some hardy species of birds were found to be present during the entire period of study which could be because of constant availability of food resources and roosting sites for these species.

The number of birds observed during all three rounds at different sites and the variation in the number of birds found could also be due to the variation in the day light hours. The average day length in winter was 11.30h, which increased to 12.11h in summer. During the winter period, average minimum temperature was 12.72ºC and maximum was 30.18ºC, while towards end of the study period, the minimum and maximum temperatures rose to 19.08ºC and 35.94ºC respectively. As noted in Table - 4 (R1-R3), the number of total species found during the second round of the observations was higher than that of the first round. It is during this period the environmental temperature rose gradually and in the third round of the observations both the minimum and maximum temperatures increased to such an extent that it could be a reason for less number of species found during the post-winter period (early summer).

In conclusion, we observed that Vadtal area was richest in species diversity followed closely by Lambhvel, Karamsad and Bakrol Road sites. Shastri Maidan area was found to be poor in species diversity although had a highest density of birds. The bird density was high in Shastri maidan while the remaining study sites showed more or less similar densities. The bird diversity was higher in Karamsad and Lambhvel Road localities followed by Bakrol and Vadtal Road areas. The bird diversity in Shastri Maidan site was the lowest. Similarly the evenness of bird species was more or less similar in all sites except for Shastri Maidan. This short-term study revealed the presence of 44 species of birds of 24 families. The study period (December 2007 - April 2008) with varying temperatures and day lengths is a transition period and yet Vallabh Vidyanagar is virtually a natural sanctuary for birds. Despite the increasing urbanization, from the last one decade no significant changes have occurred [7].

ACKNOWLEDGEMENTS

We are thankful to Head, Department of Biosciences for providing the necessary facilities for the present work. We are especially thankful to Miss Rupal A. Vasant for her keen interest and preparation of the manuscript.

REFERENCES

[1] Salim, J. and Rahul, K. (2002) *Field Methods for Bird Surveys*, Bombay Natural History Society, New Delhi. pp. 49-57.

[2] Pielou, E. C. (1966) The measurement of diversity in different types of biological collections. *J. Theor. Biol.,* **13**: 131-144.

[3] Bibby, C., Jones, M. and Marsden, S. (1998) *Expedition Field Techniques: Bird Surveys*. Geography Outdoors, Royal Geographical Society, London, pp. 109.

[4] Perrins, C. (1982) *The Encyclopedia of Birds*. Peerage Publishers, London, pp. 8-157.

[5] *The Wealth of India: Birds* (1990) Birds, Vol 2B, CSIR, New Delhi, pp.1.

[6] Ali, S. and Ripley, S. D. (1983) *Handbook of the Birds of India and Pakistan*, Oxford University Press, New Delhi, pp 1-737.

[7] Narasimhacharya A. V. R. L. (1998) Birds of Vallabh Vidyanagar. *Prajna* **8**: 29-30.

PRAJÑĀ - **Journal of Pure and Applied Sciences**
Vol. 17: 007-009, 2009 ISSN 0975 - 2595

EFFECT OF CHEMICAL TREATMENT ON ELECTROLYTIC CONDUCTIVITY AND pH OF CUT FLOWERS OF ROSE DURING POST HARVEST VASE LIFE

J. P. Patel *

Department of Biology, V. P. and R. P. T. P. Science College, Vallabh Vidyanagar, Gujarat -388 120

ABSTRACT

The present paper deals with the screening of certain potential minerals salts and plant growth regulators along with the organic nutrient sucrose in *Rosa hybrida* L. cv. 'Gladiator'. The given 20-24 hrs. treatments after about 20-24 hours of harvest. (i). Aluminium sulphate (300 mg l^{-1}) + Sucrose (5%) + GA_3 (20 mg l^{-1}) spray; (ii) Aluminium sulphate (300 mg l^{-1}) + Sucrose (5%) + Kinetin (20 mg l^{-1}) spray; (iii) Clobalt nitrate (250 mg l^{-1}) + Sucrose (5%) + Kinetin (20 mg l^{-1}) spray; (iv). Silver nitrate (10 mg l^{-1}) + Sucrose (5%) + Kinetin (20 mg l^{-1}) spray. An increase in electrolytic conductivity and pH of the cell sap was observed which can be used as an indicator of senescence during postharvest life of rose flowers.

***Keywords*: *Rosa hybrida* L., mineral salts, growth regulators, sucrose, electrolytic conductivity, pH, senescence.**

INTRODUCTION

Today commercial floriculture is most profitable agroindustry in many developed and developing countries. However, India's share in the world trade is still very low and therefore, to catch up with the export market, our approach should be scientific and well executed. The diverse agro climate in our country permits us to grow various types of tropical and subtropical plants and flowers throughout the year. Flowers due to their perishable nature, higher moisture contents, susceptibility to pests, diseases and storage and transport conditions deteriorate both in quality and quantity very fast and pose unique problems in post harvest handling. To utilize the immense potential that exist in India for supporting and export trade in cut flowers, as well as for meeting the national demand, it is essential that research should be carried out on physiology of ornamental flowers.

Rosa hybrida L. cv. 'Gladiator' flowers were taken for the present work in the post harvest studies of ornamental flowers. Roses are by far the most popular flowers in existence and are known and loved in every country of the world. Cut flowers of roses are in great demand in flori culture industry [1]. In Indian market rose cultivar 'Gladiator', the large deep red flower is the most preferred because of its size and striking colour. The present investigation aims at the study of chemical treatment on Electrolytic Conductivity and pH of cut flowers of Rose during post harvest vase life.

* Corresponding author – pateljp14@gmail.com

MATERIAL AND METHODS

Flowers of *Rosa hybrid* L. cv. Gladiator were obtained from J. K. Florist, Baroda. Rose flowers with the outer petals opened with 30-35 cm long twig were collected and brought to the laboratory. The stem part was cut under water to 20 cm with the upper pair of leaves and placed individually in tubes containing 55 ml treatment solutions. The flowers were kept in the following treatments after about 20-24 hours of harvest. Each treatment was studied in three replicates for nine days at room temperature. 1. aluminium sulphate (300 mg l^{-1}) + sucrose (5%) + GA_3 (20 mg l^{-1}) spray; 2. aluminium sulphate (300mg l^{-1}) + sucrose (5%) + kinetin (20 mg l^{-1}) spray; 3. clobalt nitrate (250 mg l^{-1}) + sucrose (5%) + kinetin (20 mg l^{-1}) spray; 4. silver nitrate (10 mg l^{-1}) + sucrose (5%) + kinetin (20 mg l^{-1}) spray.

Electrolyte leakage

Five petal discs (1 cm diameter) from each flower were taken on very alternate day and were submerged in the beaker containing 25 ml of distilled water. The petals discs were stirred continuously. After vase life for five hours, the conductivity of solution was measured using conductivity bridge (305 Systronics) and expressed in μmhos conductivity.

pH

The petals of the flowers were taken and homogenized in distilled water and centrifuged for 15 minutes at 3000 rpm. The supernatant was removed and its pH was measured (digital pH Model L1-122 of Elico Pvt. Ltd. Hyderabad.)

RESULTS

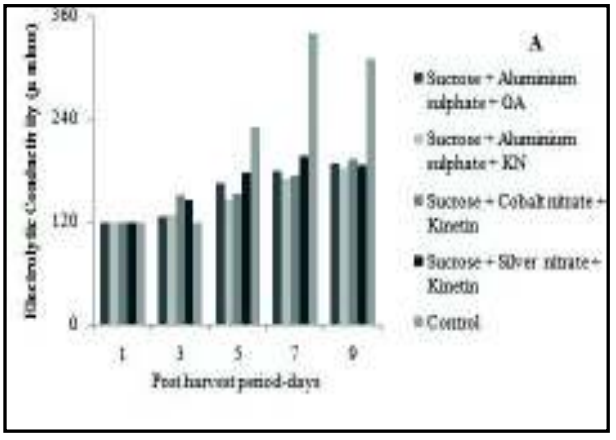

A. Electrolytic conductivity

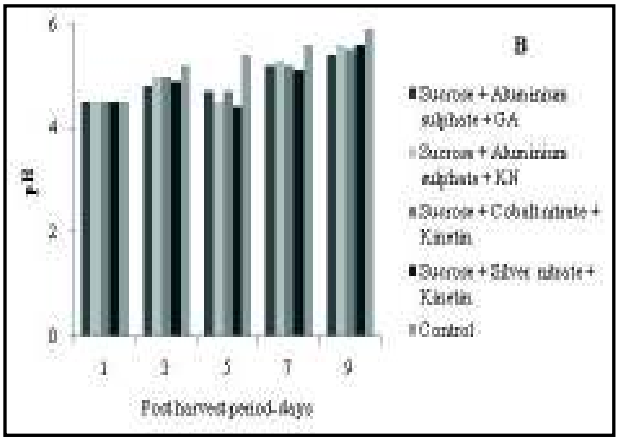

B. pH

Figure 1: Effect of vase solutions on cut flowers of rose during postharvest period.

Electrolytic conductivity of the flowers under sucrose + aluminium sulphate + GA_3 and sucrose + aluminium sulphate + kinetin treatments showed a gradual increase throughout the postharvest vaselife period. In sucrose + aluminium sulphate + GA_3 treated flowers is seen steep rise in electrolytic conductivity from third to fifth day of vaselife. Electrolytic conductivity in sucrose + cobalt nitrate + kinetin treated flowers showed a considerable rise on the third day and gradual increase from fifth to ninth day of the study. A gradual significant rise in electrolytic conductivity was noticed up to seventh day in sucrose + silver nitrate + kinetin treated flower and then declined on the ninth day of vaselife period (Fig. 1A). pH of the aqueous extract of petals of flowers under the treatment of sucrose + aluminium sulphate + GA_3, Sucrose + aluminium sulphate + kinetin and sucrose + silver nitrate + kinetin showed a gradual increase up to third day and lowered on the fifth day and gradually increased up to ninth day of vaselife. Control flowers registered gradual rise in pH throughout the postharvest period of vaselife (Fig. 1B).

DISCUSSION

Properties of cell sap like conductivity and pH can be used as objective indicators of senescence. pH is fundamental for many physiological processes connected with senescence in plant cells [2]. In present experiment on rose flowers, a sharp rise in electrolytic conductivity was observed in control flowers while in treated flowers the conductivity was very low. Same trend was observed by Khan *et al.* in cut tulip flowers [3]. pH of cell sap increased regularly in control flowers. Similar findings were reported by Derkin *et al.* in cut flowers of rose [4]. Similar finding were obtained by Amariutei *et al*. where electrolyte leakage which measured the loss of membrane integrity of petal cells, increased during vase life [1]. It has been reported that the increase in pH in ageing petals was attributed to proteolysis followed by accumulation of free ammonia. The bluing of rose petals is associated with an increase in pH. Murali and Reddy reported that in gladiolus a spike, membrane permeability assessed by electrolytic leakage was delayed when the flowers spike were held in sucrose and metal solutions [5]. The phenomenon of senescence can be marked by an increase in the activity of some hydrolytic enzymes which induce hydrolysis of cell components and a drop in the level of protein and complex molecules. Structural, physical and functional changes of membrane are intimately involved in the petal senescence. The rise in the conductivity of cell sap was correlated with the changes in pH.

CONCLUSION

Chemical and growth regulator treatment retarded senescence by maintaining the membrane integrity. Floral preservatives significantly influenced the different physiological attributes and improved the quality and vase life of Flowers of *Rosa hybrida* L. cv. Gladiator.

REFERENCES

[1] Amariutei, A., Burzo, I. and Craciun, C. (1994) Some Physiological and ultra-structural changes of Freesia cut flowers treated with silver thiosulphate. *Acta Hort.* **363:** 586-597.

[2] Barthe, Ph. and Vaillant, V. (1993) Changes in the buffering capacity of cell sap in senescing rose petals. *Scientia. Hort.* **54:** 165-174.

[3] Khan, F. U., Khan, F. A., Hayat, N. and Bhat, S. A. (2007) Influence of certain chemicals on vase life of cut tulip. *Ind. J. Plant Physiol.*, **12(2):** 127-132.

[4] Derkin, D., Vaillant, V., Arene, L. and Barthe, Ph. (1991) Effect of preservative solutions on some indicators of senescence in cut rose flowers. *Acta Hort.,* **298**: 141-144.

[5] Murali, T. P. and Reddy, T. V. (1993) Postharvest life of Gladiolus as influenced by sucrose and metal salts. *Acta Hort.*, **343**: 313-319.

PRAJÑĀ - **Journal of Pure and Applied Sciences**
Vol. 17: 010 - 016, 2009 ISSN 0975 - 2595

ELICITATION, PARTIAL PURIFICATION AND ANTIFUNGAL ACTIVITY OF β-1, 3-GLUCANASE FROM BANANA PLANTS

Janki N. Thakker, Kinjal Shah [1] and I. L. Kothari [1*]

[1]B. R. D. School of Biosciences, Satellite Campus, Bakrol, Anand, Gujarat -388 120
P. D. Patel Institute of Applied Sciences, Charotar University of Science and Technology, Education Campus Changa, Changa, Anand, Gujarat - 388 421

ABSTRACT

Elicitor prepared from the pathogenic fungi, *Fusarium oxysporum* f. sp. c*ubense*, was effective in increasing the resistance of banana plants against fusarial wilt. Elicitor treated banana plants shown increase in PR proteins. Extraction buffer (0.05 M sodium phosphate buffer, pH 7.2) was optimized for the extraction of β-1, 3-glucanase, a PR protein. A 100 kD size β-1, 3-glucanase had been partially purified using ion exchange and size exclusion chromatography which showed direct antifungal effect on the pathogenic strain. Therefore, it can be concluded that this could be one of the possible mechanism of action induced in banana plants on exposure to elicitor against fusarial wilt.

***Keywords*: *Fusarium oxysporum* f. sp. cubense, elicitor, β-1, 3-glucanase, PR protein, banana.**

INTRODUCTION

Higher plants have developed different mechanisms to protect themselves from various biotic and abiotic stresses, including pathogen attacks, wounding, exposures to heavy metals, salinity, drought, cold, air pollutants and ultraviolet rays [1]. These stresses can provoke structural and biochemical changes in plants, such as formation of cellular defence structures and production of phenolic compounds and phytoalexins [2]. In addition, a group of novel proteins are induced, which are collectively referred to as pathogenesis-related (PR) proteins. Pathogenesis Related (PR) proteins are "proteins accumulating after pathogen attack and related situation" in plants act as defence arsenals. Unlike phytoalexins, which are mainly produced by healthy cells adjacent to localized damaged and necrotic cells, PR proteins accumulate not only locally in infected and surrounding tissues, but also in remote uninfected tissues which could lead to the occurrence of systemic acquired resistance (SAR), protecting the affected plants from further infection [3, 4]. PR proteins can be categorized into 17 families [5], including β-1, 3-glucanases, chitinases, thaumatin-like proteins, peroxidases, ribosome-inactivating proteins, defensins, thionins, nonspecific lipid transfer proteins, oxalate oxidase and oxalate-oxidase-like proteins [6-8].

* Corresponding author – ilkothari@yahoo.com

PR proteins accumulate in both monocots and dicots and have proven antimicrobial activity [9]. These PR proteins are involved in recognition processes, releasing defence activating signal molecules from walls of invading pathogens.

β-1, 3-glucanase (glucan endo-1,3-β-glucosidases, EC 3.2.1.39) enzyme was included in family of PR-2 proteins, is able to catalyze endo-type hydrolytic cleavage of 1,3-β-D glucosidic linkages in β-1, 3-glucans which is a major structural component of cell walls of many pathogenic fungi [10]. Based on hydrolytic activities of β-1, 3-glucanases and their relationships to pathogen infections, β-1, 3-glucanases have been suggested as an important component of plant defence mechanisms against pathogens [11]. Synthesis of this enzyme can be induced by pathogen or other stimuli. Therefore, it has been suspected that β-1, 3-glucanases play a direct role in defending against fungi by hydrolyzing fungal cell walls, which consequently causes the lysis of fungal cells. These enzymes play an indirect role in plant defence by causing the formation of oligosaccharide elicitors, which elicit the production of other PR proteins or low molecular weight antifungal compounds, such as phytoalexins [12]. β-1, 3-glucanases are abundant and highly regulated enzymes widely distributed in plant species. There is a strong evidence that these enzymes are implicated in other diverse physiological and developmental processes in

uninfected plant such as cell elongation [13], cell division [14], fertilization [15], fruit ripening (cell wall degradation leading to fruit softening) [16], pollen germination and tube growth [17], bud dormancy (removal of phloem callose) [18] microsporogenesis (dissolution of pollen tetrads into free microspores) [19], somatic embryogenesis [20], seed germination [21], and flower formation [22].

Elicitor used in this study for induction of defence related enzymes and PR-proteins was prepared from pathogenic strain isolated from infected plants, therefore, this can be compared with vaccination mechanism in humans and animals which produce antibodies when vaccines are injected and then protect the body when the actual pathogen encounter occurs. Moreover, elicitor can also be used as source of biofertilizer and biological control agent which has its own benefit like cost reduction, ecofriendly in nature, not affecting non-target organisms and not polluting the environment as compared to chemical fertilizers. In present work, induction of β-1, 3-glucanase due to elicitation was detected and also purification of this enzyme had been carried out. After purification, direct action on fungal mycelia was determined to elucidate possible molecular mechanism for enhancing resistance in banana plants against Foc by application of elicitor.

MATERIALS AND METHODS

Plant material

Two months old banana plantlets were procured from "Cadila Pharmaceuticals" (Ahmedabad, Gujarat, India). Plantlets were planted in botanical garden (Department of Biosciences, Sardar Patel University, Vallabh Vidyanagar) in the research plots which were supplemented with farmyard manure [2:1 (w/w)]. Proper growth of the plants was checked with emergence of healthy leaves. Health of these plants was observed regularly by visual inspection.

Maintenance of fungal culture and elicitor preparation

Infected rhizomes of banana Grand naine variety showing typical symptoms of Panama disease were collected from the field. The rhizome pieces were surface sterilized and then were cut with a blade sterilized by immersing in NaOCl [10% (v/v)] for 5 minutes. Thin wedges (2-4 mm) were cut, making sure to include xylem with each wedge, since *Fusarium* species block xylem vessels during infection. Each wedge was placed on potato dextrose agar (PDA) plate in aseptic conditions and incubated at 27° C. All fungal isolates were individually grown on fresh PDA plates. Mycelium and spores were stained with lactophenol cotton blue and observed under microscope (Zeiss KS 300). Fungal mycelium was placed on fresh PDA plates, incubated at 27°C and examined daily for 10 days as followed by Patel *et al*. [23].

Elicitor preparation

Fusarium oxysporum f.sp. *cubense* (Foc) was maintained on PDA at 27°C. To obtain liquid culture of fungus, 8-mm agar plug of 3-4 wk old culture was inoculated in potato dextrose broth (PDB) and incubated at 27°C for 21 day. Later, media with mycelium was autoclaved at 121°C for 20 minutes, crushed intensely in grinder and was used as elicitor.

Standardization of protein extraction buffer

0.5 g of fresh leaf tissues was crushed in 1.5 ml of different buffers viz., potassium phosphate buffer (pH 6.0 to 10.0), sodium phosphate (pH 6.0 to 10.0); Tris HCl buffer (pH 6.0 to 10.0) in pre-chilled mortar and pestle. Extract was centrifuged at 10,000 rpm for 30 min. Supernatant was used to determine the protein content [24]. 10% SDS–PAGE [25] was done for each sample to know in which buffer the highest concentration of protein is present using Bio-Rad Mini-PROTEAN (USA) apparatus.

Comparison of protein profile of control and elicitor treated leaves

Control and elicitor treated leaf samples were collected for 7 days after inoculation of elicitor in plants. They were crushed in Tris HCl buffer (0.1 M, pH 6.8), then protein profiles of control and elicitor treated leaves were compared by using SDS-PAGE with silver stained gels.

Enzyme profiling

Gel staining activity of β-1, 3-glucanase was performed on 15% native separating gel with 5% of stacking gel.

Enzyme extraction
After one hour of inoculation of elicitor, leaf samples were collected from both the plants, powdered in liquid nitrogen, crushed in sodium phosphate buffer (0.05 M, pH 7.2) was used for β-1, 3-glucanase. Extract was centrifuged at 10,000 rpm at 4°C for 30 min. Supernatant was used as enzyme source. Samples were collected on each successive day till 7th day and processed for enzyme extraction.

Activity staining of β-1, 3-gluacanase (modified from Pan *et al*., [26])
Gel was rinsed with water, incubated with sodium acetate (0.05 M, pH 5.0), for 5 min and then incubated at 40°C for one hour in a mixture containing 75 ml of sodium acetate (0.05 M, pH 5.0) and one g of laminarin dissolved in 75 ml of water by heating in a boiling water bath. Gel was then incubated in a mixture of methanol: water: acetic acid [5:5:2, (v/v)] for 5 min, washed with water and was stained with 0.3 g of 2, 3, 5-triphenyltetrazolium chloride in 200 ml of NaOH (1.0 M) in a boiling waterbath until red bands appeared (about 10 min). Gel was then placed in 7.5% acetic acid solution for viewing.

β-1, 3-glucanase purification
Samples showing highest β-1, 3-glucanase activity, from 7 days, were further purified using cation exchange chromatography (Q sepharose, 30x1 cm dia. Column) with flow rate of 1.5 ml/minute. 1.5 ml of crude sample was charged in column. 50 fractions of 3 ml size were collected with equilibration buffer. Absorbance of all the fractions was taken at 280 nm in UV-VIS spectrophotometer and β-1, 3-glucanase activity was also measured in all fractions. Fractions, showing glucanase activity, were pooled and again charged in Sephadex G-200 column with same buffer, which was used for extraction, as elution buffer. Purity was checked by native-PAGE and glucanase gel staining activity.

Antifungal activity of purified enzymes
Mature fungal culture was harvested and added in to 50 µl of Tris buffer (0.1 M, pH 6.8) and sodium phosphate buffer (0.1 M, pH 7.2) along with 50 µl of purified enzymes sample of POX and β-1, 3 glucanase, respectively for 48 hours. Respective buffer was added in control instead of enzyme. After 48 h mycelia were stained with lactophenol cotton blue and observed under microscope as suggested by Velazhahan *et al.* [27].

RESULTS AND DISCUSSION
Molecules evoking responses in host during plant-pathogen interaction either from plant or pathogen are known as elicitors which induce plant defence genes that ultimately lead to broad-spectrum resistance [23]. An attempt has been made in present investigation to provoke defence responses in banana plants. Components of mycelial cell wall and culture filtrate to a certain extent mimic real pathogen and leads to activation of defence related enzymes and PR Proteins. In this study, purification of induced PR protein, β-1, 3-gucanase was done and also their direct action on pathogen was assessed. This clearly indicates that elicitor provoked elicitation of genes to overproduce defence related proteins in banana plants which also has direct effect on pathogen.

Standardization of extraction buffer for purification of β-1, 3-glucanase
Among the various series of buffer systems accessed, sodium phosphate buffer (0.05 M, pH 7.2) gave best result β-1, 3-glucanase which was confirmed by gel staining activity and enzyme specific assay. So for further purification work respective buffer was used.

Protein profiling of control and elicitor treated leaves
More amount of protein bands were seen in elicitor treated plant as compared to control plant treated with distilled water. Some of the induced bands are marked with arrows in Fig. 1. Lane 4 had three extra bands which has elicitor treated sample crushed in sodium phosphate buffer as compared to lane 5 having control plant with distilled water. Lane 6 and Lane 7 had elicitor and control leaves crushed in potassium phosphate buffer but clear bands were not seen in it.

17% Native gel of crude sample of control plants and elicitor treated plants also showed difference in banding patterns of proteins. Elicitor treated plant showed more and concentrated protein bands as compared to control plants which indicate the production of new proteins due to elicitation.

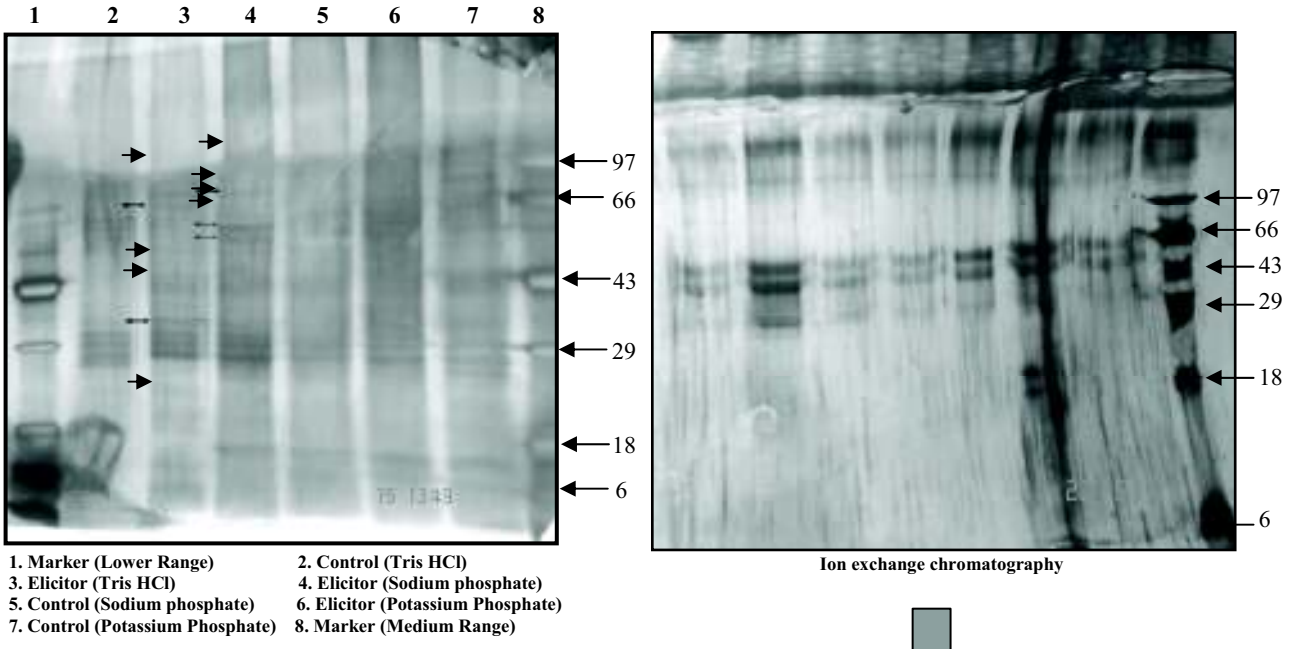

Figure 1: Comparison of protein content in control and elicitor treated plants extracted using different buffers

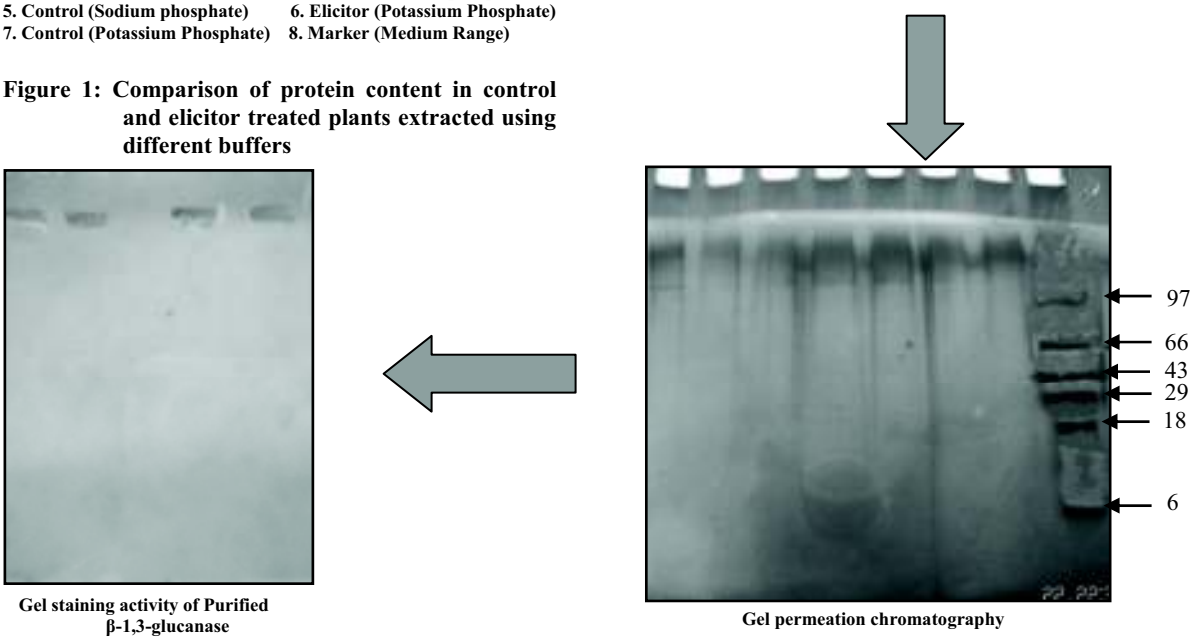

Figure 2: Purification of β-1, 3-glucanase

β-1, 3-glucanase gel staining activity

In present study increase in activity of these enzymes was observed by gel activity staining in elicited banana plants as compared to untreated plants.

For the β-1, 3-glucanase activity staining 10%, 12%, 15% and 17% gels were prepared and the best results were obtained in 15% gel, so for all the further purification steps 15% gel was used. β-1, 3-glucanase activity was detected in elicitor treated plant and no activity was detected in control plants treated with distilled water. Highest activity of β-1, 3-glucanase was seen on the 4th day. Slow induction in β-1, 3-glucanase activity of pepper was reported by Stephen and Rebecc [28] in response to inoculation with *Phytophthora capsici* and Meena *et al.* [29] reported induction of β-1, 3-glucanase in response to salicylic acid against *Cercosporidium personatum* in groundnut.

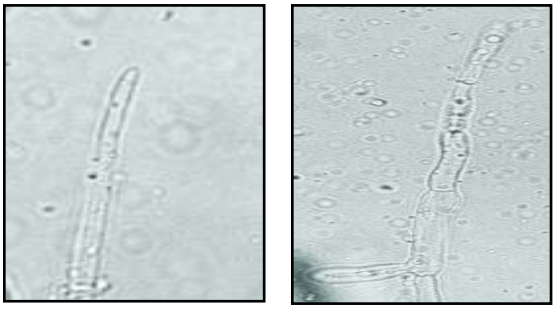

A) Control (sodium phosphate buffer, 0.1 M, pH 7.2)
B) Purified β-1,3-glucanase

Figure 3: Microscopical analysis of antifungal property of purified sample.

Purification of β-1, 3-glucanase

β-1, 3-glucanase activity in control and elicitor treated plants of different days after inoculation was checked up to 7 days and highest activity was found on the 5th day so for further purification 5th day sample was used. Crude sample had specific glucanase activity of about 10.56 U/mg. The PAGE gel showed induced band at above the 97 kD marker band and it was confirmed by doing gel staining activity (Fig. 2, A). Further purification was done by anion exchange chromatography using Q sepharose fast flow (1 x 20 cm); 50 samples (B1 fractions) were equilibrated with Tris-HCl (0.1 M, *p*H 8) and highest glucanase activity found was 16.96 U/mg. Polyacrylamide gel electrophoresis of this sample showed some bands (Fig. 2, B). Bound proteins were eluted with 0.1 to 1 M NaCl (B2 factions) which showed no glucanase activity. B1 fractions having glucanase activity was pooled and for further purification, this sample was loaded on Sephadex G-200 (gel permeation chromatography) column (1 x 20 cm). In all 25 fractions were collected and fractions from 4th-7th showed single band of ~100 kD in PAGE and highest glucanase activity was 31.93 U/mg because of higher purity. Gel staining activity showed pink color bands of glucanase (Figure 2, C). Purification steps, fold purification and yield of glucanase activity are shown in Table 1.

β-1, 3-glucanase has been purified from many plant species, usually by multi-step procedures employing ion exchange columns followed by gel filtration and hydrophobic interactions [30]. Similar techniques have been used in present work as well as in celery [28], tomato seeds [31], Pepper stems [32] young barley leaves [33] and

Table 1: Fold purification and yield of β-1, 3-glucanase enzyme with each step of purification

Steps	Total protein (mg)	Specific activity (units/mg)	Purification fold
Crude	411.6	10.56	1
Ion exchange	137.3	16.96	2.3
Gel Permeation chromatography (Sephadex G-200)	10.3	31.93	3

secretions of *Simira glaziovii* [34]. In the present study, induced β-1, 3-glucanase was investigated in elicitor treated plant and purification of same enzyme was done using Q sepharose fast flow ion exchange chromatography which is an anion exchanger and as β-1, 3-glucanase activity was found in the equilibration buffer eluted fractions only, it proved that it did not bind to matrix so sample is anionic in nature. Further purification was done using GPC using Sephadex G-200 having separation range is 3-200 kD. β-1, 3-glucanase activity was found in the 4th sample from 25 sample collected in the GPC so it shows that the enzyme had higher molecular weight. This is the first report showing purified β-1, 3-glucanase enzyme having 100kD molecular weight.

β-1, 3-glucan is an important component of fungal cell wall. So in order to protect itself from fungus, plants produce β-1, 3-glucanase (EC 3.2.1.6) enzyme to digest fungal cell wall so that it can restrict fungus entry and in turn protect itself. Similarly our results showed highest activity of β-1, 3-glucanase activity on fourth day of elicitor inoculation but no such activity was seen in control plants which were treated with buffer. Similar results of induction of β-1, 3-glucanase were observed in tobacco plants immunized by sporangiospores of blue mould pathogen, *P. tabacina* but control plants showed no induction of β-1, 3-glucanase [35]. So if this enzyme is produced in plant before the entry of pathogen it may help in protecting the plant by restricting fungus entry.

Antifungal activity of purified proteins

Microscopy results of fungal mycelia inoculated with purified enzyme β-1, 3-glucanase (Fig. 3) (stained with lacto phenol cotton blue) showed that mycelia inoculated with purified protein had swollen tip but mycelia inoculated with sodium phosphate buffer used as control for β-1, 3-glucanase were normal. These data also showed antifungal nature of the purified glucanase and its role in plant defence mechanism. Similar results were obtained by Velazhahan *et al.* [27] in which they purified chitinase enzyme of 35 kD which was induced due to elicitors derived from *Rhizoctonia solani* and it showed antifungal activity against the same fungus. β-glucan and chitin are major cell wall components of many fungi [34]. Since β-1, 3-glucanase and chitinase have shown to be capable of attacking the cell wall of pathogen *in vitro*, these enzymes have been proposed as direct defence enzymes of plants. Another potential role of β-1, 3-glucanase is related to the biological activity of cell wall constituents which were isolated from various fungi and can act as elicitors of defence reactions of plants [36]. These findings are same as ours where we are using *Fusarium* derived elicitors and it is increasing β-1, 3-glucanase activity and is having antifungal activity so in turn is increasing plant resistance.

SUMMARY AND CONCLUSION

Thus our findings in this work show that elicitor can induce PR-Proteins and enzyme like β-1, 3-glucanase which help plant to protect itself from the fungus. Antifungal activity of β-1, 3-glucanase also proves this. Therefore elicitors could be used as plant vaccines which cause plant immunization.

ACKNOWLEDGEMENT

Authors are thankful to Department of Biotechnology (DBT), Government of India, New Delhi for the financial support throughout the work.

REFERENCES

[1] Agrios, G. N. (1997) Plant Pathology. Academic Press, San Diego, CA.

[2] Bowles, D. J. (1990) Defence-related proteins in higher plants. *Annual Review of Biochemestry*, **59**: 873–907.

[3] Ryals, J. A., Neuenschwander, U. H., Willits, M. G., Molina, A., Steiner, H. Y. and Hunt, M. D. (1996) Systemic acquired resistance. *The Plant Cell*, **8**: 1809–1819.

[4] Delaney, T. P. (1997) Genetic dissection of acquired resistance to disease. *Plant Physiology*, **113**: 5–12.

[5] http://www.bio.uu.nl/~fytopath/PR-families.htm

[6] Görlach, J., Volrath, S., Knauf-Beiter, G., Hengy, G., Beckhove, U., Kogel, K. H., Oostendorp, M., Staub, T., Ward, E., Kessmann, H. and Ryals, J. (1996) Benzothiadiazole, a novel class of inducers of systemic acquired resistance, activates gene expression and disease resistance in wheat. *Plant Cell,* **8**: 629–643.

[7] Okushima, Y., Koizumi, N., Kusano, T. and Sano, H. (2000) Secreted proteins of tobacco cultured BY2 cells: identification of a new member of pathogenesis-related proteins. *Plant Molecular Biology*, **42**: 479-483.

[8] Christensen, A. B., Cho, B. H., Naesby, M., Gregersen, P. L., Brandt, J., Madriz-Ordenana, K., Collinge, D. B. and Thordal-Christensen, H. (2002) The molecular characterization of two barley proteins establishes the novel PR-17 family of pathogenesis-related proteins. *Molecular Plant Pathology*, **3**: 135–144.

[9] Sticher, L., Mani, B. M. and Metraux, J. P. (1997). Systemic Acquired Resistance. *Annual Review of Phytopathology*, **35**: 235-270.

[10] Adams, D. J. (2004) Fungal cell wall chitinases and glucanases. *Microbiology*, **150**: 2029–2035.

[11] Cordero, M. J., Raventos, D. and San Segundo, B. (1994) Differential expression and induction of chitinases and β-1, 3-glucanases in response to fungal infection during germination of maize seeds. *Molecular Plant Microbe Interaction*, **7**: 23–31.

[12] Klarzynski, O., Plesse, B., Joubert, J. M., Yvin, J. C., Kopp, M., Kloareg, B. and Fritig, B. (2000) Linear β-1, 3-glucans are elicitors of defence responses in tobacco. *Plant Physiology*, **124**: 1027–1037.

[13] Masuda, Y. and Wada, S. (1967) Effects of β-1, 3-glucanase on the elongation growth of oat coleoptile. *Botany Magazine*, **80**: 100–102.

[14] Fulcher, R. G., McCully, M. E., Setterfield, G. and Sutherland, J. (1976) β-1, 3-Glucans may be associated with cell plate formation during cytokinesis. *Canadian Journal of Botany*, **54**: 459–542.

[15] Ori, N., Sessa, G., Lotan, T., Himmelhoch, S. and Fluhr, R. (1990) A major stylar matrix polypeptide (Sp41) is a member of the pathogenesis-related proteins superclass. *EMBO Journal*, **9**: 3429–3436.

[16] Hinton, D. M. and Pressey, R. (1980) Glucanase in fruits and vegetables. *Journal of American Society for Horticulture Science*, **105**: 499–502.

[17] Meikle, P. J., Bonig, I., Hoogenraad, N. J., Clarke, A. E. and Stone, B. A. (1991) The location of (1-3)-β-glucans in the walls of pollen tubes of *Nicotiana alata* using a (1-3)-β-glucan specific monoclonal antibody. *Planta*, **185**: 1–8.

[18] Krabel, D., Eschrich, W., Wirth, S. and Wolf, G. (1993) Callase (1,3-β-D-glucanase) activity during spring reactivation in deciduous trees. *Plant Science*, **93**: 19–23.

[19] Bucciaglia, P. A. and Smith, A. G. (1994) Cloning and characterization of Tag1, a tobacco anther β-1, 3-glucanase expressed during tetrad dissolution. *Plant Molecular Biology*, **24**: 903–914.

[20] Helleboid, S., Chapman, A., Hendricks, T., Inze, D., Vasseur, J. and Hilbert, J. L. (2000) Cloning of β-1, 3-glucanases expressed during *Cichorium* somatic embryogenesis. *Plant Molecular Biology*, **42**: 377–386.

[21] Buchner, P., Rochat, C., Wuilleme, S. and Boutin, J. P. (2002) Characterization of a tissuespecific and developmentally regulated β-1, 3-glucanase gene in pea (*Pisum sativum*). *Plant Molecular Biology*, **49**: 171–186.

[22] Akiyama, T. and Pillai, M. A. (2001) Molecular cloning, characterization and *in vitro* expression of a novel endo-1, 3-β-glucanase up-regulated by ABA and drought stress in rice (*Oryza sativa* L.). *Plant Science*, **161**: 1089–1098.

[23] Patel, M., Kothari, I. L. and Mohan, J. S. S. (2004) Plant defence induced in *in vitro* propagated banana (*Musa paradisiaca*) plantlets by *Fusarium* derived elicitors. *Indian Journal Experimental Biology*, **42**: 728-731.

[24] Lowry, O. H., Rosebrough, N. J., Farr, A. L. and Randall, R. J. (1951) Protein measurement with folin phenol reagent. *Journal of Biological Chemistry*, **193**: 265.

[25] Laemmli, U. K. (1970) Cleavage of structural proteins during assembly of lead bacteriophage T-4. *Nature*, **227**: 680-685.

[26] Pan, S. Q., Ye, X. S. and Kuc, J. (1989) Direct detection of β-1, 3-glucanase isozymes on polyacrylamide electrophoresis and isoelectrofocusing gels. *Annals of Biochemistry*, **182**: 136–140.

[27] Velazhahan, R., Samiyappana, R. and Vibhayasekaran, P. (2000) Purification of an elicitor-inucible antifungal chitianase from suspension–culture Rice cells. *Phytoparasitica* **28**: 21-29.

[28] Stephen, L. K. and Rebecc, G. (1993) Affinity purification and characterization of a β-1, 3-glucanase from celery. *Plant Science*, **93**: 31-39.

[29] Meena, B., Marimuthu, T. and Velazhahan, R. (2001) Salicylic acid induces resistance in groundnut against Late leaf spot caused by *Cercospridium personatum. Journal of Mycology and Plant Pathology*, **31**: 139-145.

[30] Kauffmann, S., Legrand, M., Geoffroy, P. and Fritig, B. (1987) Biological function of pathogenesis-related proteins: four PR proteins of tobacco have β-1, 3-glucanase activity. *EMBO Journal*, **6**: 3209–3212.

[31] Yukio, M. and Hisashi, M. (2000) Development of β-1, 3-glucanase activity in germinated tomato seeds. *Journal of Experimental Botany*, **51**: 1381–1387.

[32] Young, J. K. and Byung, K. H. (1997) Isolation of a basic 34-kiloDaltons β-1, 3-glucanase with inhibitory activity against *Phytophthora capsici* from pepper stems. *Physiology and Molecular Plant Pathology*, **50**: 103-115.

[33] Maria, H. and Geoffory, L. (1993) Purification and properties of three (1-3)-Beta-D-glucanase isoenzymes from young leaves of Barley (*Hordeum vulgare*). *Biochemistry Journal*, **289**: 453-461.

[34] Felipe, A., Maura, C., Denise, E., Andre, O. and Valdirene, M. (2006) Purification and Characterization of β-1, 3-glucanase from the Secretion of *Simira glaziovii* Colleters (Rubiaceae). *Brazalian Archive of Biological Technology*, **49**: 881-888.

[35] Tuzun, S. S., Rao, M. N., Vogelie, U., Schardl, C. L. and Kuc, J. (1989) Induced systemic resistance to blue mold: Early induction and accumulation of β-1, 3-glucanases, chitinases, and other pathogenesis-related proteins (β-proteins) in immunized tobacco. *Phytopathology*, **79**: 979–983.

[36] Dravill, A. G. and Albersheim, P. (1984) Phytoalexins and their elicitors–a defence against microbial infection in plants. *Annual Review of Plant Physiology*, **35**: 243-275.

PRAJÑĀ - **Journal of Pure and Applied Sciences**
Vol. 17: 017 - 022, 2009 ISSN 0975 - 2595

QUALITATIVE PROFILING OF INDUCED PHENOLS IN DIFFERENT VARIETIES OF *ARACHIS HYPOGAEA* L. BY USING FUNGAL CULTURE FILTRATE OF *SCLEROTIUM ROLFSII [SACC.]*

Durgesh Nandini and J. S. S. Mohan *

Department of Biosciences, Sardar Patel University, Vallabh Vidyanagar, Gujarat - 388120

ABSTRACT

***Sclerotium rolfsii* infects groundnut crop and causes productivity losses. A qualitative profile of total phenols has been carried out in four different varieties of *Arachis hypogaea* L. viz. J-11, GG-20, TG-26, and TPG-41 after spraying the fungal culture filtrate (FCF) of *S. rolfsii*. As a result, the induction of phenols occurs to the tune of 30.62 fold in TG-26, 7.2 fold in GG-20, 2.3 fold in TPG-41 varieties at 96 hrs and 22.5 folds in J-11 variety at 120 hrs. Thin layer chromatography of aqueous methanol leaf extracts of groundnut plants revealed the presence of salicylic acid and coumaric acid as common phenolic compounds. However, other phenolic compounds such as tyrosine in GG-20 and TPG-41, hydroquinone in J-11 and L-phenylalanine in TG-26 varieties were also found to get induced after treatment with FCF. The phenols and phenolic compounds exhibited varied increase in presently studied groundnut varieties. Thus the present results indicate that the treatment of fungal culture filtrate successfully induce higher accumulation of phenols thereby causing systemic resistance in the worked out four different varieties of groundnut against *S. rolfsii*.**

***Keywords*: *Arachis hypogaea*, *Sclerotium rolfsii*, fungal culture filtrate, phenols, Southern blight.**

INTRODUCTION

Groundnut (*Arachis hypogaea* L.) is one of the most important oilseed crops cultivated extensively through the tropic and warm temperate regions of the world. It plays an important role in the economy of several countries. Groundnut crop is prone to attack by fungi, bacteria, virus and nematodes and cause seed rots, stem rot, wilts, blight, pod rot and foliar diseases such as rust and early and late leaf spots and bud necrosis etc. [1]. The groundnut production process from planting to storage is affected by soil borne pathogens, pre- and post harvest damage by insects and environmental conditions.

The fungus *S. rolfsii* is the main causative agent for southern blight disease or stem rot in groundnut. It may appear in plants at any time during the growing season but is more likely to cause damage in late summer and early fall as the plants approach maturity. This soil borne fungus attacks the stem of the plants near the soil and affects the central part of stem and subsequently the entire plant [2]. It causes wilting and eventual death of the parts of the plant above the infection region. *S. rolfsii* is difficult to control since the fungus spreads as mycelium in infected organic matter or as sclerotia in infected soil. Sclerotia produced on crop debris and on drying plants, serve as inoculum for the next crop. The fungus may spread more than three feet through the soil and from plant to plant with in a row. It is common to see five or six infected plants with in a row killed.

During the middle of 20th century, this disease of groundnut was controlled to some degree by fumigation or soil applied fungicides. These chemicals are often too expensive and toxic under many situations and future use of fumigants is being restricted due to environmental concerns [3]. Various methods of control have been investigated by different researchers including genetic control and chemical control. Integrated control of *S. rolfsii* on groundnut in South Africa has been investigated [4]. All of the above strategies did not yield any promising results and also affected the environment. Change in the host defense activities in various crop plants after application of biocontrol bacterial strains against soil-borne and foliar fungal diseases have also been reported by several workers [5-9]. Hence, there is a need to find alternative methods to control stem rot in groundnut so as to reduce the cost of disease control.

As an alternative to these methods, it may be possible to induce a plant defense response by exogenous applications of certain biological

* Corresponding author – jssmohan@hotmail.com

agents in order to provide protection against *S. rolfsii* in groundnut. Biological control methods are known to enhance resistance in several crop plants.

Plants have a basic defense mechanism in which, the first part is sensing the presence of the pathogen and subsequent transduction of signal in the cell. The second part of the basic defense is the localization of the pathogen through hypersensitive response (HR). It is widely known that plants can defend themselves against pathogen infection through a variety of mechanisms, local, constitutive or inducible [10].

Phenolics are well known antifungal, antibacterial and antiviral compounds occurring in plants [11]. Plants involve a rapid accumulation of phenols at the infection site, which restricts or slow down the growth of the pathogens [12]. Fungal component, fungal culture filtrate (FCF), used as elicitor might induce changes in the qualitative profile of phenols in the host plants. Thus, total phenol status has been correlated with host resistance in groundnut plants to southern blight.

Moreover, elicitors can be used as the source of bio-fertilizer and biological control which has its own benefits like cost reduction, eco-friendly in nature, not affecting non-targeted organisms, when compared to chemical controlling agents. The present investigation is mainly focused on inducing the changes in qualitative profile of phenolic compounds in different varieties of groundnut against *S. rolfsii* for controlling stem rot disease by using its fungal components in the form of FCF.

MATERIALS AND METHODS

Selection of groundnut variety and Fungi

For the present study, four varieties of groundnut viz. J-11, GG-20, TG-26, and TPG-41 grown locally in Anand district, Gujarat were selected. The fungal culture of *Sclerotium rolfsii* (ATCC 201126) was procured from Junagadh Agricultural University, Junagadh, Gujarat and maintained on potato dextrose agar medium (Hi-media, India) at 25±2°C.

Preparation of fungal culture filtrate

Fungal culture filtrate (FCF) was prepared by inoculating 8mm agar plug of fungus *S. rolfsii* in potato dextrose broth (Hi-media, India) and incubated at 25±2°C for twenty eight days. The total protein concentration of filtrate was measured by using Folin Lowry's method every week up to twenty eight days [13].

Standardization of concentration of FCF for treatment to groundnut plants

Twenty one day old FCF of *S. rolfsii* was selected for elicitor treatment on the basis of higher protein concentration. Murashige Skoog's (MS) basal medium [14] supplemented with different concentrations of FCF (5, 10, 20, 30…100%) was used for *in-vitro* germination and growth of groundnut plants. Phenylalanine ammonia lyase (PAL) and peroxidase enzyme activities were checked in fifteen days old *in vitro* grown plants at 24 hour intervals for one week. The concentration of FCF was standardized on the basis of elevated level of enzyme activities.

Peroxidase activity

The reaction mixture for peroxidase activity consisted of 1ml of 0.1M potassium phosphate buffer (pH 7.0), 200 µl of enzyme extract and 1 ml of 0.01 M orthodianisidine. To this mixture, 500µl of 20mM H_2O_2 was added and the change in absorbance was measured at 436 nm up to 3 minutes at 15 seconds interval. One unit (U) of enzyme is defined as the change in the absorbance 0.1/unit (O.D/min) under specific assay conditions [13].

Phenylalanine ammonia lyase (PAL) activity

The phenylalanine ammonia lyase assay reaction consisted of 1ml of enzyme extract, incubated at 30^{o}C with 900 µl of 150mM tris HCL (pH 8.5) containing 50mM L-phenylalanine. The deamination of phenylalanine to transcinamate was followed by measuring the absorbance of the mixture at 280 nm over a period of 5min [15]. One unit of enzyme activity was calculated as the amount of enzyme that formed 1mg cinnamic acid/hr.

Hypersensitive Response

Initially, before the elicitor application, hypersensitive (HR) response (necrotic lesions) was checked by applying the 200 µl crude FCF of *S. rolfsii* on the adaxial surface of the leaves of different varieties of groundnut grown in the experimental plots.

Elicitor Treatment to plants

In this experiment, forty five days old groundnut plants of J-11, TG-26, GG-20, and TPG-41 varieties growing in experimental plots (3X3 meter) in the department garden were used for the treatment of elicitor. Ten percent FCF was applied separately to the foliage of plants by using a hand operated atomizer. Control plants were treated with PDB and distilled water. Young leaves from five plants in each treatment were randomly excised at different time intervals (24, 48, 72, 96, 120, and 144 hrs) after elicitation with FCF to estimate the total phenols.

Estimation of total phenols

Hundred milligrams of treated plant leaves were homogenized in 80% (v/v) methanol and incubated for 24 hour at 4ºC and then centrifuged at 9200 g by using Sigma Laborzentrifugen, GmbH refrigerated centrifuge, Osterode, Germany for 10 minutes. The supernatant was collected and used as phenol extract. 200 µl of extract was added to 2.5 ml of distilled water and 500 µl of 1N Folin & Ciocalteu's reagent and incubated for 3 minutes at room temperature. 2 ml of 20% Na_2CO_3 was added to this mixture and kept in boiling water bath for one minute. The absorbance of the developed blue color was measured at 650 nm by using spectrophotometer. Total phenols were expressed as milligram phenol in terms of catechol per gram of fresh tissue.

Qualitative analysis of phenolic compounds

Qualitative analysis of plant phenolic compounds was done by using thin layer chromatography (TLC). The solvent system benzene: ethyl acetate: formic acid (5:4:1) was used for visualization of bands of phenolic acids and was confirmed by spraying vanillin sulphuric acid. The R_f values and color of spots obtained from plant extracts were compared with standard values [16].

RESULTS

Protein concentration in fungal culture filtrate (FCF) of *S. rolfsii* was measured at weekly intervals and observed gradual increase in protein concentration of FCF up to twenty one days. Protein concentration of FCF was higher (12.58mg/ml) in twenty one day old culture after the inoculation which decreased gradually till twenty eighth day. The FCF of twenty-one-day old cultures was harvested and used as elicitors for treatment.

Various concentrations (5, 10, 20, 30…100%) of *S. rolfsii* FCF were selected for elicitation in *in-vitro* grown plants on MS basal medium. Higher fold induction of PAL (120 fold at 96 hrs) and peroxidase (96 fold at 96 hrs) activities were observed in groundnut plants grown on MS medium with ten percent concentration compared to other selected concentrations of FCF (Fig. 1). The fungal culture filtrate at ten percent concentration was further used for elicitor treatment.

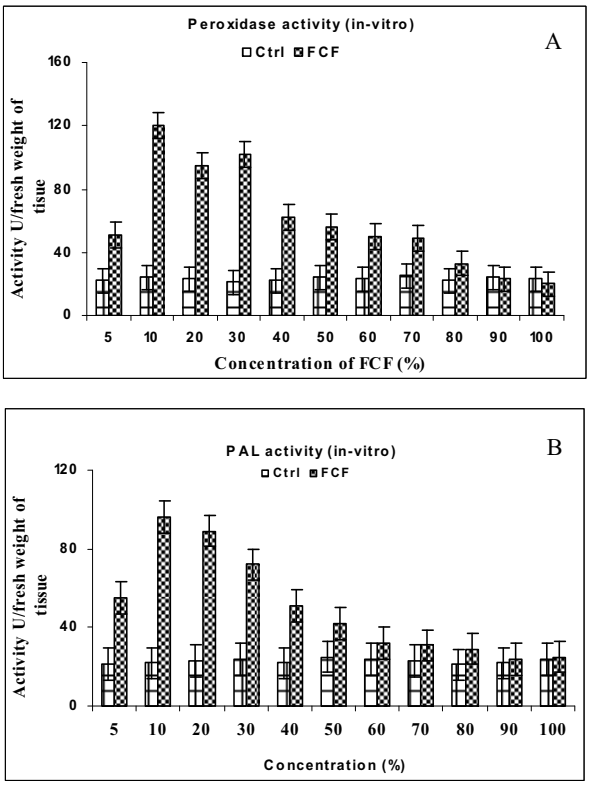

Figure 1 A & B: Activities* of Phenylalanine ammonia lyase and peroxidase enzymes respectively in the tissues of fifteen-days-old plants grown on MS medium along with different concentration of *Sclerotium rolfsii* fungal culture filtrate (5, 10, 20, 30…100%) for selection of elicitor concentration.

Hypersensitive response (HR) was detected by using the FCF directly on leaves of groundnut plants before its application as elicitor. Necrotic lesions were observed after 24 hrs at the site of elicitor application on the adaxial surface of leaves. The lesions were more prominent and distinct on treated leaves than compared to control plants.

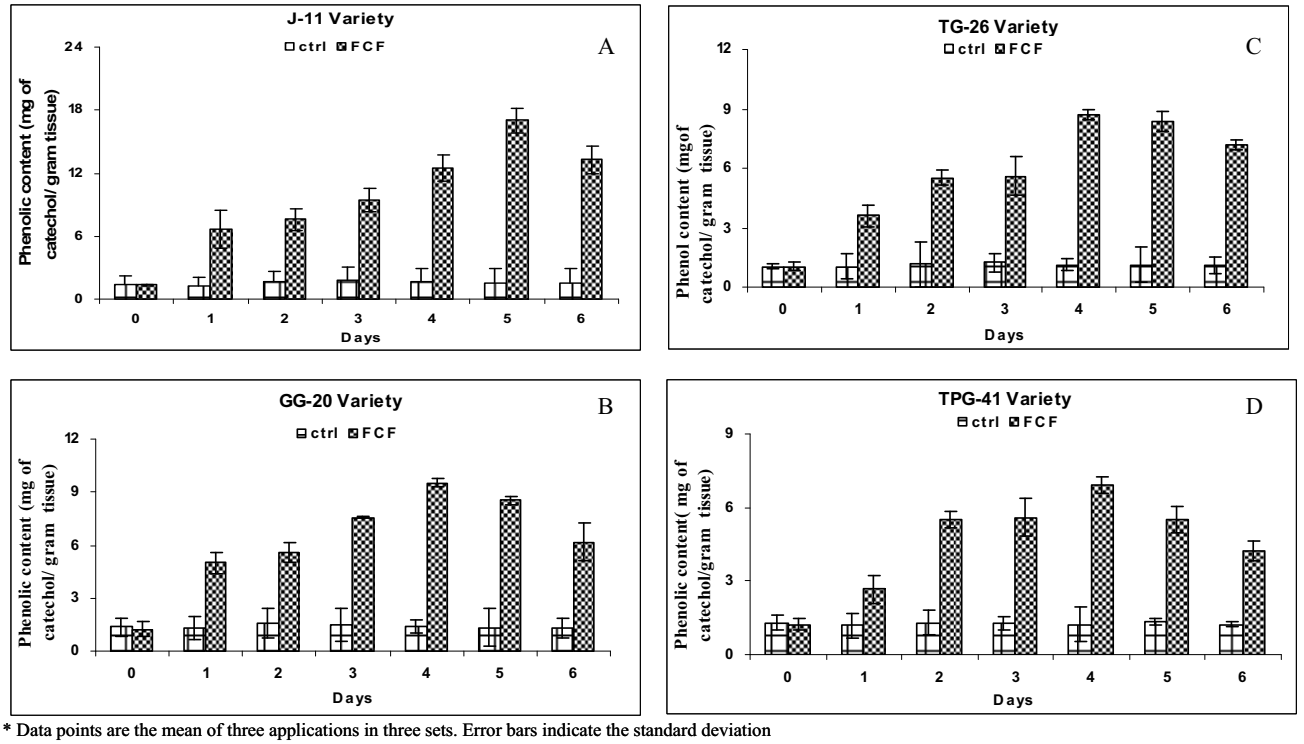

* Data points are the mean of three applications in three sets. Error bars indicate the standard deviation

Figure 2 A - D: Activities* of Induction of phenol levels in different varieties of groundnut viz. J-11, GG-20, TG-26 and TPG-41 after foliar applications of 10% FCF of *Sclerotium rolfsii* along with control.

A significant increase in total soluble phenol was detected in *S. rolfsii* FCF treated plants of four varieties i.e. J-11, TG-26, GG-20 and TPG-41 over the control plants. The amount of total phenols increased transiently by 30.6 fold in TG-26, 7.2 fold in GG-20, 2.3 fold in TPG-41 at 4th day and 22.5 fold in J-11 varieties at 5th day of treatment of elicitor (Fig. 2).

Thin layer chromatographic analysis revealed the induction of phenolic compounds after four days of treatment of FCF of *S. rolfsii* which varied among different varieties of groundnut. Salicylic acid (R_f-0.83) and coumaric acid (R_f-0.25) were observed as common phenolics induced in all varieties of groundnut under study (see Table: 1). A major band of L-tyrosine (R_f-0.49) was observed in GG-20 and TPG-41 varieties, whereas L-phenylalanine (R_f-0.56) in TG-26 variety and hydroquinone (R_f-0.73) in J-11 variety.

Table-1: Details of induction of phenolic compounds in the presently studied varieties of groundnut after treatment with fungal culture filtrate (FCF) of *Sclerotium rolfsii* observed for six days.

Sr. No.	Compounds	Rf	Colour	Days after treatment																							
				J-11 Variety						TG-26 Variety						GG-20 Variety						TPG-41 Variety					
				1	2	3	4	5	6	1	2	3	4	5	6	1	2	3	4	5	6	1	2	3	4	5	6
1	Salicylic acid	0.83	Violet	+	+	+	+	+	+	+	+	+	+	+	+	+	+	+	+	+	+	+	+	+	+	+	+
2	Coumaric acid	0.75	Light purple	+	+	+	+	+	+	+	+	+	+	+	+	+	+	+	+	+	+	+	+	+	+	+	+
3	Hydroquinone	0.73	Light grey	-	-	-	+	-	-	-	-	-	-	-	-	-	-	-	-	-	-	-	-	-	-	-	-
4	L-Phenylalanine	0.56	Deep pink	-	-	-	-	-	-	-	-	-	+	-	-	-	-	-	-	-	-	-	-	-	-	-	-
5	L-Tyrosine	0.49	Light pink	-	-	-	-	-	-	-	-	-	-	-	-	-	-	-	+	-	-	-	-	-	+	-	-
No. of Bands				2	2	2	**3**	2	2	2	2	2	**3**	2	2	2	2	2	**3**	2	2	2	2	2	**3**	2	2

DISCUSSION

During the plant pathogen interaction, the molecule hailing either from plants or pathogen known as elicitor induces the plant defense genes which ultimately lead to broad spectrum resistance [17]. In the present study, the induction of phenols and their accumulation in different varieties of *Arachis hypogaea* were provoked by using fungal culture filtrate of *Sclerotium rolfsii*. The biochemical mechanism involved in plant disease resistance is a complex phenomenon. Total phenol and phenolic acids have been considered as an important defense related compounds, whose levels are naturally higher in the resistant varieties of crops including wheat [18].

Hypersensitive Response is characterized by a rapid, localized death of tissues limiting further pathogen multiplication and spread at the site of infection [19-21]. The dying plant cells strengthen their cell walls during HR by depositing different phenolic compounds, synthesizing diverse phytoalexins and accumulating pathogenesis related (PR) proteins [22]. The induction of phenols might be due to the activation of the shikimic acid pathway through the aromatic amino acid phenylalanine and tyrosine and channeled for the synthesis of phenolics. The palms treated with biocontrol agents especially *Pseudomonas fluorescens* + *T. viride* + chitin induced the phenolics and thereby increased the resistance [23]. Similar findings were reported for groundnut against *Cercospora personatum* [9]. *Serratia plymuthica* an endophytic fungus induced the accumulation of phenolics in cucumber roots and offered resistance to *Pythium ultimum* [24]. In the present study salicylic acid and coumaric acid occurred constitutively as two common phenolics in all varieties of groundnut, while L-tyrosine in GG-20 and TPG-41 variety, hydroquinone in J-11, L-phenylalanine in TG-26 varieties were induced after the treatment with FCF of *S. rolfsii*.

The present study reveals that the phenols were synthesized at higher than normal levels in FCF treated plants of all groundnut varieties and probably showed the resistance to the fungus *S. rolfsii*. Although the role of these three estimated phenolics in disease resistance still needs confirmation, they may hasten the lignification process in the different varieties of groundnut plants. Lignin deposition and polymeric phenols has been implicated as defense responses in different plants, which offer resistant to several diseases [25]. The phenolic compounds like ferulic acid and p-coumaric acid were reported to be involved in resistance of wheat leaves to *Puccinia recondite f. sp. tritici* and also in corn leaves infected with *Colletotrichum graminicola* and were inhibitory to spore germination [26]. From the present study, it can be concluded that higher accumulation of phenols in response to treatment with *S. rolfsii* fungal culture filtrate might have induced resistance response against *S. rolfsii* in different varieties of groundnut. The use of fungal components as bio-control agents might reduce the pesticide residues in the environment and enhance the quality of the crop. Findings of this investigation might lead to development of bio-control agents to control the southern blight disease in groundnut.

ACKNOWLEDGEMENTS

Authors are very thankful to the Junagadh Agricultural University, Junagadh Gujarat for providing isolated fungal strain of *Sclerotium rolfsii*. Ms. Durgesh Nandini thank University Grants Commission, New Delhi for awarding 'UGC research fellowship for meritorious students'

REFERENCES

[1] Singh, F. and Oswalt, D. C. (1992) *Major diseases of Groundnut. Skill Development*. Series No. 6, ICRISAT Human Resource Development Program, International Crops Research Institute for the Semi-arid Troics, Patancheru, Andhra Pradesh, India pp.1-48. http:/www.icrisat.cgiar.org/Training/sds.06.pdf)

[2] Coty Wilson. (1953) *Preventing the disease of peanuts*. Oxford and IBH publication Co. pp. 448-453.

[3] Mehan, V. R., Mayee, C. D. and McDonald, D. (1994) Management of *Sclerotium rolfsii*-caused stem and pod rots of groundnut - a critical review. *Inter. J. Pest Management.* **40**: 313-320.

[4] Cilliers, A. J., Pretorius, Z. A., Van Wyk, P. S. (2003) Integrated control of *Sclerotium rolfsii* on Groundnut in South Africa. *J. Phytopathol.* **151**: 249-258.

[5] Podile, A. R. and Laxmi, V. D. V. (1998) Seed bacterization with *Bacillus subtilis*

AF1 increases phenylalanine ammonia lyase and reduces the incidence of Fusarial wilt in pigeon pea. *J. Phytopathol.* **146**: 255-259.

[6] Kishore, G. K., Pande, S. and Podile, A. R. (2005a) Chitin supplemented foliar applications of *Serratia marcescens* GPS5 improves control of late leaf spot disease of groundnut by activating defence-related enzymes. *J. Phytopathol.* **153:**169-173.

[7] Kishore, G. K., Pande, S. Rao, J. N. and Podile, A. R. (2005b) *Pseudomonas aeruginosa* inhibits the plant cell wall degrading enzymes of *Sclerotium rolfsii* and reduces the severity of groundnut stem rot. *Eur. Plant Pathol.* **113**: 315-320.

[8] Sathiyabama, M. and Balasubramanian, R. (1998) Chitosan induces resistance components in *Arachis hypogaea* against leaf rust caused by *Puccinia arachidis. Crop Prot.* **17**: 307-313.

[9] Meena, B., Radhajeyalakshmi, R., Marimuthu, T., Vidyasekaran, P., Doraiswamy, S. and Velazhahan, R. (2000) Induction of pathogenesis-related proteins, phenolics and phenylalanine ammonia lyase in groundnut by *Pseudomonas fluorescens. J. Plant Dis. Prot.* **107**: 514-527.

[10] Franceschi, V. R., Karokene, P., Krekling, T. and Christiansen, E. (2000) Phloem parenchyma cells are involved in local and distant defence responses to fungal inoculation or bark beetle attack in Norway spruce (Pinaceae). *Amer. J. Bot.* **87(3)**: 314-326.

[11] Sivaprakashan, K. and Vidyasekaran, P. (1993) Phenylalanine ammonia lyase gene for crop disease management. In: *Genetic Engineering, Molecular Biology and Tissue culture for crop pest disease management.* (Ed. Vidyasekaran P.) Daya Publishing House, Delhi, India. 113-220.

[12] Matern, U. and Kneusal, R. E. (1988) Phenolic compounds in plant disease resistance. *Phytoparasitica* **16**: 153-70.

[13] Lowry, O. H., Rosebrough, N. J., Farr, A. L. and Randall, R. J. 1951. Protein measurement with the folin phenol reagent. *J. Biol. Chem***.** 193: 265.

[14] Murashige, T. and Skoog, F. (1962) A revised medium for rapid growth and bioassays with tobacco tissue cultures. *Physiol. Plant.* **15**: 473-497.

[15] Aguilar, E. A., Turner, W. D. and Sivasithamparan, K. (2000) *Fusarium oxysporum f. sp. cubense* inoculation and hypoxia alter peroxidase and phenylalanine-ammonia lyase activities in nodal roots of banana cultivars (*Musa sp.*) differing in their susceptibility to *Fusarium* wilt. *Aus. J. Bot.* **48:** 589-596.

[16] Gagoi, R., Singh, D. V. and Srivastava, K. D. (2001) Phenol as a biochemical basis of resistance in wheat against karnal bunt. *Plant pathology* **50**: 470-476.

[17] Ricci, P. (1997) Induction of hypersensitive and systemic acquired resistance by fungal proteins. In : *The case of elicitins in plant-microbe interactions.* Vol. 3. (Eds. Stacey, G. and Keen, K. T.) Chapman and Hall, New York, 53-75.

[18] Saini, R. S., Arora, Y. K., Chaula, H. K. L. and Wagle, D. S. (1998) Total phenols and sugar content in wheat cultivars resistant and susceptible to *Ustilago nuda* (Jens) Rostrup. *Biochemie and Physiologie der pflanzen* **183**: 89-93.

[19] Gilchrist, D. G. (1998) Programmed cell death in plant defense: the purpose and promise of cellular suicide. *Ann. Rev. Phy.* **39**: 393-414.

[20] Heath, M. C. (2000) Hypersensitive response- related death. *Plant Mol Biol* **44**: 323-334.

[21] Shirashu, K. and Schulze-Lefert, P. (2000) Regulation of cell death in disease resistance. *Plant. Mol. Biol.* **44**: 371-385.

[22] Dangl, J. L., Dietrich, R. A. and Richberg, M. H. (1996) Cell death programs in plant–microbe interactions. *Plant Cell* **8**: 1793-1807.

[23] Karthikeyan, M., Radhika, K., Mathiyazhagan, S., Bhaskaran, R., Samiyappan, R. and Velazhahan, R. (2006) Induction of phenolics and defense related enzymes in coconut (*Cocos nucifera* L.) roots treated with biocontrol agents. *Braz. J. Plant Physiol.* **18(3)**:367-377.

[24] Benhamou, N., Gagne, S., Quere, D. L. and Dehbi, L. (2000) Bacterial - mediated induced resistance in cucumber: Beneficial effect of the endophytic bacterium *Serratia plymuthica* on the protection against infection by *Pythium ultimum*. *Phytopathology* **90**: 45-56.

[25] Moerschbacher, B. M., Noll, U. M., Gorrichon, L. and Reisener, H. J. (1990) Specific inhibition of lignification breaks hypersensitive resistance of wheat to stem rust. *Plant Physiology* **93**: 465-470.

[26] Southerton, S. G. and Deverall, B. J. (1990) Changes in phenolic acid levels in wheat leaves expressing resistance to *Puccinia recondite f. sp.triticia*. *Physiol. Mol. Plant Pathology* **37**: 437-450.

PRAJÑĀ - **Journal of Pure and Applied Sciences**
Vol. 17: 023-027, 2009 ISSN 0975 - 2595

LIGNIFICATION IN YOUNG BRANCHES OF *KIGELIA PINNATA JAQ.*

Sushil S. Kajal and K. S. Rao *

Department of Biosciences, Sardar Patel University, Vallabh Vidyanagar, Gujarat – 388 120

ABSTRACT

***Kigelia pinnata* is a semi deciduous fast growing tree species producing two to three flushes of shoots annually. Pattern of lignification in differentiating xylem elements of young shoots has been studied by histological and histochemical methods. The walls of cambial zone cells and the xylem derivatives undergoing expansion are rich with pectic polysaccharides. Lignin is heterogeneously distributed in the walls of xylem elements. The initiation, completion and intensity of lignin deposition vary in the walls of different xylem elements undergoing differentiation. First stage of lignification of cell walls often occurs at the cell corner middle lamella. Sequential deposition of lignin and occurrence of peroxidase activity in the cell wall areas where pectin was deposited indicates a close relationship between pectin and lignin.**

***Keywords*: cell wall, lignification, pectin, peroxidase**

INTRODUCTION

Lignin is second most abundant biopolymer after cellulose making up to 30% of the global plant biomass [1]. It is an aromatic polymer derived mainly from the polymerization of three different hydroxycinamyl alcohols: p-coumaryl alcohol, coniferyl alcohol and sinapyl alcohol deposited in the cell walls of supporting and conducting tissues such as fibers and tracheary elements of higher plants [2].

Interest in lignin gained momentum due to its role as a limiting factor of the cell wall extensibility and the cell elongation [3]. It also acts a barrier to the plant pathogens [4] and participates in wound healing [5]. Lignin composition, quantity, and distribution also affect the agro industrial uses of plant material. Digestibility and dietary conversion of herbaceous crops are affected by differences in lignin content and composition [6].

Lignin is an undesirable component in the conversion of wood into pulp and paper and remova1 of lignin is a major step in the paper making process. Lignin extraction consumes large quantities of chemicals and energy leading to a poor environmental image for the industry [7, 8]. For these reasons, new biological approaches to pulping are continuously being researched. This shows the importance of lignification which involves the deposition of lignin in the cell wall and cell wall domains of growing and differentiating plant cells. Cell wall peroxides are widely believed to be involved in the lignification process [9].

* Corresponding author – kayesrao@yahoo.com

A significant body of research over the past decade has proposed that peroxidases, laccases, and other phenol oxidases may be involved in the final steps of lignification [10, 11]. However, the exact role of these different enzymes remains as elusive as ever and little real progress has been made. On the other hand, the pattern of lignin deposition in developing xylem elements is poorly understood in trees growing under tropical climate. Therefore, the present study is aimed to understand the pattern of lignification and peroxidase activity in the walls of xylem elements in the young shoots of *Kigelia pinnata*.

MATERIALS AND METHODS

Young shoots of *Kigelia pinnata* growing in the Sardar Patel university campus were collected in the first week of March 2006. Internodal segments of growing shoots were used for histological studies and histochemical localization of pectin, lignin and peroxidise activity.

Pectins

Fresh hand cut sections obtained from young shoots were stained with ruthenium red [12]. For the localization of pectins, a marker for acidic polysaccharides which occur in pectin-rich cell walls, to visualize middle lamella and primary cell walls. A solution of 0.02% ruthenium red in distilled water was used and, after 10 min of staining, sections were washed for 10 min with running tap water and mounted in 50% (v/v) glycerol.

Lignin localization
Transeverse hand section was cut from shoots showing secondary growth. Lignin was visualized using phloroglucinol/ HCl [13], where phloroglucinol in acidic conditions gives red product primarily by reaction with lignin cinnamaldehyde groups. Sections were incubated for 5min in 10% phloroglucinol (w/v) in 100% EtOH followed by 3 min incubation in concentrated HCl.

Peroxidase activity
Histochemical localization of peroxidase was performed using benzidine as substrate dissolved in absolute ethanol, in the presence of 1 mM H_2O_2. Sections were incubated for 20-30 min at 25°C in the dark. Peroxidase activity, when present, was visualized by brown staining under light microscope.

The stained sections were observed using binocular research microscope and photographed using Zeiss Image Analyzer.

RESULTS
Pectin localization
The pattern of pectin distribution in cambial cell walls and differentiating xylem elements was studied by using ruthenium red. The cambial zone was wide with differentiating xylem elements. The newly formed cambial cells and enlarging derivatives had very thin walls and stained pink with ruthenium red indicating the presence of pectinc-rich polysaccharides (Fig. 1A). Among the xylem derivatives differentiating vessels were prominent with their larger diameter and thin primary walls stained intensely with ruthenium red. The differentiating elements with secondary walls did not give any reaction with ruthenium red (Fig. 1A).

Pectin in vessel walls remains for very short period. Many of cambial derivatives towards xylem showed lignified vessels whereas other xylem elements showed no sign of lignification (Fig. 1B). The differentiating elements with secondary walls did not give any reaction with ruthenium red. Vessel walls are the first constituents to lose pectin from its walls followed by its associated parenchyma cells and then ray parenchyma. At this stage the vessel lumen becomes round and the walls start lignifying. Among the phloem elements, the middle lamella of fibers shows more lignin than that in the secondary cell walls (Fig. 1C).

Lignin localization
Phloroglucinol-HCl reaction was used to localize lignin deposition in the cell walls. Phloroglucinol-HCl staining provides a fairly reliable estimate of the extent of lignifications in plant tissues.

Secondary xylem of *Kigelia pinnata* displayed a developmental gradient from thin-walled cambial cells to mature xylem characterized by a lignified secondary wall. Light microscopy histochemistry was used to determine the timing of the appearance of lignin in the developing xylem, a key event in wood formation. In the phloroglucinol stained sections, the cell wall areas to display evidence of phenolic deposition were the middle lamellae and cell corners (Fig. 1C & D).

Both the xylem vessels and associated parenchyma cells away from cambium reacted intensely with phloroglucinol to give bright red color (Fig. 2A). The fibers gave reddish–orange colour. Vessel walls appeared as the most rapid depositors of lignin among xylem constituents. Lignin staining with phlorglucinol was most intense at cell corner and middle lamella in axial parenchyma and fibers (Fig. 2A). On the other hand lignification in vessel walls was equally intense. Ray parenchyma in differentiating xylem showed least lignin deposition as compared to walls of other xylem elements (Fig. 2B). Ray parenchyma and axial parenchyma in matured xylem showed lignification throughout their walls. Xylem derivatives immediate to the cambium did not give any reaction with phloroglucinol.

Peroxidase activity
Peroxidase activity was visualized using benzidine as a substrate. Development of brown colour indicated the presence of enzyme activity along cell walls. The cambial zone and its immediate derivatives did not show any colouration with benzidine. Intense brown colouration was observed in the developing vessel elements and the associated parenchyma cells (Fig. 2C).The brown colour was first observed at cell corners and middle lamella but gradually the whole cell wall stained intense brown. Both the

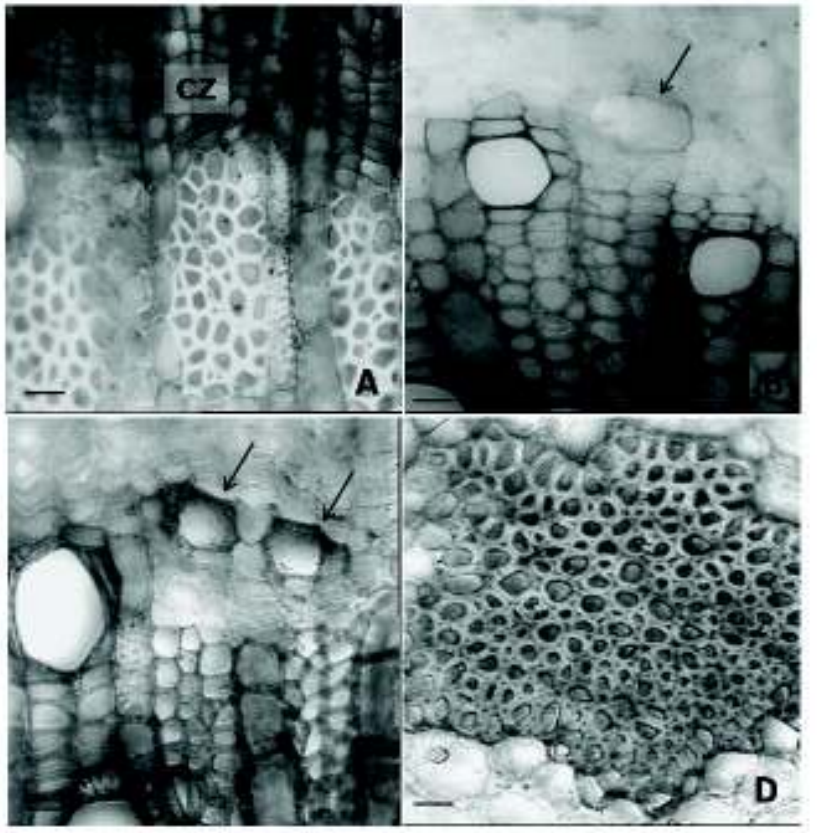

Figure 1

(A) T.S of twig of *Kigelia pinnata* showing cambial zone (CZ) containing pectin.
(B) Vessel elements showing beginning of lignin deposition
(C) Phloem fibers showing lignin deposition at middle lamella.
(D) T.S of twig of *Kigelia pinnata* differentiating vessel element.

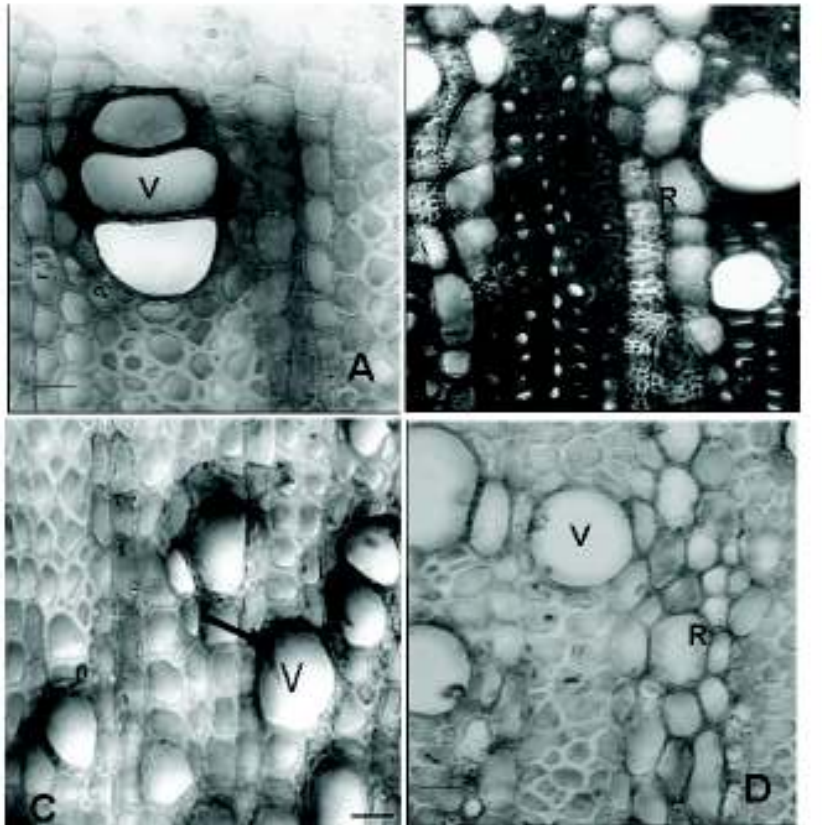

Figure 2

(A) Walls of vessel elements (V) showing intense lignification.
(B) Walls of ray parenchyma showing weak reaction with phloroglucinol.
(C) Vessel walls showing intense peroxidase activity.
(D) Ray parenchyma and vessel walls showing intense peroxidase activity.

axial parenchyma and ray parenchyma showed peroxidase activity but it was more intense in ray parenchyma cells (Fig. 2D). The reaction was often more intense in the middle lamella of axial parenchyma and xylem fibers, whereas like lignin, peroxidase activity was localized throughout the walls of vessels. Similar results were obtained when syrinzaldehyde was used as a substrate in place of benzidine.

DISCUSSION

Like all living systems, the plant cell wall assembly is the result of synergistically and spatio-temporally controlled biosynthesis networks interacting to give rise to supramolecular structure which are more complex than the simple summation of their elementary components. The present histochemical work on young shoots of *Kigelia* demonstrates the sequential changes occurring in the walls leading to lignification. Cambial zone cells and the differentiating xylem derivatives are characterized by the presence of pectin polysaccharides indicating the growing nature of the cells. Ca-pectate is known to occur in precise domains of the cell wall such as the inner and the outer surface of primary cell wall and the middle lamella and act as cementing material between two adjacent cells and it also determine the porosity of the cell wall, have important functions in cell growth and differentiation [14,15]. In the cell wall, unesterified pectins are cross-linked by ca^{2+} to form calcium pectate structure which is abundant in the middle lamella and also in cell corners [16].

The completion of cell expansion is followed by the deposition of secondary wall material between the primary wall and the plasma membrane. The secondary walls of woody plants are described as composite materials consisting of tight mixtures of polysaccharides, glycoproteins and polyphenols, organized around the crystalline and amorphous cellulose microfibril framework, that are deposited after the cessation of primary wall expansion [17]. Initiation of secondary wall thickening in differentiating xylem tissue of *Kigelia* is always accompanied by deposition of lignin in middle lamella/ cell wall, as reported earlier [18]. To detect lignin with phloroglucinol, an acidic condition is needed to develop the red colour indicating the presence of coniferylaldehyde and cinnamaldehyde groups [19, 20].

First stage of lignification often occurs after the deposition of pectins at the cell corner and middle lamella, the two zones rich in Ca-pectate [18]. Sequential deposition of lignin in the areas where pectin was deposited indicates close relationship between these two components. Penel et *al*., [21] proposed that Ca-pectate bound peroxidases could be involved in the initiation of lignin deposition and as middle lamella is composed of pectic polysaccharides, as it shows maximum peroxidase activity during initial stages of lignification. The involvement of a specific peroxidase in this catalytic step has been largely examined due to the interest in the control of the metabolic steps involved in the synthesis and composition of these polymers [22]. According to Terashima *et al.*, [23] the formation of bonds between carbohydrates and oligolignols would liberate Ca^{2+} and peroxidases from carbohydrates, and lignin deposition would convert the carbohydrate hydrophilic gel into a hydrophobic gel, pushing peroxidases, water and ions towards the inner part of cell wall. Once initiated at the site of pectins, peroxidase and lignin polymerization may continue, supposedly penetrating the pores with the pectic architecture.

The results showing co-localization of peroxidase and lignin are correlative and in accordance with earlier results [24]. Absence of peroxidase activity in mature xylem elements confirms its activity during lignification only. However, it is interesting to note the ray cell walls showing highest peroxidase activity and weak reaction with phloroglucinol. It could be possible that being the living cells in secondary xylem they were producing peroxidase needed for the polymerization of monolignol in the cell walls of the adjacent dead xylem elements like vessels and fibers. However, this localization needs to be confirmed at ultra-structural level.

REFRENCES

[1] Lewis, N. G. and Davin, L. B. (1998) The biochemical control of monolignol coupling and structure during lignan and lignin biosynthesis. In: Lewis, N. G. and Sarkanen, S. (Eds), Lignin and Lignan Biosynthesis. ACS Symposium Series **697,** American Chemical Society, Washington, DC, 334–361.

[2] Hatfield, R. and Vermerris, W. (2001) Lignin formation in plants. The dilemma of

linkage specificity. *Plant Physiol.* **126**: 1351-1357.

[3] Müsel, G., Schindler, T., Bergfeld, R., Ruel, K., Jacquet, G., Lapierre, C., Speth, V. and Schopfer, P. (1997) Structure and distribution of lignin in primary and secondary cell walls of maize coleoptiles analyzed by chemical and immunological probes. *Planta* **201**: 146-159.

[4] Nicholson, R. L. and Hammerschmidt, R. (1992) Phenoloc compounds and their role in disease resistance. *Ann. Review Phytopathology*. **30**: 369-389.

[5] Hawkins, S. and Boudet, A. (1996) Wound-induced lignin and suberin deposition in a woody angiosperm (*Eucalyptus gunnii* Hook.): Histochemistry of early changes in young plants. *Protoplasma* **191**: 96–104.

[6] Akin, D. E., Hanna, W. W., Snook, M. E, Himmelsbach, D. S, Barton, F. E and Windham W. R. (1986) Normal-12 and brown midrib-12 sorghum. 11. Chemical variations and digestibility. *Agron. J.* **78***:* 832-837.

[7] Higuchi, T. (1985) Biosynthesis of lignin. In: Higuchi, T. (Ed.)*, Biosynthesis and Biodegradation of Wood Components*. Academic Press, New York, pp 141-160.

[8] Odendahl, S. (1994) Environmental protection and consumer demands: a review of trends and impacts. *Pulp Pap-Can* **95**: 144–148.

[9] Syrjanen, K. and Brunow, G. (2000) Regioselectivity in lignin biosynthesis: the influence of dimerization and crosscoupling biosynthesis. *J. Chem. Soc. Perkin Trans* **1**: 183–187.

[10] McDougall, G. J., Stewart, D., and Morrison, I. M. (1994). Cell-wall-bound oxidases from tobacco (*Nicotiana tabacum*) xylem participate in lignin formation. *Planta* **194**: 9–14.

[11] Richardson, A., Stewart, D., and Mc.Dougall, G. J. (1997) Identification and partial characterization of a coniferyl alcohol oxidase from lignifying xylem of Sitka spruce (*Picea sitchensis*). *Planta* **203**: 35–43.

[12] Vallet, C., Chabbert, B., Czaninski, Y., and Montis, B. (1996) Histochemistry of lignin deposition during schlrenchyma differentiation in stems. *Annals of Botany*. **78**: 625-632.

[13] Gahan, P. B. (1984) *Plant Histochemistry and Cytochemistry*, Academic press, Florida.

[14] Ridley, B. L., O'Neill, M. A. and Mohnen, D. (2001) Pectins: structure, biosynthesis, and oligogalacturonide-related signaling. *Phytochemistry* **57**: 929–967.

[15] Jarvis, M. C., Briggs, S. P. H. and Knox, J. P. (2003) Intercellular adhesion and cell separation in plants. *Plant Cell Environ* **26**: 977–989.

[16] Gugliemino, N., Liberman, M., Catesson, A. M., Mareck, A., Part, R., Mataftschive S., and Goldberg, R. (1997) Pectin methylesterases from poplar cambium and innder bark : localization, properties, and seasonal changes. *Planta* **202**: 70-75.

[17] Ruel, K., Chevalier-billosta, V., Guillemin, F., Sierra, J. B. and Joseleau, J. P. (2006) The wood cell wall at the ultrastructural scale-formation and topochemical organization. *Ciencia Y techologia* **8**: 107-116.

[18] Terashima, N., Fukushima, K., He, L. and Takabe, K. (1993) Comprehensive model of the lignified plant cell wall. In: Jung, H. G., Buxton, D. R., Hatfield, R. D. and Ralph, J. *Forage Cell Wall Structure and Digestibility*, *American Society of Agromony, Madison*, USA, 247-270.

[19] Sarkanen, K. V. and Ludwig, C. (1971) Definition and nomenclature. In: Sarkanen K. V. and Ludwig, C. H. (Eds), *Lignins: Occurrence, formation, structure and reaction. Wiley Interscience, New York: 1-18.*

[20] Geiger, H., and Fugger, H. (1979) Uber den chemismusder wiesner-reaction of lignin. *Naturforschung* **34B**: 1471-1472.

[21] Penel, C., Carpin, S., Crèvecoeur, M., Simon, P. and Greppin, H. (1999) Binding of peroxidases to Ca^{2+}-pectate: possible significance for peroxidase function in cell wall. *Plant Peroxidase Newsletter* **14**: 33–40.

[22] Bernards, M. A. and Lewis, N. G. (1998) The macromolecular aromatic domain in suberized tissue: a changing paradigm. *Phytochemistry* **47**: 915-933.

[23] Terashima, N. (2000). Formation and ultrastructure of lignified plant cell walls. In: Kim, Y. S. (Ed.), *New horizons in wood anatomy*. Gwangju: Chonnam National University Press, 169–180.

[24] Higuchi, T. (1997) Biochemistry and molecular biology of wood. Berlin: Springer-Verlag.

PRAJÑĀ - **Journal of Pure and Applied Sciences**
Vol. 17: 028-032, 2009 ISSN 0975 - 2595

REMOVAL OF CADMIUM, MERCURY AND LEAD FROM AQUEOUS SOLUTION USING MARINE MACROALGAE AS LOW COST ADSORBENTS

Nirmal Kumar, J. I. [*], Rita N. Kumar [1] and Cini Oommen

P. G. Department of Environmental Science and Technology, Institute of Science and Technology for Advanced Studies and Research (ISTAR), Vallabh Vidyanagar, Gujarat – 388 120
[1]N. V. Patel College of Pure and Applied Sciences, Vallabh Vidyanagar, Gujarat – 388 120

ABSTRACT

Biosorption potential of a brown seaweed, *Sargassum ilicifolium* and two green seaweeds, *Caulerpa sertularioides* and *Chaetomorpha* sp. were compared for cadmium, mercury and lead removal at various initial concentrations (20 to 80 mg L^{-1}) and two different contact periods (60 and 120 minutes). The metal uptake increased with increase in initial concentration by *S. ilicifolium* from 20 to 60 mg L^{-} while *C. sertularioides* and *Chaetomorpha* sp exhibited increase from 20 to 80 mg L^{-1}. Highest value for Langmuir constant q_{max} was recorded by *C. sertularioides* for Hg (50.00 mg g^{-1}). The values of Freundlich model constant (n) for biosorption by *S. ilicifolium* ranged between 2.353 to 5.348 which indicate good adsorption. The Cd uptake values in the different seaweeds were in the order *Chaetomorpha* sp.> *S. ilicifolium*>*C. sertularioides*. Hg uptake values followed the sequence *C. sertularioides*>*S. ilicifolium*>*Chaetomorpha* sp. The metal uptake values for Pb displayed the order *Chaetomorpha* sp.>*C. sertularioides*>*S. ilicifolium*.

Keywords: **Biosorption, heavy metals, isotherms, metal uptake, seaweeds.**

INTRODUCTION

Natural waters across the globe are being besieged with several chemical and biological contaminants. Ever-increasing industrialization and urbanization have augmented the discharge of various noxious contaminants, heavy metals being the most harmful. Aqueous heavy metal pollution has become a serious threat and is of great environmental concern due to their non-biodegradable and persistant nature and accumulation throughout the food chain. Among heavy metals, lead and cadmium have high priority for removal from aqueous environments [1, 2]. Removal of these pollutants from aqueous effluents has conventionally been accomplished through a range of abiotic processes [3, 4]. In recent times, growing interest has been observed in the application of materials of biological origin in heavy metal removal. Certain types of biomass like algae, marine algae, bacteria, yeast and higher plants can retain relatively high quantities of metal ions by "passive" sorption and/or complexation. This process is known as biosorption in contrast to bioaccumulation, an active mode of metal accumulation by living cells which depends on the metabolic activity of the cell [5]. The sequestering behaviour of biological materials for cationic or anionic species has been well accepted and reported during the past few decades and the idea has been potentially applied to the removal of some pollutant ions from aqueous wastes and industrial effluents [6, 7].

Brown marine alga, *Ecklonia radiata* exhibited high uptake capacities for lead, cadmium and copper from aqueous solutions, with marked lead sorption [8]. Antunes *et al.* [9] investigated the influence of different experimental parameters such as initial pH, shaking rate, sorption time, temperature, equilibrium conditions and initial concentrations on the removal of copper ions from aqueous solutions by *Sargassum* sp. Senthilkumar *et al* [10] compared ten different seaweeds on the basis of lead uptake at different pH conditions and reported brown algae, *Turbinaria conoides* to exhibit maximum lead uptake. Sheng *et al.* [11] used two locally harvested brown marine algae, *Sargassum* sp. and *Padina* sp., for the removal of cations (Cd^{2+} and Cr^{3+}) and an anion ($Cr_2O_7^{2-}$) from dilute aqueous solutions. The potential use of the brown seaweed, *Ecklonia* biomass as a bioreductant for reducing Cr (VI) was examined in a continuous packed-bed column by Park *et al.* [12]. The current study aims to investigate brown and green marine macroalgae for their heavy metal biosorption capacities from aqueous solution at different initial concentrations of the heavy metals Cd, Hg and Pb and at different

* Corresponding author – istares2005@yahoo.com

contact period (time) of dry biomass. The optimum time period for adsorption of heavy metals is 60, 90 minutes and in very few cases 120 minutes [13]. Therefore, in the present study two different contact periods (60 and 120 minutes) were selected. The concentration of heavy metals was selected in aqueous solution, keeping in mind the fact that surface water, groundwater and marine water generally have heavy metal concentrations not more than 1 or 2 ppm (permissible limits) [14]. Thus, four heavy metal concentration 20, 40, 60 and 80 mg L^{-1} were chosen for the current study

MATERIALS AND METHODS

Seaweeds

Fresh samples of marine seaweeds *Sargassum ilicifolium*, *Caulerpa sertularioides* and *Chaetomorpha* sp. were collected from Okha Port (22°28'N and 69°05'E), Gulf of Kutch, Northwest coast of India in January 2009. The algae were cleaned at the site of collection to remove the adhering dirt and soil particles and washed with deionised water to remove particulate material from their surfaces. The washed seaweeds were first air dried and then oven-dried at 80°C to constant weight. The dried biomass was ground and passed through a 2mm mesh size sieve and stored in polyethylene bottles.

Biosorption experiment and analytical method

All the experiments were conducted at a constant temperature of 25±2°C following the modified method of Suresh Kumar *et al.* [15]. Batch equilibrium biosorption experiments were carried out at in 250 ml Erlenmeyer flasks containing cadmium nitrate, mercuric chloride and lead nitrate solutions (150 ml) of known concentrations, i.e. 20, 40, 60 and 80 mg L^{-1}, prepared using analytical grade chemicals. Pre-weighed amounts of algal biomass (100 mg) were added to each flask and the mixtures were agitated on a rotary shaker at 180 rpm for two different contact periods, 60 and 120 minutes. Controls for each concentration without the addition of heavy metals were also maintained. After the respective contact periods, the solutions were separated from the biomass by filtration and all the filtrates were analyzed using Inductively Coupled Plasma-Optical Emission Spectroscopy (ICP-OES; Perkin Elmer Optima-3300 RL) at Sophisticated Instrumentation Centre for Applied Research and Testing (SICART), Vallabh Vidyanagar, Gujarat, India. All the biosorption experiments were conducted in triplicates to substantiate the results. The data shown are the mean values of three replicate determinations.

Metal uptake capacity

The amount of metal sorbed at equilibrium, q (mg g^{-1}), which represents the heavy metal uptake was calculated from the difference in metal concentration in the aqueous phase before and after biosorption according to the following equation [16]:

$$q = V(Ci-Ce)/W$$

where V is the volume of metal solution (L), Ci and Ce are the initial and equilibrium concentration of metal in solution (mg L^{-1}), respectively and W is the mass of dried alga (in g). The percentage reduction of the heavy metals by all the macroalgae was also estimated from the difference of initial metal concentration and the metal concentration in the filtrates.

Biosorption isotherms

The experimental data obtained were fitted to Langmuir and Freundlich equations, widely used in biosorption studies. Freundlich equation model is expressed as:

$$q = K\,Ce^{1/n}$$

In this model, K (L g^{-1}) and 1/n are the constants to be determined from the data. For a good adsorbent, $0.2<1/n<0.8$, and a smaller value of 1/n indicates better adsorption and formation of rather strong bond between the adsorbate and adsorbent. Langmuir equation is expressed as:

$$q = q_{max}bCe/1+bCe$$

where q_{max} (mg g^{-1}) is the amount of adsorption corresponding to complete monolayer coverage, i.e., the maximum adsorption capacity and b (L mg^{-1}) is the Langmuir constant.

RESULTS AND DISCUSSION

Biosorption capacities of brown seaweed, *Sargassum ilicifolium* and two green seaweeds, *Caulerpa sertularioides, Chaetomorpha* sp. were compared for cadmium, mercury and lead removal at various initial concentrations (20 to 80 mg L^{-1}) and two different contact periods (60 and 120 minutes) [Fig. 1 (a) to (c)]. *S. ilicifolium* showed Cd uptake with q values

between 10.92 to 27.85 mg g^{-1}. The values for Hg uptake ranged from 9.38 to 27.60 mg g^{-1}. Pb uptake values fluctuated from 7.07 to 17.34 mg g^{-1}. *C. sertularioides* exhibited Cd uptake values in the range of 1.19 to 20.51 mg g^{-1}, Hg uptake values from 10.41 to 47.45 mg g^{-1} and Pb values from 6.03 to 21.58 mg g^{-1}. For *Chaetomorpha* sp., the Cd uptake values were recorded between 7.98 to 31.55 mg g^{-1}, Hg values between 3.73 to 20.02 mg g^{-1} and Pb values between 7.52 to 35.08 mg g^{-1}. Similar observations were made by Prasanna Kumar *et al.* [17] for the removal of copper from aqueous solution using a marine green alga, *Ulva fasciata* with maximum adsorption capacity of 26.88 mg/g. Sheng *et al.* [18] investigated the biosorption performance of four marine algae *Sargassum* sp., *Padina* sp., *Ulva* sp. and *Gracillaria* sp. for removal of lead, copper, cadmium, zinc, and nickel from dilute aqueous solutions and observed that *Sargassum* sp. and *Padina* sp. showed the highest potential for the sorption of the metal ions, with the maximum uptake capacities ranging from 0.61 to 1.16 mmol/g for *Sargassum* sp. and 0.63 to 1.25 mmol/g for *Padina* sp.

Influence of different initial concentrations and contact period was evident on the equilibrium sorption capacity of all the sorbents. A substantial increase in Cd uptake with increase in initial concentration was observed in *S. ilicifolium* while Hg and Pb uptake increased from 20 to 60 mg L^{-1} but decreased at 80 mg L^{-1}. *C. sertularioides* exhibited a decrease in Cd uptake with an increase in initial concentration. However, in sharp contrast, Hg and Pb uptake values demonstrated marked increase with increase in initial metal concentration from 20 to 80 mg L^{-1}. A similar pattern was observed for Cd and Pb uptake by *Chaetomorpha* sp. Biosorption capacity with reference to contact period of the biomass exhibited a similar pattern for all the metals studied. All the three algae revealed higher q values for all the metals at 120 minutes. Similar results were obtained by Ahalya *et al.* [19]. The Cd uptake values in the different seaweeds were in the order *Chaetomorpha* sp.> *S. ilicifolium* > *C. sertularioides*. Hg uptake values followed the sequence *C. sertularioides* > *S. ilicifolium* > *Chaetomorpha* sp. The metal uptake values for Pb displayed the order *Chaetomorpha* sp. > *C. sertularioides* > *S. ilicifolium*.

Percent reduction by the seaweeds for all the three heavy metals was calculated [Fig. 1 (d) to (f)]. Maximum Cd reduction was observed by *S. ilicifolium* (97.64%) at an initial concentration of 20 mg L^{-1} at 120 minutes while minimum reduction was seen by *C. sertularioides* (3.66%) at 60 mg L^{-1} at 60 minutes. The highest percentage of Hg reduction was witnessed by *C. sertularioides* (95.68%) at 60 mg L^{-1} at 120 minutes whereas the lowest reduction was observed for *Chaetomorpha* sp. (15.96%) at 80 mg L^{-1} at 60 minutes. *Chaetomorpha* sp. exhibited greatest Pb reduction (98.56%) at 20 mg L^{-1} at 120 minutes and the least reduction was seen by *S. ilicifolium* (29.64%) at 80 mg L^{-1} at 60 minutes. The results of the current study corroborated with the findings of Kumar and Kaladharan [20] where 49.27% reduction for Zn, 97.63 % reduction for Cd, 78.44% reduction for Pb and 74.10% reduction for Cu was observed by the biosorbent from *S. wightii*.

Freundlich and Langmuir isotherms were established for the biosorption process for different heavy metals (Fig. 2). Langmuir model served to estimate the maximum metal uptake values where they could not be reached in the experiments. The constant b represents affinity between the sorbent and sorbate. Highest value for q_{max} for Cd biosorption was calculated for *S. ilicifolium* (28.57 mg g^{-1}) while *C. sertularioides* and *Chaetomorpha* sp. exhibited higher values for Hg (50.00 mg g^{-1}) and Pb (37.037 mg g^{-1}) biosorption, respectively (Table 1). For Langmuir equation, R^2 ranged from 0.203 to 0.983.

The Freundlich model predicts that the metal concentration on the adsorbent increased as there was an increase in the metal concentration in the aqueous solution. The value of *n*, of the Freundlich model, falling in the range of 1 to 10, indicates substantially better sorption. The values of the model constants for all the metals are represented in Table 1. The values of n for *S. ilicifolium* ranged between 2.353 to 5.348 which indicate good adsorption when compared to *C. sertularioides* and *Chaetomorpha* sp. R^2 value for the equation varied from 0.042 to 0.952 for the Metals studied (Table 1). Langmuir model provided a better fit than Freundlich model as depicted by higher values of correlation

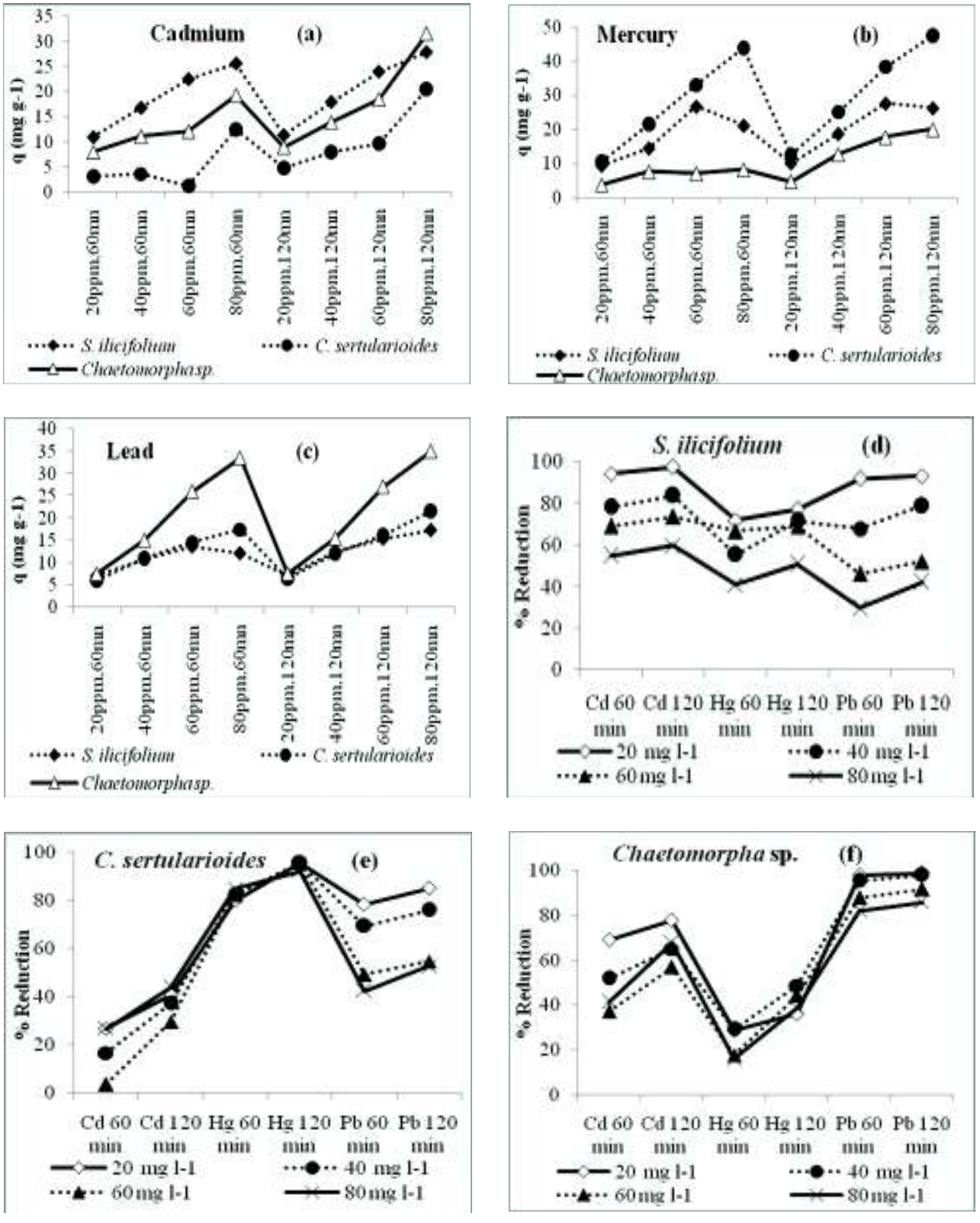

Figure 1: (a) to (c) Heavy metal uptake of cadmium, mercury and lead by dried biomasses of various marine algae and (d) to (f) Metal reduction (%) by the three marine algae at different initial concentrations and variable contact period.

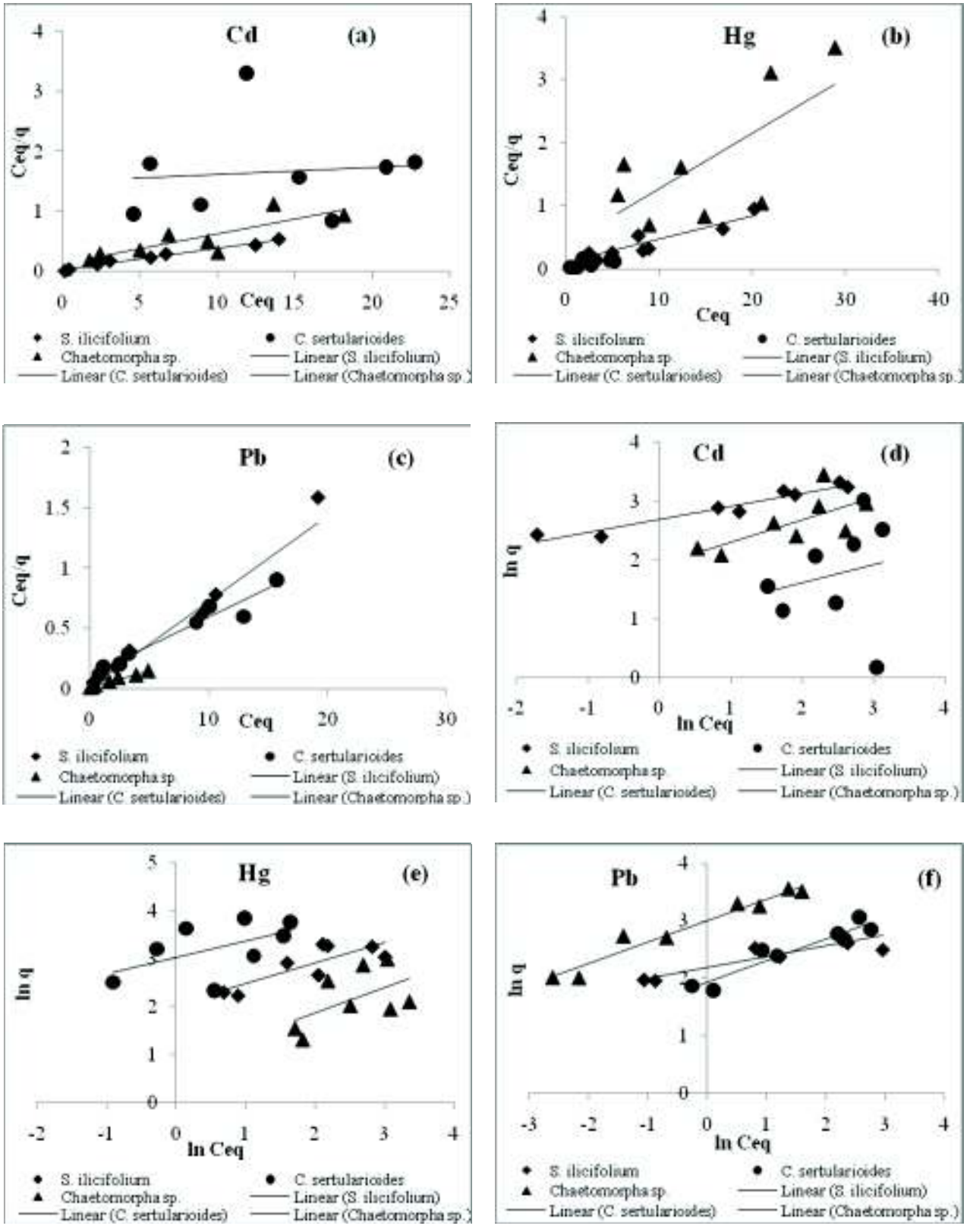

Figure 2: Langmuir plots for metal removal (a) Cd (b) Hg (c) Pb and Freundlich plots for metal removal (d) Cd (e) Hg (f) Pb.

Table 1: Isotherm constants for biosorption by dried biomasses of various marine algae.

Isotherm Constants	*S. ilicifolium*			*C. sertularioides*			*Chaetomorpha* sp.		
	Cd	Hg	Pb	Cd	Hg	Pb	Cd	Hg	Pb
Freundlich									
n	**4.484**	**2.353**	**5.348**	**3.215**	**2.959**	**2.659**	**2.632**	**1.905**	**2.695**
R^2	**0.934**	**0.661**	**0.816**	**0.042**	**0.287**	**0.906**	**0.482**	**0.284**	**0.952**
Langmuir									
q_{max}(mg g^{-1})	**28.571**	**27.778**	**14.286**	**2.667**	**50.000**	**21.277**	**20.408**	**11.494**	**37.037**
b (L mg^{-1})	**0.921**	**0.336**	**4.673**	**0.264**	**0.526**	**0.416**	**0.371**	**0.219**	**2.079**
R^2	**0.983**	**0.858**	**0.947**	**0.203**	**0.404**	**0.944**	**0.690**	**0.484**	**0.980**

coefficients R^2. The findings of the study reinforce the potential of green seaweed, *Chaetomorpha* sp. for heavy metal uptake and its proposed use as an efficient biosorbent material.

CONCLUSION

The present work assessed the biosorption performance of a brown and two green marine macroalgae for the removal of Cd, Hg and Pb from aqueous solutions. *Chaetomorpha* sp recorded the highest metal uptake capacity for Cd and Pb while maximum Hg sequestration was observed in *C. sertularioides*. The concentration of the heavy metals analyzed during the study decreased significantly during the experimental period, proving the marine macroalgae to be excellent biosorbents. The main advantages of using these marine algae as biosorbent are abundant availability of the material and economic feasibility. Thus, the use of green marine macroalgae for the development of efficient biosorbent materials can be considered an ecofriendly and cost-effective approach for heavy metal removal.

ACKNOWLEDGEMENTS

Authors are thankful to Mr. Jagdeesh Rao, Executive Director, Foundation for Ecological Security, Anand, Gujarat for financial assistance of this research project and Sophisticated Instrumentation Centre for Applied Research and Testing (SICART), Vallabh Vidya Nagar for providing instrumentation facility for ICP.

REFERENCES

[1] Volesky, B. (2001) Detoxification of metal-bearing effluents: biosorption for the next century. *Hydrometallurgy*, **59**: 203-216.

[2] Rama, M. P., Alonso, J. A., López, C. H. and Vaamonde, E. T. (2002) Cadmium removal by living cells of the marine microalga *Tetraselmis suecica*. *Bioresource Technology*, **84**: 265-270.

[3] Yabe, M. J. S. and Oliveira, E.de. (2003) Heavy metals removal in industrial effluents by sequential adsorbent treatment. *Advances in Environmental Research*, **7**: 263-272.

[4] Oubagaranadin, J. U. K., Sathyamurthy, N. and Murthy, Z. V. P. (2007) Evaluation of Fuller's earth for the adsorption of mercury from aqueous solutions: a comparative study with activated carbon. *Journal of Hazardous Materials*, **142**: 165-174.

[5] Wase, J. and Forster, C. F. (1997) *Biosorbents for metal ions*, Taylor & Francis, London.

[6] Kapoor, A. and Viraraghavan, T. (1995) Fungal biosorption-An alternative treatment option for heavy metal bearing wastewaters: A review. *Bioresource Technology*, **53**: 195-206.

[7] Bailey, S. E., Olin, T. J., Bricka, R. M. and Adrian, D. D. (1999) A review of potentially low-cost sorbents for heavy metals. *Water Research*, **33(11)**: 2469-2479.

[8] Matheickal, Jose T. and Yu, Qiming. (1996) Biosorption of lead from aqueous solutions by marine algae *Ecklonia radiate*. *Water Science and Technology*, **34(9)**: 1-7.

[9] Antunes, Wallace M., Aderval, Luna S., Henriques, Cristiane A. and Antonio, Carlos

A. da Costa. (2003) An evaluation of copper biosorption by a brown seaweed under optimized conditions. *Electronic Journal of Biotechnology*, **6(3)**: 174-184.

[10] Senthilkumar, R., Vijayaraghavan, K., Thilakavathi, M., Iyer, P. V. R. and Velan, M. (2007) Application of seaweeds for the removal of lead from aqueous solution. *Biochemical Engineering Journal*, **33(3)**: 211-216.

[11] Sheng, Ping Xin, Lai, Heng Tan, Paul, Chen J. and Yen-Peng, Ting. (2005) Biosorption performance of two brown marine algae for removal of chromium and cadmium. *Journal of Dispersion Science and Technology*, **25(5)**: 679-686.

[12] Park, Donghee, Yeoung-Sang Yun, Dae, Sung Lee, Seong-Rin Lim and Jong, Moon Park (2006) Column study on Cr (VI)-reduction using the brown seaweed *Ecklonia* biomass. *Journal of Hazardous Materials,* **B137**: 1377-1384.

[13] Vijayaraghavan Kuppusamy, Jegan Joseph Raj, Palanivelu Kandasamy and Manickam Velan (2004) Copper removal from aqueous solution by marine green alga *Ulva reticulate*. *Electronic Journal of Biotechnology*, **7(1)**: 61-71.

[14] Maiti, S. K. (2001) *Handbook of methods in environmental studies. Vol. 1: Water and wastewater analysis*. ABD Publishers, Jaipur, India, pp. 16-20.

[15] Suresh Kumar K., Ganesan K. and Subba Rao, P. V. (2008) Heavy metal chelation by non-living biomass of three color forms of *Kappaphycus alvarezii* (Doty) Doty. *Journal of Applied Phycology*, **20**: 63-66.

[16] Basha, Shaik, Murthy, Z. V. P. and Jha, B. (2006) Biosorption of hexavalent chromium by chemically modified seaweed, *Cystoseira indica*. *Chemical Engineering Journal*, **137**: 480-488.

[17] Prasanna Kumar, Y., King, P. and Prasad, V. S. R. K. (2006) Removal of copper from aqueous solution using *Ulva fasciata* sp. - A marine green algae. *Journal of Hazardous Materials*, **137(1)**: 367-373.

[18] Sheng, Ping Xin, Yen-Peng, Ting, Chen, J. Paul and Liang Hong. (2004) Sorption of lead, copper, cadmium, zinc, and nickel by marine algal biomass: characterization of biosorptive capacity and investigation of mechanisms. *Journal of Colloid and Interface Science*, **275(1)**: 131-141.

[19] Ahalya, N., Kanamadi, R.D. and Ramachandra, T. V. (2005) Biosorption of chromium (VI) from aqueous solutions by the husk of Bengal gram (*Cicer arientinum*). *Electonic journal of Biotechnology*, **8(3)**: 258-264.

[20] Kumar, Vinoj V. and Kaladharan, P. (2006) Biosorption of metals from contaminated water using seaweed. *Current Science*, **90(9)**: 1263-1267.

PRAJÑĀ - **Journal of Pure and Applied Sciences**
Vol. 17: 035 - 039, 2009 ISSN 0975 - 2595

BIOCHEMICAL ALTERATIONS INDUCED BY CHRONIC EXPOSURE OF CHLOROQUINE IN SWISS ALBINO MICE

P. Mehta [*], J. J. Dattani, D. K. Rajput, N. Moid, H. N. Highland and K. R. Desai[*]

Department of Zoology, University School of Sciences, Gujarat University, Ahmedabad, Gujarat -380 009

ABSTRACT

The present study was undertaken to determine biochemical changes induced by antimalarial drug, Chloroquine Phosphate (CQ) on certain tissues of mice (*Mus musculus*). Healthy adult male Swiss albino mice weighing between 30-40gm were used for the study. 200mg/kg body weight/day of Chloroquine phosphate (CQ) was administrated through oral route for 45 days. Control animals were given distilled water for the same duration (45 days). Liver, kidney, and brain tissues were biochemically investigated for toxic effects post treatment. Results obtained exhibited significant decrease in protein levels of liver ($p<0.01$) and brain ($p<0.001$). Cholesterol level was found to be increased significantly in kidney ($p<0.01$) and liver ($p<0.001$). Creatinine concentration was significantly ($p<0.001$) elevated in kidney. Succinate dehydrogenase (SDH) activity significantly ($p<0.01$) decreased in brain. Thus, use of choloroquine for longer duration stipulates austere monitoring, as chronic usage may lead to development of many adverse effects in the humans.

***Keywords*: chloroquine toxicity, protein, cholesterol, SDH, creatinine.**

INTRODUCTION

Malaria is still considered a major health problem in many of the developing countries of Asia and Africa. The annual death rate of malaria exceeds over a million people. Chloroquine is a commonly used antimalarial drug that belongs to the quinolone family. Chloroquine is cheap and until recently, was very effective, which made it the antimalarial drug of choice for many years in most part of the world. Comparative antimalarial drug trials in humans revealed that chloroquine was more effective as an antimalarial than quinidine and quinine [1]. Subsequently, it was developed as the first choice drug for prophylaxis and treatment of all types of malaria due to susceptible strains of *P. falciparum*, *P. ovale, P. vivax and P. malariae* [2].

Chloroquine has a quinoline ring like that of quinine and a side chain identical to that of quinacrine. The chloride atom in the seventh position appears to be critical to its antimalarial activity [2]. It specifically inhibits the malarial parasites digestive pathway for haemoglobin. There are two enantiomers, the (-) chloroquine being less active than (+) chloroquine enantiomer relatively active against chloroquine resistant strains of *Plasmodium falciparum* [3]. Chloroquine has adverse effects on various tissues though it is known to be well tolerated when given in prophylactic dosages, withdrawal of drugs and reversal of side effects is also documented at higher dosages and their prolonged usage can result in adverse influences [4].

Some of the ill effects of chloroquine at therapeutic dosage are dizziness, headache, diplopia, disturbed visual accommodation, dysphasia, nausea, malaise and pruritus of palms, soles and scalp. It can also cause visual hallucinations, confusion and occasionally frank psychosis. It can also exacerbate epilepsy. When used as prophylactic drug at 300mg of the base/week, it can cause retinal toxicity after 3-6 years (after 50-100g of chloroquine). Intra muscular injection of chloroquine can cause hypotension and cardiac arrest, particularly in children. Retinal toxicity is more serious and may be irreversible [5]. These side effects do not warrant stoppage of treatment.

Hence, the current work aims to study the influence of chloroquine on certain tissues like liver, kidney and brain of mice.

MATERIALS AND METHODS

Animals

Healthy adult male albino mice (*Mus musculus*) of Swiss strain, weighing between 30-40gm obtained from the Cadila Healthcare, Ahmedabad, Gujarat, India, were used for the experiment. The animals

* Corresponding author – ketalak60@yahoo.co.in

were maintained in an air conditioned animal house at temperature of 26±2°C and exposed to 10-12 hours of day light, provided food chow and water *ad libitum.* Treated animals were caged separately and a maximum of five animals per cage were maintained. The treatment was given daily before feeding so as to avoid interference with food intake. All oral treatments were given by a feeding gavage attached to a hypodermic syringe.

Preparation of dose

Pure CQ (~99%) was generously gifted by IPCA laboratories. It was dissolved in the double distilled water. The Dose of antimalarial drug (i.e. Chloroquine) was selected on the basis of the LD_{50} value in accordance with oral LD_{50} doses for Rat and Mouse and mean oral lethal doses for Human [6]. Chloroquine phosphate was given orally at a dosage of 200 mg/kg body weight/day for 45 consecutive days.

Data collection

At the end of each treatment, the animals were weighed on an animal weighing balance and sacrificed. The kidney, liver, brain (Cerebral hemisphere) of both control and treated animals were dissected out and blotted free of blood, weighed on Citizen Balance to the nearest milligram and utilized to study the different parameters.

Parameters

Protein estimation in brain (cerebral hemisphere), liver and kidney homogenate in both control and treated groups was done by the method of Lowry *et al.* [7]. Level of cholesterol in brain (cerebral hemisphere), liver and kidney was estimated by the method of Zlatkis *et al.* [8]. SDH activity was estimated by the method of Beatty *et al.* [9]. Creatinine was estimated by method of Merck [10].

Statistical Analysis

Test for statistical significance between control and chloroquine treated animals was done using Student's t test.

RESULTS

In Kidney, protein level insignificantly decreased by chloroquine treatment in treated group as compared to control animals. The cholesterol level in kidney was augmented significantly ($p<0.01$) after 45 days of chloroquine treatment as compared to control animals. Due to the chloroquine treatment creatinine level was significantly ($p<0.001$) increased in treated group as compared to control animals [Table 1].

Table 1: Showing the protein, cholesterol and creatinine concentrations in the kidney of control and treated groups of mice.

Groups	Protein mg / 100 mg fresh weight	Cholesterol mg / 100 mg fresh weight	Creatinine mg / 100 mg fresh weight
Group-1 Control	19.52 ± 0.34	1.28 ± 0.63	229.06 ± 1.51
Group-2 CQ Treated	17.85 ± 2.41^{NS}	4.10 ± 0.85*	327.07 ± 1.26 ***

Values are mean ± S.E, *** p<0.001, * p<0.01, NS-insignificant, n = 10

After, treatment of chloroquine for 45 days, protein level of liver exhibited a significant ($p<0.01$) decline. A significant ($p<0.001$) increase in the cholesterol content of the liver post treatment with chloroquine was observed [Table 2].

Table 2: Showing biochemical parameters in liver.

Groups	Protein mg / 100 mg fresh weight	Cholesterol mg / 100 mg fresh weight
Group-1 Control	19.76 ± 0.31	0.79 ± 0.07
Group-2 CQ Treated	16.69 ± 0.72 *	2.78 ± 0.45 ***

Values are mean ± S.E, *** p < 0.001, * p < 0.01, n = 10

In brain, the protein level of cerebral hemispheres recorded a significant ($p<0.001$) rise after the treatment with chloroquine as compared to values of control animals. The cholesterol level in brain was insignificantly elevated after chloroquine treatment. The brain SDH activity reduced significantly ($p<0.01$) following the treatment with chloroquine in comparison to control animals [Table 3].

Table 3: Showing biochemical parameters in brain.

Groups	Protein mg / 100 mg fresh weight	Cholesterol mg / 100 mg fresh weight	SDH µg formazan formed/ 15 minutes/mg protein
Group-1 Control	11.58 ± 0.69	2.11 ± 0.23	190.62 ± 1.26
Group-2 CQ Treated	21.29 ± 2.07 ***	2.47 ± 0.13 ^{NS}	172.52 ± 1.71 *

Values are mean ± S.E, *** p < 0.001, *p < 0.01, NS-insignificant, n = 10

DISCUSSION

Malaria is one of the most widespread parasitic infections of humans due to its high morbidity and

mortality which greatly affects both economic productivity and livelihood [11]. Approximately 40% of world's population is at risk to this epidemic. Each year 300-500 million people suffer from acute malaria and 1.5-2.5 million face death as a result of the disease annually [12, 13, 14]. CQ has been the most frequently used drug for the first-line treatment of malaria infections in many tropical countries because it is effective against all forms of malaria, relatively easy to manufacture and chemically stable. Thus it is readily stored and transported even under extreme climatic conditions [15]. Prolonged use of chloroquine in the prophylaxis of malaria and therapy of rheumatoid diseases has several side effects. Clinically most serious effects involve functional and physiological loss of vital organs like eyes and the skeletal muscles [16, 17, 18]. The present work was undertaken in order to understand the toxic effects of chloroquine administration on some soft tissues of male albino mice *Mus musculus* of Swiss strain for the duration of 45 days.

Chloroquine administration decreased the protein level in liver and kidney and increased the protein content in the brain of treated mice. The alterations in protein level of liver, kidney and brain might be due to changes in its synthesis or metabolism. De-Feo *et al.* reported a therapeutic dose of CQ which led to a decrease in protein turnover in humans [19].

Chloroquine is known to be concentrated in lysosomes which play important role in the conformational conversion of protein. Shyng *et al.* showed that these conformational changes like conversion of α-helical structure into β-pleated sheet altered the physical features of the protein [20]. The pathological isoform of these proteins are heat resistant and protease resistant forming prion proteins [20]. Kitamoto *et al.* reported that these protease resistant proteins accumulate in muscle fiber and this pathological condition is called Chloroquine Myopathy which is characterized by degenerated muscle fiber with numerous autophagic, rimmed vacuoles [21]. Matsunga *et al.* reported that pH is the crucial factor in determining the conformational state of some amyloidgenic proteins and increase in pH might be responsible for biosynthesis of prion molecules that are accumulated [22]. Thus chloroquine also inhibits proteolysis leading to increased protein level in brain.

In our study, cholesterol content was increased in all the three organs (liver, kidney and brain) after chloroquine exposure for 45 days. Yamamoto *et al.* demonstrated an increased concentration of phospholipids and cholesterol in the liver, spleen and kidney [23, 24]. Nilsson *et al.* reported that chronic CQ treatment caused a 3-fold increase in the phospholipids concentration and a 10-fold increase in gangliosides level in the skeletal muscle [25]. Fredman *et al.* documented similar increase in chloroquine treated miniature pigs, which conform to our findings [26].

Succinate dehydrogenase (SDH) is an enzyme involved in the Kreb's cycle. A decrease in its activity may affect the conversion of succinate to fumarate and may alter the function of Krebs cycle thus, also altering the energy metabolism of the tissue. SDH is a mitochondrial enzyme and hence any change in the structure or function of mitochondria may influence its activity. Chloroquine crosses the blood brain barrier and has been reported to accumulate in the brain and other tissues. Chloroquine was found to accumulate in the cytoplasm and mitochondria of various organs [27]. This may affect the SDH activity and cause alterations in energy metabolism of tissue. Chloroquine treatment for 45 days in mice exhibited changes in mitochondrial respiratory activity in brain. Chloroquine is known to affect the enzymes of energy metabolism and SDH being one of the enzymes may be affected by it. Deepalakshmi *et al.* showed reduction in mitochondrial NADH dehydrogenase, succinate dehydrogenase, and cytochrome C oxidase activities following CQ treatment in rats, which is in agreement with our study [28].

Creatinine is a marker enzyme of kidney function. In the present work, level of creatinine was found to be increased in kidney. Earlier reports suggest that antimalarial drugs decrease creatinine clearance, thereby increasing the level of creatinine in kidney [29]. Whether chloroquine affects glomerular filtration or tubular excretions of creatinine remains to be investigated. A significant increase in creatinine content might mean that there is cellular injury causing enzyme

leakage from the liver into the bloodstream. There might be alteration of functional capacity of tubular excretion so creatinine which is a product of protein metabolism is increased in mice kidney. However, urea, creatinine and electrolytes (Na^+, K^+, HCO^- , and Cl^-) are the most sensitive biochemical markers employed in the diagnosis of renal damage because creatinine is excreted through the kidney while the electrolytes are reabsorbed and excreted in the tubules. So in cellular damage, there will be retention of creatinine in the blood and no re-absorption and excretion of electrolytes by the tubules as noticed by Mulla *et al.* [30]. Creatinine is a toxic byproduct of protein metabolism that needs to be excreted by the kidney, therefore marked increase in serum creatinine confirms an indication of functional damage to the kidney [31]. Creatinine is more specific to the kidney since kidney damage is the only significant factor that increases serum creatinine level [32]. Therefore the increase in creatinine level noticed in the present study is a classical sign suggesting adverse effect on kidney by the exposure arising from CQ treatment.

In conclusion, results of our study suggest that prolonged exposure to the antimalarial drug chloroquine phosphate potentiates several adverse effects on vital tissues of host. Contemplating the risks to humans due to widespread use of these quinoline derivatives, these findings suggest the necessity of proper instructions and careful monitoring by doctors when prescribing chloroquine for longer duration for prophylaxis as it can produce some undesirable effects. Further this work also identifies the need for more such studies in future which could throw light on other aspects of antimalarial drug toxicity and its ameliorative treatments.

REFERENCES

[1] Bruce-Chwatt, L. J., (1981) *Chemotherapy of malaria*. 2nd ed. WHO Monograph Series 27. World Health Organization, Geneva.

[2] Pandey, A. V., Bisht, H., Babbarwal, V. K., Srivastava, J., Pandey, K. C. and Chauhan, V. S. (2001) Mechanism of malarial haem detoxification inhibition by chloroquine. *Biochem. J.* **355**: 333-238.

[3] Krishna, S. and White, N. J. (1996) Pharmacokinetics of quinine, chloroquine and amodiaquine. *Clin. Impli. Clin. Pharmacokinet.,* **30**: 263-299.

[4] Reynolds, J. E. F. (1982) *Martindale the extra pharmacopoeia*. 28th ed. The Pharmaceutical Press, London,.

[5] Ogunbayo, O. A., Adisa, R. A., Ademowo, O. G. and Olorunsogo, O. O. (2006) Incidence of chloroquine induced oxidative stress in the blood of rabbit. *Int. J. Pharmacol.*, **2(1)**: 121-125.

[6] Walum, E. (1998) Acute oral toxicity. Alternative Testing Methodologies. Environ. *Health Perspect.,* **106(2)**: 497-503.

[7] Lowry, O. H., Rosebrough, N. J., Farr, A. L. and Randall, R. J. (1951) Protein measurement with Folin-phenol reagent. *J. Biol. Chem.***193**: 265-275.

[8] Zlatkis, A., Zak, B. and Boyle, A. (1953) A new method for the direct determination of serum cholesterol. *J. Lab. Clin. Med.*, **41**: 486-492.

[9] Beatty, C. H., Basinger, G. M., Dully, C. C. and Bocek, R. M. (1966) Comparision of red and white voluntary skeletal muscle of several species of primates. *J. Histochem. Cytochem.* **14**: 590-600.

[10] Merck, E. (1974) Estimation of creatinine. In: Clinical Laboratory, 11th ed. *Medico-Chemical Investigation Methods*, E. Merck Co; Darmstadt. Germany: p. 7-19.

[11] Sachs, J. and Malaney, P. (2002) The economic and social burden of malaria. *Nature,* **415**: 680-685.

[12] Breman, J. G., Egan, A. and Keusch, G. T. (2001) The intolerable burden of malaria: a new look at the numbers, *Am. J. Trop. Med. Hyg.,* **64(1–2)**: iv-vii.

[13] Carter, R. and Mendis, K. N. (2002) Evolutionary and historical aspects of the burden of malaria. *Cli. Microbiol. Rev.,* **15**: 564 – 594.

[14] Hay, S. I., Guerra, C. A., Tatem, A. J., Noor, A. M. and Snow, R. W. (2004) The global distribution and population at risk of malaria: past, present, and future. *Lancet Infect Dis.* **4(6)**: 327-336.

[15] Ginsburg, H. (2005) Should chloroquine be laid to rest? *Acta Trop.,* **96**: 16-23.

[16] Goldman, L. and Preston, R. H. (1957) Reactions to chloroquine observed during the treatment of various dermatologic disorders. *Am. J. Trop. Med.*, **6**: 654-657.

[17] Hobbs, H. E., Sorsby, A. and Freedman, A. (1959) Retinopathy following chloroquine therapy. *Lancet ii*: 478-480.

[18] Whisnant, J. P., Espinosa, R. E., Kierland, R. R. and Lambert, E. H. (1963) *Proc. Staff Meet. Mayo Clin*. **38**: 501-513.

[19] De-Feo. P., Volpi, E., Lucidi, P., Cruciani, G., Santeusanio, F., Bolli, G. B. and Brunetti, P. (1994) Chloroquine reduces whole body proteiolysis in humans. *Am. J. Physiol.* **267**: E183-E186.

[20] Shyng, S. L., Huber, M. T. and Harris, D. A. (1993) A prion protein cycles between the cell surface and an endocytic compartment in cultured neuroblastoma cells. *J. Biol. Chem.,* **268**: 15922-15928.

[21] Kitamoto, T., Shin, R. W. and Doh-Ura, K. (1992) Abnormal isoform of prion protein accumulates in the synaptic structures of the central nervous system in patients with Creutzfeldt-Jakob disease. *Am. J. Path.,* **140**: 1285-1294.

[22] Matsunaga, Y., Zerovnik, E. and Yamada, T. (2002) Conformational changes preceding amyloid-fibril formation of amyloid-beta and stefin B: parallels in pH dependence. *Curr. Med. Chem.,* **9**: 1717-1724.

[23] Yamamoto, A., Adachi, S., Ishikawa, K., Yokomura, T., Kitani, T., Nasu, T., Imoto, T. and Nishikawa, M. (1971) Studies on drug-induced lipidosis: III. Lipid composition of the liver and some other tissues in clinical cases of "Niemann-Pick-like Syndrome" induced by 4, 4'-Diethylaminoethoxyhexestrol. *J. Biochem.* **70**: 775-784.

[24] Yamamoto, A., Adachi, S., Matsuzawa, Y., Ketani, T., Hiraoka, A. and Seki, K. I. (1976) Studies on drug-induced lipidosis: VII. Effects of bis-β-diethylaminoethylether of hexestrol, chloroquine, homochlorocyclizine, prenylamine, and diazacholesterol on the lipid composition of rat liver and kidney. *Lipids.* **9**: 616-622.

[25] Nilsson, O., Fredman, P., Klinghardt, G. W., Dreyfus, H. and Svennerholm, L. (1981) Chloroquine-induced accumulation of ganglio sides and phospholipids in skeletal muscles. *Eur. J. Biochem.* **116**: 565-571.

[26] Fredman, P., Klinghardt, G. W., Nilsson, O. and Svennerholm, L. (1982) Lipid accumulation in liver, spleen, lungs and kidneys of miniature-pigs after chloroquine treatment. *Biochem.J.,* **201**: 581-588.

[27] Adelusi, S. A., Dawodu, A. H. and Salako, L. A. (1982) Kinetics of the uptake and elimination of chloroquine in children with malaria. *British J. Pharmacology,* **14**: 483-487.

[28] Deepalakshmi, P. D., Parasakthy, K., Shanthi, S. and Devaraj, N. S. (1994) Effect of chloroquine on rat liver mitochondria. *Ind. J. Exp. Biol.,* **32**: 797-799.

[29] Landewe, R. B. M., Vergouwen, M. S. C., Goeithe, H. S., Van rijthoven, A. W. A. M., Breedveld, F. C. and Dijkmans, B. A. C. (1995). Antimalarial drug induced decrease in creatinine clearance. *J. Rheumatology,* **22(1)**: 34-37.

[30] Mulla, M. S., Thavara, U., Tawatsin, A., Kong-Ngamsuk, W. and Champoosri, J. (2001). Mosquito burden and impact on the poor; measures and costs for personal protection in some, communities in Thailand. *J. Am. Mosquito Control Assoc.,* **17**: 153-159.

[31] Panda, N. C. (1999). Kidney In: *Textbook of Biochemistry and Human Biology*. 2nd ed. Prentice Hall India, pp: 296-290.

[32] Cheesbrough, M. (1998). Clinical chemistry tests in: District laboratory practice in tropical countries campbridege new edition part I, pp: 331-363.

PRAJÑĀ - **Journal of Pure and Applied Sciences**
Vol. 17: 040-047, 2009 ISSN 0975 - 2595

IMPACT OF CHROMIUM DURING EARLY GERMINATION OF FENUGREEK IN INTERACTION WITH COPPER, ZINC, LEAD AND CADMIUM

M. Nataraj,* Arpita Parmar and Mafatlal M. Kher

Department of Biosciences, Sardar Patel University, Vallabh Vidyanagar, Gujarat – 388 120

ABSTRACT

Chromium is one of the heavy metals known to cause oxidative damages to plants. When plants are exposed to more than one element, the effects may be independent, synergistic additive or antagonistic. The present paper deals with the effect of chromium (Cr^{6+}) on germination of *Trigonella foenum-graecum* seeds when treated along with either: Cu, Zn, Pb, or Cd. The present study suggests that Cu and Zn are antagonistic and Pb and Cd are either synergistic or additive. However Zn at higher concentrations was synergistic.

***Keywords*: *Trigonella foenum-graecum,* catalase, peroxidase, superoxide dismutase, proline.**

INTRODUCTION

Rapid industrialization and urbanization has resulted in the deterioration of water, air and land quality. Natural water sources are contaminated with several heavy metals arising from mining wastes and industrial discharges. The tremendous increase in the use of heavy metals over the past few decades has eventually resulted in an increased flux of metallic substances in the environment. Among the heavy metals, some are essential for plant growth, but when present at elevated levels in soils, they are generally toxic and can ultimately cause the death of plants. The possible adverse effects of heavy metal pollution and their phytotoxic effects have been reported by several workers [1, 2]. The contamination of soil with heavy metals results in phytotoxicity [3]. Metal toxicity largely depends upon environmental factors such as pH, salinity, hardness, nitrate, phosphate and calcium. Various interactions can occur when plants are exposed to enormous concentrations of more than one trace element. Such combination effects were categorized by Berry and Wallace [4] as independent, in which the yield response with the stressor having greater effect, additive, in which stressors act on same step in yield production process and effect is given by the added dose of stressors, synergistic, in which the total effect is greater than that of the most of the active stressor or antagonistic in which the combined effect is smaller than the effect of the most active stressor alone. In the present investigation the influence of Cu, Zn, Pb and Cd on germination of Fenugreek seeds when treated along with chromium was undertaken.

* Corresponding author – nattusamy@yahoo.com

MATERIALS AND METHODS

The certified seeds of Gujarat fenugreek-1 (GF-1) were procured from Department of Agronomy, Anand Agriculture University Anand. The seeds were surface sterilized with 0.1% $HgCl_2$ [5]. Solutions of different concentration (1.25, 2.5, 5.0, 10.0 mg/L) of heavy metals were prepared using potassium dichromate (Cr^{6+}), cadmium chloride (Cd), zinc sulphate (Zn), copper sulphate (Cu) and lead nitrate (Pb) in distilled water. Ten seeds were placed on petri plates over Whatman paper no-1 filter paper and treated with 2 ml of different concentrations of combinations of heavy metals like Cr and Cu, Cr and Zn, Cr and Pb and Cr and Cd. Distilled water and solution of different concentrations (1.25, 2.5, 5.0, 10.0 mg/L) of chromium alone were used as control. For every treatment three replicates, each with 8-10 seeds were maintained. The fresh solutions were applied after 48 hours to respective petri plates. After 7 days seedling were selected from each petri dish and biochemical analysis like total soluble protein, free proline content, enzyme assay for anti-oxidative enzymes like catalase, peroxidase and superoxide dismutase were carried out.

Measurement of root length and shoot length

The root length was measured from the point at which root hairs were observed and the rest of the portion was measured as shoot length.

Biochemical analysis

Enzyme Assay

Catalase and Peroxidase assays were carried out from the fresh seedlings of Cr and Cu, Cr and Zn and Cr and Cd treated fenugreek against control seedlings. Known weights of fresh tissues were homogenized with cold 0.1M potassium phosphate Buffer (pH-7) then centrifuged at 10,000 rpm for 30 minutes, at 4°C and the supernatant was used for catalase assay.

Catalase assay done using the protocol of Beers and Sizer [6]. The substrate for assay was 0.005M H_2O_2 (commercially available 30% H_2O_2 solution) prepared in the cold buffer. The tissue extract was used as an enzyme source. The reaction mixture containing 3.0 ml phosphate buffer, 2 ml H_2O_2 and 1ml enzyme was allowed to react at 20°C for 1 min. The enzyme activity was stopped by addition of 0.7N H_2SO_4 and the reaction mix was titrated with 0.01N $KMnO_4$.The values obtained were then converted into unit activity.

Peroxidase assay was done according to the procedure of Chance and Machly [7] in which 0.01M O-dianisidine was allowed to react with the enzyme in presence of 20 mM H_2O_2 at 30°C for 5 min. The reaction was stopped by addition of 2 N H_2SO_4 and the absorbance was measured at 430 nm in a spectrophotometer against reagent blank.

Superoxide dismutase assay was done according to the procedure described by Sadsivam and Manickam [8]. Known weight of tissues were homogenized in 50 mM potassium phosphate buffer (pH-7.8), in a pre-chilled pestle and mortar and the homogenate was centrifuged at 4°C for 10 min. at 10,000 rpm for the enzyme assay.

Total soluble proteins

The total soluble protein content was determined according to Lowry's [9] method by using bovine serum albumin (BSA) as a standard. The metal treated seeds of fenugreek were homogenized in an ice-cold mortar and pestle with extraction buffer containing 20 mM Tris Base (pH-8), 0.25M Sucrose, 5% PVP and 3 µl of ß-mercaptoethanol. Then the homogenate were centrifuged at 12000 rpm for 20 minutes and the supernatant was used for protein assay.

Proline content

Free proline content was estimated following the procedure of Bates *et al*. [10]. Fresh seedlings were homogenized in 3% aqueous salicylic acid and homogenate was filtered through Whatman filter paper No.1. To an aliquot of 2 ml filtrate, 2 ml of acid ninhydrin was added followed by addition of 2 ml glacial acetic acid and boiling for 1 hour. After incubation, the mixture was quickly cooled under running tap water and extracted with 4 ml toluene and the free proline was estimated from the organic phase at 520 nm against a reagent blank. The amount of proline in the sample was calculated using a standard curve prepared from pure proline.

RESULTS AND DISCUSSION

Root length

When the seeds of fenugreek were treated with Cr along with Cu or Zn an increase in the root length was observed except in seeds treated with low concentration of Cr along with high concentrations of Cu and Zn in comparison control treated only with Cr. however the seeds treated with Pb and Cd, along with Cr showed a decrease in the root length compared with the seeds treated with Cr alone suggesting the synergistic effect. At lower concentration of Pb, development and extension of main root is much more affected than the lateral roots [11]. The phytotoxic effects of Cd include inhibition of seed germination, seedling growth [12] and reduction of root elongation [13]. Cd and Pb are toxic heavy metals and so when seeds of fenugreek were treated with Pb and Cd along with Cr, it shows decrease in root length because the interaction of the two metals show synergism, in which one metal increases the toxicity of the another and ultimately the effect higher toxicity. The highest root length has been found in 2.5 ppm of Zn along with 5 ppm of Cr with 44.32% increase than the control. Where as highest 81.4% decrease in root length found in 10 ppm Cd along with the 2.5 ppm of Cr. However there was a marked decline in root length at higher concentrations of Cu and Zn along with low concentrations of Cr. The results suggest that an antagonistic effect by Cu and Zn was observed when Cr concentration is higher along with higher concentration of Cu and Zn. But at low concentration of Cr along with high concentrations of Cu and Zn, synergistic effect by Cu and Zn was observed. This could be

because the Cu and Zn being micronutrients show an antagonistic effect at low concentrations but at higher concentrations show synergistic effect. The relative concentrations of metals could be an important factor than absolute concentrations of individual metals (Table 1).

Shoot length

There is a reduction in shoot length in seeds treated with Cu and Zn, along with the lower concentration of Cr. However at higher concentrations of Cr along with Cu an increase in the shoot length was observed. The seeds treated with 5ppm and 10ppm of Zn exhibited reduction in shoot length. The seeds which are treated with Cd and Pb, showed a decrease in shoot length, compared with the seeds treated with Cr alone. The highest increase in the shoot length has been found at 2.5 ppm of Cu along with the 10 ppm of Cr. It is 105% higher than the control and the highest decrease 64.49% was recorded in 10 ppm of Cd and 10 ppm of Cr. The results suggest that the Pb, Cd and higher concentrations of Zn have a synergistic effect in toxicity (Table 2).

Catalase

Catalase analysis carried out has showed that in seeds treated with Cd and Pb along with Cr, there is an increase in the catalase activity compared to the seeds treated with Cr alone. However seeds treated with Cu and Zn, there was a decrease in the unit activity. The highest activity has been found in the seeds treated with 5 ppm of Cd along with 1.25 ppm of Cr. The activity is 6 fold higher than the control. The highest reduction in the unit activity has been found in 2.5 ppm of Cu and Zn along with 1.25 ppm of Cr compared to the control. There is 34% decrease in the unit activity. In present study higher % increase in catalase activity in Cd and Pb treated seeds along with Cr, indicates their antioxidant defence mechanism. Exposure to heavy metals causes oxidative stress in plants and produces H_2O_2 and free radicals. Although H_2O_2 plays an important role in certain tasks in plant cell [14] control of H_2O_2 is essential to prevent oxidative damage to membrane and proteins. Catalase activity has been found highest in Cd treated seeds along with Cr. The activity in present experiment is more than double, which shows an additive effect of metals, where as seeds which were treated with Cu and Zn along with Cr, shows a decrease in enzyme activity means it shows an antagonistic effect (Table3).

Peroxidase

The seeds treated with Cu along with Cr, showed decrease in peroxidase activity, than the seeds treated with Cr alone. Where as in Cd and Pb treated seeds, there is an increase in the activity of peroxidase enzyme. The highest activity has been found in 2.5 ppm of Pb along with 1.25 ppm of Cr, which is 7 fold higher than the control. The highest decrease has been shown in 10 ppm of Cu along with 2.5 ppm Cr, which is 74% higher than the control. This enzyme activity increases significantly with increase in the metal concentration. At some concentrations, the activity has been found to be more than twice, which shows an additive effect, where in the seeds treated with Cu, it shows an antagonistic effect. Cd and Pb enhance the effect of Cr resulting in a many fold increase in activity than the control, where as Cu and Zn decrease the toxicity of Cr, and the effect is antagonistic. However at the higher concentrations of Zn, the seedlings exhibited increased enzyme activity (Table 4).

Superoxide dismutase

The activity of superoxide dismutase has been found to be lower in the seeds treated with Cu along with Cr, but the seeds which were treated with Cd and Pb along with Cr showed high activity. In the present experiment the highest activity was found in 1.25 ppm of Zn along with 2.5 ppm of Cr. It shows 2 fold increase in SOD activity. The highest decrease of 66.58% was noticed in the seeds treated with 10 ppm of Zn and 1.25 ppm of Cr. These observations suggest that the impact of Zn is dependent on relative concentration of Cr (Table 5).

Total protein

At lower concentrations of heavy metals, the concentrations of total soluble protein decreases. The seeds treated with Cu and Zn along with 1.25 ppm of Cr show a decrease in protein content. But in Cd and Pb treated seeds there is an increase in protein content. As the concentration of Zn increases, the concentration of total protein increases. The highest increase in protein content was found in seeds treated with 10 ppm of Pb along with 1.25 ppm of Cr. It showed a one fold

Table 1: Effect of heavy metal stress on root length.

Metal conc. (mg/lit.)	Root length (cm)				
	Control	Treated			
	Cr	Cr + Cu	Cr + Zn	Cr + Pb	Cr + Cd
D. W.	20.55 ± 0.003	-	-	-	-
1.25	23.51 ± 0.003	-	-	-	-
1.25 + 1.25	-	62.05 ± 0.013	26.61 ± 0.003	21.77 ± 0.002	14.51 ± 0.001
1.25 + 2.5	-	41.12 ± 0.004	30.64 ± 0.007	24.19 ± 0.004	45.96 ± 0.006
1.25 + 5	-	116.93 ± 0.001	33.06 ± 0.003	19.35 ± 0.001	16.93 ± 0.002
1.25 + 10	-	80.64 ± 0.024	54.83 ± 0.007	32.25 ± 0.002	25.8 ± 0
2.50	27.78 ± 0.004	-	-	-	-
2.5 + 1.25	-	64.51 ± 0.029	78.22 ± 0.006	10.48 ± 0	98.38 ± 0.002
2.5 + 2.5	-	35.48 ± 0	47.58 ± 0.008	18.54 ± 0.003	51.61 ± 0.022
2.5 + 5	-	14.51 ± 0.001	29.83 ± 0.006	13.7 ± 0.004	29.03 ± 0
2.5 + 10	-	42.42 ± 0.006	25 ± 0.003	9.67 ± 0.005	47.58 ± 0
5.00	55.26 ± 0.016	-	-	-	-
5 + 1.25	-	76.61 ± 0.001	70.96 ± 0.011	2.96 ± 0.003	17.74 ± 0.002
5 + 2.5	-	104.03 ± 0.006	54.80 ± 0.007	25.80 ± 0.001	26.61 ± 0.001
5 + 5	-	54.83 ± 0.004	63.70 ± 0.007	45.16 ± 0.002	30.64 ± 0.001
5 + 10	-	189.90 ± 0.004	48.38 ± 0.002	36.29 ± 0.005	17.14 ± 0.002
10.00	32.08 ± 0.002	-	-	-	-
10 + 1.25	-	100.00 ± 0.016	13.70 ± 0.002	41.10 ± 0.001	74.19 ± 0.016
10 + 2.5	-	142.74 ± 0.005	72.58 ± 0.002	59.67 ± 0.017	37.09 ± 0.005
10 + 5	-	159.67 ± 0.004	29.83 ± 0.006	21.77 ± 0.007	45.16 ± 0.012
10 + 10	-	130.64 ± 0.002	55.64 ± 0.008	34.28 ± 0.003	103.22 ± 0.014

Table 2: Effect of heavy metal stress on shoot length.

Metal conc. (mg/lit.)	Soot length (cm)				
	Control	Treated			
	Cr	Cr + Cu	Cr + Zn	Cr + Pb	Cr + Cd
D. W.	2.78 ± 0.60	-	-	-	-
1.25	3.23 ± 0.67	-	-	-	-
1.25 + 1.25	-	2.27 ± 1.17	2.94 ± 0.83	2.68 ± 0.73	1.62 ± 0.28
1.25 + 2.5	-	1.40 ± 0.54	3.02 ± 0.42	2.70 ± 0.55	1.76 ± 0.64
1.25 + 5	-	2.05 ± 0.75	1.59 ± 0.57	2.46 ± 0.25	1.43 ± 0.51
1.25 + 10	-	2.25 ± 1.08	2.88 ± 0.74	1.7 ± 0.81	1.50 ± 0
2.50	2.54 ± 0.92	-	-	-	-
2.5 + 1.25	-	3.33 ± 0.50	1.80 ± 0.45	3.05 ± 0.48	1.60 ± 0.53
2.5 + 2.5	-	3.12 ± 1.02	3.62 ± 0.54	2.48 ± 0.53	2.53 ± 0.25
2.5 + 5	-	3.13 ± 0.70	3.01 ± 0.46	2.38 ± 0.90	2.40 ± 0.69
2.5 + 10	-	2.34 ± 0.87	2.92 ± 0.59	2.23 ± 0.94	1.30 ± 0.36
5.00	2.85 ± 0.71	-	-	-	-
5 + 1.25	-	3.42 ± 0.81	1.95 ± 1.10	2.39 ± 0.89	2.40 ± 0.53
5 + 2.5	-	3.00 ± 1.24	2.69 ± 0.95	2.00 ± 0.90	2.56 ± 0.49
5 + 5	-	3.53 ± 1.26	2.23 ± 0.70	1.50 ± 0.91	2.47 ± 0.45
5 + 10	-	2.99 ± 0.80	2.22 ± 0.94	1.94 ± 1.00	1.43 ± 0.40
10.00	2.9 ± 0.59	-	-	-	-
10 + 1.25	-	3.87 ± 0.96	2.75 ± 0.64	2.26 ± 0.61	2.67 ± 0.76
10 + 2.5	-	5.97 ± 1.44	3.13 ± 0.81	2.22 ± 0.81	1.50 ± 0.50
10 + 5	-	2.89 ± 0.69	3.15 ± 0.43	1.39 ± 0.87	2.07 ± 0.40
10 + 10	-	3.37 ± 0.55	2.69 ± 0.44	2.18 ± 0.73	1.03 ± 0.05

Table 3: Effect of heavy metal stress on catalase activity.

Metal conc. (mg/lit.)	Unit activity (Unit/ml/min.)				
	Control	Treated			
	Cr	Cr + Cu	Cr + Zn	Cr + Pb	Cr + Cd
D. W.	1.01 ± 0.043	-	-	-	-
1.25	1.15 ± 0.047	-	-	-	-
1.25 + 1.25	-	1.51± 0.01	1.39± 0.047	2.4± 0.047	6.5± 0.025
1.25 + 2.5	-	0.76± 0.02	0.75± 0.047	2.91± 0.092	6.25± 0.025
1.25 + 5	-	1.39± 0.05	1.395± 0.047	2.45± 0.025	7.72± 0.56
1.25 + 10	-	0.83± 0.02	1.518± 0.047	2.53± 0.047	6.71± 0.047
2.50	1.17 ± 0.047	-	-	-	-
2.5 + 1.25	-	0.88± 0	1.77± 0.047	4.68± 0.047	6.45± 0.047
2.5 + 2.5	-	1.64± 0.05	0.885± 0.047	2.65± 0.43	6.1± 0.058
2.5 + 5	-	1.72± 0.03	1.645± 0.047	2.53± 0.047	6.96± 0.036
2.5 + 10	-	1.37± 0.04	1.139± 0.047	3.42± 0.26	6.76± 0.025
5.00	1.5 ± 0.019	-	-	-	-
5 + 1.25	-	1.29± 0.02	1.695± 0 .025	3.04± 0.13	6.45± 0.047
5 + 2.5	-	1.14± 0.05	0.961± 0.030	2.15± 0.047	5.19± 0.43
5 + 5	-	1.69± 0.08	1.341± 0.075	2.78± 0.047	5.54± 0.12
5 + 10	-	2.28± 0	1.898± 0.047	2.024± .047	6.48± 0.43
10.00	1.26 ± 0.033	-	-	-	-
10 + 1.25	-	1.01± 0.01	1.847± 0.075	2.278± .047	6.2± 0.26
10 + 2.5	-	1.77± 0.02	1.569± 0.064	1.51± 0.047	7.21± 0.047
10 + 5	-	1.08± 0	1.189± 0.025	2.66± 0.73	6.55± 0.30
10 + 10	-	1.26± 0	1.012± 0.047	3.29± 0.13	5.69± 0.25

Table 4: Effect of heavy metal stress on peroxidase activity.

Metal conc. (mg/lit.)	Unit activity (Unit/ml/min.)				
	Control	Treated			
	Cr	Cr + Cu	Cr + Zn	Cr + Pb	Cr + Cd
D. W.	78.47 ± 0.039	-	-	-	-
1.25	11.42 ± 0.011	-	-	-	-
1.25 + 1.25	-	25.40 ± 0.020	12.50 ± 0.011	43.62 ± 0.003	71.29 ± 0.046
1.25 + 2.5	-	19.20 ± 0.009	25.25 ± 0.020	91.37 ± 0.027	53.76 ± 0.034
1.25 + 5	-	15.06 ± 0.021	28.00 ± 0.018	46.37 ± 0.009	70.11 ± 0.051
1.25 + 10	-	45.70 ± 0.014	73.50 ± 0.037	64.12 ± 0.004	73.05 ± 0.015
2.50	26.39 ± 0.036	-	-	-	-
2.5 + 1.25	-	28.05 ± 0.010	30.25 ± 0.014	35.50 ± 0.005	66.70 ± 0.006
2.5 + 2.5	-	10.90 ± 0.027	64.50 ± 0.011	32.87 ± 0.009	54.23 ± 0.006
2.5 + 5	-	24.90 ± 0.003	83.25 ± 0.015	52.37 ± 0	36.59 ± 0.012
2.5 + 10	-	22.30 ± 0.012	37.25 ± 0.001	75.25 ± 0.016	71.41 ± 0.006
5.00	36.54 ± 0.026	-	-	-	-
5 + 1.25	-	24.40 ± 0.106	43.50 ± 0.003	54.62 ± 0.014	55.41 ± 0.005
5 + 2.5	-	17.10 ± 0.002	40.75 ± 0.028	38.62 ± 0.005	43.52 ± 0.004
5 + 5	-	26.40 ± 0.043	30.50 ± 0.002	87.37 ± 0.007	57.41 ± 0.022
5 + 10	-	67.50 ± 0.004	31.25 ± 0.019	91.25 ± 0.028	33.18 ± 0.004
10.00	23.55 ± 0.004	-	-	-	-
10 + 1.25	-	9.87 ± 0.034	25.50 ± 0.005	34.75±0.003	38.00 ± 0.003
10 + 2.5	-	23.80 ± 0.018	25.50 ± 0.025	62.37±0.017	31.18 ± 0.003
10 + 5	-	32.20 ± 0.029	35.25 ± 0.007	79.25±0.022	38.35 ± 0.013
10 + 10	-	41.00 ± 0.009	45.00 ± 0.018	69±0.005	42.82 ± 0.013

Table 5: Effect of heavy metal stress on superoxide dismutase activity.

Metal conc. (mg/lit.)	Unit activity (Unit/ml/min.)				
	Control	Treated			
	Cr	Cr + Cu	Cr + Zn	Cr + Pb	Cr + Cd
D. W.	0.80 ± 0.001	-	-	-	-
1.25	0.74 ± 0.003	-	-	-	-
1.25 + 1.25	-	0.60 ± 0.001	0.73 ± 0.003	0.87 ± 0	1.20 ± 0.003
1.25 + 2.5	-	0.70 ± 0	0.60 ± 0.003	1.40 ± 0.010	2.63 ± 0.004
1.25 + 5	-	0.90 ± 0.001	1.13 ± 0.003	1.03 ± 0.001	1.43 ± 0.008
1.25 + 10	-	1.15 ± 0.001	0.50 ± 0.003	1.07 ± 0.003	0.63 ± 0.001
2.50	1.43 ± 0.003	-	-	-	-
2.5 + 1.25	-	0.75 ± 0.001	4.03 ± 0.002	1.63 ± 0.016	1.00 ± 0.013
2.5 + 2.5	-	1.55 ± 0.002	0.80 ± 0.005	1.03 ± 0.001	0.80 ± 0.005
2.5 + 5	-	1.45 ± 0.003	0.90 ± 0.004	1.07 ± 0.005	1.10 ± 0.003
2.5 + 10	-	0.55 ± 0	1.63 ± 0.004	0.96 ± 0.002	1.40 ± 0.001
5.00	1.56 ± 0.002	-	-	-	-
5 + 1.25	-	0.65 ± 0.002	1.33 ± 0.004	1.86 ± 0.022	1.1 ± 0.002
5 + 2.5	-	0.75 ± 0.001	2.23 ± 0.004	1.13 ± 0.001	0.77 ± 0.001
5 + 5	-	0.55 ± 0.002	1.36 ± 0.001	1.40 ± 0.009	1.60 ± 0
5 + 10	-	0.90 ± 0.001	3.90 ± 0.006	1.50 ± 0.001	1.03 ± 0.005
10.00	1.77 ± 0.002	-	-	-	-
10 + 1.25	-	1.60 ± 0.002	1.40 ± 0.003	0.93 ± 0	1.03 ± 0.001
10 + 2.5	-	1.25 ± 0.002	0.80 ± 0.002	0.87 ± 0	0.80 ± 0.002
10 + 5	-	1.35 ± 0	0.86 ± 0.002	1.13 ± 0.003	1.37 ± 0.001
10 + 10	-	1.00 ± 0.002	0.93 ± 0.003	1.10 ± 0.002	1.53 ± 0

Table 6: Effect of heavy metal stress on total soluble protein.

Metal conc. (mg/lit.)	Amount of protein (mg/gm of tissue)				
	Control	Treated			
	Cr	Cr + Cu	Cr + Zn	Cr + Pb	Cr + Cd
D. W.	46.89 ± 0.011	-	-	-	-
1.25	42.54 ± 0.009	-	-	-	-
1.25 + 1.25	-	25.40 ± 0.007	34.28 ± 0.002	32.83 ± 0.003	38.64 ± .002
1.25 + 2.5	-	19.20 ± 0.007	32.72 ± 0.005	35.32 ± 0.006	28.67 ± 0.01
1.25 + 5	-	15.06 ± 0.008	40.00 ± 0.004	27.42 ± 0.001	27.63 ± .001
1.25 + 10	-	45.70 ± 0.008	35.58 ± 0.002	92.25 ± 0.011	32.62 ± 0.002
2.50	32.76 ± 0.004	-	-	-	-
2.5 + 1.25	-	28.05 ± 0.006	51.42 ± 0.006	31.16 ± 0.007	43.42 ± 0.007
2.5 + 2.5	-	10.90 ± 0.002	37.42 ± 0.003	74.18 ± 0.004	25.55 ± 0.01
2.5 + 5	-	24.90 ± 0.005	34.54 ± 0.003	63.16 ± 0.005	24.93 ± 0.003
2.5 + 10	-	22.30 ± 0.005	41.81 ± 0.002	67.53 ± 0	36.98 ± 0.009
5.00	52.81 ± 0.003	-	-	-	-
5 + 1.25	-	24.40 ± 0.007	35.84 ± 0.007	30.54 ± 0.001	30.12 ± .006
5 + 2.5	-	17.10 ± 0.004	36.36 ± 0.002	34.49 ± 0.003	26.80 ± 0.006
5 + 5	-	26.40 ± 0.001	62.85 ± 0.002	31.79 ± 0.005	31.37 ± 0.007
5 + 10	-	67.50 ± 0.026	37.14 ± 0.003	49.45 ± 0.003	32.62 ± 0.001
10.00	31.75 ± 0.003	-	-	-	-
10 + 1.25	-	9.87 ± 0.002	32.98 ± 0.005	42.18 ± 0.007	19.94 ± 0.002
10 + 2.5	-	23.80 ± 0	33.76 ± 0.002	61.09 ± 0.002	28.25 ± 0
10 + 5	-	32.20 ± 0.003	39.74 ± 0.003	57.14 ± 0.009	27.22 ± 0.005
10 + 10	-	41.00 ± 0.007	56.36 ± 0.011	34.28 ± 0.003	35.32 ± .002

Table 7: Effect of heavy metal stress on proline content.

Metal conc. (mg/lit.)	Unit activity (Unit/ml/min.)				
	Control	Treated			
	Cr	Cr + Cu	Cr + Zn	Cr + Pb	Cr + Cd
D. W.	20.55 ± 0.003	-	-	-	-
1.25	23.51 ± 0.003	-	-	-	-
1.25 + 1.25	-	62.05 ± 0.013	26.61 ± 0.003	21.77 ± 0.002	14.51 ± 0.001
1.25 + 2.5	-	41.12 ± 0.004	30.64 ± 0.007	24.19 ± 0.004	45.96 ± 0.006
1.25 + 5	-	116.93 ± 0.001	33.06 ± 0.003	19.35 ± 0.001	16.93 ± 0.002
1.25 + 10	-	80.64 ± 0.024	54.83 ± 0.007	32.25 ± 0.002	25.80 ± 0
2.50	27.78 ± 0.004	-	-	-	-
2.5 + 1.25	-	64.51 ± 0.029	78.22 ± 0.006	10.48 ± 0	98.38 ± 0.002
2.5 + 2.5	-	35.48 ± 0	47.58 ± 0.008	18.54 ± 0.003	51.61 ± 0.022
2.5 + 5	-	14.51 ± 0.001	29.83 ± 0.006	13.70 ± 0.004	29.03 ± 0
2.5 + 10	-	42.42 ± 0.006	25.00 ± 0.003	9.67 ± 0.005	47.58 ± 0
5.00	55.26 ± 0.016				
5 + 1.25	-	76.61 ± 0.001	70.96 ± 0.011	2.96 ± 0.003	17.74 ± 0.002
5 + 2.5	-	104.03 ± 0.006	54.80 ± 0.007	25.80 ± 0.001	26.61 ± 0.001
5 + 5	-	54.83 ± 0.004	63.70 ± 0.007	45.16 ± 0.002	30.64 ± 0.001
5 + 10	-	189.9 ± 0.004	48.38 ± 0.002	36.29 ± 0.005	17.14 ± 0.002
10.00	32.08 ± 0.002	-	-	-	-
10 + 1.25	-	100.00 ± 0.016	13.70 ± 0.002	41.10 ± 0.001	74.19 ± 0.016
10 + 2.5	-	142.74 ± 0.005	72.58 ± 0.002	59.67 ± 0.017	37.09 ± 0.005
10 + 5	-	159.67 ± 0.004	29.83 ± 0.006	21.77 ± 0.007	45.16 ± 0.012
10 + 10	-	130.64 ± 0.002	55.64 ± 0.008	34.28 ± 0.003	103.22 ± 0.014

increase than control, where as the highest decrease was found in 1.25 ppm of Cu along with 10 ppm of Cr. There is a 68.92% decrease in the protein content. The soluble protein content in germinating seeds is an important indicator of their physiological state. In germinating seeds, both essential and non essential heavy metals induce formation of thiol rich non translated proteins, known as metal binding peptides as phytochelatins and certain translated proteins. This probably plays a central role in the homeostatic control of metal ions in plants [15]. In present study the decrease in protein content shows an antagonistic effect of heavy metals. At higher concentration, Zn shows a synergistic effect. Cd and Pb along with the Cr, shows a synergistic effect and increase in the amount of total protein (Table 6).

Proline

In present experiment proline content increases in Cu along with Cr treated seeds except 5 ppm of Cu along with 2.5 ppm of Cr. The same result has been found in seeds treated with Zn along with Cr. The highest value has been found in 10 ppm of Cu along with 5 ppm of Cr. It is 2.5 fold increase in than the control. Where as highest decrease has been found in 2.5 ppm of Pb along with 5 ppm of Cr. It shows 94.65% decrease in proline content. Proline is a substance which induces osmotic adjustment. It has been suggested that proline is a source of energy, carbon and nitrogen for recovering tissue [16]. The percentage increase is clearly showing that fenugreek is trying to the metal stress. Proline increases the stress tolerance of plants through such functions as osmoprotectant [17], the protection of enzyme against denaturation and the stabilization of protein synthesis [18]. In addition proline could be involved in the metal chelation in the cytoplasm [19] especially in the case of metal stress, an inhibitor of lipid peroxidation [20], an $^{\cdot}OH$ scavenger [21] and single O_2 scavenger [22]. In present study it has been found that the seeds treated with Cu and Zn shows increase in proline content which is tolerance behaviour, where as in Cd and Pb treated seeds a reduction in proline content which is not tolerance behaviour (Table 7). Wallace *et al.* [23] measured the growth of bean plants, *Phaseolus vulgaris* (Fabaceae), in

soil culture with additions of Cd, Li, Cu and Ni. Leaf dry weights were reduced by Cu and Ni. Combinations of Cu and Ni decrease the yield by 68%, which indicated a synergistic effect of the two metals. Combination treatments with Cd and Zn resulted in synergistic and additive effects on the growth of both roots and shoots. Interactions of Zn and Cu on the growth of three species of *Brassica* (Brassicaceae) were described by Ebbs and Kochian [24].

CONCLUSION

The micronutrients copper and zinc showed antagonistic effect at low concentration when treated along with chromium. However at higher concentrations these metals showed synergistic effect. Lead and cadmium, being metals of no physiological importance to plants, mostly showed synergistic effects.

REFERENCES:-

[1] Antonovies, J., Bradhave, A. D. and Turner, R. G. (1971) Heavy metal tolerance in plants. *Adv. Ecol. Res.* **75**: 1-85.

[2] Chiba, S. and Takashashi, K. (1977) Studies on heavy metal pollution in agricultural land (2) Absorption of cadmium and growth retardation in forage crops. *Bull. Shikou Agri. Exper. Station* **30**: 49-73.

[3] Chaney, R. L., Hundermann, P. T., Palmen, W. T., Small, R. J., White, M. C., and Decken, A. M. (1987) Compositing municipal residances and Sludge information transfer Inc., Rockvilla M. B. *Proc. National Conference*. pp. 86-87.

[4] Berry, W. L. and Wallace, A. (1981) Toxicity: the concept on relationship to the dose response curve. *J. Plant Nutrition* **3**: 13-19.

[5] Young, A. P. (1926) Facultative parasitism and host range of fungi. *Amer. J. Botany*.**13**: 502-520.

[6] Beers, R. F. Jr. and Sizer, I. W. (1952) A spectrophotometric method for measuring the breakdown of hydrogen peroxide by catalase. *J. Biol. Chem.* **195**: 133–140.

[7] Chance, B. and Maehly, A. C. (1955) *Meth. Enzymol.*, **11**: 773-775.

[8] Sadasivam, S. and Manickam, A. (1996). Carbohydrates. In: *Methods in Biochemistry*. Sadasivam S, Manickam A, (Eds.), New Age International Pvt. Ltd, New Delhi, pp. 11–12.

[9] Lowery, O. H., Rosebrough, N. J., Farr, A. L. and Randall, R. L. (1951) Protein measurement with Folin phenol reagent. *J. Biol. Chem.* **193**: 265-275.

[10] Bates, L. S., Waldren, R. P. and Teare I. D. (1973) Rapid determination of free proline for water stress studies. *Plant and Soil* **39**: 205-207.

[11] Obroucheva, N. V., Bystrova, E. I., Ivanov V. B., Anupova, O. V. and Seregin I. V. (1998) Root growth responses to lead in young maize seedlings. *Plant and Soil* **200**: 55-61.

[12] Fargasová, A. (2001) Phytotoxic Effects of Cd, Zn, Pb, Cu and Fe on *Sinapis alba* L. Seedlings and their accumulation in roots and shoots. *Biologia Plantarum*, **44(3)**: 471-473.

[13] Rascio, N., Dalla Vecchia, F., Ferrertti,M.,Merlo, L. and Ghisi, R. (1993) Some effects of cadmium on maize plants. *Arch. Env. Contam. Toxi.* **25**: 244-249.

[14] Low, P. S. and Merida, J. R. (1996) The oxidative burst in plant defense: function and signal transduction. *Physiol. Plant.* **96**: 533-542.

[15] Steffens, J. S. (1990) The heavy metal binding peptides of plants. *Ann. Rev. Plant Physiol. Plant Mole. Biol.* **41**: 553-575.

[16] Stewart, G. R. and Lee, J. A. (1974) The role of proline accumulation in halophytes. *Planta* **120**: 279-289.

[17] Taylor, C. B. (1996) Proline and water deficit: Ups, down, ins and outs. *Plant cell*, **8**: 1221-1224.

[18] Shah, K. and Dubey, R. S. (1998) Effect of cadmium on proline accumulation and ribonuclease activity in rice seedlings: Role of proline as a possible enzymes protectant. *Biologia Plantarum*. **40**: 121-130.

[19] Farago, M. E. and Mullen, W. A. (1979) Plants which accumulate metals. IV. A possible copper-proline complex from the roots of *Armeria meritima. Inorganic Chimica Acta* **32**: L93-L94.

[20] Mehta, S. K and Gaur, J. P. (1999) Heavy metal induced proline accumulation and its role in ameliorating metal toxicity in *Chlorella vulgaris*. *New Phytology*. **143**: 253-259.

[21] Smirnoff, N. and Cumbes, Q. J. (1989) Hydroxyl radical scavenging activity of compatible solutes. *Phytochemistry* **28**: 1057-1060.

[22] Alia, M. P. and Matysik, J. (2001) Effect of proline on the production of singlet oxygen. *Amino Acids* **21**: 195-200.

[23] Wallace, A., Romney, E. M., Alexander, G. V. Soufi S. M. and Patel P. M. (1977) Some Interactions in Plants Among Cadmium, Other Heavy Metals, and Chelating Agent. *Agronomy J.* **69**: 18-20.

[24] Ebbs, S. D. and Kochian, L. A. (1997) Toxicity of Zn and Cu to *Brassica* species. Implication for phytoremediation. *J. Environ. Quality*, **26:** 776-781.

PRAJÑĀ - **Journal of Pure and Applied Sciences**
Vol. 17: 048 - 050, 2009 ISSN 0975 - 2595

METABOLIC OBSERVATIONS ON ZINC INDUCED TOXICITY ON *LEMNA POLYRRIZA* L.

Krupa Unadkat and Punita Parikh*

Department of Botany, Faculty of Science, M. S. University of Baroda, Vadodara, Gujarat - 390 002

ABSTRACT

The influence of Zn toxicity on *Lemna polyrrhiza L* was investigated using biochemical parameters as stress indicators. Lemna plants (*Lemna polyrrhiza L*) were cultured in Hoagland's medium which was supplemented with various Zn concentrations (1, 3, 5, 7 and 9 ppm Zn) and were separately harvested after 3, 6 and 9 days. The toxicity symptoms of Zn ions showed chlorosis on the leaves of the test plants. There were significant decrease in chlorophyll, protein and carbohydrate when the exposure time and concentrations of the metal ion increased. However 1 ppm Zn ion concentration increased chlorophyll and carbohydrate content of the plants. Higher concentration of the metal ion significantly reduced all the biochemical parameters under study.

***Keywords*: *Lemna polyrrhiza,* Zn ion, metal toxicity, chlorosis.**

INTRODUCTION

Pollution of environment by toxic metals arises as a result of various industrial activities and has turned these metal ions into major health issue [1]. Although several adverse effects of the toxic metals have been known for a long time, exposure to heavy metals continues, and is even increasing in some parts of the world, in particular in less developed countries. Heavy metal pollution is also a multi-element problem in many areas [2]. The accumulation of Cd and Zn in biotic systems as a consequence of human activities is becoming a major environmental problem. These elements easily taken up by plants and then enter the food chain, resulting in a serious health issue for humans. The increasing levels of heavy metals in the environment, their entry into the food chain, and the overall health effects are of major concern to researchers in the field of environmental biology. Zinc plays an important role in many biochemical functions within plants. Zinc is an essential component over 300 enzymes. In most of these enzymes, zinc makes up an integral component of the enzyme structure. The most distinct zinc deficiency symptoms – stunted growth and little leaf are presumably related to disturbances in the metabolism of auxins and indole acetic acid (IAA) [3]. Zinc is a major industrial pollutant of the terrestrial as well as aquatic environment. General symptoms of zinc toxicity are wilting, necrosis of old leaves, and reduced plant growth. Zinc toxicity inhibits chlorophyll formation in young leaves [4]. Photosynthesis and transpiration are also reduced by high concentrations of zinc.

Therefore, the present study was undertaken to investigate the effect of Zn on chlorophyll, protein and carbohydrate content to determine the biochemical response of Zn stress on *Lemna polyrrhiza L*

MATERIALS AND METHODS

The test plants *Lemna polyrrhiza* L. were collected from the pond at Harani, Vadodara. They were allowed to acclimatize for 15 days. Plants were washed thoroughly under a running tap water and were grown and propagated for 4 weeks in quarter strength Hoagland's solution [5] containing (mM): 1.25 $Ca(NO_3)_2$, 1.5 KNO_3, 0.5 KH_2PO_4, 0.5 $MgSO_4$ and 0.25 NaCl, and (μM): 11.5 H_3BO_3, 2.3 $MnCl_2$, 0.026 H_2MoO_4 and 11.2 FeEDTA. Plants of same size were selected for the experiment. In the pilot scale experiment, the test plants were exposed to wide range of the metal ion concentrations i.e.10, 20, 30, 40, 50, 60, 70, 80, 90 and 100 ppm. It was noticed that the plants were unable to survive in the concentration range between 20-100 ppm Zn ions. In the subsequent experiments it was revealed that the concentration mortality (LC_{50}) of Zinc sulphate on exposed plants was 9 ppm during 240 hrs.

* Corresponding author – punitaparikh@gmail.com

Therefore, the trace element under study $ZnSO_4$ (Zn) were supplied at 1, 3, 5, 7 and 9 ppm for 3, 6 and 9 days. Nutrient solution devoid of trace element served as a control. Both the control and the treated solutions were maintained at pH 5.5 using dilute HCl or NaOH. Experimental plants (in triplicates) were placed in nutrient solution. Solutions were replenished every 3 days to prevent depletion of metals and nutrients. After each experimental period, harvested plants were washed in running tap water and rinsed with deionized water. Extraction and estimation of Total chlorophyll was done using method [6]; Total soluble protein by Lowry's method [7] and Carbohydrates by Anthrone method [7] in the test plants.

Each result shown in the figures was the mean of at least three replicated treatments. Standard deviation was used to examine the differences between each treatment and the level of statistical significance was set at P = 0.05.

RESULTS

Chlorophyll Content

The results of effect of Zn metal ion concentration on total chlorophyll content of *L. polyrrhiza* is represented in Table 1. It was observed that 1 ppm concentration of the metal ion marginally increased the chlorophyll following 3 days treatment period. Thereafter, the chlorophyll content showed gradual decline as the treatment period and the metal ion concentration increased. The prolonged exposure of 9 days to high concentration of Zn i.e. 9 ppm significantly reduced (45%) chlorophyll than the control.

Table 1: Effect of Zn ion on chlorophyll content of *L. polyrriza.*

Concentration of Zinc Metal (ppm)	Chlorophyll (mg/g)		
	Days of Treatment		
	3 days	6 days	9 days
Control	1.7 ± 1.90	2.2 ± 0.24	2.5 ± 0.07
1	2.4 ± 0.80	2.1 ± 0.14	1.5 ± 0.25
3	1.7 ± 0.20	1.7 ± 0.10	1.5 ± 0.50
5	1.7 ± 0.31	2.0 ± 0.08	1.4 ± 0.06
7	1.8 ± 0.12	1.3 ± 0.05	0.6 ± 0.06
9	1.5 ± 0.03	1.1 ± 0.17	0.95 ± 0.30

Protein Content

All the experimental concentrations gradually declined protein content as the period of treatment increased from 3 to 9 days (Table 2). It also decreased with increased metal ion concentrations in all the treatment periods. Protein showed 49% reduction when the plants were treated with 9 ppm Zn ions following exposure of 9 days.

Table 2: Effect of Zn ion on protein content of *L. polyrriza.*

Concentration of Zinc Metal (ppm)	Protein Content (mg/g)		
	Days of Treatment		
	3 days	6 days	9 days
Control	0.70 ± 0.05	0.72 ± 0.01	0.73 ± 0.05
1	0.69 ± 0.05	0.67 ± 0.06	0.58 ± 0.05
3	0.61 ± 0.01	0.59 ± 0.01	0.57 ± 0.03
5	0.55 ± 0.03	0.50 ± 0.01	0.55 ± 0.01
7	0.55 ± 0.02	0.46 ± 0.04	0.40 ± 0.01
9	0.50 ± 0.02	0.41 ± 0.02	0.35 ± 0.03

Total Carbohydrates Content

Data presented in Table 3 showed that total carbohydrate content revealed a slight rise at 1 ppm metal ion concentration following 3 days treatment period. Thereafter, a negative correlation was recorded with the increased metal ion concentrations and the treatment period.

Table 3: Effect of Zn ion on carbohydrate content of *L. polyrriza.*

Concentration of Zinc Metal (ppm)	Carbohydrate (mg/g)		
	Days of Treatment		
	3 days	6 days	9 days
Control	4.2 ± 0.10	4.2 ± 0.10	4.5 ± 0.10
1	4.8 ± 0.30	3.6 ± 0.20	3.6 ± 0.10
3	3.0 ± 0.10	2.7 ± 0.05	2.7 ± 0.05
5	2.9 ± 0.05	2.5 ± 0.10	2.4 ± 0.05
7	2.3 ± 0.05	2.3 ± 0.05	2.0 ± 0.05
9	2.3 ± 0.05	2.3 ± 0.05	2.0 ± 0.05

DISCUSSION

In the present work, when the test plants were exposed to Zn ion concentration from 3 ppm to 9 ppm significantly reduced total chlorophyll at all the treatment periods. The results were similar to those reported previously by Baryla *et al*. [8]. Benavides *et al*. [9] had reported that the reason for the loss of chlorophyll following heavy metal exposure was due to the distortion of the

chlorophyll ultrastructure, inhibition of the synthesis of photosynthetic pigments and enzymes of the Calvin cycle or reduction in the chloroplast density and size which led to the damage of the photosynthetic cycle. Xun [10] had explained that the Cd and Zn weakened the capacity of resisting ROS, resulting in lipid peroxidation or de-esterification, and then led to damages to structure of the chloroplast membrane. Jiang *et al*. [11] had reported that the combined pollution by Cd and Zn caused the structure of the chloroplast to be damaged.

However, total chlorophyll content of the test plants was more at 1 ppm Zn ion concentration after 3 days treatment period. This might be due to its role as micronutrient promoting growth at very low concentration [12].

The soluble protein contents for all the treatments reached minimum values in all the treatment period studied as compared with the treatment without Zn. Hu *et al*. [13] speculated that the accumulation of Zn in the plants led to a breakdown of protein synthesis systems, or the inhibition of protein synthesis or the speeding up of the decomposition of protein. The decline in proteins also leads to decrease in RNA content and increased the activity of hydrolytic enzymes, such as protease and RNAase due to heavy metal stress.

Hendawy and Khalid reported that *Salvia officinalis* under zinc application resulted in a marked decrease of essential oil percentage, total carbohydrates and proline content [14]. A concentration dependent decrease in plant height, fresh weight, chlorophyll, carbohydrate and protein content as well as NR activity was observed by Vijaykumar *et al*. under varying concentrations of Zinc in black gram [15]. Our results are in accordance with these previous reports. It strongly suggests that Zn though micronutrient exhibits its inhibitory effect at higher concentrations. The decline in carbohydrate might be due to alteration in metabolic pathway due to Zn induction in the test plants.

REFERENCES

[1] Waisberg, M., Joseph, P., Hale, B. and Beyersmann, D. (2003) Molecular and cellular mechanisms of cadmium carcinogenesis. *Toxicology*, **192**: 95–117.

[2] An, Y. J., Kim, Y. M., Kwon, T. I. and Jeong, S.W. (2004) Combined effects of copper, cadmium, and lead upon *Cucumis sativus* growth and bioaccumulation. *Sci. Total Environ*., **326**: 85–93.

[3] El-Sherif, A. F., Shehata, S. M. and Youssif, R. M. (1990) Response of tomato seedlings to zinc application under different salinity levels. *Egypt. J. Hort. Sci*., **17**: 131-142.

[4] Kaya, C., Higgs, D. and Burton, A. (2000) Plant growth, phosphorus nutrition and acid phosphatase enzyme activity in three tomato cultivers grown hydroponically at different zinc concentrations. *J. Plant Nutri.,* **23**: 569-579.

[5] Hoagland, D. R. and Arnon, D. I. (1938) The water culture method for growing plants without soil. *Calif. Agrl. Expt. Sta. Cir*., **347**: 1-39.

[6] Arnon, D. I. (1949) Copper enzymes in isolated chloroplast. Polyphenol oxidase in *Beta vulgaris*. *Plant Physiol*., **24**: 65-71.

[7] Sadasivam, S. and Manikam, A. (1991) In: *Biochemical Methods* (2nd Ed), New Age International (P) Ltd., New Delhi pp: 8-195.

[8] Baryla, A., Carrier, P., Franck, F., Coulomb, C., Sahut, C. and Havaux. M. (2001) Leaf chlorosis in oilseed plants (*Brassica napus*) grown on cadmium-polluted soil: causes and consequences for photosynthesis and growth. *Planta*, **212**: 696-709.

[9] Benavides, M. P., Gallego, S. M. and Tomaro, M. L. (2005) Cadmium toxicity in plants. *Braz. J. Plant Physiol*., **17**: 21-34.

[10] Xun, Q. S. (2004) *Response of Hydrilla verticillata (Linn. f.) Role to Cd, Cu, Zn stress*. Ph. D. thesis, Nanjing Normal University.

[11] Jiang, H. M., Yang, J. C. and Zhang, J. F. (2007) Effects of external phosphorus on the cell ultrastructure and the chlorophyll content of maize under cadmium and zinc stress. *Environ. Pollut*., **147**: 750-756.

[12] Wang, H., Wang, P. F. and Zhang, H. (2009) Use of phosphorus to alleviate stress induced by cadmium and zinc in two submerged macrophytes *Afri. J. Biotech.,* **8(10)**: 2176-2183.

[13] Hu, Z. B, Wang, H. Z, Wu, J. J. and Xu, J. M. (2005) Ecological effects of both single and combined pollution of Cd and bensulfuron-methyl on soil microorganisms. *J. Zhejiang Univ. Agric. Life Sci.*, **31(2)**: 151-156.

[14] Hendawy, S. F. and Khalid, Kh. A. (2005) Response of Sage (*Salvia Officinalis* L.) Plants to Zinc Application Under Different Salinity Levels. *J. App. Sci. Res.* **1(2)**: 147-155.

[15] Vijay Kumar, S., Satish Kumar, G., Alok, S., UdaiPal, S. and Singh, V. P. (2007) Effect of zinc on growth and nr activity in black gram antagonized by magnesium and sucrose. *Ind. J. Plant Physiol.,* **12**: 95-99.

PRAJÑĀ - **Journal of Pure and Applied Sciences**
Vol. 17: 051-054, 2009 ISSN 0975 - 2595

THE PHYSIOLOGICAL ACTION OF 2, 4 DICHLOROPHENOXYACETIC ACID ON THE GROWTH OF *EICHHORNIA CRASSIPES*

Rita N. Kumar,[*] Sudeshna Chakraborty and Nirmal Kumar [1]

Department of Biological & Environmental Sciences, N. V. Patel College of Pure & Applied Sciences, Vallabh Vidyanagar, Gujarat – 388 120
[1]P.G. Department of Environmental Sciences, Institute of Science & Technology for Advanced Studies & Research (ISTAR), Vallabh Vidyanagar, Gujarat – 388 120

ABSTRACT

The present paper deals with the study of effect of different concentrations of herbicide 2, 4 D on an aquatic weed, *Eichhornia crassipes*. Various concentrations of herbicide i.e. 1 ppm, 2 ppm, 4 ppm and 6 ppm were applied to *E. crassipes* plants in duplicate sets. The total carbohydrates, proteins and chlorophylls content were estimated for a period of ten days at regular intervals of three days. During the present study it was found out that the concentration of these primary metabolites and chlorophyll pigments decreased with the increasing concentration of 2, 4 D till nine days.

***Keywords*: *Eichhornia crassipes*, herbicide, 2, 4 D, total carbohydrate, protein, chlorophyll**

INTRODUCTION

Many attempts have been made for controlling the excess growth of *Eichhornia crassipes*, an abnoxious weed by using various physical, chemical and biological methods [1, 2]. Among the various chemicals experimented, the use of herbicide is more popular and various herbicides are reported to be used for control of this weed [2]. 2, 4 D is a synthetic herbicide of phenoxy or phenoxyacetic acid family that causes disruption of plant hormone responses [3, 4]. The herbicide is a systemic herbicide (dispersed throughout the plant) and can be absorbed through roots [5]. It poisons the plant by causing rapid cell division and abnormal growth. The symptoms of injury in susceptible plants include: cupping and curling of stems and leaves, stunting of growth and production of ethylene. Rapid and characteristic physiological responses to herbicide activity in aquatic plants have potential for monitoring the treatment effect in laboratory evaluations and operational applications.

Eichhornia crassipes, an aquatic macrophyte popularly known as water hyacinth is a free floating aquatic weed belonging to the family Pontederiaceae [6]. Due to the invasive nature of this macrophyte, its removal from the wetlands poses a severe problem. Difficulties with nuisance aquatic plant infestations can be the results of watershed-level problems [5-10]. Generally one herbicide application is effective for control of macrophyte density for one growing season only and more frequent harvesting is necessary for control. Out of several measures of control for macrophytes, the chemical control typified by the use of herbicides is gaining preference [8]. The primary advantage of the use of herbicides is comparatively low cost [11, 12]. No attempt has been made so far to study the effect of 2, 4 D on *E.crassipes* .The present work, therefore, has been carried out to find out the effect of this herbicide on total carbohydrate, protein and chlorophyll pigments of *E. crassipes*.

MATERIALS AND METHODS

For the present investigation, the plants of *Eichhornia crassipes* having uniform height, size and equal number of leaves were collected from Bakrol pond situated in Bakrol village. Plants were brought to the laboratory and washed thoroughly under running tap water to remove adhered soil particles and other impurities. The plants were kept in tap water in plastic troughs for one week prior to experiment. Different concentrations such as 1 ppm, 2 ppm, 4 ppm and 6 ppm of herbicide (2, 4D) were prepared in 20 liter of water and experimental sets were arranged in duplicate for each treatment. Control trough was maintained without addition of herbicide. The plants were allowed for acclimatization and growth for seven days. The quantitative analysis of total proteins, total carbohydrates and total chlorophylls was carried out for 9 days at an

* Corresponding author – nvpas2009@gmail.com

interval of three days from young leaves as per the methodologies of Lowery *et al.* [13], Witham *et al.* [14] and Vernon [15] respectively. The standard deviation of the obtained data was carried out and was plotted in the graph.

RESULTS AND DISCUSSION

During the present investigation it was observed that the higher dosage of herbicide showed a detrimental effect on the growth of the macrophyte. The plant showed visible symptoms of die back at tips and margins of leaves followed by progressive chlorosis. The plants which were susceptible to the action of 2, 4D showed various morphological and histological responses suggesting that physiological reactions of the cells were affected [16].

The primary metabolites like total carbohydrate, proteins, and pigments like total chlorophylls were found in decreased concentration. The standard deviation of the results indicates a significant difference among the obtained values. The concentration of total carbohydrate decreased gradually from 0.317 to 0.031 mg.g^{-1} FW with an increase in the concentration of herbicide. The lowest i.e. 0.031 mg.g^{-1}FW was recorded at 6ppm on 9th day of the treatment. A similar decrease in carbohydrate content was observed till tenth day in *Eichhornia crassipes* treated with Isoproturon with about 75% decline in total sugars by Rana & Kumar [17]. The carbohydrate content was found slightly increased in *Eichhornia* plants of control set (Fig 1). The present findings are in accordance with that of Rasmusse [16] who also reported the decrease in the total carbohydrate, after the addition of 2, 4D on *Dandelion* sp. This could be due to more utilization of the carbohydrates as a result of increased respiratory activity of plants following herbicide treatment [16].

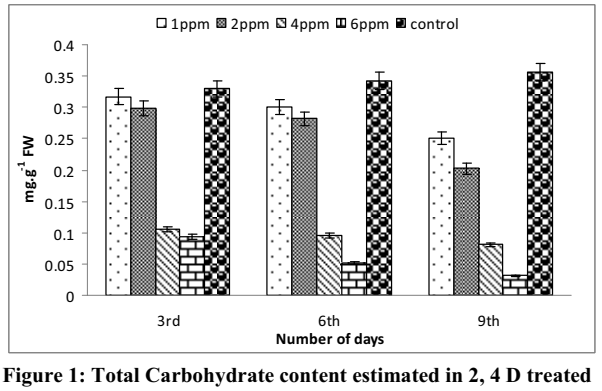

Figure 1: Total Carbohydrate content estimated in 2, 4 D treated *E. crassipes* leaves.

The protein content decreased gradually from 0.224 mg.g^{-1} FW to 0.14mg.g^{-1} FW at all the concentrations of herbicide, except in the plants treated with 2 ppm concentration on 6th day, while the protein content was comparatively higher (0.298 mg.g^{-1}FW) in the plants of control set and they exhibited slight rise in their concentration till ninth day (Fig. 2). Sprecher *et al*. [18] while working on physiological and diagnostic effect of herbicide on the macrophytes such as *Elodea canadensis*, *Potamogeton pectinatus* and *Vallineria americana*, recorded decline in protein content with increased application of herbicide Triclopyr. The present results indicate that herbicides prevent active uptake of amino acids thus indirectly affecting the synthesis of the proteins [19].

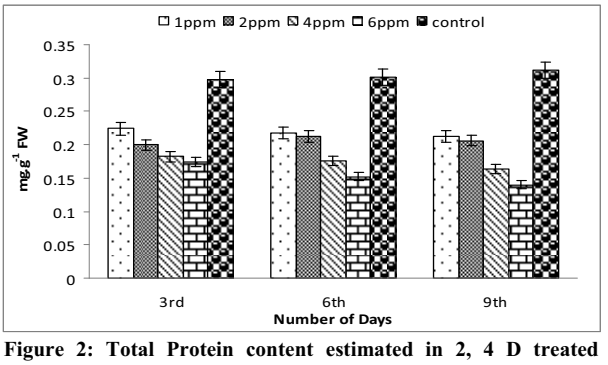

Figure 2: Total Protein content estimated in 2, 4 D treated *E.crassipes* leaves.

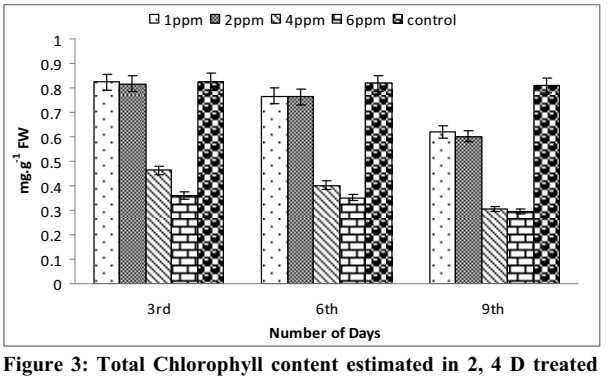

Figure 3: Total Chlorophyll content estimated in 2, 4 D treated *E.crassipes* leaves.

The chlorophyll content of leaves decreased in all the concentrations of herbicide. The initial chlorophyll decline was slow, but after sixth day of treatment rapid reduction occurred at 1and 2 ppm concentrations. The plants of control set showed a slight rise in chlorophyll values till tenth day (Fig. 3). Sprecher *et al.* [20] recorded similar decline of total chlorophyll with application of the herbicide Fluridone on two different aquatic macrophytes: *Myriophyllum spicatum* and

Hydrilla verticillata. The decrease in the pigment content may be due to reduced photosynthetic activity of leaves caused as a result of stress following the herbicide treatment [21].Herbicide of urea derivatives like monouron, cotaron, linuron and others are known to initiate leaf tip die back followed by chlorosis similar to isoproturon [22]. Izawa [23] reported photosystem-II (PS-II) as the site of action by inhibition the electron transfer between the primary electron acceptor and the plastoquinon (PQ). It could be the reason that chlorophyll degradation and disorganization cause the reduction in chlorophyll content. The decrease in chlorophyll content in herbicide treated water hyacinth plants might be due to the induction of inhibition of photosynthesis which ultimately kills the plants which was also reported in unicellular algae when treated with similar urea derivatives [23].

The plants treated with 2 and 4 ppm herbicide concentrations showed the symptoms of wilting after 6th day of treatment, while plants treated with 6ppm concentration were killed from 9th day of treatment onwards. The above results may be because of the fact that 2, 4 D causes disruption of plant hormone responses which ultimately affects the metabolic pathway of the plant causing its death [4]. Parsons *et al* [24] studied the effect of 2, 4D on the growth of a macrophyte, *Myriophyllum spicatum* and concluded that application of the herbicide had reduced the biomass and frequency of macrophyte.

From the present investigation it can be concluded that the higher dosage of 2, 4D can control the growth of *Eichhornia crassipes* by affecting its basic physiological processes.

REFERENCES

[1] Varshney, C. K. and Rzoska, J. (1976). Aquatic weeds in South East Asia, Jaunk B. (Ed.), Publ, HAQUE.

[2] Gopal, B. and Sharma, K. P. (1981). Water Hyacinth (Eichhornia crassipes), most troublesome weed of the world. Hindasia Publications, Delhi.

[3] Karr, J. R., and Gorman, O. T. (1975) Effects of land treatment on the aquatic environment. Non-point source pollution seminar, sec. 108 (a), Demonstration projects progress reports, Chicago, November 20, 1975. Report no. EPA-905/9-75 007.

[4] Paterson, M. (2004). 2, 4, D-ethylhexyl analysis of risks to endangered and threatened salmon and steelhead, Ph.D. thesis, Submitted to Environmental Field Branch Office of Pesticide Programs.

[5] Chanpaign, I. L. (1994). Herbicide Handbook, Seventh Edition, Ahrens, W. H. (Ed.) Published by Weed Society of America.

[6] Chukwuka, K. S. and Uka, U. N. (2007) Effect of water hyacinth (Eichhornia crassipes) infestation on zooplankton populations in Awa Reservoir, Ibadan South West Nigeria. *Journal of Biological Sciences,* 7(6): 865-869.

[7] Edmondson, W. T. (1977) Tropic equilibrium of Lake Washington. Corvallis, OR: U.S. Environmental Protection Agency, Office of Research and Development. pp. 36

[8] Edmondson, W. T. (1991) The uses of ecology: Lake Washington and beyond. Seattle: University of Washington Press. pp. 329.

[9] Karr, J. R., and Schlosser, I. J. (1978) Water resources and the land-water interface. Science, 201(43): 229-234.

[10] Doppelt, B., Scurlock, M., Frissell, C. and Karr, J. (1993) Entering the watershed: a new approach to save America's river ecosystems. Covelo, C A: Island Press. pp. 510.

[11] Gupta, O. P. (1973) Aquatic weed control. World Crops, 25(4): 182-190.

[12] Dunst, R., and Nichols, S. A. (1979) Macrophyte control in a lake management program. In: Aquatic plants, lake management and ecosystem consequences

of lake harvesting. Proceedings of a Conference, Center for Biotic Systems, Institute of Environmental Studies, University of Wisconsin, Madison. pp. 411-418.

[13] Lowry, O. H., Rosebrough, N. J., Farr, A. L. and Randall, R. J. (1951). Protein measurement with the folin phenol reagent. *J. Biol. Chem,* 193: 265-275.

[14] Witham, E. H., Blayder, D. F. and Devlin, R. M. (1971). Experiments in Plant Physiology, Van Nostrand Reinhold Co., New York.

[15] Vernon, L. P. (1960). Spectrophotometric determination of chlorophylls and pheophytin in plant extracts. *Anal. Chem.,* 32: 1144-1150.

[16] Rasmusse, L. W. (1947). The physiological action of 2,4 Dichlorophenoxyacetic acid on Dandelion Taraxacum officinale. Plant physiology, 377-392.

[17] Rana, B. C. and Kumar, N, J. I. (1993) Effect of isoproturon on growth and metabolites of water hyacinth. *Indian Bot. Contactor,* 10: 47-49.

[18] Sprecher, S. L., and Stewart, A. B. (1995) Triclopyr effects on peroxidase activity in target and non-target aquatic plants. *Journal of Aquatic Plant Management,* 33: 43-48.

[19] Mann, J. D., Jordan, L. S. and Day, B. E. (1965) A Survey of Herbicide for their effect upon protein synthesis. *Plant Physiology,* 840-843.

[20] Sprecher, S. L., Stewart, A. B. and Brazil, J. M. (1993). Peroxidase changes as indicators of herbicide induced stress in aquatic plants. *Journal of Aquatic management,* 31: 45-50.

[21] Khan, M. S., Chaudhry, P., Wani, P. A., and Zaidi, A. (2006). Biotoxic effects of the herbicides on growth, seed yield and grain protein of green gram. *Journal of Applied Science and Environmental Management,* 10(3): 141- 146.

[22] Kumar, N, J. I. and Rana, B. C. (1994). Response of Eichhornea crassipes to isoproturon. Ecobiology, 6(3): 225-227.

[23] Izawwa, S. Photosynthesis-I, eds : Trebst A and Avron M, Springer- Vernag Berlin pp 266-268.

[24] Parsons, J. K., Hamel, K. S., Madson, J. D. and Getsinger, K. D. (2001). The use of 2,4 D for selective control of an early infestation of Eurasion watermilfoil in Loon Lake, Washington. Journal of Aquatic Plant Management, 39: 117-125.

PRAJÑĀ - **Journal of Pure and Applied Sciences**
Vol. 17: 055-057, 2009 ISSN 0975 - 2595

EFFECT OF PLANT GROWTH RETARDANTS AND PINCHING ON GROWTH, FLOWERING AND YIELD OF GAILLARDIA (*GAILLARDIA PULCHELLA* FOUG.) CV. LORENZIANA

M. Y. Saiyed, R. G. Jadav*, A. B. Parmar and K. M. Chauhan

Department of Horticulture, B. A. College of Agriculture,
Anand Agricultural University, Anand, Gujarat - 388 110

ABSTRACT

An experiment was carried out to study the effect of plant growth retardants and pinching on growth, flowering and yield of Gaillardia (*Gaillardia pulchella* Foug.) cv. Lorenziana at nursery of the Department of Horticulture, A.A.U., Anand during the month of November, 2007 to April, 2008. The treatments comprised of two different concentrations of CCC (500 and 1000 ppm), MH (50 and 100 ppm), PP333 (25 and 50 ppm) sprayed at 30 days and 60 days after transplanting, pinching and control (water spray). The results revealed that CCC 1000 ppm was found most effective for obtaining maximum plant spread (50.92 cm^2), more number of branches (53.84), bigger size of flower (6.04 cm), more number of flowers per plant (26.37), per hectare (19,53,333), higher yield (7.42 t/ha) and shelf life (37.82 hrs) of gaillardia.

***Keywords*: Gaillardia, growth retardant, pinching, cycocel, maleic hydrazide, paclobutrazol.**

INTRODUCTION

Gaillardia belongs to Asteraceae family; native of South-Western United States and Mexico. It is popularly known as blanket flower due to it's colour and spreading habit. It resembles a blanket. It is one of the most popular flowers in India because of its easy cultivation, wide adaptability to varying soils and climatic conditions with long duration of flowering habit and attractive flower colour. The gaillardia is mainly grown for its cut flowers and the loose flowers are used for making garlands, used in religious occasion and for decoration during social functions. Its gorgeously coloured flowers are best arranged in copper bowls or simple plain-coloured vases. There are many varieties of gaillardia found in the country but in Anand region, the most important cultivated variety is 'Lorenziana' which belongs to annuals with double flowers of many attractive colours mentioned earlier. Recently, scientists have given more attention towards the regulation of plant growth, increasing yield and quality of flowers by using some plant growth retardants and pinching. Keeping the above facts in view, the present investigation was carried out to know the effect of different growth retardants and pinching on growth, flowering and yield of Gaillardia (*Gaillardia pulchella* Foug.) cv. Lorenziana

MATERIALS AND METHODS

An experiment was conducted to study the effect of plant growth retardants and pinching on growth, flowering and yield of Gaillardia (*Gaillardia pulchella* Foug.) cv. Lorenziana was conducted at the nursery of the Department of Horticulture, B.A. College of Agriculture, Anand Agricultural University, Anand, during November, 2007 to April, 2008. The treatments comprised of two different concentrations of cycocel CCC (500 and 1000 ppm), maleic hydrazide MH (50 and 100 ppm), and paclobutrazol PP333 (25 and 50 ppm) sprayed at 30 days and 60 days after transplanting, pinching and control (water spray). A control was maintained by spraying distilled water. The experiment was laid out in a randomized block design with 14 treatments, replicated thrice. In pinching treatment, the plants were pinched after 30 DAT. The spray of plant growth retardants was done twice at 30 (S_1) and 60 (S_2) days after transplanting (DAS). The plants were transplanted on November 22, 2007 with a spacing of 45 cm × 30 cm. The observations on plant growth yield and quality parameters were recorded and subjected to statistical analysis.

* Corresponding author – rg_jadav@yahoo.co.in

Table 1: Effect of plant growth retardants and pinching on growth, yield and quality of Gaillardia.

Sr. No.	Treatments (ppm)	Height of the plant (cm)	Spreading of plant (cm^2)	Number of branches	Days required to first flower opening after transplanting	Days required to 50% flowering after Transplanting	Flower yield per hectare (t)	Shelf life (hrs)
1	S_1T_1 CCC 500	62.12	50.63	50.66	73.23	86.52	7.25	35.85
2	S_1T_2 CCC 1000	61.81	50.92	53.84	74.03	87.48	7.42	37.82
3	S_1T_3 MH 50	59.46	49.42	50.45	66.67	83.25	6.11	37.52
4	S_1T_4 MH 100	58.50	49.47	48.63	71.50	84.77	6.00	36.55
5	S_1T_5 PP333 25	65.94	48.23	46.55	76.00	88.23	5.83	35.55
6	S_1T_6 PP333 50	65.49	49.59	42.89	75.52	88.22	5.68	33.55
7	S_2T_1 CCC 500	68.34	48.86	44.32	76.08	86.98	6.63	35.25
8	S_2T_2 CCC 1000	66.09	47.33	45.11	75.25	88.42	6.87	36.50
9	S_2T_3 MH 50	65.16	47.36	42.16	74.03	86.37	5.80	36.40
10	S_2T_4 MH 100	65.62	47.47	42.87	74.08	86.78	5.75	35.55
11	S_2T_5 PP333 25	67.20	47.25	41.24	78.05	86.10	5.53	34.50
12	S_2T_6 PP333 50	69.33	47.34	41.38	79.23	86.90	5.66	33.45
13	Pinching	69.46	46.24	40.76	79.58	99.08	5.57	31.15
14	Control (Water spray)	69.73	45.29	37.09	81.20	99.50	5.00	29.20
S.Em. ±		2.21	1.50	1.47	2.29	2.90	0.20	1.07
C.D. at 5%		6.43	NS	4.28	6.65	8.42	0.59	3.10
C.V. %		13.73	13.66	12.69	3.26	14.67	5.51	12.28

Where, S_1 = First spray at 30 DAT, S_2 = Second spray at 60 days of DAT, DAT = Days after transplanting, T_1-T_6 = Treatments

RESULTS AND DISCUSSION

The data presented in Table 1 exhibited significant differences among the different treatments in respect of growth, flowering and yield parameters. The plant height was significantly retarded by MH 100 ppm (58.50 cm) followed by MH 50 ppm (59.46 cm). That may be due to the antiauxin effect on MH with stimulation of dwarfing properties and nullification of apical dominance [1]. These results are in close conformity with the finding of Khimani *et al*. [2] and Patel [3] in Gaillardia. The data presented in Table 1 showed that the maximum number of branches under the treatment CCC 1000 ppm (53.84) which was followed by CCC 500 ppm (50.66). Similar results have been reported by Makwana in gaillardia [4]. There was no significant effect of various plant growth retardants and pinching on plant spread but maximum plant spread was recorded with CCC 1000 ppm (50.92 cm^2) followed by CCC 500 ppm (50.63cm^2) at 120 DAT. Early flowering (66.67 DAT) and 50 per cent flowering (83.25 DAT) were recorded by treatment MH 50 ppm. These results are in agreement with result obtained by Makwana [4].

The maximum number of flowers per plant, per plot and per hectare was obtained by the application of CCC 1000 ppm (26.37, 1055 and 19, 53,333, respectively) as compared to control (20.30, 812 and 15,03,457, respectively) and other treatments. Similar results were also recorded by Makwana [4] and Poshiya *et al.,* [5], in Gaillardia, and Singh *et al.,* [6] in marigold. However, CCC 500 ppm and CCC 1000 ppm was most effective concentration for increasing growth, flowering and yield of Gaillardia.

CONCLUSION

From the above findings it can be concluded that an application of CCC 500 ppm is found beneficial and cost effective for getting higher yield of Gaillardia (*Gaillardia pulchella* Foug.) cv. Lorenziana, as it gave higher flower yield and the highest net realization (77,240 Rs. ha^{-1}) with highest CBR (1:3:45).

REFERENCES

[1] Crafts, A. C., Currier, H. B. and Day, B. E. (1950) Response of several crop plants and weed to maleic hydrazide, *Hilgardia,* **20**: 57-80.

[2] Khimani, R. A., Patil, A. A. and Kanamadi, V. C. (1994) Effect of growth retardants on growth and flower production of gaillardia (*Gaillardia pulchella* var. 'Picta Fouger'). In: *Floriculture Technology, Trades and Trends.* Prakash, J. and Bhandari, K. R. (eds.), Oxford and IBH Publishing Co. Pvt. Ltd., New Delhi, pp. 119-121.

[3] Patel, S. L. (1997) Effect of plant growth regulators on growth, flowering and flower yield of annual gaillardia (*Gaillardia pulchella* Foug.) var. 'Lorenziana'. M.Sc (Agri.) Thesis, Navsari Agricultural University, Navsari.

[4] Makwana, M. K. (1999) The effect of plant growth regulators on growth, yield and quality of gaillardia (*Gaillardia pulchella*) cv. 'Lorenziana'. M.Sc. (Agri.) Thesis, Gujarat Agricultural University, Gujarat.

[5] Poshiya, V. K., Kataria, G. K. and Chovatia, V. P. (1995) Effect of growth substances on growth and yield in gaillardia. *J. Applied Hort.,* **1(1 & 2)**: 99-100.

[6] Singh, R. and Rathore, S. V. S. (1992) Effect of different growth regulators on growth and flowering of African marigold (*Tagetes erecta* L.). *Prog. Hort.,* **24(1-2)**: 92-95.

PRAJÑĀ - **Journal of Pure and Applied Sciences**
Vol. 17: 058-064, 2009 ISSN 0975 - 2595

CERTAIN BIOCHEMICAL CHANGES ASSOCIATED WITH THE GROWTH AND RIPENING OF MULBERRY (*MORUS ALBA* L.) FRUIT

Neeta B. Gol, T. V. Ramana Rao * and Prakash R. Patel

Department of Biosciences, Sardar Patel University, Vallabh Vidyanagar, Gujarat – 388 120

ABSTRACT

The biochemical composition and enzymatic changes were analyzed in the fruit of *Morus alba* at its five sequential developmental stages. A declining trend of chlorophylls and carotenoids occurs simultaneously with an increase in the anthocyanins content. As the Mulberry fruit proceeds towards ripening a concomitant sharp increase occurs in the quantity of sugars, but the amount of total starch, protein and ascorbic acid decreases. The changes in the activity of enzymes such as amylase, invertase, catalase and peroxidase involved in a number of catabolic and anabolic reactions indicate that these enzymes also have active role in the process of Mulberry fruit growth and ripening. The specific activity of invertase and cell wall degrading enzymes such as PG, cellulase and PME showed higher activity throughout the growth and ripening stages. The present study manifests that with rich source of sugars and antioxidants the fruit of *Morus alba* can be used as a natural food. Besides, since a significant amount of anthocyanins also found to get accumulated in the ripening Mulberry fruit, it may also be used as a natural food colorant. Due to significant medicinal and economic importance, Mulberry fruits are recommended for their commercial exploitation.

***Keywords*: fruit, growth and ripening, *Morus alba*, biochemical changes.**

INTRODUCTION

Mulberry (*Morus alba* L.) is a medicinally important plant which belongs to the genus *Morus* of the family Moraceae. It is a monoecious or dioecious plant growing up to 10 - 12 m height, with alternate leaves, unisexual to bisexual flowers in the leaf axils, and fleshy fruits (sorosis). Globally the Mulberry plant is mainly used as feed for the silk worm [1]. In addition to the use of young leaves and stems of Mulberry plants as a delicious vegetable, the leaves and the roots of *M. alba* have also been used in traditional medicine as a cathartic, analgesic, diuretic, antitussive, sedative, hypotensive and antiphlogistic and for the treatment of edema [2]. The other uses of *M. alba* are as a hypoglycemic [3], cardioprotective [4], and neuroprotective agent [5]. Besides, Mulberry fruits are also valued well (consumed fresh, in juice or as preserves). The Mulberry fruit has been used as a medicinal agent to nourish the blood and for the treatment of weakness, fatigue, anemia and premature graying of hair. Further, Mulberry plants are used as animal feed and also these plants finding place in landscaping [1].

Oh *et al.* [6] reported that the Mulberry plant contains flavonoids, coumarine and stilbene, which have hepatoprotective and free radical scavenging activity. In addition, some phenolic compounds from *M. alba* have been reported to have antioxidant properties and also it has been demonstrated that *M. alba* is clinically effective in the treatment and prevention of diabetes [6].

However, a perusal of literature reveals that most of the studies have been carried out on the comparison between chemical composition of ripened fruits of White (*Morus alba*), Red (*Morus rubra*) and Black (*Morus nigra*) Mulberry plants, but in spite of finding a very high medicinal value with the fruits of *Morus alba* due consideration is not given to study the physiological and biochemical changes associated with their growth and ripening. Therefore, it is envisaged that the results of the present study would be useful in determining the maturity indices for harvesting of Mulberry fruit for its commercial exploitation.

MATERIALS AND METHODS

The presently worked out fruit of Mulberry (*Morus alba*) was collected at its sequential stages of growth viz. young, mature, pre-ripened, ripened and post-ripened stages, from the Mulberry plants grown in the vicinity of Vallabh Vidyanagar, Gujarat, India. From the plants selected for collection of fruit samples, 10 – 20 fruits were collected for each of the presently worked out parameters during the period between April to

* Corresponding author – tadapanenirao@yahoo.com

May of 2009. The stage of the development of the fruit was decided based on the appearance of the colour and size of the fruits and they were categorized into five sequential stages viz. young, mature, pre-ripened, ripened and post-ripened stages. After recording the length, diameter and fresh weight of these fruits (Fig. 1, Table 1), they were subjected for their biochemical analyses.

Figure 1: Fruit of *Morus alba* at its sequential stages of growth and ripening.

Table 1: Fresh weight, length, diameter, pH and titrable acidity of *Morus alba* fruit at its sequential stages of growth and ripening.

Parameters	Stages of growth and ripening				
	Young	Mature	Pre-ripened	Ripened	Post-ripened
Fresh weight (gms)	0.16 ± 0.01	0.21 ± 0.06	0.35 ± 0.04	0.69 ± 0.09	1.06 ± 0.07
Length (cms)	1.50 ± 0.15	1.70 ± 0.10	2.00 ± 0.12	2.20 ± 0.17	2.60 ± 0.06
Diameter (cms)	0.50 ± 0.03	0.60 ± 0.05	0.70 ± 0.03	0.80 ± 0.05	0.90 ± 0.05
pH	4.52 ± 0.03	4.81 ± 0.01	5.09 ± 0.09	6.21 ± 0.01	7.30 ± 0.03
Titrable acidity (%)	5.63 ± 0.46	5.33 ± 0.37	4.31 ± 0.411	3.71 ± 0.46	2.30 ± 0.34

The titrable acidity, which is expressed as citric acid %, has been determined by titrating 5-ml juice with 0.1N sodium hydroxide using phenolphthalein as an indicator [7]. The quantitative analyses of pigments such as chlorophyll 'a', chlorophyll 'b', total chlorophylls and anthocyanins, starch, total soluble sugars, reducing, non-reducing sugars and ascorbic acid were carried out as per the methods cited by Thimmaiah [8], while the method of Wang *et al*. [9] was followed for estimating the amount of total carotenoids. The amount of proteins and total phenolic contents were quantified by following the methods of Lowry *et a*l. and Bray and Thorpe respectively [c.f. 8].

While the activity of hydrolyzing enzymes (amylase and invertase) and cell wall degrading enzymes: pectinmethylesterase (PME), polygalactoranase (PG) and cellulase have been evaluated as per the methods cited by Thimmaiah [8], Devi [10] is followed for assessing the activity of antioxidant enzymes (catalase and peroxidase).

The data presented in this paper is the mean and standard deviation (S.D.) of three replicates for each of the parameters tested for the present study and that has been subjected to statistical analysis using Duncan's multiple range test (DMRT) [11].

RESULTS AND DISCUSSION

As the Mulberry fruit continues its growth the pH of the fruit increases from 4.5 at young stage to 7.3 at its post-ripened stage. The titrable acidity of the fruit was found to get decreased from 5.63 % at young stage to 2.30 % at its post-ripened stage (Table 1). A gradual decrease in the titrable acidity of the ripening Mulberry fruit corresponds to increase in the pH of the fruit flesh. Willis *et al*. [12] opined that the change in pH is mainly due to the leakage of organic acids from the vacuole.

Fruit colour is known to serve as an index for determining the ripening stage and optimal harvest time for various fruits. As the fruit of *Morus alba* ripens, a visual change occurs in its color from green to reddish black. The quantitative analysis of the pigments (Chlorophylls) reveals that the amount of Chl. 'a', Chl. 'b' and Total Chl. were very high in the young Mulberry fruit, but thereafter they decline gradually and their declining trend continues till the post-ripened stage. The maximum amount of Chl. 'a' was found to be 0.061 mg/gm in the first stage (i.e. young stage), while the Chl. 'b' and Total Chl. of same stage were 0.038 mg/gm and 0.100 mg/gm respectively, but as the fruit

proceeds towards post-ripened stage the amount of all kinds of chlorophylls were found to get declined (i.e. 0.003 mg/gm of Chl. 'a', 0.002 mg/gm of Chl. 'b' and 0.004 mg/gm of Total Chl.). Thus it may be concluded that during ripening process the amount of Chl. 'a', Chl. 'b' and Total Chl. declined by 20 fold, 19 fold and 25 fold respectively (Table 2). Perhaps, as Willis *et al*. [12] stated that this kind of decline in the amount of chlorophyll may be due to the loss of chlorophyll as a part of a transition of the chloroplasts into chromoplasts containing yellow and red carotenoid pigments. More or less similar kinds of changes were noticed in case of carotenoids of presently studied Mulberry fruit.

The young stage of Mulberry fruit is found to have higher accumulation of carotenoids that reaches to the tune of 42.42 mg/gm, but subsequently they get declined gradually up to the post-ripened stage. In contrast, the present study further revealed that anthocyanins increased significantly in Mulberry fruit from its young stage (2.80 mg/100gm) to the post-ripened stage (31.85 mg/100gm) (Table 2). Thus the results of the present study are in accordance with the findings of Merzlyak *et al*. [13] who stated that the degradation of chlorophyll is accompanied by the biosynthesis of one or more pigments, usually either carotenoids or anthocyanins. More or less a similar rise in the rate of anthocyanins accompanied by a decrease in the rate of chlorophyll was recently noticed during the ripening of strawberry and tomato fruits by Yuhua *et al*. [14] and Wang *et al*. [9] respectively.

Sugars, either in free state or as derivatives play an essential role in imparting attractive colour, flavour, appearance and texture to the fruits. As the fruit of Mulberry grows, the amount of sugars increases from 11.12 mg/gm in the young Mulberry fruit to 45.65 mg/gm at post ripened stage, which is four fold rise and statistically also this rise is significant. Consistency was observed in case of reducing as well as non-reducing sugars measuring 26.92 mg/gm and 18.74 mg/gm respectively at post-ripened stage (Table 3). According to Mazumdar and Majumder [7] starch is the major storage polysaccharide found in the fruits. In contrast to sugars, the amount of starch was found to get decreased by 2 fold from 122.03 mg/gm at young stage to 61.19 mg/gm at the post-ripened stage (Table 3). Thus the results of the present study are in accordance with the findings of Vishal and Neerja [15] who reported a steady increase in the quantity of total and reducing sugars throughout the period of growth and maturation of Kiwi fruit, while noticing starch degradation and increase in sugars (i.e. glucose, fructose and sucrose). Likewise, Sabir *et al.* [16] also made a more or less similar kind of observation in the apple fruit and opined that the increase in the sugar content may be due to the hydrolysis of polysaccharides or due to less acidity and ascorbic acid contents. Based on these views it may be concluded that the increase in the levels of sugars during the ripening of Mulberry fruit may be due to the mobilization of starch reverses within the fruit.

Proteins are said to be the ubiquitous components of all living tissues, although occurring in low concentration in fruits they are involved in metabolism during growth, development and ripening of fruits. The amount of protein content in the currently worked out Mulberry fruit is found to be increased gradually from 1.90 mg/gm to 7.94 mg/gm at young fruit stage to pre-ripened stage respectively, but subsequently it exhibits inconsistency in its quantity by having a declining trend at the ripening stage and a very high quantity of it (14.99 mg/gm) occurs at post-ripened stage (Table 4). However, the level of protein increased, probably indicating that particular proteins were being synthesized during ripening. These results support the findings of Davis and Cocking [17] who also reported increase in the protein content in tomato fruit during the climacteric period but they noticed this kind of increase during the later stages of ripening. However, a similar kind of increase in the protein synthesis has been reported in many fruits during their early climacteric period [e.g. Drouct and Hartman; Tucker and Laties; and Sharma; (c.f.18)].

Table 2: Proximate composition of pigments of *Morus alba* fruit during its growth and ripening.

Pigments	Stages of growth and ripening				
	Young	Mature	Pre-ripened	Ripened	Post-ripened
Chlorophyll 'a' (mg/gm)	0.061 ± 0.0019^{e}	0.038 ± 0.0010^{d}	0.015 ± 0.0009^{c}	0.004 ± 0.0004^{b}	0.003 ± 0.0002^{a}
Chlorophyll 'b' (mg/gm)	0.038 ± 0.0022^{d}	0.023 ± 0.0005^{c}	0.007 ± 0.0009^{b}	0.003 ± 0.0003^{a}	0.002 ± 0.0004^{a}
Total chlorophylls (mg/gm)	0.100 ± 0.0029^{e}	0.061 ± 0.0012^{d}	0.022 ± 0.0001^{c}	0.007 ± 0.0002^{b}	0.004 ± 0.0002^{a}
Total carotenoids (mg/gm)	42.42 ± 0.859^{d}	27.43 ± 0.473^{c}	10.28 ± 0.701^{b}	2.66 ± 1.126^{a}	2.39 ± 0.136^{a}
Total anthocyanins (mg/100gm)	2.80 ± 0.377^{a}	4.36 ± 0.377^{b}	7.88 ± 1.027^{c}	23.37 ± 0.621^{d}	31.85 ± 1.619^{e}

Values of means followed by different alphabets are statistically significant according to Duncan's multiple range test (DMRT) at 5 % level. (n = 3).

Table 3: Changes in the carbohydrate contents of the fruit of *Morus alba* at its sequential stages of growth and ripening.

Carbohydrates (mg/gm)	Stages of growth and ripening				
	Young	Mature	Pre-ripened	Ripened	Post-ripened
Total soluble sugars	11.12 ± 0.395^{a}	14.03 ± 0.600^{b}	20.47 ± 0.236^{c}	29.40 ± 0.298^{d}	45.65 ± 0.506^{e}
Reducing sugars	1.38 ± 0.165^{a}	2.40 ± 0.201^{b}	4.10 ± 0.315^{c}	11.73 ± 0.344^{d}	26.92 ± 0.539^{e}
Non-reducing sugars	9.74 ± 0.237^{a}	11.63 ± 0.402^{b}	16.37 ± 0.280^{c}	17.68 ± 0.245^{d}	18.74 ± 0.043^{e}
Starch	122.03 ± 1.997^{c}	99.95 ± 4.437^{b}	94.46 ± 1.481^{b}	62.66 ± 4.114^{a}	61.19 ± 7.339^{a}

Values of means followed by different alphabets are statistically significant according to Duncan's multiple range test (DMRT) at 5 % level. (n = 3).

Phenols, which are known as the substances of the aromatic compounds in fruits have been found to be 0.728 mg/gm in the fruit of Mulberry at its young stage, but they declined to 0.486 mg/gm at pre-ripened stage. However, eventually a significant increase in the level of phenols occurs in the ripened (0.670 mg/gm) and post-ripened fruit (1.386 mg/gm) (Table 4). Thus the results of the present study supports the opinions of Kumar and Goswami [19] that the significant accumulation of total phenols in the early stages act as a protection mechanism to the phytohormones (auxins, gibberellins, cytokinins), which play an important role in cell division and cell enlargement. However, phenols of the Mulberry fruit eventually exhibit a declining trend, which even reported earlier by Kumar and Goswami [19]. A decrease in the ascorbic acid content during and after ripening (i.e. 18.24 mg/100 gm to 11.60 mg/gm) of presently worked out Mulberry fruit suggest that ascorbic acid catabolized faster to meet the increased respiratory requirements during ripening. This result also suggests that the ripening shifted the redox balance to the oxidative side. The decrease of ascorbic acid content was reported in different fruits by Rousi and Aulin [20].

Table 4: Changes in the content of Proteins, Phenols and Ascorbic acid in the fruit of *Morus alba* at its sequential stages of growth and ripening.

Proteins, Phenols and Ascorbic acid (mg/gm)	Stages of growth and ripening				
	Young	Mature	Pre-ripened	Ripened	Post-ripened
Total proteins	1.90±0.207^{a}	5.01±0.569^{b}	7.94±0.372^{d}	6.52±0.205^{c}	14.99±0.065^{e}
Total phenols	0.728±0.005^{c}	0.830±0.014^{d}	0.486±0.006^{a}	0.670±0.014^{b}	1.386±0.006^{e}
Ascorbic acid	18.24±1.66^{b}	22.11±1.91^{c}	16.58±1.66^{b}	16.04±0.96^{b}	11.60±1.66^{a}

Values of means followed by different alphabets are statistically significant according to Duncan's multiple range test (DMRT) at 5 % level. (n = 3).

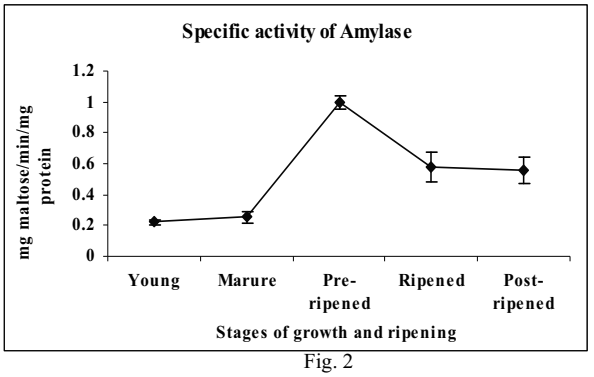

Fig. 2

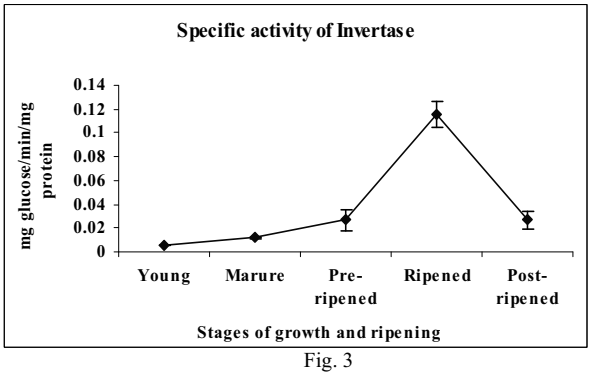

Fig. 3

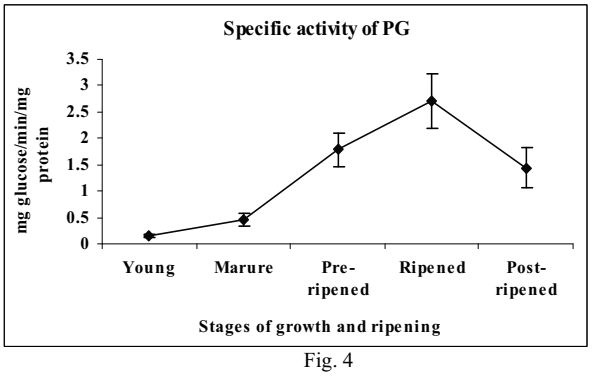

Fig. 4

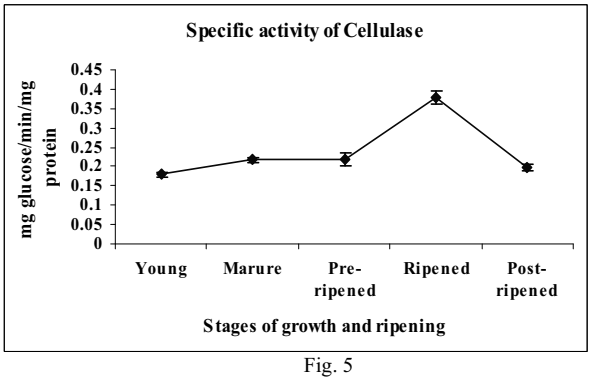

Fig. 5

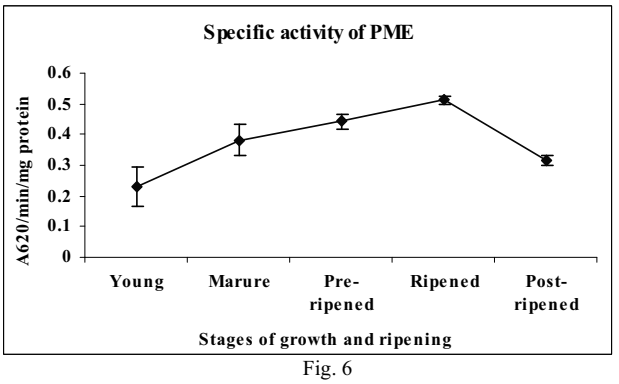

Fig. 6

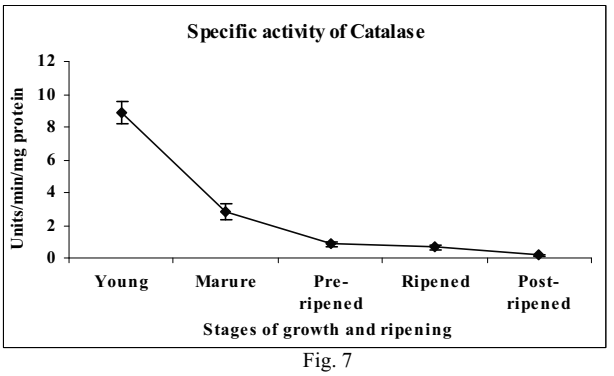

Fig. 7

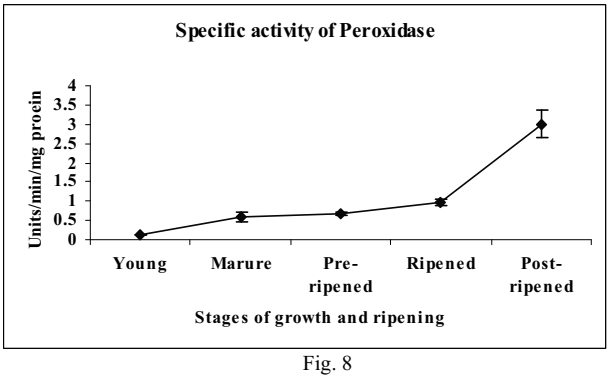

Fig. 8

Fig. 2-8: Graphical representation of the specific activity of the enzymes of *Morus alba* fruit at its sequential stages of growth and ripening.

Amylase enzyme is known to hydrolyze starch. The present study reveals that the specific activity of amylase enzyme increases from young stage (0.23 mg maltose released/min/mg protein) to pre-ripened stage (1.00 mg maltose released/min/mg protein), but in the ripened stage it decreases to 0.59 mg maltose released/min/mg protein, while more or less it remained consistent till post-ripened stage (Fig. 2). However, Lima *et al*. [21] opined that the climacteric rise in mango fruit is marked by an appreciable increase in the activity of amylase due to reducing and non-reducing sugars contents and a decrease in the starch content. Perhaps this may be due to the hydrolysis of starch into sugars (viz. glucose, fructose or sucrose) and increased activity of amylase due to the presence of starch. In contrast to amylase, a

consistent and gradual increase in the specific activity of invertase was found all throughout the course of growth and ripening of Mulberry fruit with 0.027 glucose released/min/mg proteins at its pre-ripened stage; 0.12 glucose released/min/mg protein at ripened stage (Fig. 3). Dilley also reported a more or less similar kind of increased invertase activity in different fruits during their early stages of fruit development but with ultimate decline of it [22].

All the three enzymes that are involved in cell wall softening, polygalacturonase (PG), pectinmethylesterase (PME) and cellulase are positively accelerated cell wall softening and degradation could directly influence fruit growth, development and the fruit maturity [23]. A positive correlation has been reported between the appearance of polygalacturonase (PG) and initiation of softening in a number of fruits like guava (EI-Zoghbi,), papaya (Paull and Chan) and mango (Roe and Bruemmer) [c.f. 24]. The specific activity of PG, PME as well as cellulase are found to get increased from young stage to the ripened stage, but later on declined. During the course of present study the specific activity of PG was noted to be 1.79 mg glucose released/min/mg protein in the pre-ripened stage, while in the ripened stage it was found to be 2.71 mg glucose released/min/mg protein and 1.44 mg glucose released/min/mg protein in the post-ripened stage (Fig. 4). Thus the results of the present study are in agreement with the findings of Selvaraj who reported higher values of PG activity in certain fruits from the young to the ripened stages [25]. The cellulase enzyme of the currently studied fruit exhibits a steady and gradual increase in its specific activity (from 0.18 mg glucose released/min/mg protein at young stage to 0.38 mg glucose released/min/mg protein at ripened stage), except in the post-ripened stage where it decreases significantly (0.20 mg glucose released/min/mg protein) (Fig. 5). The presently obtained values of the specific activity of cellulase are also in agreement with the findings Bonghi and Ferrarese [26] who stated that the cellulase is associated with fruit growth and development at initial stage and with fruit softening at late stage. It was presumed that cellulase could accelerate cell division and regulate growth and development of cell. In addition, cellulase activity rose rapidly with concomitant increase of fruit growth. The specific activity of PME was also low with 0.23 mg glucose released/min/mg protein at the young stage, but eventually it increased significantly up to 0.51 mg glucose released/min/mg protein in the ripened stage (Fig. 6). A similar kind of increase in the PME activity has been reported during ripening by Nunan *et al* [27].

According to Chance *et al*. [28] Catalase and Peroxidases [PO] are enzymes of a homoproteinaceous nature (oxido-reductase) that catalyze the oxidation of various organic compounds. During the course of present study the specific activity of catalase was found to get declined from 8.91units/min/mg protein at young stage to 0.16 units/min/mg protein at post-ripened stage (Fig. 7). In case of peroxidase, its specific activity was noticed to be increased from 0.13 units/min/mg protein at young fruit stage to 2.99 units/min/mg protein at post-ripened fruit stage, which shows a remarkable increase by 23 fold (Fig. 8). Therefore, the results of the present investigation are in agreement with the view of Jimenez *et al.* [29] who stated that the antioxidant system, which includes catalase, super oxide dismutase, some peroxidase and many other enzymes, plays a crucial role in the ripening process.

CONCLUSION

From the foregoing account it may be concluded that the fruit of *Morus alba*, being a rich source of sugars and antioxidants, can be used as a natural food. Since a significant amount of anthocyanins also get accumulated in the ripening Mulberry fruit it also may be used as a natural food colourant. Due to these kinds of medicinal and economic importance Mulberry fruits can be recommended for their commercial exploitation.

REFERENCES

[1] Venkatesh, K. R. and Seema, C. (2008) Mulberry: Life enhancer. *J. Med. Plants Res.,* **10**: 271-278.

[2] Taro, N. (1999) The chemistry and biosynthesis of isoprenylated flavonoids from moraceous plants. *Pure Appl. Chem*., **71**: 1115-1118.

[3] Hesham, A., Abdel, N. B., Jari, S. and Kalevi, P. (2005) Hypolipidemic and antioxidant effect of *Morus alba L* (Egyptian Mulberry) root bark fractions supplementation in cholesterol - fed rats. *J Ethanopharmaco,* **78**: 2727-2733.

[4] Enkhmaa, B., Shiwaku, K., Katsube, T., Kitajima, K., Anuurad, E. and Yamasaki, M. (2005) Mulberry (*Morus alba L.*) leaves and their major flavonal quercetin 3-(6-malonylglucaside) attenuate athero-sclerotic lesion development in LDL receptor-deficient mice. *J. Nutr*., **135**: 729-734.

[5] Kang, T. H., Oh, H. R., Jung, S. M., Ryu, J. H., Park, M. W. and Park, Y. K. (2006) Enhancement of neuroprotection of Mulberry leaves (*Morus alba* L.) prepared by the anaerobic treatment against ischemic damage. *Biol. Pharm. Bull.*, **29**: 270-274.

[6] Oh, H., Ko, E. K., Jun, J. Y., Oh, M. H., Park, S. U. and Kang, K. H. (2002) Hepatoprotective and radical scavenging activities of preflavonoids, coumarin and stilbene from *Morus alba*. *Planta Med.*, **68**: 932-934.

[7] Mazumdar, B. C. and Majumder, K. (2003) *Methods on physico-chemical analysis of fruits*, Daya Publishing House, Delhi, India.

[8] Thimmaiah, S. K. (1999) *Standard methods of biochemical analysis*. Kalyani Publishers, New Delhi, India.

[9] Wang, Z., Ying, T., Bao, B. and Huang, X. (2005) Characteristics of fruit ripening in tomato mutant. *epi. J*. Zhejiang *Univ. Sci*. **68(6)**: 502-507.

[10] Devi, P. (2001) *Principles and methods in plant molecular biology*, Biochemistry and Genetics. Agrobios, Jodhpur, India.

[11] Bliss, C. I. (1967) *Statistical methods for research in the natural sciences*, Statistics in biology, McGraw Hill Book Company.

[12] Willis, R. B. H., Mc Glasson, W. B., Graham, D., Lee, T. H. and Hall, E. G. (1996) *Postharvest- An introduction to the physiology and handling of fruit and vegetables* - Indian edition, CBS Publishers and Distributors, New Delhi, India.

[13] Merzlyak, M. N., Solovchenko, A. E. and Gitelson, A. A. (2003) Reflectance spectral features and non-destructive estimation of chlorophyll, carotenoid and anthocyanin content in apple fruit. *Postharvest Biol. and Tech*., **27**: 197-211.

[14] Yuhua, L., Ryozo, S., Hirobumi, M. and Sanevuki, K. (2001) Regulation of anthocyanin biosynthesis during fruit development in 'Nyoho' Strawberry. *J. Japan. Soc. Hort. Sci.*, **70(1)**: 28-32.

[15] Vishal, S. R. and Neerja, S. R. (2003) Studies on fruit growth and organic metabolites in developing kiwifruit. *Ind. J. Plant Physiol*, **8**: 138-140.

[16] Sabir, S. M., Ali Shah, S. Z. and Afzal, A. (2004) Effect of chemical treatment, wax coating, oil dipping and different wrapping materials on physio-chemical characteristics and storage behavior of Apple. *Pak. J. Nutr.* **3(2)**: 122-127.

[17] Davies, J. W. and Cocking, E. S. (1967) Protein synthesis in tomato fruit tissue: The site of synthesis and the pathway of carbon into protein. *Planta*, **76**: 285-305.

[18] Singh, R. R. and Sharma, R. M. (2000) Structure, cellular components and composition of fruits and vegetables. In: Verma, L. R., Joshi, V. K., (Eds.), *Postharvest technology of fruits and vegetables*, Indus Publishing Co., New Delhi. India, pp. 76-93.

[19] Kumar, S. and Goswami, A. K. (1985) Phenol content and peroxidase system in developing apple fruits. *I. J. Hort*., **42**: 184.

[20] Rousi, A. and Aulin, H. (1977) Ascorbic acid content in relation to ripeness in fruit of six (*Hyppophae rhamnoides* L.) clones from Pyharanta, SW Finland. *Ann. Agric. Fenn*., **16**: 80-87.

[21] Lima, L., De, C., Chitarra, O. A. B. and Chitarra, M. I. F. (2001) Changes in amylase activity, starch and sugars contents in mango fruits pulp Cv. (Tommy Atkins) with spongy tissue. *J. Braz. Arch. Bio. And Tech*., **44(1)**: 59-62.

[22] Dilley, D. R. and Hulme, A. C. (1970) *Enzymes*, In: Hulme, A. C., (Ed.), Biochemistry of fruits and their products, Academic Press, London, Vol. 1, pp. 159-178.

[23] Zhao, Y. F., Lin, H. T., Lin, J. F. and Chen, S. J. (2006) A review of cell wall-degrading enzymes in fruit softening and their control. *J. Zhongkai Univ. Agri. Tech.*, **19(1)**: 65-70.

[24] Prasanna, V., Prabha, V. and Tharanathan, R. N. (2007) Fruit ripening phenomena- An overview. *Cri. Rev. Food Sci. Nutr.*, **47**: 1-19.

[25] Selvaraj, Y. (1993) Changes in enzymes activity in ripening pineapple fruit. *Ind. J. Hort*., **50(4)**: 310-317.

[26] Bonghi, C. and Ferrarese, L. (1998) Endo-β-1, 4-glucanases are involved in peach fruit growth and ripening and regulated by ethylene. *Physiol. Planta.*, **102**: 346-352.

[27] Nunan, K. J., Davies, C., Robinson, S. P. and Fincher, G. B. (2001) Expression patterns of cell wall-modifying enzymes during grape berry development. *Planta*, **214**: 257-264.

[28] Chance, B., Sies, H., Boveris, A. (1979): Hydroperoxide metabolism in mammalian organs. *Physiol. Rev.,* **59**: 527-605.

[29] Jimenez, A., Cressen, G., Kular, B., Firmin, J., Robinson, S. and Verhoeyen, M. (2002) Changes in oxidative process and components of the antioxidant system during tomato fruit ripening. *Planta*, **214**: 751-758.

PRAJÑĀ - **Journal of Pure and Applied Sciences**
Vol. 17: 065-067, 2009 ISSN 0975 - 2595

DISSOCIATION CONSTANTS OF SOME DERIVATIVES OF 4 – AMINO BENZOIC ACID IN MIXED

Shipra Baluja,* Pranav Inamdar and Mehul Bhatt

Department of Chemistry, Saurashtra University, Rajkot, Gujarat - 360 005

ABSTRACT

The dissociation constants of some derivatives of 4-amino benzoic acid measured by Calvin Bjerrum pH titration method in DMF-water and DMSO-water (60:40 v/v) systems at 308.15 K. It is observed that dissociation constant depends on the solvent and substituents group present in the compound.

***Keywords*: 4-amino benzoic acid, Schiff base, dissociation constant, pH.**

INTRODUCTION

Para amino benzoic acid is a biological important entity. Small amount of p- amino benzoic acid is present in B-complex vitamins and multivitamin formulas. It is essential nutrients for microorganism and some animals. It has various applications in medical field. It enhances the effect of cortisone [1], acts as an antioxidant to protect skin from sunburn [2], used in dermatomyositis [3], peyronie's disease [4] and pemphigus [5] etc. Further, it increases the ability of some infertile women to become a pregnant [6]. Therefore, it was of interest to study the dissociation constant of some new derivatives of p-amino benzoic acid.

The dissociation constant provides useful information about structure, toutomeric equilibria, solvent-solute interactions etc. [7]. Various workers have reported the dissociation constants of Schiff bases [8-10]. In continuation with our previous work [11], in the present paper, dissociation constant of some derivatives of 4 – amino benzoic acid have been studied in 1- 4 dioxane-water system at 308.15 K by Calvin Bjerrum pH titration method. Now onwards, these derivatives are designated as ligands.

MATERIALS AND METHODS

The structures of synthesized ligands are given in Figure 1. All the ligands were recrystallized and their purity was checked by thin layer chromatography. The characterization was done by IR, NMR and mass spectral analysis. The physical constants of these ligands are given in Table 1.

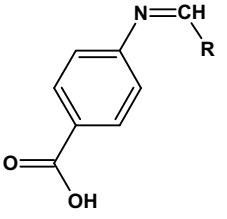

Where, R=
HPI 1 = -4 OCH_3 C_6H_4 HPI 2 = -C_6H_5
HPI 3 = -4 Cl C_6H_4 HPI 4 = -C_4H_3O
HPI 5 = -CH=CH C_6H_4 HPI 6 = -2 OH C_6H_4
HPI 7 = -4 OH, 3 OCH_3 C_6H_3 HPI 8= -3 NO_2 C_6H_4

Figure 1: General structure of derivatives of 4-Amino benzoic acid.

Table 1: Physical constants of derivatives of p-amino benzoic acid.

Code	M.F.	M. Wt. g	R_f* Value	M.P. °C	Yield %
HPI-1	$C_{15}H_{10}NO_3$	255.27	0.61	186	62
HPI-2	$C_{14}H_{11}NO_2$	225.24	0.51	170	45
HPI-3	$C_{14}H_{10}NO_2Cl$	256.69	0.45	217	52
HPI-4	$C_{12}H_9NO_3$	215.20	0.48	212	59
HPI-5	$C_{16}H_{13}NO_2$	251.28	0.58	172	63
HPI-6	$C_{14}H_{11}NO_3$	241.24	0.41	260	57
HPI-7	$C_{15}H_{13}NO_4$	271.27	0.52	115	55
HPI-8	$C_{13}H_9N_2O_4$	270.23	0.34	250	65

The Calvin Bjerrum pH titration method was used to determine dissociation constants of synthesized ligands.

For this, the following sets of mixtures were prepared for titration:

(I) 0.80 ml HNO_3 (0.1M) + 11.20 ml water + 24.00 ml 1, 4 – Dioxane + 4.0 ml $NaNO_3$ (1.0 M).

(II) 0.80 ml HNO_3 (0.1M) + 11.20 ml water + 22 ml 1, 4 – Dioxane + 2.0 ml ligand solution (0.1M) + 4.0 ml $NaNO_3$ (1.0 M).

* Corresponding author – shipra_baluja@rediffmail.com

Thus, total volumes (V^0) in each set = 40.0 ml and 1, 4 – Dioxane: water ratio was 60:40 (v/v).

A Systronic pH meter (Model No. EQ 664) was used for the pH determination. The systronic glass electrode and a saturated calomel electrode were used as indicator and reference electrodes respectively. Before measurement, the pH meter was calibrated with buffer solutions of known pH in acidic and basic range.

The above mentioned solutions were allowed to attain a constant temperature (308.15 K) and then titrated against standard NaOH solution (0.5 M) under an inert atmosphere of nitrogen. The change in the pH of solution with each addition of alkali was recorded.

RESULTS AND DISCUSSION

The titration curves obtained in the above two titrations are designated as the acid titration curve and ligand titration curve respectively. The average number of protons associated with compound ($\overline{n_H}$) can be calculated by Irving and Rossotti equation.

$$\overline{n_H} = Y - \left\{\left(V'' - V'\right)\left(N^0 + E^0\right)\right\} \Big/ \left\{\left(V^0 + V'\right)T_L^0\right\} \quad \ldots(1)$$

where Y is the number of replaceable protons per molecule.

For the ligands HPI-6 and HPI-7, Y is taken to be 2 whereas for rest of the ligands, its value is 1. $V^{/}$ and $V^{//}$ are the volume of alkali required at the same pH for both acid and ligand titration curves respectively. V^0 is the initial volume of the solution. N^0, E^0 and T^0_L are the initial total concentration of the alkali, acid and ligand respectively.

The evaluated values of $\overline{n_H}$ for all the ligands are given in Table 2. It is observed that for the ligands HPI-1 to HPI-5 and HPI-8, the formation curve extend from 0 to 1. Whereas for HPI-6 and HPI-7, $\overline{n_H}$ values extend over the range from 0 to 2, indicating two dissociation steps.

Three methods have been used for the evaluation of dissociation constants:

(i) Half-integral method: In this method, dissociation constants were evaluated from the plot of $\overline{n_H}$ verses pH.

The pK_1^H values for HPI-1 to HPI-5 and HPI-8 are evaluated at $\overline{n_H}$ = 0.5. Whereas for HPI-6 and HPI-7, pK_1^H values are determined at $\overline{n_H}$=1.5 and $\overline{n_H}$ = 0.5. All these values are given in Table 2.

(ii) Average method: The dissociation constants for HPI-1 to HPI-5 and HPI-8 were then calculated by equation (2) at several pH.

$$\log pK_1^H = pH + \log [\overline{n_H} / (\overline{n_H} - 1)] \quad \ldots.. (2)$$

From these evaluated pK_1^H values, the average pK_1^H can be calculated using several points close to 0.5 and 1.5 and are given in Table 2.

Table 2: The log pK_1^H values for all the ligands calculated by Half-integral method and point wise calculation.

Compound code	Half-integral Method	Point wise calculation
HPI-1	9.16	9.02
HPI-2	9.90	9.63
HPI-3	7.75	7.55
HPI-4	9.55	9.41
HPI-5	9.44	9.57
HPI-6	8.83	8.97
HPI-7	9.30	9.37
HPI-8	8.41	8.56

As $\overline{n_H}$ values are between 0 and 2, for HPI-6 and HPI-7 ligands, the dissociation constants for all the points below $\overline{n_H}$=1 were calculated by equation (2) whereas for all the points above $\overline{n_H}$=1, the equation (3) was used.

$$\log pK_2^H = pH + \log [(\overline{n_H} - 1) - (2 - \overline{n_H})] \quad \ldots.(3)$$

The values of pK_1^H and pK_2^H were calculated and averages of these values are given in Table 2. (iii) Least square method: This method is applicable to only those ligands which have two replaceable hydrogens. So, for HPI-6 and HPI-7, following equation (4) is used to calculate pK_1^H and pK_2^H values which are reported in Table 2.

$$[\overline{n}_H/(\overline{n}_H - 1)].1/(1/\text{antilog}pH) = [(2 - \overline{n}_H)/(\overline{n}_H - 1)].(1/\text{antilog pH}).pK_1^H.pK_2^H - pK_1^H \quad \ldots. (4)$$

The comparison of pK_1^H values shows that acidic character increases in the order: HPI-3> HPI-8> HPI-1> HPI-5> HPI-4> HPI-2. The acidic character depends on the type of substituent group. Table 2 shows that introduction of an electronegative group like –Cl or $-NO_2$ increases the acidic strength. Similar results were also

observed by other workers with compound containing –Cl, -Br or NO_2 groups [7, 11, 12]. Further the presence of methoxy group (as in HPI-1) also causes the acidic character to increase. In HPI-4, the presence of lone pair of electrons on oxygen may cause the molecule to have a tendency to accept hydrogen rather to donate, which may cause decrease in acidic character in HPI-4.

The presence of intramolecular hydrogen bonding also plays an important role in deciding the acidic strength of a compound. Weaker the intramolecular H-bond, larger will be the acidic strength or vice-versa.

Thus in HPI-2 stronger hydrogen bonding may cause minimum acidic strength, which is followed by HPI-4 and HPI-5.

Comparison of HPI-6 and HPI-7 shows that HPI-6 is more acidic than HPI-7. The presence of –OH at ortho position to $–OCH_3$ decreases the acidity in HPI-7 as comparison to only –OH group at ortho position, as in HPI-6. Thus, overall comparison of acidic character of all ligands shows that HPI-6 and HPI-7 are more acidic than HPI-1, HPI-2, HPI-4 and HPI-5, but less acidic than HPI-3 and HPI-8.

REFERENCES

[1] Wiesel, L. L., Barritt, A. S. and Stumpe, W. M. (1951) The synergistic action of para-aminobenzoic acid and cortisone in the treatment of rheumatoid arthritis. *Am. J. Med. Sci*., **222**: 243-248.

[2] Wills, I. and Kligman, A.M. (1970) The Quest for More Effective Sunscreens. *Arch. Dermatol.*, **102**: 405-417.

[3] Grace, W. J., Kennedy, R. J. and Formato, A. (1963) Therapy of Scleroderma and Dermatomyositis. *NY State J. Med.*, **63**: 140 -144.

[4] Zarafonetis, C. J. D. (1959) Treatment of Peyronie's disease with potassium para-amino benzoate, *J. Urol.* **81**: 770-772.

[5] Zarafonetis, C. J. D., Curtis, A. C. and Shaw, J. M. (1956) Treatment of Pemphigus with Potassium para-aminobenzoate. *Am. J. Med. Sci.*, **231**: 30-50.

[6] Sieve, B. F. (1942) The clinical effects of a new B-complex factor, para-amino benzoic acid, on pigmentation and fertility. *South Med. Surg.,* **104**: 135-139.

[7] McDanial, D. H., Brown, H. C. and Haffinger, E. A. (1955) Brande and F. Nachod, "Determination of organic structure by physical methods", Academic Press, Inc, N. W.

[8] Blázquez, M., Pineda, T., Sevilla, J. M., Domínguez, M. and García-Blanco, F. (2004) The Schiff base between pyridoxal-5′-phosphate (PLP) and hexylamine. Formation of the unprotonated form of the imine by reaction of the unprotonated PLP and free amine. *J. Phys. Org. Chem.,* **4**:372-380.

[9] Ögretir, C., Dal, H., Berber, H. and Taktak, F. F. (2006) Spectroscopic Determination of Acid Dissociation Constants of Some Pyridyl Shiff Bases. J. Chem. Eng. Data, **51:** 46–50.

[10] Öğretir, C., Görgün, K., Özkütük, M. and Sakarya, H. C. (2009) Determination and evaluation of acid dissociation constants of some novel benzothiazole Schiff bases and their reduced analogs by spectroscopy ARKIVOC 197-209.

[11] Baluja, S. H., Bhalodia, R. H. and Kasundra, P. K. (2009) Dissociation constant of some derivatives of 5-aminoisophthalic acid in mixed solvents by calvin Bjerrum pH titration method". *Russ. J. Phys. Chem.*, In Press.

[12] Magausson, L. B., Cpostmus, C. and Craig, C. A. (1963) Coordination in solutions I.Acid strengths of phenol derivatives in water. *J. Am. Chem. Soc*., **85**: 1711-1715.

PRAJÑĀ - **Journal of Pure and Applied Sciences**
Vol. 17: 068-073 2009 ISSN 0975 - 2595

SYNTHESIS AND SPECTROPHOTOMETRIC STUDIES OF Fe (III)-HMCNP COMPLEX AND THEIR USE AS AN ANALYTICAL REAGENT

Shailesh M. Dave, Kapil L. Dubal, Vijay R. Ram, Atul H. Bapodra and Hitendra S. Joshi *

Department of Chemistry, Saurashtra University, Rajkot, Gujarat -360 005

ABSTRACT

In the present investigation, 4-Hydroxy-8-methylcoumarin derivatives and their metal complexes of Fe(III) were synthesized and characterized using spectrophotometric method. Metal complex of Fe (III) with 4-Hydroxy-8-methylcoumarin chalcones [1-(4'-hydroxy-8'-methyl coumarin-3'-yl)-3-o-nitrophenyl-2-propene-2-one] was also determined by mole ratio and Job's method. The complexes of metal formed with coumarin derivatives were compared with standard reagents.

***Keywords*: 4-Hydroxy-8-methylcoumarin; 1-(4'-hydroxy-8'-methyl coumarin-3'-yl) -3-o-nitrophenyl-2-propene-2-one; spectrophotometric determination; Fe (III) complex, Beer's law, Mole ratio method, Job's method.**

INTRODUCTION

The theory of metal based mixed valence complexes (MBMV) is well documented [1, 2]. The synthesis of hydroxy coumarins is of great interest due to their wide applications as chelating agents [3]. Hydroxy coumarin derivatives form complexes with V, Ti (IV), Zr (IV), Pr, Sm, Gd, etc,[4-8].

The physico chemical studies of coumarins with chelating groups at appropriate positions and their metal-complexes revealed that the ligands could be proved as a potential analytical reagent [9-13].

The present communication deals with synthesis of HMCNP [1-(4'-hydroxy-8'-methyl coumarin-3'- yl) - 3 – o – nitrophenyl – 2 – propene – 2 - one], HMCNP complex with Fe (III) metal ion, which may be used as an analytical reagent. It belongs to chalcone series [14]. Chalcones are the compounds which are obtained by the condensation of aromatic ketone with an aldehydes; which is cheated with Fe (III). The ligand is found to form complexes with above metal ion in different pH range. The absorption spectra of the complex were recorded on Shimadzu UV-160-A Spectrophotometer and the effects of pH on the absorption values were studied. The composition of complex was determined by Yoe and Jones mole ratio and Job's method [15, 16]. Same has been supported from thermo gravimetric analysis [17].

* Corresponding author – drhsjoshi49@gmail.com

The proposed structure of the synthesized compounds and complexes were assigned and proposed on the basis on the basis of ^{1}H NMR, IR spectra data and spectrophotometric studies.

MATERIALS AND METHODS

All chemicals used throughout this work were of analytical grade. The absorbance measurements were done on a Shimadzu UV-160-A Spectrophotometer. The pH of the solutions were measured on EQUIPTRONICS 614 pH meter and solutions of required pH were obtained using sodium-acetate-acetic acid, sodium acetate-HCl, NH_3-NH_4Cl or Borax-HCl buffers of suitable concentration. The stoichiometric ratios of metal to reagent in the complexes were determined by Job's method, Yoe and Jones mole ratio method and gravimetrically. The whole experimental work was carried out at 25˚C.

Preparation of 4-hydroxy-8-methyl coumarin [18-28]

To a well stirred mixture of o-cresol (10.8 g, 0.01mol), malonic acid (10.4 g, 0.1mole) and phosphorus oxychloride (40 ml) was added to anhydrous zinc chloride (30 g) in small portion. The reaction mixture was heated with stirring on a waterbath at 70°C for 18-20 hrs. The content was cooled and poured into ice-water to get solid; the obtained solid was filtered and washed with water. It was then treated with sodium carbonate solution and filtered. The filtrate was acidified with dilute

hydrochloric acid. The precipitates were washed with water and crystallized from methanol. Yield was 75%, m.p. 225˚C.

Synthesis of 3-Acetyl-4-hydroxy-8-methyl coumarin [29-32]

4-hydroxy-8-methyl coumarin (1.56 g, 0.01mole) was dissolved in mixture of acetic acid (5 ml) and phosphorus oxychloride (4 ml) and was heated on waterbath for half an hour. The reaction mixture was poured into ice-cold water; the product was isolated and crystallized from ethanol. Yield was 85%, m.p. 110˚C.

Synthesis of 1-(4'-hydroxy-8'-methyl coumarin-3'-yl)-3-o-nitrophenyl-2- propene-2-one (HMCNP)

A solution of 3-acetoacetyl-4-hydroxy coumarin (1.98g, 0.01mole), o-nitrobenzaldehyde (1.06g, 0.01mole) and piperidine (1 ml) as a catalyst in chloroform (50 ml) was refluxed with for 6 hours on a water bath. The excess chloroform was distilled off and the residue was washed with methanol and crystallized from dioxane. Yield was 68%, m.p.120˚C. ^{1}H NMR 400 MHz ($CDCl_3$): δppm: 2.46 (s, 3H, Ar-CH_3), 6.54-6.57 (d, 1H, J=15.6Hz, –CH=), 6.85-6.89 (d, 1H, J=15.6Hz,–CH=), 7.11-8.45 (m, 7H, Ar-H); IR (KBr, cm^{-1}): 3402, 3112, 2950, 2850, 2337, 1724, 1604, 1442, 1384, 1261, 1195, 771; Analytical Calculated for $C_{19}H_{13}O_6N$: C, 64.95; H, 3.70; N, 3.99 ; Found : C, 64.91; H, 3.69; N, 3.95% respectively.

Preparation of standard solution of Fe (III)

Ferric chloride (anhydrous) 2.0276 g was dissolved in double distilled water, containing a little free acid and was diluted to 250 ml to get 0.05M stock solution of ferric chloride. This solution was standardized gravimetrically using Na_2EDTA. It was diluted to get desired concentration as and when required.

Effect of pH

To study of the effect of pH, a series of solutions were prepared by taking 1 ml (0.005 M) ferric chloride solution and 3 ml (0.02M) HMCNP reagent solution. pH of the solution were adjusted to 2.0, 2.5, 3.0 and 3.5 with sodium acetate – hydrochloric acid buffer. The coloured solution was then diluted to 25 ml keeping the final concentration of alcohol 75%. The absorbance spectrum of each solution was obtained between 200 to 800 nm. It is observed that colour intensity was maximum at pH 2.5, indicates that maximum complex formation takes place at this pH. The results are presented in Table 1.

Table 1: Complexation with Fe (III) at different pH values.

pH	Buffer	Absorbance
2.0	Na – acetate – hydrochloric acid	0.246
2.5	Na – acetate – hydrochloric acid	0.271
3.0	Na – acetate – hydrochloric acid	0.218
3.5	Na – acetate – hydrochloric acid	0.184

Gravimetric determination of Fe (III) with HMCNP

A 1.0% solution of the reagent in dioxane was used. Ferric chloride solution (0.05 M, 10 ml) was taken in a clean beaker, diluted to about 100 ml with distilled water and pH of the solution was adjusted to 2.0 to 3.0 using sodium acetate-hydrochloric acid buffer. The solution was warmed at 60˚C and small excess of reagent HMCNP was added (1%, 30 ml). The precipitates obtained were digested on water bath for 60 minutes at 60˚C. The precipitates were filtered through a previously weighed sintered glass crucible (G4) and washed with warm water. The chelate was dried to constant weight at 110-115˚C in hot air oven, cooled and weighed.

The experiment was repeated at different pH of the solution. The experiment was also repeated with different aliquots keeping the optimum pH to evaluate its applicability.

Spectrophotometric study of Fe (III) complex

The Fe (III) - HMCNP chelate is soluble in chloroform, benzene, carbon tetrachloride, DMF, ethyl acetate. This enabled to verify the Beer's law and its application for spectrophotometric determination.

Absorption Spectra

To record the absorption spectra, 5 mg of chelate was dissolved in 25 ml of chloroform and absorbance of this solution was measured at different wave length in the range of 350-600 nm. The absorbance was plotted against wave length to get absorption spectra. It was observed that the absorbance of the coloured solution of chelate

increases continuously towards the lower wave length. A shoulder is observed at 500 nm and hence all the measurements were carried out at 500 nm. Absorption Spectra of Fe (III)-HMCNP complex is shown in Figure 1.

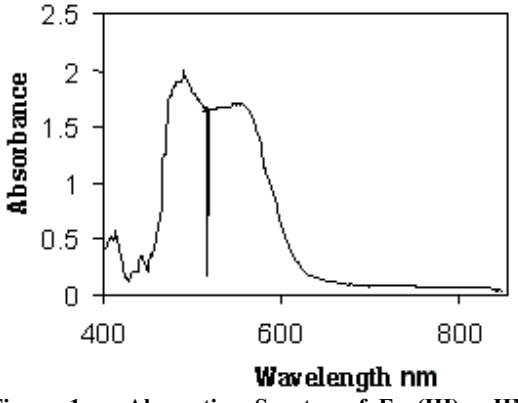

Figure 1: Absorption Spectra of Fe (III) - HMCNP Complex.

Effect of the reagent concentration

A series of solutions were taken, keeping the concentration of ferric ion constant (0.005 M, 1ml) while the amount of (0.05 M) reagent HMCNP was varied. The absorbances of the solutions after development of color, were recorded at 500nm. The absorbance was found to increase till addition of approximately 8 times excess of the reagent. Thus, about 8 times excess of the reagent found to be essential for maximum complex formation.

Verification of Beer's Law

To 10 ml of solution (0.01 M) of the reagent solution in each set of 25 ml volumetric flask, 2 ml buffer solution (pH 2.5) was added. Varying amount of Fe(III) solution (0.005 M) were added and the contents were made upto the mark with ethanol and distilled water to make final volume. Absorbances were measured at 500nm against reagent blank prepared in ideal condition. Absorbance values were plotted against the Fe (III) content. A straight line is passing through the origin of graph that indicates the obeyance of Beer's law. The standard graph thus obtained may be used for the determination of ferric ion in an unknown solution using HMCNP reagent. The results are presented in Table 2. The graph is shown in Figure 2. Molar absorptivity calculated from Beer's law plot was found to be 11×10^2 lit $mol^{-1}cm^{-1}$ for Fe (III)-HMCNP reagent at 500nm.

Composition of Chelate

The composition of Fe (III) chelate with the reagent HMCNP has been determined on the basis of Job's method and by Yoe and Jones mole ratio method.

Table 2: Verification of Beer's law.

Fe (III) solution in ml	Fe (III) concentration in ppm	Absorbance at 500nm
0.3	3.35	0.048
0.6	6.70	0.096
0.9	10.05	0.144
1.2	13.40	0.190
1.5	16.75	0.241
1.8	20.10	0.259

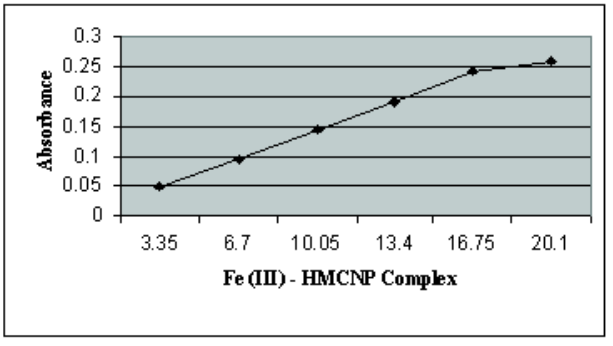

Figure 2: **Verification of Beer's law.**

Composition of Fe (III)-HMCNP complex by Job's method

A series of 11 solutions was prepared from a (different) standard Iron solution (0.005M) and HMCNP reagent solution (0.005M) in various proportions (as shown in Table 3) and adjusted so that total volume remain 12 ml. Each solution was buffered by the addition of 2ml of acetate buffer (pH 2.5). These solutions were then diluted to 25ml using dioxane as a diluent. Absorbance of these solutions was recorded at 500nm against metal ion blank. The results are presented in Table 3 and graph is shown in Figure 3. From the graph, it has been observed that maximum absorbance found at 0.5 ratio of metal ion concentration to the total metal and ligand concentration, which indicates the formation of 1:1 (M : L) complex.

Yoe and Jones mole ratio method

In this method, equimolar solutions of the Fe (III) ion as well as the reagent (0.005 M) were used. A series of solutions were prepared, keeping the reagent solution (6.0 ml, 0.005 M) constant while varying the amount (from 1 to 9.0 ml, of 0.005 M) pH of the solutions were adjusted to 2.5. These

solutions were diluted to 25 ml in volumetric flasks. Absorbance were recorded at 500 nm and plotted against the ratio of concentration of metal ion to reagent. The results are presented in Table 4 and Graph shown in Figure 3.

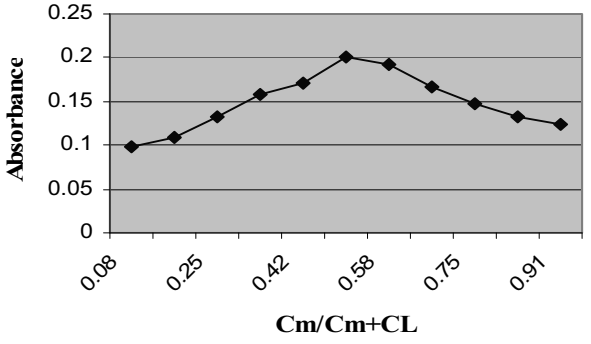

Figure 3: Result of Job's method of continuous verification.

Table 3: Data obtained from Job's method of continuous verification.

Metal ion solution (0.005M) ml.	Ligand solution (0.005M) ml.	$C_m/C_m + C_L$	Absorbance at 500nm
1.	11	0.08	0.098
2.	10	0.17	0.110
3.	9	0.25	0.132
4.	8	0.33	0.158
5.	7	0.42	0.172
6.	6	0.50	0.201
7.	5	0.58	0.192
8.	4	0.66	0.166
9.	3	0.75	0.147
10.	2	0.83	0.132
11.	1	0.91	0.124

Where C_m and C_L are concentrations of metal ion and ligand respectively

Table 4: Data obtained from Yoe and Jones mole ratio method.

Fe(III) solution (0.005M) ml.	Ligand solution (0.005M) ml.	$Cm + C_L$	Absorbance At 500nm
1.	6	0.17	0.066
2.	6	0.33	0.113
3.	6	0.50	0.182
4.	6	0.66	0.212
5.	6	0.83	0.226
6.	6	1.00	0.241
7.	6	1.16	0.241
8.	6	1.33	0.241

Where C_m and C_L are concentrations of metal ion and ligand respectively

It is evident from the graph that absorbance gradually increases upto molar composition of metal to the reagent and after that it becomes constant indicating 1:1 stoichiometry of the complex.

RESULTS AND DISCUSSION

In the current paper, 4-Hydroxy-8-methylcoumarin was synthesized by the condensation of o-cresol with malonic acid. 4-Hydroxy-8-methylcoumarin was acetylated and subjected to Fries migration to give 3-acetoacetyl-4-hydroxy-8-methylcoumarin. The acetyl coumarin was condensed with o-nitro benzaldehyde to yielded compound 1-(4'-hydroxy-8'-methyl coumarin-3'-yl)-3-o-nitrophenyl-2- propene-2-one.

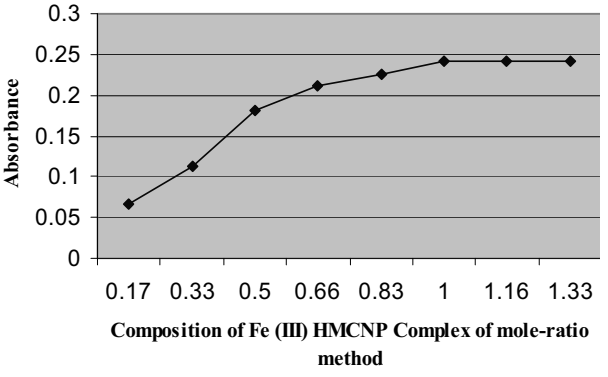

Figure 4: Result of Yoe and Jones mole ratio method.

In the present study the reagent HMCNP form complexes with Fe (III) in the various range of pH.

The composition of complexes determined by mole ratio and Job's method, was found to be 1:1 (M: L), this has also supported by gravimetric analysis. The synthesized reagents are quite stable at 25°C for long time without decomposition. The reagents are well suited as gravimetric reagents.

CONCLUSION

Apart from any theoretical significance that may be attached to a knowledge of the formation constants and spectra of the Fe(III) HMCNP complexes. HMCNP has been proposed as a colorimetric reagent and as an indicator for complexometric titrations for Fe(III). This work has revealed the superior stability of solutions of the highly purified reagent. It has demonstrated the significance of control of pH and of excess reagent necessary to insure that the solutions

prepared for photometric measurement should have the same degree of complex formation. From the finding, it is concluded that, coumarin derivatives as an analytical reagent has found extensively used in analytical determination of various metal ions.

ACKNOWLEDGMENTS

The authors are thankful for facilities & grants given under UGC- Special Assistance Programme (DRS) Department Research Support (Sanction letter No. 540/6/DRS/2004 (SAP-I) Dt. 26/03/2004, and Department of Science & Technology New Delhi Fund for Improvement of Science & Technology (FIST) (Sanction letter No. SR/FST/CSI-072/2003 Dt. 24/12/2003 and Department of Chemistry, Saurashtra University, Rajkot – 360 005 (INDIA) for providing facilities.

REFERENCES

[1] Hush, N. S. (1967) Intervalence-transfer absorption. II. Theoretical considerations and spectroscopic data. *Prog. Inorg. Chem,* **8:** 391-444.

[2] Meyer, T. J. (1978) Optical and thermal electron transfer in metal complexes. *Acc. Chem. Res.*, **11(3):** 94-100.

[3] Anschuetz R. (1903) On a New Class more Aromatically, the Tetronic Acid of Related Compounds. *Chem. Ber.,* **36:** 463-466.

[4] Singh, H. B. (1973) Complexation reactions of dihydroxy coumarins-I : Study of gallium(III)-4-phenyldaphnetin (4-phenyl-7,8-dihydroxycoumarin) complexes. *Journal of Inorganic and Nuclear Chemistry,* **35(1):** 187-199.

[5] Katyal, M. and Singh H. (1968) Analytical applications of hydroxycoumarins. *Talanta*, **15(10):** 1043-1054.

[6] Kalara A. K., (1971) Spectrophotometric determination of ruthenium (III) using diphenylcarbazone. *Microchimica Acta.*, **59(5):**788-793.

[7] Vyas, K. B., Jani, G. R. and Hathi M. V. (2009) Potentiometric studies on transition metal complexes of substituted derivative of coumarin-Part 1. *E-Journal of Chemistry*, **6(4):**1121-1124

[8] Charyulu, K., Jagannadha K., Omprakash, K. L., Pal, A. V. Chandra, Reddy, M. L. N. (1985) Stability constants of copper(II), nickel(II), cobalt(II) and zinc(II) complexes with some hydroxycoumarins**.** *J. Indian Chem. Soc.*, **62(2):**121-123.

[9] Kalra, A. K., Singh, H. B. and Singh, R. P. (1972) Spectrophotometric study of the vanadium (IV) complex with 4-phenyl-7,8-dihydroxycoumarin (4-phenyldaphnetin. *J. Indian Chem. Soc.*, **49(1):** 97-102.

[10] Singh, H. B., Srivastava, S. and Maheshwari, S. (1982) Syntheses and characterization of five coordinate titanium (IV) and niobium (V) complexes with some dihydroxycoumarins**.** *Journal of the Institution of Chemists (India)*, **54(6):** 276-280.

[11] Pokhariyal, G. P., Lal, B. (1997) Some trivalent lanthanide complexes of 8-acetyl-7-hydroxy-4-methylcoumarin *J. Indian*. *Chem. Soc.*, **74(6):** 492-493.

[12] Gudasi, K. B. and Goudar, T. R. (1997) Synthesis of lanthanide (III) complexes with 2-(3-coumarinylthioacetyl) benzimidazole. *J. Indian Chem. Soc.* **74(10):**, 786-788.

[13] Popat, K. H., Nimavat, K. S., Vasoya, S. L. and Joshi, H. S. (2003) Synthesis, anticancer, antitubercular and antimicrobial activity of 6-carbethoxy-5-(3'-chlorophenyl)-3-aryl-2-cyclohexenones and 6-aryl-4-(3'-chlorophenyl)-3-oxo-2, 3a, 4, 5-tetrahydro-1H-indazoles. *Indian J. Chem.*, **42B(6):** 1497-1501

[14] Bakry, R. S., Razak, O. A., Walily, A. F. and Belal S. F. (1998) Spectrophotometric investigation of the formed chelate between timonacic

and palladium (II) and its analytical applications. *J. Pharm. Biomed. Anal*., **17 (1):** 95-101.

[15] Malik, A. K., Kaul, K. N., Lark, B. S., Faubel, W. and Rao, A. L. J. (2001) Spectrophotometric determination of cobalt, nickel palladium, copper, ruthenium and molybdenum using sodium isoamylxanthate in presence of surfactants. *Turk. J. Chem.*, **25:** 99-105.

[16] Mwelase, S. R. and Bariyanga, J. (2002) MALDI time-of-flight mass spectrometry and thermogravimetric analysis of Mg (II), Ca (II), Cu (II), Zn (II) and Pt (II) adducts with monomethoxypolyethylene glycol 5000. *Journal of Molecular Structure*, **608(2-3)**, 235-244.

[17] **a).** Anschutz R. (1909) The Benzotetronic Acid Group I *Ann*., **367:** 169-218.
b). Harford A. D. and Hill D. W. (1937) Reactions of o-hydroxybenzylidene diacetophenones. VII. Flavylium salts from dihydrochalcones. *J. Chem. Soc.* 41-42.

[18] Kneyuki, H. (1962) The reactions of esters with acyl chloride in the presence of aluminum chloride. IV. Formation of tribenzoylmethane *Bull. Chem. Soc. Japan*, **35:** 5235-5236.

[19] Sonn, A. (1917) 4-Hydroxycoumarins. *Ber.*, **50:** 1292-1305.

[20] Boyd, J and Robertson, A. (1948) The chemistry of the insoluble red woods; a new synthesis of 4 - hydroxycoumarins. *J. Chem. Soc.*, 2174-2176

[21] Hoesch, Kurt. (1915) A new synthesis of aromatic ketones. I. Preparation of some phenol ketones**.** *Ber.*, **48:** 1122-1133.

[22] **a).** Iguchi S. (1952) The antibacterial properties of compounds containing the tricarbonylmethane group. VI. 3-Acyl-4-hydroxycoumarin containing substituents in the benzene nucleus. *Yakugaku Zasshi*,**72:** 122-127
b). Iguchi, S. and Utsugi, N. (1953) 3-Acyl-4-hydroxycoumarins containing substituents in the benzene nucleus. IV. Syntheses of 3-acyl-5-methyl-4,7-dihydroxycoumarins and their antibacterial properties. *Yakugaku Zasshi* **73:** 1290-1294.

[23] Garden, J. F., Hayes, N. F. and Thomson, R. H. (1956) Synthesis of 4-hydroxycoumarins. *J. Chem. Soc.,* 3315-3318.

[24] Ziegler, E. and Junek, H. (1955) 4-Hydroxycoumarin. I. A new synthesis of 4-hydroxycoumarin and its derivatives. *Montch.*, **86**: 29-38.

[25] Ziegler, E. and Junek, H. (1956) 4-Hydroxycoumarin. III. A new synthesis of 3-substituted 4-hydroxycoumarins. *Montch.*, **87:** 212-217.

[26] Shah, V. R., Bose, J. L. and Shah, R. C. (1960) New synthesis of 4-hydroxycoumarins. *J. Org. Chem.*, **25:** 677-679.

[27] Dallacker F., Kratzer P. and Lipp M. (1961) Derivatives of 2,4-pyronone and 4-hydroxycoumarin. *Ann.*, **643**: 97-109.

[28] Dholakia, V. N., Parekh, M. G. and Trivedi, K. N. (1968) 4-Hydroxycoumarins. II. pyrones from 4-hydroxycoumarins. *Aust. J. Chem.*, **21(9):** 2345-2347.

[29] Eisenhauer, H. R., Link, K. P. (1953) 4-Hydroxycoumarins. XIV. The reaction of 4-hydroxycoumarin with aromatic acid chlorides. *J. Am. Chem. Soc.*, **75:** 2046-2049.

[30] Stahmann, M. A., Wolff, I. and Link, K. P. (1943) Hydroxycoumarins. I. Synthesis of 4-hydroxycoumarins. *J. Am. Chem. Soc.*, **65:** 2285-2287.

PRAJÑĀ - **Journal of Pure and Applied Sciences**
Vol. 17: 074-078 2009 ISSN 0975 - 2595

APPLICATION OF THERMOMETRIC TECHNIQUE FOR EVALUATION OF CORROSION INHIBITION IN MILD - STEEL IN PRESENCE OF UREA AND ITS DERIVATIVES IN AQUEOUS HYDROCHLORIC ACID MEDIUM

M. B. Mapara *

Department of Chemistry, M. B. Patel Science College, Anand, Gujarat - 388 001

ABSTRACT

Studies in corrosion behavior of mild-steel in aqueous hydrochloric acid solution were carried out using conventional weight-loss and thermometric technique in presence of urea and its substituted derivatives. The plot of log(C) vs. log (θ/1-θ) suggests that all the inhibitors obey Langmuir adsorption isotherm equation. Percent inhibition efficiency has been determined from the result of conventional weight-loss and thermometric technique, which are in good agreement. The result of thermometric technique can be satisfactorily used for the evaluation of corrosion inhibition in mild-steel in presence of urea and its substituted derivatives in aqueous hydrochloric acid medium considering its simplicity, quickness and reliability.

***Keywords*: corrosion inhibition, urea, thermometric technique.**

INTRODUCTION

Iron and ferrous alloys have been extensively used under different condition in chemical industries in handling alkalis, acids and salt solutions. Bothiraja and Sethuraman studied the corrosion of mild-steel in hydrochloric acid [1]. The Influence of tramadol [2-[(dimethylamino) methyl]-1-(3-methoxyphenyl) cyclohexanol hydrate] on corrosion inhibition of mild steel in acidic media have been studied by Prabhu *et al*. [2]. The "N-benzyl-N,N-bis[(3,5-dimethyl-1H-pyrazol-1-yl)methyl]amine was used as a corrosion inhibitor for steel in 1 M HCl by Tebbji *et al.* [3]. The effect of *Azadirachta indica* leaves extract as an inhibitor in 0.5 M sulphuric acid against corrosion in copper was studied by Valek and Martinez [4].

The corrosion inhibition of mild steel in acidic media by a new triazole derivative has been studied by Bentiss *et al.* [5]. The effect of thiourea and its derivatives as an inhibitor for corrosion of iron in acidic medium have been studied by Pillai and Narayan [6]. Inhibitions of corrosion of mild-steel by phenylthiosemicarbazides of nontraditional oils have been studied by Toliwal and Jadav [7]. Uses of ethanolamides as corrosion inhibitor have been studied [8]. Inhibition effect of some fatty acid oxadiazoles on the corrosion have been reported [9].

* Corresponding author – drmbmapara@gmail.com

MATERIALS AND METHODS

Weight Loss

For complete immersion test the specimens of size 5.5 x 2.5 x 0.2 cm were completely immersed in 250 mL of corrosive electrolyte solution. The concentration of plain hydrochloric acid solution studied were 0.1 M, 0.5 M, 1.0 M and 2.0 M. The effect of concentrations of urea and its derivatives on mild steel were studied to understand the corrosion behavior in presence of these compounds. The immersion period was ranging from 60 minutes to 24 hours in different acid concentrations. Total immersion tests were carried out at 303K with and without urea and its derivatives. From the results of weight-loss measurements the corrosion rate (mdd), inhibition efficiency (IE%) and surface coverage (θ) were calculated.

Thermometric Technique

For the thermometric study, test specimen of size 2.5 x 1.0 x 0.2 cm was immersed in 20 mL of acid solution. The test were carried out in the concentration of 1.0 M and 2.0 M acid solutions, using 1, 5, 10 and 25 mM of urea and its derivatives. Digital thermometer with 0.01^{o}C precision was used in Dewar flask. The change in temperature was recorded at the regular interval of time. The results were used to calculate reaction number (RN) and inhibition efficiency (IE%) as given below.

$$RN = (T_{max} - T_i) / t \qquad \text{---------} \qquad (1)$$

Where, T_{max} and T_i are the maximum and initial temperature in minutes in the experiments to attain T_{max}.

Inhibition efficiency was calculated as-

$$IE\% = (RN_b\text{-}RN_{inh}) / RN_b \times 100 \text{ -----} \quad (2)$$

RESULTS AND DISCUSSION

It has already been established that at higher concentration of acid solution, corrosion behavior of mild-steel can be considered to be predominantly chemical in nature. Urea and its derivatives might have formed a bond with metal and the molecule might have also been chemisorbed at the metal surface. Successive decrease in reaction number (RN) and temperature difference (ΔT), suggest decrease in corrosion rate in presence of urea and its derivatives. These decrease in reaction number (RN) and temperature difference (ΔT) can again be linked up with protective power of these compounds. Decreases in reaction number (RN) with the addition of inhibitors suggest adsorption of the compound on the corroding surface. Decrease in temperature difference (ΔT) also indicates the effect of the added compounds. It is clear from the Fig. 1 & 2 that the behavior is characterized by an initial period during which the temperature remains constant or varies very slightly. This part of the curves can be described as incubation period in which pre-immersion oxide film protects the metal from acid attack or an induction period which will be the time required for the break-down of the film and start of attack. Inhibition efficiency can be very well judged by knowing the extent to which reaction number is affected. The plots of reaction number (RN) versus log C indicate that all the compounds form chemisorbed monolayer protective film on the corroding surface. Similarly, variation in delay in time as a function of log C can also be interpreted on the same line. However, adsorption may be of weaker since the time necessary to reach (T_{max}) clearly establishes good amount of inhibition particularly when higher concentrations were employed.

The results make it evident that thermometric technique can be satisfactorily employed to study corrosion behavior of mild-steel in hydrochloric acid solution in absence and presence of urea and its derivatives. Generally, considerable inhibition in presence of thiourea may be attributed to the presence of two polar functional groups having nitrogen and sulphur atoms. It is generally agreed that the polar functional group is the reaction centre for the establishment of chemisorptions process. Urea contains two N-atoms having non-bonding electron pair on each nitrogen atom, which can become reaction centre. Urea offers inhibition but to a very less extent. Phenylurea is more effective than urea, which is due to the phenyl group at N-atom of urea. The introduction of phenyl group in urea has decreased the corrosion rate probably due to the negative charge of π-electrons of aromatic ring.

In p-chlorophenylurea presence of chloro group has shown more effect on the corrosion process but lesser effective compared to p-nitrophenylurea. The introduction of chloro group did not provide additional reaction centre due to its comparatively lower electron withdrawing tendency. In case of p-nitrophenylurea the introduction of electron withdrawing $–NO_2$ group has remarkable increase in inhibitive efficiency because of the additional reaction centre established by N and O atoms of $–NO_2$ group. Chemisorptions of the additives are shown by linearity of log (θ/1-θ) vs. log C, from the results presented in Table - 1 & 2. It is evident that thermometric technique can be satisfactorily employed to study the corrosion behavior of mild-steel in hydrochloric acid solution in presence and absence of urea and its derivatives.

CONCLUSION

From the present investigation, following conclusions can be drawn:

1. Linearity of plot of log (θ/1-θ) vs. log C in presence of urea and its derivatives suggests that they functions through adsorption by Langmuir isotherm.
2. Thermometric technique is simple and quick. However, it is found more useful when reaction is highly exothermic.
3. Variation in delay time as a function of log C has resulted in parabolic curves indicates that all the compound form chemisorbed mono-layer protective film on the corroding surface.
4. Trends in reaction number, temperature difference and time necessary to reach Tmax in thermometric corrosion tests can be satisfactorily used to know corrosion rate and inhibitive power of the organic additives.

TABLE 1: Influence of different concentration of urea and its derivatives on corrosion rate (mdd), inhibition efficiency (IE%) and surface coverage (θ) of mild-steel in 2 M HCl solution.

Inhibitors concentration (mM)		Corrosion Rate (mdd) (mgm/dm^2/day)	Inhibition Efficiency (IE%)	Surface Coverage (θ)	Log (θ/1-θ)
Blank		12023.45	-	-	-
Thiourea	1	6118.73	49.11	0.4911	-0.0150
	5	4431.84	63.14	0.6314	0.2337
	10	3776.56	68.59	0.6859	0.3391
	25	2604.28	78.34	0.7834	0.5583
Methyl urea	1	6551.57	45.51	0.4551	-0.0782
	5	4762.49	60.39	0.6039	0.1831
	10	4025.45	66.52	0.6652	0.2981
	25	3248.73	72.98	0.7298	0.4315
Phenyl urea	1	8285.36	31.09	0.3109	-0.3456
	5	5954.01	50.48	0.5048	-0.0080
	10	4880.31	59.41	0.5941	0.1654
	25	3412.25	71.62	0.7162	0.4020
p-Nitro phenyl urea	1	9692.10	19.39	0.1939	-0.6188
	5	7151.55	40.52	0.4052	-0.1667
	10	6086.27	49.38	0.4938	-0.0107
	25	4433.04	63.13	0.6313	0.2335
p-Chloro phenyl urea	1	10165.83	15.45	0.1545	-0.7385
	5	8097.79	32.65	0.3265	-0.3144
	10	7208.06	40.05	0.4005	-0.1751
	25	5818.14	51.61	0.5161	0.0279
Urea	1	10627.53	11.61	0.1161	-0.8815
	5	9098.14	24.33	0.2433	-0.4927
	10	8340.66	30.63	0.3063	-0.3550
	25	7322.28	39.10	0.3910	-0.1924

Specimen area : 30.70 sq.cm. Immersion period: 1 hr. Temperature: 30 ± 1°C

TABLE 2: Influence of urea and its derivatives on temperature difference (ΔT), time to reach maximum temperature (Δt), reaction number (RN) and inhibition efficiency (IE%) during corrosion of mild-steel in 2 M HCl solution.

Inhibitor and its concentration (mM)		Temp. difference T_{max} (ΔT) °C	Time to reach (Δt) Min.	Reaction number (RN) °C Min^{-1}	Inhibition Efficiency (IE%) calculated from	
					Thermo- metric method	Weight-loss method
Blank		26.3	150	0.1754	-	-
Thiourea	1	20.0	225	0.0890	49.23	49.11
	5	15.0	235	0.0639	63.54	63.24
	10	13.7	250	0.0548	68.73	68.59
	25	10.1	265	0.0382	78.19	78.34
Methyl urea	1	20.1	210	0.0958	45.37	45.51
	5	14.8	215	0.0692	60.50	60.39
	10	12.8	220	0.0584	66.67	66.52
	25	10.8	230	0.0472	73.09	72.98
Phenyl urea	1	22.9	190	0.1206	31.24	31.09
	5	17.3	200	0.0868	50.51	50.58
	10	14.5	205	0.0711	59.43	59.41
	25	10.3	210	0.0493	71.87	71.62
p-Nitro phenyl urea	1	24.0	170	0.1413	19.42	19.39
	5	18.2	175	0.1045	40.49	40.51
	10	15.8	180	0.0883	49.62	49.38
	25	12.7	200	0.0638	63.20	63.13
p-Chloro phenyl urea	1	24.4	165	0.1482	15.46	15.45
	5	19.7	170	0.1162	33.70	33.65
	10	18.4	175	0.1052	40.00	40.05
	25	15.7	185	0.0849	51.56	51.61
Urea	1	24.7	160	0.1544	11.92	11.81
	5	21.8	165	0.1325	24.44	24.33
	10	20.6	170	0.1214	30.77	30.63
	25	19.2	180	0.1067	39.12	39.10

Surface area of specimen: 3.2 sq.cm. Temperature: 30 ± 1°C

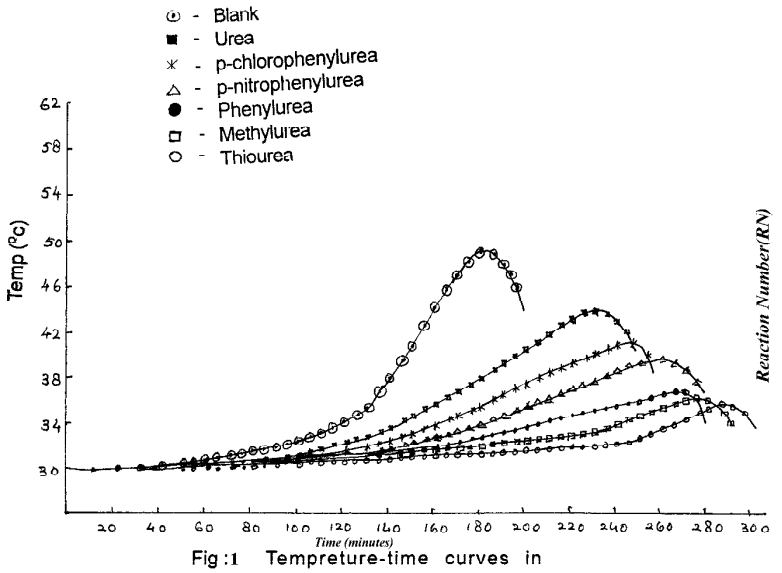

Fig :1 Tempreture-time curves in absence and presence of 25mM of urea and its derivatives for mild-steel in 1.0M HCL solution.

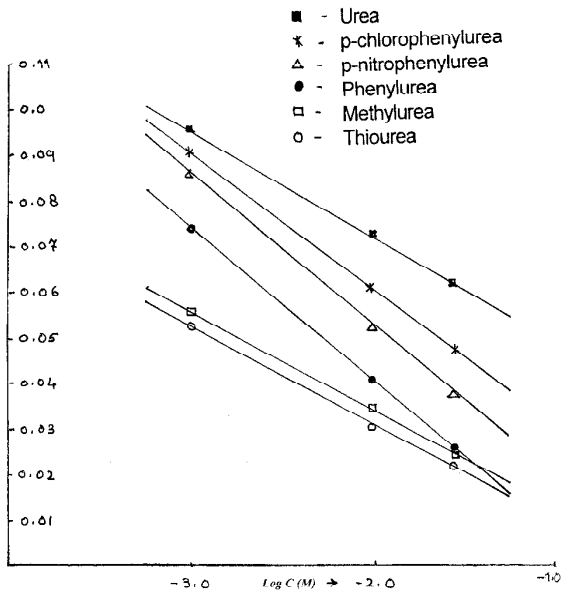

Fig :1 Reaction Number(RN) as a function of inhibitor concentration (Log C) of mild-steel in 1.0M HCL solution containing urea and its deratives.

Figure 1B: Temperature time curves in absence and presence of 25 mM of urea and its derivatives for mild-steel in 1 M HCl solution.

Figure 1B: Reaction Number (RN) as a function of inhibitor concentration (Log C) of mild-steel in 1 M HCl solution containing urea and its derivatives.

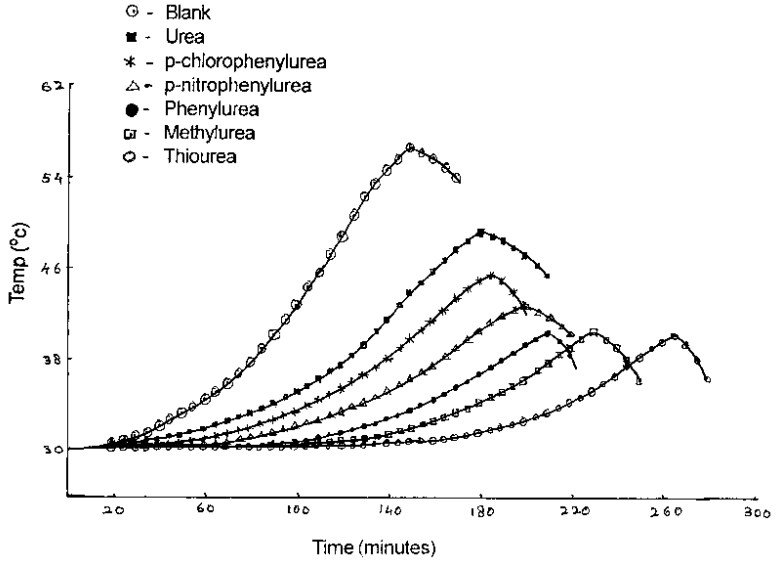

Figure 2B: Temperature time curves in absence and presence of 25 mM of urea and its derivatives for mild-steel in 2 M HCl solution.

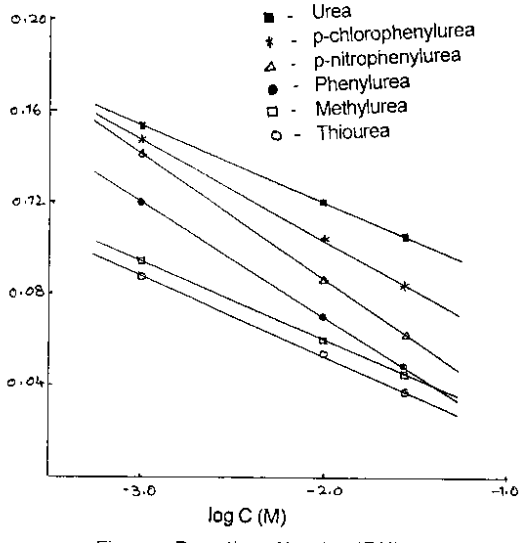

Figure 2B: Reaction Number (RN) as a function of inhibitor concentration (Log C) of mild-steel in 2 M HCl solution containing urea and its derivatives.

5. Inhibition efficiency result obtained with thermometric technique is in fair agreement with those obtained with weight-loss method.

REFERENCES

[1] BothiRaja, P. and Sethuraman, M. G. (2008) Inhibitive effect of black pepper extract on the sulphuric acid corrosion of mild steel. *Material Letters* **62(17-18)**: 2977-2979.

[2] Prabhu, R. A., Shanbhag, A. V. and Venkatesha, T. V. (2007) Influence of tramadol [2[(dimethylamino)-methyl]-1-(3- methoxyphenyl) cyclohexanol hydrate] on corrosion inhibition of mild steel in acidic media. *Journal of Applied Electrochemistry* **37(4)**: 491-497.

[3] Tebbji, K., Bouabdellah, I., Aouniti, A., Hammouti, B., Oudda, H., Benkaddour, M., and Ramdani, A. (2007). N-benzyl-N,N-bis[(3,5-dimethyl -1H-pyrazol-1-yl) methyl]amine as corrosion inhibitor of steel in 1 M HCl. *Material Letters* **61(3)**: 799-804.

[4] Valek, L., and Martinez, S. (2007) Copper corrosion inhibition by *Azadirachta indica* leaves extract in 0.5 M sulphuric acid. *Material Letters* **61(1)**: 148-151.

[5] Bentiss, F., Lagrenée, M., Traisnel, M. and Hornez, J. C. (1999) The corrosion inhibition of mild steel in acidic media by a new triazole derivative. *Corrosion Science* **41**: 789-803.

[6] Pillai, K. C. and Narayan, R. (1978) Inhibition of corrosion of iron in acids by thiourea and derivatives. *Journal of the Electrochem Society* **125**: 1393-1397.

[7] Toliwal, S. D. and Jadav, K. (2009) Inhibition of mild steel by phenyl thiosemicarbazides of non traditional oil. *Journal of Scientific and Industrial Research* **68**: 235-241.

[8] Chaudhary, R. S., Tyagi, D. K., Rani, M. and Kumar, A. (2007) Corrosion inhibition of mild steel by ethanolamides in hydrocholric acid. *Journal of Scientific and Industrial Research* **66**: 47-51.

[9] Rafiquee, M. Z. A., Saxena, N., Khan, S. and Quraishi, M. A. (2007) Some fatty acid oxadiazoles for corrosion inhibition of mild steel in HCl. *Indian Journal of Chemical Technology*,**14**: 576-583.

PRAJÑĀ - **Journal of Pure and Applied Sciences**
Vol. 17: 079-085, 2009 ISSN 0975 - 2595

RECYCLING OF FOOD GRADE PLASTICS PACKAGING FILMS FOR VARIOUS APPLICATIONS

Neeraj Jindal, Lokesh Sharma, Manish Patel, Mehul Choksi and Neetha John*

Plastics Technology, Institute of Science and Technology for Advanced Studies and Research (ISTAR), Vallabh Vidyanagar, Gujarat – 388 120

ABSTRACT

Food grade plastics films were recycled effectively and efficiently by simple and economical methods. Different routes were followed and a comparative study was conducted. The plastics films were blended with virgin plastics and formulated with different additives to make them more polar and reactive. The mixing of plastics films with virgin plastics and other additives were performed on two roll mill and specimens were prepared on different processing machines like film extrusion, injection moulding, compression moulding etc. The major areas were the recycled compounds used are injection moulding, extrusion, metal adhesion etc.

Keywords **: Recycling, plastics films, packaging, hot melt adhesives.**

INTRODUCTION

Polyethylene films for packaging have a very long life span [1]. They are tough, chemical and moisture resistant. They are also puncture resistant so that heavy or sharp edged products do not damage them. They have good clarity and are easy to work with [2, 3]. They are not affected by temperature extremes and are UV stabilized. These films are available in clear, black and a variety of colors and they may be made from renewable resources such as starch and cellulose [4, 5]. Polyethylene films are environmentally friendly and not harmful to foodstuffs. They are found to be ideal for food packaging. No harmful substances are used during the manufacturing and the preparation and there are no vapors, which are hazard to health [6]. They offer especially good protection to the packaged goods. They can be used for a multitude of applications and provide protection not only to foodstuffs and medications but also for screws, bearings, furniture and construction fittings.

These films can be made into biodegradable polymer films [7], which have a proprietary additive that allows oxidative degradation breaking the long carbon chains down into smaller pieces. The oxidative degradation is triggered by sunlight, heat, and mechanical stress. The film becomes brittle and the molecular fragments are then further broken down by microbial action to carbon dioxide, water and natural substances [8, 9].

Amount of plastic waste generated annually it is estimated that 56% of all plastics waste is used in packaging, three-quarters of which is from households. It is estimated that only 7% of total plastic waste arising are currently being recycled [10]. A report on the production of carrier bags made from recycled rather than virgin polyethylene concluded that the use of recycled plastic resulted in the following environmental benefits [11, 12]. Reduction of energy consumption by two-thirds, production of only a third of the sulphur dioxide and half of the nitrous oxide, reduction of water usage by nearly 90% and reduction of carbon dioxide generation by two-and-a-half times [13, 14].

The disposal of plastics products also contributes significantly to their environmental impact. Because most plastics are non-degradable, they take a long time to break down. With more and more plastics products, particularly plastics packaging, being disposed of soon after their purchase, the landfill space required by plastics waste is a growing concern [15, 16].

In the present work a novel method for recycling of plastics films is proposed. This method not only reduces the waste disposal problems but also convert waste plastics into more useful products. The recycled plastics material was to be used making packaging films, moulded articles, hot melt adhesives etc. Virgin LDPE is to be blended with recycled plastics in various proportions. In

* Corresponding author – neethajob@yahoo.co.in

order to increase the processibility and polarity, EVA, PVA and polyethylene wax were added to the system.

EXPERIMENTAL

Materials used

Low density polyethylene (LDPE), Grade 22FA02 supplied by Reliance, Baroda, Ethylene vinyl acetate, EVA, PE wax, polyvinyl alcohol (PVA) etc were commercial grade.

LDPE based food grade packaging films used as recycled plastics.

Adherents: Leather was collected from the foot wear industry; galvanized iron (GI) Metal sheets were used as metal adherent and plastics sheets were molded using compression moulding machine with virgin LDPE material used as plastics adherent.

Experimental work

Preparation of Recycled Plastics films

The collected films were washed by water and detergents to remove the impurities and fat or oil in the films by keeping the films in the solution for 3 hours, and dried. The films were washed again using toluene to remove printing from the films. The films were finally washed with detergent solution again to remove the solvent and then dried completely.

Mixing and Processing

Blends of different ratios were prepared as per the formulations in Table 1, in a laboratory two roll mill at 120° to 130°C temperature. Test specimens were prepared using injection molding machine, compression moulding and blown film plant.

Table 1: Formulations of the blends with recycled LDPE.

Ingredients	No. 1	No.2	No. 3	No 4
LDPE	100 Parts	100 Parts	100 parts	100 parts
Waste LDPE	5, 10, 15, 20 parts	20 parts	20 parts	20 parts
EVA	-	2, 4, 6, 8 parts	-	2, 4, 6, 8 parts
PVA	-	-	2, 4, 6, 8 parts	6 parts
WAX	-	5 parts	5 parts	5 parts

Mechanical Properties

Tensile specimens were tested on universal testing machine. The testing speed was 50mm/min. Percentage elongation and modulus at ultimate elongation was also measured. The test was conducted as per ASTM D 638. Specimens for Izod impact test were kept in cantilever position and pendulum load was used. The energy required for breaking the specimens was recorded as impact strength which was conducted as per ASTM D 256. Sheets specimens were taken for estimating Rockwell hardness in L scale as per ASTM D 785. Abrasion loss was determined using Taber abrader as per ASTM D 1044. Dart impact strength of the films was conducted as per ASTM D1709. Rectangular pieces were used for flexural strength and measured using universal testing machine as per ASTM D 790 and Durometer hardness measured in shore D scale as per ASTM D 2240.

Physical Properties

The specimens were cut from the sheets and immersed in chemicals for 24 hours at room temperature. The change in weight was measured and percentage was calculated. Specimens were tested for the flammability with horizontal clamping methods as per ASTM D 635**.** The joints were tested for peel strength on UTM Shimadzu, Japan; model AG100KNG as per ASTM D903.

Differential Scanning Calorimeter (DSC) (ASTM D3417)

A sample of 10 to 20 mg in an aluminum sample pan was placed into the differential scanning calorimeter. The sample was heated at a controlled rate (usually 10°/min) and a plot of heat flow versus temperature is produced. The resulting thermo gram was analyzed.

RESULTS AND DISCUSSION

Figure 1 and 2 shows the impact strengths of blends of LDPE/ recycled plastics with varying the amount of recycled plastics. Figure 2 shows the impact strength with combination of EVA and PVA in the LDPE/ recycled plastics blends. Impact strengths in all the blends were found to be increasing. This proves the miscibility of the recycled Plastics with virgin LDPE and recycled plastics can be added to the virgin LDPE, recycled plastics does not show variations, but with PVA and EVA shows increase in impact strength to a

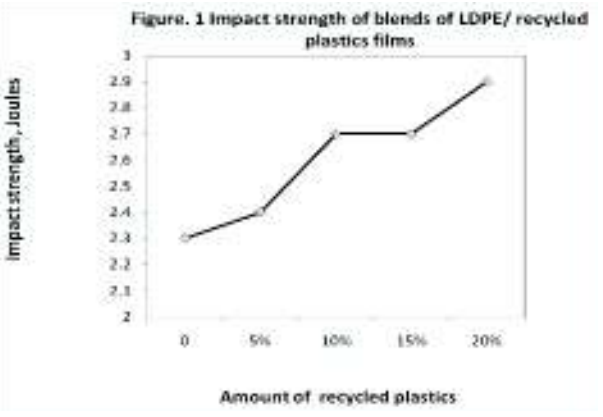
Figure. 1 Impact strength of blends of LDPE/ recycled plastics films
Impact strength, Joules
3
2.9
2.8
2.7
2.6
2.5
2.4
2.3
2.2
2.1
2
0
5%
10%
15%
20%
Amount of recycled plastics

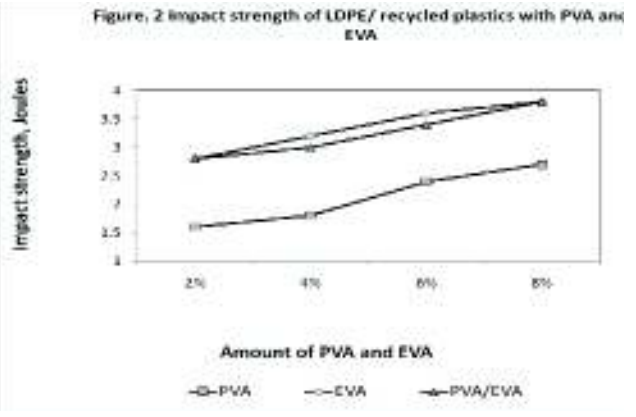
Figure. 2 Impact strength of LDPE/ recycled plastics with PVA and EVA
Impact strength, Joules
4
3.5
3
2.5
2
2%
4%
6%
8%
Amount of PVA and EVA
PVA
EVA
PVA/EVA

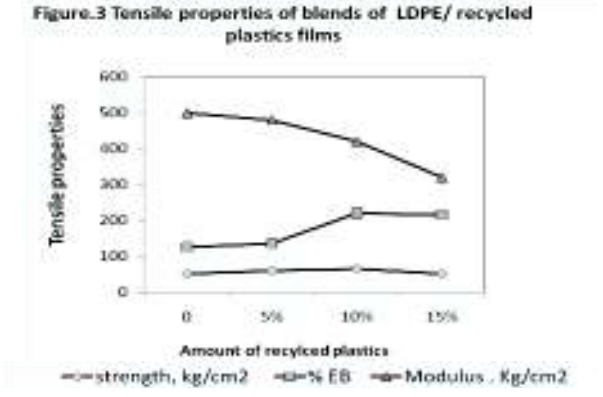
Figure.3 Tensile properties of blends of LDPE/ recycled plastics films
Tensile properties
600
500
400
300
200
100
0
0
5%
10%
15%
Amount of recycled plastics
strength, kg/cm2
% EB
Modulus , Kg/cm2

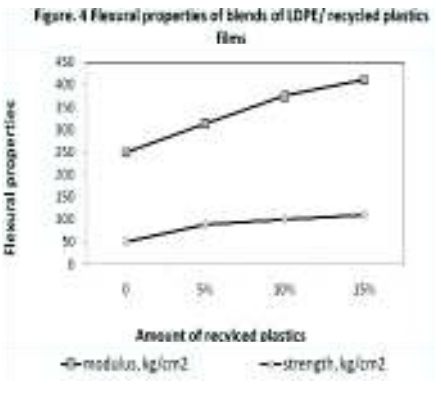
Figure. 4 Flexural properties of blends of LDPE/ recycled plastics films
Flexural properties
450
400
350
300
250
200
150
100
50
0
0
5%
10%
15%
Amount of recycled plastics
modulus, kg/cm2
strength, kg/cm2

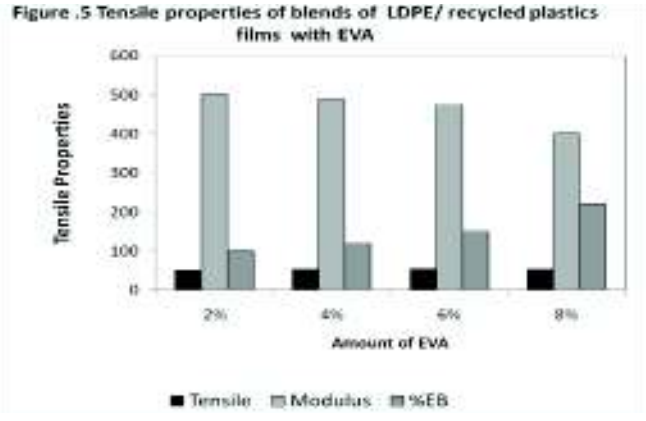
Figure .5 Tensile properties of blends of LDPE/ recycled plastics films with EVA
Tensile Properties
600
500
400
300
200
100
0
2%
4%
6%
8%
Amount of EVA
Tensile
Modulus
%EB

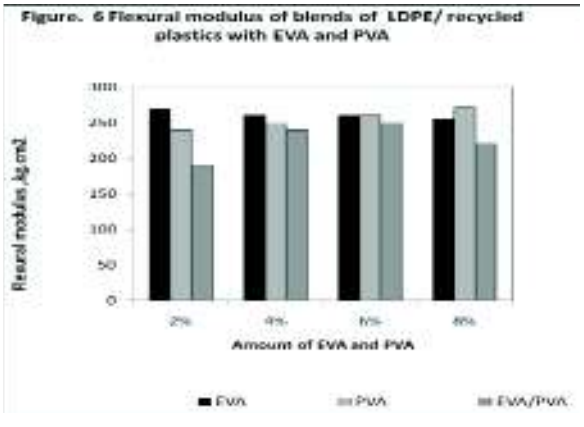
Figure. 6 Flexural modulus of blends of LDPE/ recycled plastics with EVA and PVA
Flexural modulus ,kg/cm2
Amount of EVA and PVA
EVA
PVA
EVA/PVA

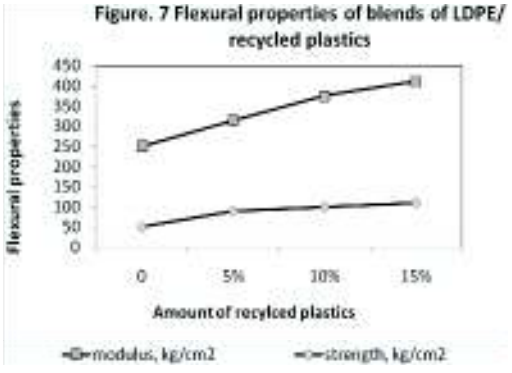
Figure. 7 Flexural properties of blends of LDPE/ recycled plastics
Flexural properties
450
400
350
300
250
200
150
100
50
0
0
5%
10%
15%
Amount of recycled plastics
modulus, kg/cm2
strength, kg/cm2

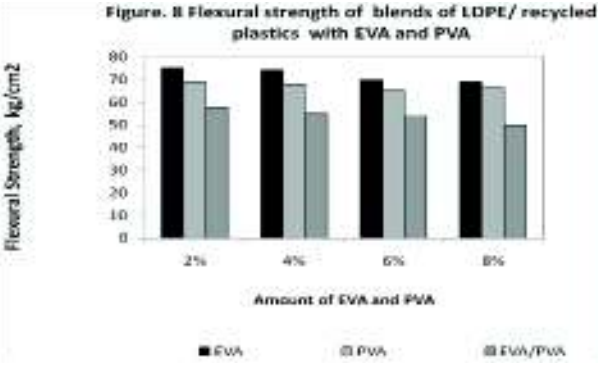
Figure. 8 Flexural strength of blends of LDPE/ recycled plastics with EVA and PVA
Flexural Strength, kg/cm2
80
70
60
50
40
30
20
10
0
2%
4%
6%
8%
Amount of EVA and PVA
EVA
PVA
EVA/PVA

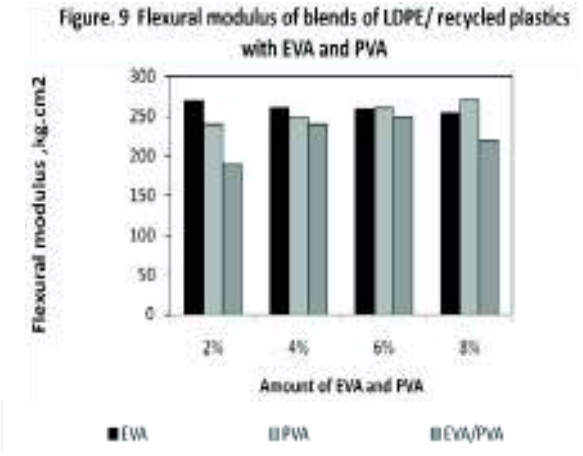

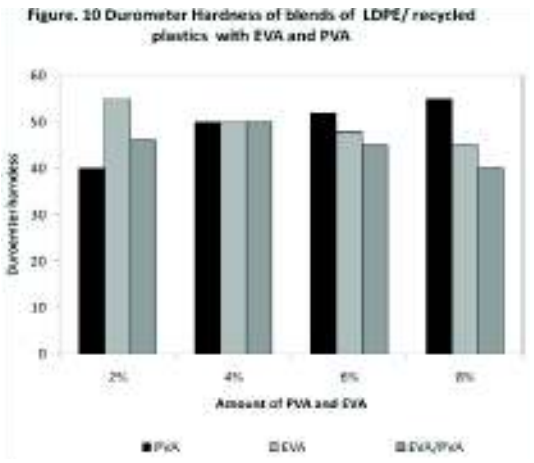

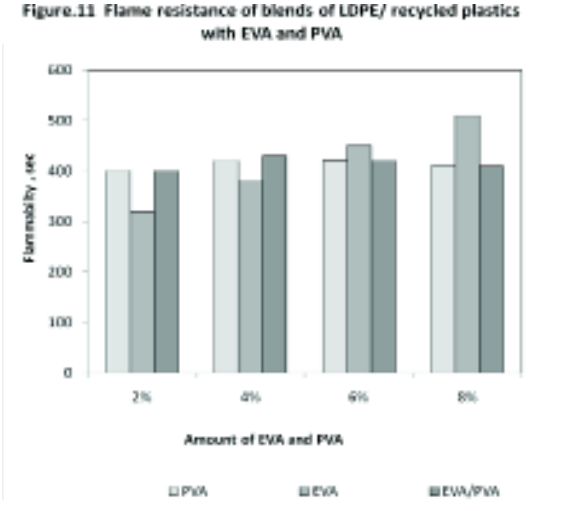

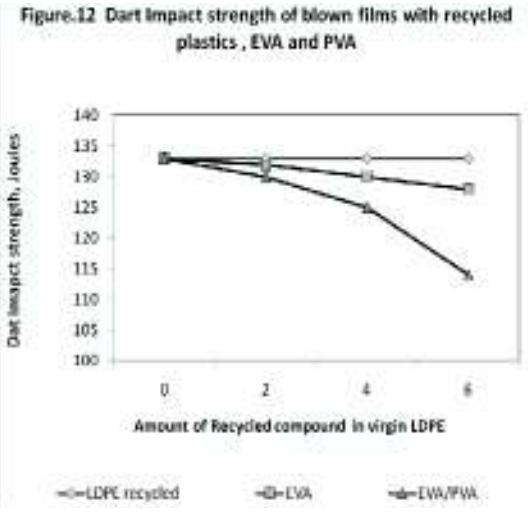

very greater extend. Toughness of the matrix is found to be increased with PVA and the amount is more significant in EVA. EVA is a flexible material and increases the flexibility and impact strength.

Figure 3 shows the tensile properties of blends of LDPE/ recycled plastics. The results indicated that the tensile strength does not vary, tensile modulus decreased and elongation at break decreased. This is due to the increased flexibility imparted by recycled plastics. The stiffness of recycled plastics is lower compared to virgin LDPE. Figures 4-6 show the tensile strength of the blends LDPE/ recycled plastics with EVA, PVA and EVA/PVA combined respectively. Tensile strength and modulus with EVA is slightly lower but elongation increases as EVA is flexible material. In case of PVA and in PVA/EVA blends, Tensile strength and modulus increases as the amount increases. All properties show an optimum level of addition for property enhancement. EVA and PVA can increase the polarity and miscibility of the blends therefore recycled LDPE addition does not decreases the original properties of the blends.

Figure 7 shows the flexural strength and flexural modulus of blends of LDPE/ recycled plastics. It is found that by the addition of LDPE recycled enhancement in flexural strength and modulus of the blends were observed. The total stiffness of the compounds is improved by addition of recycled plastics and blending with EVA, PVA and EVA/PVA mixture. Figure 9 shows the flexural modulus of the LDPE/ recycled plastics blends with EVA, PVA and EVA/PVA mixture. The flexural strength and modulus of all blends are not affected but shows increasing trends even though all contain the recycled LDPE. Thus it indicates that recycled LDPE can be added without affecting the properties.

Figure 10 shows the Durometer hardness (shore D) of the LDPE/ recycled blends. In case of PVA hardness increases initially and then decreases on further increase in PVA. In the blends with EVA hardness decreases as EVA is a flexible and soft material compared to LDPE.

Figure 11 shows the EVA based blends the flammability increases to a greater extend with the amount of EVA and in all other cases flammability increasers marginally. Therefore LDPE recycled can be added to virgin LDPE and can be used in flame-retardant application also.

Figure 12 shows the dart impact strength of the films prepared using blends of LDPE/ recycled plastics blended with virgin LDPE. In case of EVA and PVA blend compound there is a decrease in dart impact due to the addition of blends and this is due to the lower miscibility of PVA with virgin LDPE. In case of recycled plastics and EVA dart impact strength remain unchanged. It gives the confirmation that recycled plastics can be easily added to the virgin LDPE without affecting the impact properties of the films. PVA is polar material and shows very less compatibility with LDPE thus decreases the impact strength of LDPE films.

Table 2: Volume and Surface Resistivity of the blends.

Samples	Volume resistivity, ohm	Surface resistivity, ohm
0, 5, 10, 15 & 20 % in LDPE/ recycled plastics blends	$92.4x10^{10}$	$26.3x10^{10}$
2. 4, 6, 8 % PVA in LDPE/ recycled plastics blends	$41.36X10^{12}$	$108.8x10^{12}$
2. 4, 6, 8 % EVA in LDPE/ recycled plastics blends	$37.6x10^{12}$	$92.4x10^{12}$
2. 4, 6, 8 % EVA + PVA in LDPE/ Recycled plastics blends	$48.88x10^{12}$	$81.6x10^{12}$

Table 3: Chemical Resistance of the compounds.

Samples	Weight loss in gm 1N NaOH	Weight lose in gm, 1N HCl
0, 5, 10, 15, 20 % recycled plastics in blends	0.001	0.002
2, 4, 6, 8 % EVA in LDPE/ recycled plastics blends	0.020	0.000
2, 4, 6, 8 % PVA in LDPE/ recycled plastics blends	0.000	0.000
2, 4, 6, 8 % EVA + PVA in LDPE/ recycled plastics blends	0.009	0.011

Table 4: Abrasion loss of the compounds.

Samples	Abrasion Resistance, weight loss (gm/cycles)
0% recycled plastics in blends	2.4×10^{-5}
5% / recycled plastics / LDPE blends	2.6×10^{-5}
10% recycled Plastics/ LDPE blends	3.4×10^{-5}
15% recycled plastics / LDPE blends	3.0×10^{-5}
2, 4, 6, 8 %EVA in recycled plastics / LDPE blends in	$2.4x10^{-5}$
2, 4, 6, 8 % PVA in recycled plastics/LDPE blends	$4x10^{-6}$
2, 4, 6, 8 % EVA+PVA in recycled plastics/LDPE blends	$6x10^{-6}$

Table 5: Adhesion strength, Plastics to Plastics bonding.

Samples: Adhesive joints : Plastics to Plastics	Load (Kg/F)
0, 5, 15, 20 % recycled plastics /LDPE blends	120
2, 4, 6, 8, % EVA in recycled plastics /LDPE blends	130
2, 4, 6, 8 % PVA in recycled plastics /LDPE blends	134
2, 4, 6, 8 % EVA+PVA in recycled plastics /LDPE blends	134

Table 2 shows that there is no change in resistivity values of the compounds when blended with recycled LDPE and also with EVA and PVA. Table 3 shows the chemical resistance of the compounds in 1N NaOH and 1N HCl. It is evident that by blending with recycled LDPE there is no change in chemical resistance. The weight loss of the sample was very negligible in both solutions. Table 4 shows the abrasion resistance of the compounds which were also extremely small in all types of compounds.

Joints of metal to metal, leather to leather and plastics to plastics were prepared out of the compounds which contain recycled LDPE. The joints were made using hot melt adhesives based on the blends prepared. Bond ability is found to be very good. In case of leather to leather joint the leather adherent breaks around 130-135 Kg/F and joints were unaffected. In Metal to Metal Bonding bond Strength was greater than 250 Kg/F. This indicates that the recycled compounds can be very well used as hot melt adhesives, shows excellent bond strengths. In all the types of adherents the results were similar.

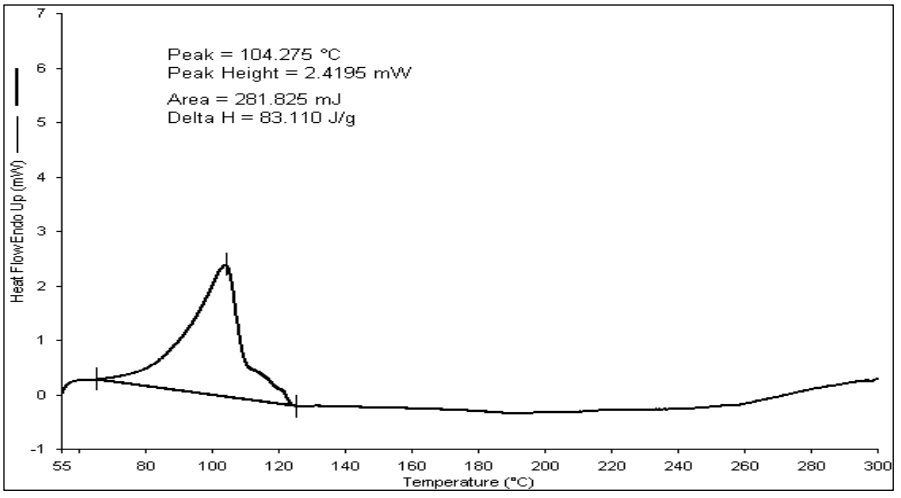

DSC Curve 1: Blend of LDPE/recycled plastics (20 %)

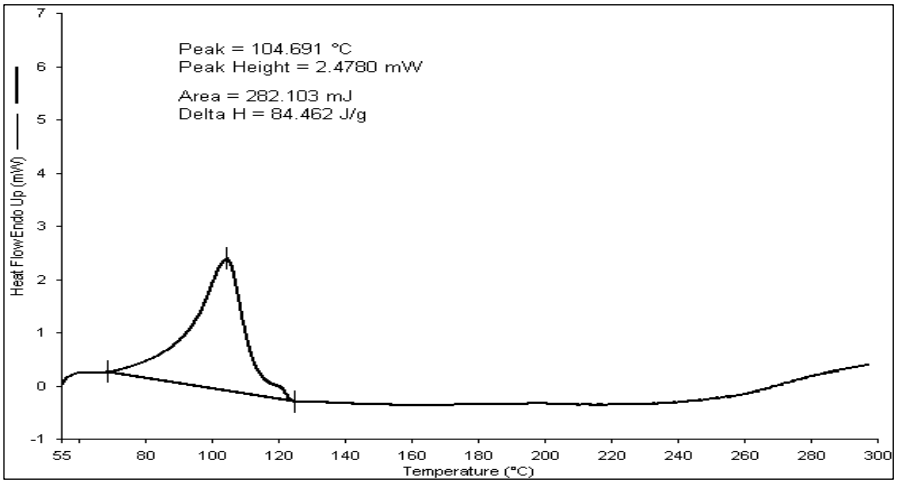

DSC Curve 2: Blend of LDPE/ recycled plastics with (8%) EVA

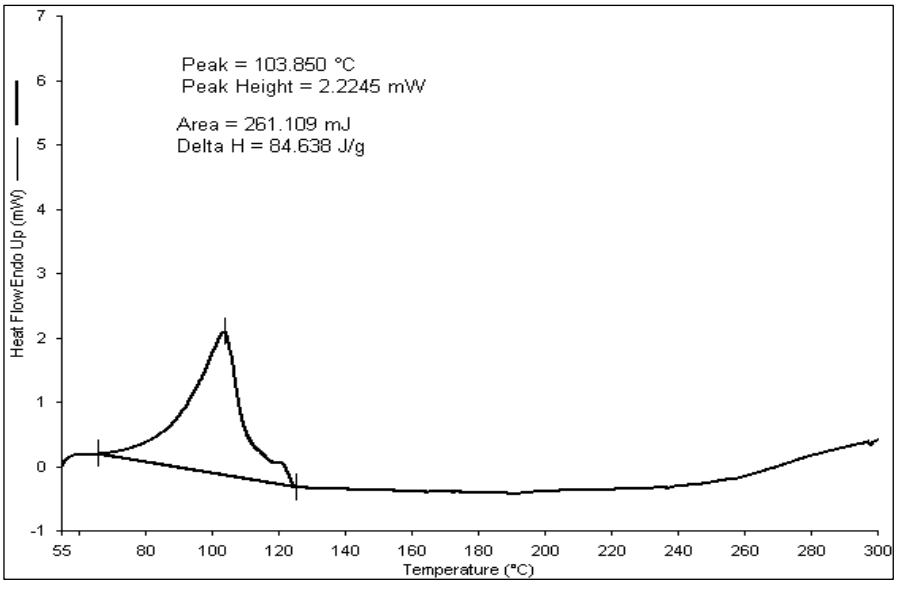

DSC Curve 3: Blend of LDPE/ recycled plastics with (8%) PVA and EVA

From DSC peaks (DSC Curves 1-3) melting temperature of all the blends are found to be equal and peak height, area and enthalpy remains same. It confirms that the addition of LDPE pouches doesn't vary its melting characteristics. The peak melting point is around 103 ^{0} C peak area 260 mJ and delta H 84 J/gm which are common to all blends. This confirms that blending virgin LDPE with recycled LDPE does not make any change in processing characteristics, therefore very easily processed with maximum usage of recycled plastics.

CONCLUSIONS

Recycled plastics films were blended with virgin LDPE in different ratios. The blends were further modified with EVA and PVA. Mechanical properties, chemical properties, flammability, resistivity and DSC thermogram were estimated.

The blends were used making injection molding specimens, compression molding sheets, blown films and also used in hot melt adhesives for substrates like metal to metal, plastics to plastics and leather to leather. Joints were exhibiting superior bond strengths. The recycled plastics based compounds were added to film grade virgin LDPE for making blown films. The films were of high quality and the process for making the recycled compounds were very simple and cost effective. The waste plastics films were converted into useful products thus it opens an easy way of disposal of used plastics packaging films.

REFERENCES

[1] Brydson, J. J. A. (1995) *Plastics Materials*, Butterworth, London.

[2] Brydson, J. A. (1994) *Specialty Rubber*, Rapra Review 74.

[3] Hensen, F. (1997) *Plastics Extrusion Technology*, Hanser Publication, New York.

[4] Fält, S., Wågberg, L., Vesterlind, E. L., Larsson, P.T. (2004) Model films of cellulose II – improved preparation method and characterization of the cellulose film. *Cellulose,* **11(2)**: 151-162.

[5] Weng, M. (1991) Sorbic Anhydride as Antimycotic Additive in Polyethylene Food Packaging Films. *Journal of Food Science*, **56**: 274–275.

[6] Frank Esposito (2010) Oxo-biodegradable additive suppliers rebut critics. *Plastics News*, 2.

[7] Wilfried Paulus, Dylingowski, P. J. and Hamel, R. G. (2006) Microbial degradation of plastics. In: *Directory of Micro-bicides for the Protection of Materials A Handbook,* pp-340.

[8] Otey, H.F. and Doane, M.W. (1984) In: *Starch: Chemistry and technology*" 2nd Edn, Academic Press, New York, pp-384.

[9] Rachel Cernansky, (2009) "Recycling plastic is tricky business, and many plastics are better off as garbage", *Discover science Technology the future.* pp-240.

[10] Read, P. S. Phillips (2003), M. C. C. Armijo de Vega, *Delivering more sustainable Waste Management in Mexico, Resources, Conservation and Recycling*, **39(3)**: 187-296.

[11] Inyang, H. I., de Brito Galvao, T.C. and Hilger, H. (2003) Utilization of Wastes Resources. *Conservation and Recycling,* **39(1)**: 1-105.

[12] Gonçalves, S. P. C., Martins-Franchetti, S. M. and Chinaglia, D. L. (2009) Biodegradation of the Films of PP, PHBV and Its Blend in Soil. *Journal of Polymer and Environment,* **17(14)**: 12.

[13] Issam, A. M., Poh, B. T., Abdul Khalil, H. P. S. and Lee, W. C. (2009) Adhesion Properties of Adhesive Prepared from Waste Polystyrene. *Journal of Polymer and Environment,* **1(3)**: 22.

[14] Hilary, I. Inyang, Terezinha Cássia de Brito Galvão and Helene Hilger (2003) Waste recycling within the context of industrial ecology. *Resources, conservation and recycling* **39**: 1.

[15] Shih-Cheng, Pan, Chin-Chi, Lin and Dyi-Hwa, Tseng (2003) Reusing sewage sludge ash as adsorbent for copper removal from wastewater. *Resources, conservation and recycling,* **39(1)**: 39.

PRAJÑĀ - Journal of Pure and Applied Sciences
Vol. 17: 086-090 2009 ISSN 0975 - 2595

STUDY OF REVERSAL IN INHIBITION OF CORROSION OF MILD STEEL IN H_2SO_4 AT HIGHER CONCENTRATION OF THIOUREA BY ELECTROCHEMICAL IMPEDANCE SPECTROSCOPY

N. S. Patel,* S. Jauhari and G. N. Mehta

Applied Chemistry Department, S. V. National Institute of Technology, Surat, Gujarat - 395 007

ABSTRACT

The inhibition effect of thiourea against mild steel corrosion in 1 N H_2SO_4 solutions was evaluated using potentiodynamic polarization, linear polarization and electrochemical impedance spectroscopy. Mild steel working electrode was exposed along with Pt counter electrode and saturated calomel reference electrode in stagnant 1 N H_2SO_4 solution at an ambient temperature. Corrosion behavior of mild steel in absence and presence of 2 mM, 5 mM, 10 mM, 20 mM, 50 mM and 100 mM of thiourea was studied. It was found that at higher concentration of 50 mM and 100 mM of thiourea, the reversal in inhibition of the corrosion was observed.

Keywords: **mild steel, thiourea, electrochemical impedance spectroscopy, acid corrosion.**

INTRODUCTION

The corrosion of iron and mild steel (MS) is a fundamental academic and industrial concern that has received a considerable amount of attention [1]. A study of the mechanism of the action of corrosion inhibitors has relevance both from the point of view of the search for new inhibitors and also for their effective use [2]. Huge amount of acid solutions are used in the chemical industry for removal of the undesired scales and rust. The addition of corrosion inhibitors effectively secures the metal against an acid attack. Inhibitors are generally used in these processes to control metal dissolution [3] and, during past decade many organic inhibitors have been studied in different media [4-7].

Thiourea (TU) is an effective inhibitor for corrosion of MS in acidic media [8-10], especially in industrial operations such as pickling, descaling, cleaning, acidization of oil wells, to protect metals and alloys. It acts as a protective film and is superior to amine-based inhibitors in acidic media. This kind of inhibitor simultaneously acts in both anodic and cathodic areas. Sulfur containing compounds, such as TU, are very effective corrosion inhibitors for steel in acidic conditions because sulfur atom is easily protonated in acidic solution and a stronger electron donor than nitrogen [11, 12]. Therefore sulfur atom is more strongly adsorbed to the metal surface. It has been observed that adsorption mainly depends on the presence of π-electrons and heteroatoms, which induce greater adsorption of the inhibitor molecules onto the surface of metal. Mechanism of action of inhibitors considers that most chemical reactions can be treated as acid–base interactions [13]. Based on this concept, TU would act as a rather strong base due to its sulfur, which serves as an electron donor. On the other hand, Fe^{3+}, Fe^{2+} and metallic Fe would behave like acids. Herein, they act as electron acceptors, with higher acidity corresponding to higher oxidation state. This interaction with the inhibitor would proceed mainly due to the presence of long-range electrostatic forces [13]. TU has been studied in HCl, H_2SO_4, HNO_3 and H_3PO_4 at various concentrations like 2, 5, 10, 20 and 50 mM by thermometric and weight loss methods using similar concentrations [8], TU was evaluated as an effective inhibitor in HCl and H_2SO_4 by Linear Polarization Resistance (LPR) and Tafel extrapolation methods [9]. It was observed that at the lower concentrations of 2 and 5 mM of TU, the inhibition efficiency was comparatively low because of removal of the inhibitor layer on the metal surface due to hydrodynamic effect. Moreover, at the higher concentration of 50 mM of TU, the reversal in inhibition was observed due to reduction of TU on the TU layer [14, 15] which was studied by above stated electrochemical techniques and by A C impedance technique.

In this paper TU is again evaluated only in stagnant 1 N H_2SO_4 at an ambient temperature

* Corresponding author – niketan.ptl@gmail.com

(30°C) using recently imported CHI680B A C impedance analyzer (USA) with three electrodes system in order to study the effect of TU on the reversal of inhibition at much higher concentration of 100mM also assuming that at 100mM, there might be retardation in the reversal of inhibition.

EXPERIMENTAL

Inhibitor Preparation

The molecular formula of TU is shown in Fig. 1. The choice of the compound is based on molecular structure considerations; the presence of N, S, O atoms is likely to facilitate the adsorption of the compound on the metal surface.

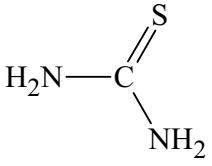

Figure 1: Molecular structure of TU.

Preparation of Specimens

Cylindrical working electrodes of MS containing 0.09% P, 0.37% Si, 0.01% Al, 0.05% Mn, 0.19% C, 0.06% S and the remainder Fe, were used for the electrochemical polarizations and impedance measurements. The surface preparation of the mechanically polished specimens were carried out using different grades of emery papers, degreased with acetone dried at room temperature and then stored in a desiccator before use.

Electrochemical and impedance measurements

A three-electrode cell of Borosil glass, consisting of a working electrode (WE) of MS, a pure platinum counter electrode (CE), and saturated calomel electrode (SCE) as a reference electrode, was used for the measurements. The electrolytes used were acidic solutions maintained at 30°C. The AC impedance measurements are shown as Nyquist plots and polarization data as Tafel plots. CH Electrochemical analyzer model 608 C (USA) was used for this purpose. Polarization resistance measurements were carried out with a scan rate of 0.01 V/s at −10mV to +10mV vs. corrosion potential (E_{corr}) of the working electrode measured against SCE. Polarization curves obtained again with the scan rate of 0.01 V/s in the range of −250mV to +250mV vs. E_{corr}. Impedance measurements were carried out at the E_{corr}; 60 min after the electrode had been immersed in the test solution. The frequency range studied was 0.1Hz to 1000Hz. The A.C. signal was 5 mV peak-to-peak with 12 data points per decade.

RESULTS AND DISCUSSION

The potentiodynamic polarization data are shown as the Tafel plots for MS in 1 N H_2SO_4 with the addition of various concentrations of the additive in Fig.1. The corrosion kinetic parameters such as corrosion potential (E_{corr}), corrosion current density (I_{corr}), anodic and cathodic Tafel slopes (b_a and b_c) were derived from these curves and are given in Table 1. The values of inhibition efficiency (E_I %) are calculated using the following equation.

$$E_I\% = 100 \times \frac{I_{corr} - I_{corr(inh)}}{I_{corr}} \qquad \text{..... (1)}$$

Where I_{corr} and $I_{corr(inh)}$ are the values of corrosion current densities of MS without and with the additive, respectively, which were determined by extrapolation of the cathodic and anodic Tafel lines to the corrosion potential E_{corr}.

The inhibiting properties of the tested TU have also been evaluated by the determination of the polarisation resistance. The corresponding polarisation resistance (R_p) values of MS in 1 N H_2SO_4 in the absence and presence of different concentrations of the additive are given in Table-1. The inhibition efficiency (E_{Rp}%) was defined as follows:

$$E_{Rp}\% = 100 \times \frac{R_{P(inh)} - R_P}{R_{P(inh)}} \qquad \text{..... (2)}$$

R_p and $R_{p(inh)}$ are the polarisation resistance in the absence and in the presence of the inhibitor, respectively.

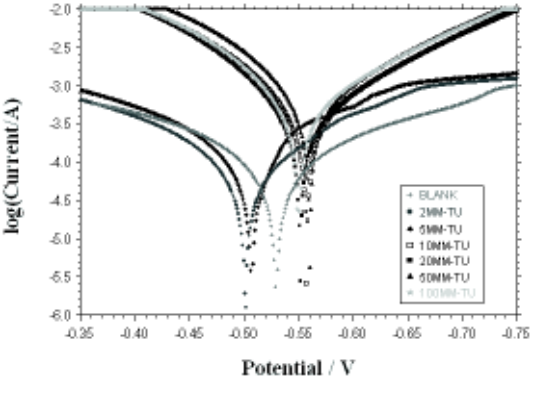

Figure 2: Tafel plots showing effect of TU on corrosion of MS in H_2SO_4 medium.

Table 1: Effect of TU on MS in 1N H_2SO_4 media (Electrochemical polarizations studies).

Concentration of inhibitor (ppm)	E_{corr} V	Tafel Constant (mV/decade) ba	bc	Corrosion Current Density (mA/cm^2)	R_p (ohm cm^2)	E_I %	E_{Rp}%
0mM TU	-0.5308	80	120	5.914	06	-	-
2mM TU	-0.5024	80	115	2.465	11	58.3	45.5
5mM TU	-0.5096	75	115	1.986	15	66.4	60.0
10mM TU	-0.5569	70	110	1.364	26	76.9	76.9
20mMTU	-0.5535	65	100	0.995	39	83.2	84.6
50mMTU	-0.5613	70	115	1.684	24	71.5	75.0
100mMTU	-0.5512	75	105	2.065	14	65.1	57.1

From the Table 1, it is observed that the I_{corr} values gradually decreased with increase in the concentration of inhibitor from 2 mM to 20 mM, with respect to the blank. Further, increase in the concentration up to 50 mM to 100 mM, there was a sharp decrease in the values of I_{corr}. It could be derived from this decrease that there was some kind of reversal trend established.

The R_p values of MS in 1N H_2SO_4 in the absence and presence of different concentrations of the tested inhibitor are also given in Table 1. From the results, R_p values gradually increased with increase in the concentration of inhibitor from 2 mM to 20 mM and E_{Rp}% increases to attain 84.6% at 20 mM. Here also the above reversal trend continued as R_p values for 50 mM & 100 mM decrease with increase in the concentration. The values of inhibition efficiency of TU obtained by electrochemical methods are in good agreement.

The corrosion behavior of MS in 1N H_2SO_4, in absence and the presence of various concentrations of TU were also investigated by electrochemical impedance spectroscopy (EIS) technique. The resultant Nyquist plots are shown in Fig. 3. The values of inhibition efficiency (E_R %) were calculated by the equation as follows.

$$E_R\% = 100 \times \frac{R_{t(inh)} - R_t}{R_{t(inh)}} \qquad \text{..... (3)}$$

Where R_t and $R_{t(inh)}$ are the charge-transfer resistance values in absence and the presence of the inhibitor, respectively.

To obtain the values of double layer capacitance (C_{dl}), the values of frequency at which the imaginary component of the impedance is maximum $-Z_{im(max)}$ was found and used in the following equation with corresponding R_t values:

$$C_{dl} = \frac{1}{2\pi f_{\max} R_t} \qquad \text{..... (4)}$$

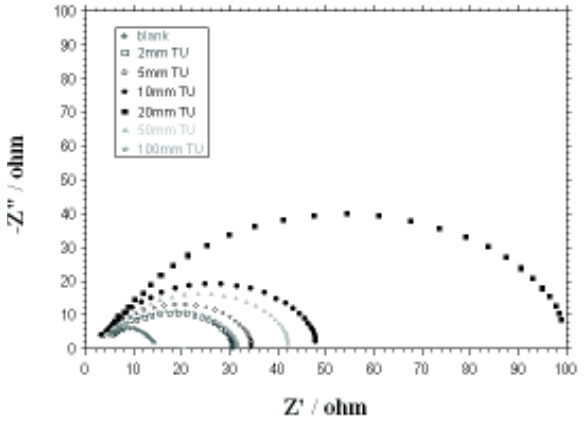

Figure 2: Nyquist plots showing effect of TU on corrosion of MS in H_2SO_4medium.

The existence of a single semicircle in Nyquist plot shows that there was only single charge transfer process during the anodic dissolution of MS and remained unaffected in the presence of TU added in the acid. The value of real impedance (Z') for blank was only 15 Ohms which indicated that there was least charge transfer resistance (R_t) of the corrosion reactions. There was gradual increase in the diameter of each semicircle of the Nyquist plot when the concentration was raised from 2 to 20 mM. This increase of the diameters clearly reflected that the R_t values also increased from 15 to 100 Ohms at concentration of 20 mM due to formation and gradual improvement of the barrier layer of the inhibitive molecules (IE 85 %), and as a result the acid corrosion rate of MS gradually decreased. Decrease in the R_t values confirms the reversal trend at 50 mM & 100 mM concentrations.

Table 2: Data from electrochemical impedance measurements of mild steel in 1 N H_2SO_4 for various concentrations of TU.

Concentration of inhibitor (ppm)	R_t Ohm.cm^2	Cdl μF/cm^2	Inhibition Efficiency IE (%)
0mM TU	15	148.2	-
2mM TU	28	123.9	46.4
5mM TU	35	105.6	57.1
10mM TU	48	90.5	68.8
20mMTU	100	82.3	85.0
50mMTU	41	94.6	63.4
100mMTU	31	111.2	51.6

Table 2 embodies various parameters such as R_t and C_{dl}. There was a gradual decrease in values of C_{dl} with increase in the concentration of TU. The double layer between the charged metal surface and the solution is considered as an electrical capacitor [16]. The adsorption of the TU on the electrode decreases its electrical capacity because they displace the water molecule and others ions originally adsorbed on the surface. The decrease of this capacity with increasing TU concentrations (except at 50 mM & 100 mM) may be associated with the formation of a protective layer at electrode surface. And the results obtained from EIS show the similar trend as those obtained from electrochemical polarisations.

The reversal trend in the results at 50 mM is observed and it is further continued even at higher concentration of 100 mM may be due to the degradation of the TU layer adsorbed by the reduction of TU in to corrosive species like HS^- ions [17] and H_2S [18] or due to protonation of TU [19] which might have catalyzed the H_2 evolution reaction.

CONCLUSIONS

- Corrosion of mild steel in stagnant 1 N H_2SO_4 at 30^{o}C was effectively inhibited by TU.
- There was gradual increase in inhibition with the gradual increase from 2 mM, 5 mM, 10 mM and 20 mM of concentration of TU, the reversal in inhibition, was observed when the concentration of TU was further increased from 20 mM to 50 mM and 100 mM due to reduction and protonation of TU because of the degradation of adsorbed layer of the inhibitor.
- The results of the electrochemical polarizations and EIS were all in very good agreement to support the above conclusions.

REFERENCES

[1] Uhlig, H. H. and Revie, R. W. (1985) *Corrosion and Corrosion Control*, Wiley, New York, pp.1-185.

[2] Trabanelli, G. (1991) Inhibitors - An Old Remedy for a New Challenge. *Corrosion*, **47**: 410-419.

[3] Schmitt, G. (1984) Application of inhibitors for acid media. *British Corr. J.,* **19**: 165-176.

[4] Tebbji, K., Bouabdellah, I., Aouniti, A., Hammouti, B., Oudda, H., Benkaddour, M. and Ramdani, A. (2007) N-benzyl-N, N-bis [(3, 5-dimethyl- 1H – pyrazol – 1 -yl) methyl] amine as corrosion inhibitor of steel in 1 M HCl. *Material Letters*, **61**: 799-804.

[5] Bentiss, F., Gassama, F., Barbry, D., Gengembre, L., Vezin, H., Lagrenee, M. and Traisnel, M. (2006) Enhanced corrosion resistance of mild steel in molar hydrochloric acid solution by 1, 4-bis (2- pyridyl) - 5H –pyridazino [4, 5-b] indole: Electrochemical, theoretical and XPS studies. *App. Surface Sci.*, **252**: 2684-2691.

[6] Prabhu, R. A., Shanbhag, A. V. and Venkatesha, T. V. (2007) Influence of tramadol [2- [(dimethylamino) methyl] -1 - (3- methoxyphenyl) cyclohexanol hydrate] on corrosion inhibition of mild steel in acidic media. *J. App. Electrochem.*, **37**: 491-497.

[7] Avci, G. (2008) Corrosion inhibition of indole-3-acetic acid on mild steel in 0.5M HCl. *Colloids and Surfaces A: Physicochemical Engineering Aspect*, **317**: 730-736.

[8] Mehta, G. N. (1979) *Electrochemical Techniques for the study of Passivity and Evaluation of Inhibitors*, Ph. D. Thesis, South Gujarat University, Surat.

[9] Mehta, G. N. (1988) Tafel intercept and linear polarisation resistance techniques to study acid corrosion of mild steel & effect of thiourea. *Bull. Electrochem.*, **4**: 111-115.

[10] Shamis-El-Din, A. M., Hosary, A. A., Saleh, R. M. and Abd-El-Kader, J. M. (1977) Peculiarities in the behavior of thiourea as corrosion inhibitor. *Werkstattund Korros*, **28**: 26-31.

[11] Agrawal, R. and Namboodhiri, T. K. G. (1989) The inhibition of sulphuric acid

corrosion of 410 stainless steel by thioureas, *Corrosion Sci.*, **30**: 37-52.

[12] Ali, S. A., Saeed, M. T. and Rahman, S. V. (2003) The isoxazolidines: a new class of corrosion inhibitors of mild steel in acidic medium, *Corrosion Sci.,* **45**: 253-266.

[13] Mansfeld, F. B. (1993) Determination of Coating Deterioration with Electrochemical Impedance Spectroscopy. *Corrosion,* **49**: 726.

[14] Ateya, B. G., El-Anadouli, B. E. and El-Nizamy F. M. (1984) The effect of thiourea on the corrosion kinetics of mild steel in H_2SO_4. *Corrosion Sci.*, **24**: 497-507.

[15] Ateya, B. G., El-Anadouli, B. E. and El-Nizamy F. M. (1984) The adsorption of thiourea on mild steel. *Corrosion Sci.*, **24**: 509-515.

[16] Bentiss, F., Lagrenée, M., Traisnel, M. and Hornez, J. C. (1999) The corrosion inhibition of mild steel in acidic media by a new triazole derivative. *Corrosion Sci.*, **41:** 789-803.

[17] Makrides, A. C. and Hackerman, N. (1955) Effect of thiourea compounds on dissolution rate of iron and mild steel - adsorption and inhibition, steady state and potential. *Ind. Eng. Chem.*, **47**: 1773.

[18] Parsons, R. (1961) The structure of the mercury-electrolyte interphase in the presence of thiourea. *Proc. Royal Soc.***, 261**: 79-90.

[19] Pillai, K. C. and Narayan, R. (1978) Inhibition of corrosion of iron in acids by thiourea and derivatives. *J. Electrochem Soc.*, **125**: 1393-1397.

PRAJÑĀ - **Journal of Pure and Applied Sciences**
Vol. 17: 091-093, 2009 ISSN 0975 - 2595

CHEMICAL REFINING AND ITS EFFECT ON COLOUR OF THE VEGETABLE OIL

Sibban Singh *

Department of Industrial Chemistry, Institute of Science and Technology for Advanced Studies and Research (ISTAR), Vallabh Vidyanagar, Gujarat – 388 120

ABSTRACT

Crude cottonseed oil is one of the dark colour fatty oil of oleic-linoleic group used for edible purposes in India. In the present investigation it has been tried to refine it chemically by alkali (sodium hydroxide) and study its effect on the reduction in colour of the oil. The experiments were carried out by varying the excess amount of alkali and its concentration to remove the free fatty acids present in the oil. The acid value of refined oil changes by using higher amount of excess alkali but proportionally increasing oil loss and resulting poor yield of refined oil. It was concluded that the optimum level of excess amount of alkali was 12% at 15% concentration (w/v) in order to reduce the colour value.

Keywords: **crude cottonseed oil, free fatty acid, refining and pigments.**

INTRODUCTION

Cottonseed oil [1] is one of the edible oils popularly used in India. In natural form it is very dark in colour which must be reduced to light colour prior to its application. It also contains free fatty acids (FFA) which poses many problems while frying operation resulting bad flavour and odour in the cooked items. Therefore its removal becomes essential. Gossypol and related pigments of cottonseed oil readily combine with caustic soda and thus are removed more or less completely by alkali refining process. Oils that are presumably coloured by carotenoid pigments are also lightened by alkali refining, although it is probable that the pigments are physically adsorbed on the soap formed by the alkali rather than chemically combined. The absorptive capacity of the soap is limited, however other vegetable oils such as palm oil, tung oil etc., which are very strongly coloured by carotene, are apparently little affected with by alkalis. The cottonseed oil is chemically refined by the addition of sodium hydroxide at a level sufficient to neutralize the free fatty acids present in the oil [2]. An excess amount of sodium hydroxide is required to reduce colour of the refined oil. The amount of sodium hydroxide depends on the FFA content and other impurities present in the crude oil. The caustic used in alkali refining process is normally diluted to 8.0 to 14.0% although higher concentration is occasionally used to reduce the colour. Any soap remaining after the primary soap-stock separation from refine oil is removed by hot water washing. In this step, 10-15% water is added at a temperature sufficient to prevent emulsification (generally 180-195^{0}F). Various researches and developments have been done about reducing the impurities present in cottonseed oil [3-7]. In the present study the effort has been made to conduct experiments on removal of FFA from crude cottonseed oil with alkali of different concentrations using variable excess amounts with a view to achieve least acid value and colour of the product.

MATERIALS AND METHODS

The crude cottonseed oil used for the present experimental work was procured from M/s ARCOGUL (Anand Regional Co-operative Oilseeds Growers Union Limited), Chikhodara, Gujarat. Sodium hydroxide required for chemical refining process was purchased from Chiti-Chem. Corporation, Baroda. All other chemicals used for analytical work were of A R grade obtained from M/s S.D. Fine Chemicals, Boisar, Maharashtra.

The physico-chemical characteristics of experimental oil sample such as Specific gravity, Acid value, Saponification value, Iodine value and Refractive index were determined by AOCS methods [8]. The percentage of free fatty acid is approximately half of acid value of the oil calculated as oleic acid. Gardner scale [9] was used to measure the colour value of the oil sample.

* Corresponding author – sibban_singh@yahoo.co.in

Chemical refining of crude cottonseed oil

100 gm of oil sample was taken into 250 ml beaker and stirred for 5 – 10 min by maintaining the temperature at 60 – 70 ^{0}C. Then after the calculated amount of caustic soda solution as per free fatty acid content of oil was added slowly to it. It was further stirred for one to one and half an hour at same temperature. The soap-stock thus formed was allowed to settle down and then separated with the help of separating funnel. The upper layer was made free from alkalinity by washing with hot distilled water. The washed oil thus obtained was dried by heating for 10-15 min under vacuum and then it was analyzed for colour, acid value and yield of refined oil. The experiments were repeated for different proportion of excess amount of alkali over stoichiometrically needed such as 5%, 8%, 12%, 16% and 20% each treated for five different concentrations e.g. 6%, 9%, 12%, 15% and 18% taken as weight by volume.

RESULTS AND DISCUSSION

The cottonseed oil sample was procured from ARCOGUL (Anand regional co-operative oilseeds growers union limited) chikhodra, Gujarat. It was analyzed for its physico-chemical characteristics and the results were depicted in Table 1. It is clear from the table that acid value of crude oil is 5.7 i.e. 2.9 % FFA. Also the colour of oil is 11 on gardner scale (10% solution in acetone).

Table 1: Physico–chemical characteristics of experimental crude cottonseed oil*.

Sr. no	Characteristics	Value
1	Specific gravity at 30^{0}C	0.917
2	Colour** (gardner scale)	11.0
3	Acid value	5.8
4	Saponification value	192.0
5	Iodine value	105.8
6	Refractive index at 40^{0}C	1.4650

* -- average of two determination with variation up to ±0.5
** -- 10% solution in acetone

On the basis of these results the experiments were conducted to neutralize the FFA from crude cottonseed oil with caustic soda solution by varying the percentage of excess amount of alkali and also its concentration. Table 2 shows the effect of different concentrations on colour, acid value and percentage yield by taking 4% excess alkali. Results show that with the increase in concentration of solution, the colour of oil and acid value decreases from 6.5 to 4.5 and 1.6 to 1.0 respectively. However, there is no significant change in yield of oil.

When 8% excess alkali was used, the colour and acid value were further lowered down to 4.0 and 0.7 respectively as obvious from the Table 3. In this case yield was comparatively poor than that provided with 4%. This is because of higher losses of oil due to saponification and emulsification occurring during the process.

Table 2: Chemical refining of crude cottonseed oil with 4% excess alkali.

Sr. No.	Alkali concentration (%)	Analysis of refined oil		
		Colour	Acid value	% Yield
1	6	6.5	1.6	96.8
2	9	6.0	1.4	96.2
3	12	5.5	1.3	96.3
4	15	5.0	1.2	96.4
5	18	4.5	1.0	96.6

Table 3: Chemical refining of crude cottonseed oil with 8% excess alkali.

Sr. No.	Alkali concentration (%)	Analysis of refined oil		
		Colour	Acid value	% Yield
1	6	6.0	1.4	94.0
2	9	5.0	1.1	92.5
3	12	5.0	1.0	91.0
4	15	4.5	0.8	91.3
5	18	4.0	0.7	92.0

Similar trend in changes in colour, acid value and yield were observed upon refining with 12%, 16% and 20% excess alkali as the results presented in Table 4, Table 5 and Table 6 respectively. It is apparent from these tables that oil losses are very high with higher doses of alkali i.e. with 16% and 20% excess amount of alkali it is 13.7% and 14.4% respectively when treated by 15% (w/v) alkali solution. But higher losses can not be compromised with the negligible refining benefits in terms of reduction in colour of the final product as each drop of oil is important because of its cost factor. Therefore, on the basis of above results an optimum level of caustic soda may be used as 12% excess of theoretically calculated amount on the basis of FFA content of crude cottonseed oil.

Table 4: Chemical refining of crude cottonseed oil with 12% excess alkali.

Sr. No.	Alkali concentration (%)	Analysis of refined oil		
		Colour	Acid value	% Yield
1	6	5.0	1.3	91.0
2	9	4.5	1.2	90.5
3	12	4.0	1.0	90.0
4	15	4.0	0.8	89.6
5	18	3.5	0.6	89.0

Table 5: Chemical refining of crude cottonseed oil with 16% excess alkali.

Sr. No.	Alkali concentration (%)	Analysis of refined oil		
		Colour	Acid value	% Yield
1	6	4.0	1.3	88.9
2	9	3.5	1.1	88.0
3	12	3.5	0.8	87.7
4	15	3.0	0.7	86.3*
5	18	2.5	0.6	85.8

* 13.7% oil loss

Table 6: Chemical refining of crude cottonseed oil with 20% excess alkali.

Sr. No.	Alkali concentration (%)	Analysis of refined oil		
		Colour	Acid value	% Yield
1	6	3.5	0.9	86.4
2	9	3.5	0.8	86.0
3	12	3.0	0.6	85.8
4	15	3.0	0.6	85.6*
5	18	2.5	0.5	85.0

* 14.4% oil loss

CONCLUTION

From the present study following conclusion can be drawn.

1. As the percentage of excess amount of alkali increases, the colour and FFA of refined oil decreases.
2. The colour and FFA decreases with the concentration of caustic soda solution.
3. Optimum level of caustic soda may be used as 12% excess with the view of reduction in colour and losses of oil.

ACKNOWLEDGEMENT

Author is thankful to the Director, Institute of Science and Technology for Advanced Studies and Research (ISTAR), Vallabh Vidyanagar, for providing the facilities required for carrying out the present study.

REFERENCES

[1] Lynn, J. A. and King, C. C.(1996) Cottonseed oil. In: *Bailey's Industrial Oils and Fats Products,* Hui, Y.H., (Ed.), John Wiley and Sons, New York, Vol. 2, pp. 176-183.

[2] Gad, T. E. and El-Zalaki, E. M. (2006) Effect of sodium hydroxide and other salts on gossypol content of cottonseed meal and oil. *Fette, Seifen, Anstrichmittel,* **82:** 407-411.

[3] Attia, M., Abbasy, M., El-Nockrashy, A. S. and Shoeb, Z. E. (2006) Cottonseed colour fixed pigments. Part III. Prevention of colour fixation and removal of colour-fixed pigments. *Nahrung,* **25**: 607-615.

[4] Attia, M., Taha, F. S., Mustafa, H. M. and El-Nockrashy, A. S. (2006) Bench-scale treatments of colour-fixed cottonseed oil. *Nahrung,* **32**: 281-284.

[5] Gad, T. E. and El-Zalak, E. M (2006) Total gossypol content and properties of cottonseed oil as affected by borax treatment before and after oil storage. *Fette, Seifen, Anstrichmittel*, **82**: 228–232.

[6] Helmy, H. E., Taha, F. S. and Abd El-Motal, E. A. (2006) Effect of phospholipids, free fatty acids and soapstock on colour fixation of cottonseed oil. *Nahrung,* **38**: 70-77.

[7] Helmy, H. E., Taha, F. S. and Abd El-Motal, E. A. (2006) Treatments of phospholipids to prevent or decrease colour fixation in cottonseed oil. *Nahrung*, **38**: 418-426.

[8] AOCS (1990) *Official Methods and Recommended Practices of the American Oils Chemists' Society*, Firestone, D., (Ed.), AOCS Press, Champaign.

[9] Methods of Sampling and test for oils and fats, Bureau of Indian Standards, BIS: (part II) (1976). pp. 548.

PRAJÑĀ - Journal of Pure and Applied Sciences
Vol. 17: 094-098, 2009 ISSN 0975 - 2595

STUDIES ON CYANOETHYLATION OF *PLANTAGO OVATA* SEED HUSKS (PSYLLIUM)

D. K. Raval,* J. K. Parmar, J. P. Patel [1] and M. R. Prajapati [2]

Department of Chemistry, Sardar Patel University, Vallabh Vidyanagar, Gujarat - 388 120
[1]N. V. Patel College of Pure & Applied Sciences, Vallabh Vidyanagar, Gujarat - 388 120
[2]United Phosphorus Limited, 11, G. I. D. C. Industrial Estate, Vapi, Gujarat - 396 195

ABSTRACT

Cyanoethylation of *Plantago ovata* seed husks (Isabgol; Psyllium), was carried out by acrylonitrile in a DMSO/H_2O medium. The effects of reaction influencing factors like concentration of sodium hydroxide and acrylonitrile, solid:liquid ratio in the reaction mixture, reaction period and temperature were studied. The products were characterized by determination of degree of cyanoethylation, IR-spectroscopy and by thermogravimetry. The effect of sonication on the reaction has also been studied. The percentage of nitrogen in the cyanoethylated husks were found to be in the range of 7.20% - 12.50%.

***Keywords*: cyanoethylation, *Plantago ovata* seed husk (*Psyllium*), etherification on polysaccharide, thermogravimetry.**

INTRODUCTION

Modification of polysaccharides into, carboxymethyl, hydroxyethyl and cyanoethyl derivatives find number of industrial applications. More particularly cyanoethylated derivative of fenugreek gum [1], cellulose [2], bagasses [3] stack have been prepared or manufactured industrially. They are found in good commodity applications like high dielectric diods, glass carbon electrodes, flocculating agents, detergent additives, thermomolding composites, fiber hot-pressed composites [4 – 8].

One of the important natural polysaccharide is *psyllium* obtained from *Plantago ovata* seed husks. This is commonly known as Isabgol and abundantly available in the local market. The unmodified form is a very good pharmaceutical product as a mild laxative. Structurally it is a highly branched polysaccharide with 1→4 and 1→3 linked xylan backbone variously substituted at O-2 and O-3 with arabinose, xylose and an aldobiouronic acid identified as 2-O-(galactopyranosyluronic acid) rhamnose [9].

Till now its modification has not been studied academically or technically except a few instances [10–13]. Thus it was thought to undertake modification of *Plantago ovata* seed husk through its hydroxyl functionality. In current study the cyanoethylethers of *Plantago ovata* seed husk have been prepared and reaction conditions have been optimized. The products have been characterized by usual chemical methods along with the instrumental techniques such as Infra-Red (IR) spectroscopy and Thermogravimetric analysis (TGA). The effect of sonication on the cyanoethylation has also been studied.

MATERIALS AND METHODS

Preparation of Cyanoethyl-Isabgol (CEI)

5.0 g (37.8 mM) Isabgol powder in 10-30 ml DMSO was mixed with 25 ml 2-10% (12.5-62.5 mM) aqueous solution of sodium hydroxide. The reaction mass was thoroughly mixed and the homogeneous paste thus obtained was kept for ½ hour at room temperature with occasional stirring. 25-65 ml (0.38-0.98 M) acrylonitrile (AN) was added drop wise to this reaction mass over a period of 30 minutes. The desire temperature (0-30°C) of the reaction medium was achieved either by using ice/salt system or by heating the reaction bath. The reaction mass was occasionally stirred throughout the course of reaction (3-48 hrs). After the completion of the desired period, the reaction mass was treated with required amount of acetic acid in order to neutralized the excess of sodium hydroxide present in the system. The precipitation of the product was carried out by dumping the reaction mass into the non-solvent (200 ml of 80% methanol) followed by vigorous stirring for 10 min. The above procedure for precipitation was repeated thrice taking fresh methanol each time.

* Corresponding author – aanal.virat@gmail.com

The product thus obtained was dried in an oven at 60°C to the constant weight and ground to approximately equal particle size.

Degree of substitution of the Cyanoethyl-Isabgol (CEI)

The degree of substitution per anhydroglucose unit (AGU) was calculated from the nitrogen content of the product. The nitrogen content was determined by the Kjeldahl's method for the determination of percent (%) nitrogen for the product. The degree of substitution (DS) for Cyanoethyl-Isabgol can be derived from following formulae.

Degree of Substitution for %N content up to 7.567 = %N / 7.567 (1)

Degree of Substitution for %N content more than 7.567 = 1 + (%N found - 7.567)/4.198 (2)

Reaction efficiency (R.E.) of Etherification

The reaction efficiency for the cyanoethylation of Isabgol was determined by the following equation:

$$R.E. = \frac{\text{Moles of reagent cosumed actually for etherification}}{\text{Moles of reagent taken initially}} \times 100 \quad (3)$$

The various reaction parameters studied for the cyanoethylation are concentration of NaOH, Acrylonitrile, liquid:solid ratio, reaction time and temperature. The results obtained are presented in the Table 1 to 5. The effect of sonication on cyanoethylation of Isabgol is depicted in Table 6.

RESULTS AND DISCUSSION

A set of products obtained upon cyanoethylation of Isabgol Husk were characterized by determination of %N, Reaction Efficiency (R.E.), Thermogravimetry and Infra-Red (IR) spectroscopy. The experimental data comprising of the effects of reaction influencing factors are given in Table 1 to 6.

Effect of Sodium Hydroxide Concentration

Table 1 shows the effect of sodium hydroxide concentration on %N and R.E. of cyanoethylation of Isabgol. %N found to decrease from 11.41% to 7.22% with increase in the sodium hydroxide concentration in the cyanoethylation of Isabgol. This may be due to the fact that cyanoethylated polysaccharide undergoes partial alkaline hydrolysis under the influence of higher concentration of sodium hydroxide to yield ultimately carboxymethyl polysaccharide [14]. Beside, acrylonitrile may also undergo side reaction in the presence of excess of sodium hydroxide via conversion of nitrile group, which result in the decrement in the nitrogen content [1]. The R.E. was also found to decrease from 5.95 to 3.76% with increase in the sodium hydroxide concentration from 37.5 to 62.5 mM.

Table 1: Effect of sodium hydroxide concentration on D.S. and R.E. on cyanoethylation of Isabgol.

No	Amount of sodium hydroxide		Product (g)	%N	D.S.	R.E. (%)
	% NaOH	mM				
1	2	12.5	4.0	10.36	1.66	5.41
2	4	25.0	4.2	10.83	1.77	5.65
3	6	37.5	4.8	11.41	1.91	5.95
4	8	50.0	4.3	7.33	0.96	3.82
5	10	62.5	4.5	7.22	0.95	0.95

Isabgol: 5.0 g; Acrylonitrile: 45.0 ml; Dimethyl sulfoxide: 10.0 ml; Reaction Time: 24 hrs; Reaction Temperature: 20°C.

Table 2: Effect of acrylonitrile concentration on D.S. and R.E. on cyanoethylation of Isabgol.

No.	Amount of acrylonitrile		Product (g)	%N	D.S.	R.E. (%)
	ml	mM				
1	25	379	4.9	11.03	1.82	10.36
2	35	531	4.9	11.03	1.82	7.40
3	45	683	4.8	11.41	1.91	5.95
4	55	853	4.8	11.93	2.04	5.09
5	65	987	4.8	11.93	2.04	4.31

Isabgol: 5.0 g; 6% sodium hydroxide: 25.0 ml; Dimethyl sulfoxide: 10.0 ml; Reaction Time: 24 hrs; Reaction Temperature: 20°C.

Effect of Acrylonitrile Concentration

Table 2 presents the data regarding %N and R.E. of cyanoethylation of Isabgol with increase in acrylonitrile concentration. %N was found to increase from 11.03%, with increase in the acrylonitrile concentration, and finally reached a constant level of 11.93%. The enhancement in the %N and hence Degree of Substitution (D.S.) of the cyanoethylated *Plantago ovata* seed husk could be associated with greater availability of acrylonitrile molecules in the vicinity of the *Plantago ovata* molecules at higher acrylonitrile concentrations. The molecules of Isabgol are present in the excess of the reagent acrylonitrile and their reaction would rely on the availability of acrylonitrile molecules in their proximity. This increased number of acrylonitrile molecules

would lead to increase %N and D.S. of cyanoethyl-Isabgol. As a result, the Reaction Efficiency (R.E.) of cyanoethylation decreases from 10.36% to 4.31% as the acrylonitrile concentration increase. This reflects the amount of unreacted acrylonitrile when taken in large excess in the reaction mixture.

Table 3: Effect of liquid:solid ratio on D.S. and R.E. on cyanoethylation of Isabgol.

No.	Amount of Dimethyl sulfoxide		Liquid/ solid ratio	Product (g)	%N	D.S.	R.E. (%)
	ml	mM					
1	10	140	13.84	4.8	11.93	2.04	5.09
2	15	211	14.61	4.8	11.03	1.82	4.71
3	20	281	15.38	4.8	9.22	1.39	3.94
4	25	352	16.15	4.5	8.55	1.23	3.65
5	30	422	16.92	4.3	7.42	0.98	3.17

Isabgol: 5.0 g; 6% sodium hydroxide: 25.0 ml; Acrylonitrile: 55.0 ml; Reaction Time: 24 hrs; Reaction Temperature: 20°C.

Effect of Liquid-Solid ratio

Table 3 shows the effect of liquid:solid ratio on the reaction parameters. It was controlled by varying the amount of DMSO from 10 to 30 ml which was used as the reaction medium. %N and R.E. were found to be decreased gradually from 11.93% to 7.42% and 5.09% to 3.77% respectively in the range of liquid:solid ratio studied (13.84 to 16.92). This may be due to the decrement of acrylonitrile molecules in the vicinity of hydroxyl groups of the *Plantago ovata* with increase in the liquid content. It is quit obvious that the total liquid content of the reaction mass was increased with increasing the stated ratio while the total amount of Isabgol and acrylonitrile were remained unchanged. Hence, the concentration of acrylonitrile molecules available in the vicinity of hydroxyl groups gradually decrease with increase in liquid:solid ratio [2].

Effect of Reaction Time

Table 4 shows the effect of reaction time on the cyanoethylation of Isabgol. % N and R.E. were found to increase in the initial stage of the reaction and then it leveled off as reaction proceeded [15]. The time interval over which reaction was studied ranges from 3 to 48 hrs. From the beginning of reaction up to 3 hrs, the reaction was observed to be very fast. This can be conformed by the value of %N obtained which is 10.46 % at the end of 3 hrs. Upon increasing the period from 3 to 6 hrs and then from 6 to 12 hrs, the increment of only 1.13 and 0.34 %N were observed respectively. Further increasing the reaction time 12 to 48 hrs there was no increment in the %N observed at all i.e. after 12 hrs of reaction period a maximum level of substitution has been obtained under the chosen set of reaction conditions.

Table 4: Effect of Reaction Time on D.S. and R.E. on cyanoethylation of Isabgol.

No.	Reaction Time (hrs)	Product (g)	%N	D.S.	R.E. (%)
1	3	4.8	10.46	1.69	4.46
2	6	4.9	11.59	1.95	4.95
3	12	4.9	11.93	2.04	5.09
4	18	4.7	11.93	2.04	5.09
5	24	4.8	11.93	2.04	5.09
6	48	4.7	11.93	2.04	5.09

Isabgol: 5.0 g; 6% sodium hydroxide: 25.0 ml; Acrylonitrile: 55.0 ml; Dimethyl sulfoxide: 10.0 ml; Reaction Temperature: 20°C

Effect of Reaction Temperature

Table 5 shows the effect of temperature on the cyanoethylation of Isabgol. The temperature range on which reaction studied was 0°C to 30°C. Both, %N and R.E. were found to increase up to 10°C and reach the maximum value of 12.49% and 5.33% respectively. With increase in the temperature from 10°C to 30°C, %N and R.E. gradually decrease up to 11.48% and 4.90% respectively. The decrease in the %N with increase in the temperature may be due to the partial conversion of cyanoethylated groups of the product into carboxyethyl groups under the influence of alkali [1, 3, 16].

Table 5: Effect of Reaction Temperature on D.S. and R.E. on cyanoethylation of Isabgol.

No.	Reaction Temperature (°C)	Product (g)	%N	D.S.	R.E. (%)
1	0	4.9	10.58	1.72	4.51
2	10	4.8	12.49	2.17	5.33
3	20	4.9	11.93	2.04	5.09
4	30	4.7	11.48	1.93	4.90

Isabgol: 5.0 g; 6% sodium hydroxide: 25.0 ml; Acrylonitrile: 55.0 ml; Dimethyl sulfoxide: 10.0 ml; Reaction Time: 12 hrs.

Effect of Sonication

The ultrasonic vibrations have found pronounced effects when the cyanoethylation of Isabgol was performed using ultrasonic cleaner UC500. The remarkable increase in the %N and R.E. respectively of 10.11% and 4.31% are observed only in 5 min of the sonication period. Further increase of 5 min in sonication time (from 5 min to 10 min) there observed an increase of 0.99 %N content and 0.43% in R.E. Any increase in sonication time further from 10 min caused surprised decreased in the values of %N from 11.10% to 8.46% as well as R.E. from 4.75% to 3.61%. The results are shown in Table 6.

Table 6: Effect of sonication on D. S. and R. E. on cyanoethylation of Isabgol.

No.	Sonication Time (min)	Product (g)	%N	D.S.	R.E. (%)
1	5	1.6	10.11	1.60	4.31
2	10	1.5	11.10	1.84	4.74
3	15	1.5	10.81	1.77	4.61
4	20	1.3	9.36	1.42	3.99
5	25	1.4	8.46	1.21	3.61

Isabgol: 2.0 g; 6% sodium hydroxide: 10.0 ml; Acrylonitrile: 22.0 ml; Dimethyl sulfoxide: 4.0 ml; Reaction Temperature: 30ºC; Frequency: 22.0 KHz

Characterization by Thermogravimetric Analysis (TGA)

Du-Pont Model 951 thermogravimetric analyzer was employed to carry out study of Cyanoethyl-Isabgol. The sensitivity and precision of mass measurements are 0.2% and 0.4% respectively. The samples were powdered to the same average mesh size and dried carefully in vacuum desiccator. 10 mg of exact weight of sample was taken for each Thermo Gravimetric Analysis (TGA). The Initial Decomposition Temperature (IDT) dropped very much down from 245°C (for unmodified Isabgol) to the range of 147–182°C for various samples. This is very clear-cut and sound evidence that the cyanoethylated products start to decompose at an earlier stage than the Isabgol. During the later stages of degradation all of the cyanoethyl derivatives behave nearly similar to the native Isabgol. This statement is based on the much lesser deviations observed in the values of T_{50}, T_{max} and Integral Procedural Decomposition Temperature (IPDT) along the columns. IPDT was estimated by Doyle's method [17] to cover the whole range of degradation on TG-thermograms. Cyanoethyl ether degraded in two steps, the first step was found to have higher activation energy than the other, for all the samples. Hence, the Cyanoethyl-Isabgol samples are considered to have much less thermal stability. This may be due to the presence of –CN (nitrile) groups attached to the polysaccharide backbone. However, the Cyanoethyl-Isabgol was found more stable than the native Isabgol when the thermal stability was decided on the basis of T_{max} [18]. The values of T_{max} are in the range of 312.5°C to 325°C compared to 310°C for native Isabgol. Table 7 shows the results obtained from TGA characterization of CEI.

Characterization by Infra-Red (IR) Spectroscopy

The spectra of Isabgol and cyanoethyl-isabgol were recorded on Nicolate 400D spectrophotometer using KBr pellets. The most striking evidence for the presence of –CN group shows the band at 2250 cm^{-1}[19]. A couple of new bands were observed at 1587 cm^{-1} and 1520 cm^{-1} due to N-H bending vibrations arising from secondary amine and amide group [20]; due to the transformation of –CN group in the presence of sodium hydroxide and water to $–CONH_2$ group. The strong and broad band extending from 1200-950 cm^{-1} consisting of several close bands which are typical of all cellulosic fibers has been found to change to a relatively transparent region and having only a few individual weaker bands [21].

Table 7: Thermal parameters of Cyanoethyl-Isabgol.

No.	D.S.	IDT (ºC)	T_{10} (ºC)	T_{50} (ºC)	IPDT (ºC)	E_1	E_2	E_3	Char yield (%)
						Kcal M^{-1}			
1	-	245.0	112.5	305.0	310.0	32.28	1.54	-	2.49
2	1.45	147.5	157.5	307.5	325.0	9.31	1.83	-	2.50
3	1.56	170.0	182.5	310.0	325.0	11.59	2.20	-	4.73
4	1.76	162.5	175.0	267.5	312.5	13.99	2.62	-	-
5	1.94	177.5	195.0	297.5	312.5	17.11	2.61	-	3.68
6	2.12	182.5	202.5	302.5	312.5	17.61	2.73	-	1.00

ACKNOWLEDGEMENTS

The authors are grateful to University Grants Commission, Government of India, New Delhi for the financial assistance in part in form of Minor Research Project to D. K. Raval. J. K. Parmar is thankful to UGC for the award of Meritorious Research Fellowship. Our obligation is due to Mr. N. H. Shastri, Museum Curator for granting permission to perform the experiments on ultrasonic cleaner UC500 in the University Museum. The infrastructural and other facilities provided by Heads of the department are also gratefully acknowledged.

REFERENCES

[1] El-Molla, M. M., (1998) Technical and feature articles - Chemical modification of fenugreek gum: Part II - Cyanoethylation *American dyest. Rep.*, **87**: 47.

[2] (a) Dong, Y.-G., Xiao-Ling, G. and Zhen-Qi (2000) Cyanoethyl cellulose prepared by homogeneous and nonhomogeneous reaction *buckwheat husk*, *Ziran Kexueben*, 30(3), 214-216; (b) Schleicher, H., Lakanoff, B. and Philipp, B. (1974) Effect of the cellulose structure and preactivation on the cyanoethylation process. *Faserforsch. Textiltech*, **25:** 179-83.

[3] Hassan, M. L., El-Wakil, N. A. and Sefain, M. Z. (2001) Thermoplasticization of bagasse by cyanoethylation. *J. Appl. Polym. Sci.*, **79:** 1965-1978.

[4] Ryosuke, N., Hiroshi, O. and Motoyasu, F. (2000) saccharide derived monomers, their manufacture and dielectric polymers obtained from the monomers. *Japan Kokai Tokkyo Koho*, **122**: 888.

[5] Lin, B., Sun, X. Y. and Xu, J. R. (2003) Preparation and application of cyanoethylchitosan modified electrode *Yingyong Huaxue*, **20:** 963-967.

[6] (a) Malinowski T. P. (1961) Flocculation **US 3001933**; (b) Walker H. M. (1962) Drilling fluid **US 3032498**; (c) Wilson A. R. (1959) Water-emulsion paints containing cyanoethylated starch **US 2881143**.

[7] Pallaske, M. (2003) Environmentally friendly wood preservation process by cyanoethylation of wood in the presence of catalysts **DE 10140224**.

[8] Hassan, M. L. (2002) Dielectric properties of cyanoethylated bagasse composites. *Polymer Plastic Technology and Engineering*, **41:** 589-600.

[9] Kennedy, J. F., Singh, J. S. and David, A. T. (1979) Structural data for the carbohydrate of ispaghula husk of *Plantago ovata* Forsk, *Carbohydr. Res.*, **75:** 265-274.

[10] Shirsand, S. B., Sarasija, S., Para, M. S., Swamy, P. V. and Nagendra K. D. (2009) *Plantago ovata* mucilage in the design of fast disintegrating tablets, *Indian J. Pharm. Sci.*, **71:** 41-45.

[11] Khasgiwal, P. C. and Mithal, B. M. (1975) Derivatives of *Plantago Ovata* seed husk gum. Part I. Carboxyl derivatives, *Indian J. Pharm.,* 37, 53-55.

[12] Jain, A. K. and Mithal, B. M. (1976) Derivatives of *Plantago Ovata* seed husk gum. Part II. Methoxy derivative, *Indian J. Pharm.,* 38, 15-17.

[13] Trivedi, J. H., Dholakia, A. B., Patel, K. H. and Trivedi, H. C. (2009) Photoinduced graft copolymerization of methylacrylate onto sodium salt of partially carboxymethylated psyllium. *Trends in Carbo. Res.*, **1:** 38-46.

[14] Feit, B. A. and Zilkha, H. (1963) Kinetics and mechanism of the cyanoethylation of alcohols. *J. Org. Chem.*, **28:** 406-410.

[15] Saha, A. K., Das, S., Basak, R. K., Bhatta, D. and Mitra, B. C. (2000) Improvement of functional properties of jute-based composite by acrylonitrile pretreatment *J. Appl. Polym. Sci.*, **78:** 495-506.

[16] Khalil, M. I., Beliakova, M. K. and Aly, A. A. (2001) Preparation of some starch ethers using the semi-dry state process. *Carbohydr. Polym.*, **46:** 217-226.

[17] Doyle, C. D. (1961) Estimating thermal stability of experimental polymers by empirical thermogravimetric analysis. *Anal. Chem.* **33:** 77-79.

[18] Sefain, M. Z., Naoum, M. M., Fadl, M. H. and El-Wakil, N. A. (1994) Thermal behavior of cyanoethylated cellulose. *Thermochim Acta*, **231:** 257-65.

[19] Khalil, E. M. A. and El-Wakil, N. A., (2000) Infrared absorption spectra of cyanoethylated cellulose fibres. *Cellulose Chemistry & Technology* **34:** 473-479.

[20] Weissberger, A. (1956) *Chemical Application of Spectroscopy*, Interscience, New York, pp. 520-527.

[21] O'Connor, R. T., DuPre, E. F. and Mitcham D., (1958) Applications of infrared absorption spectroscopy to investigations of cotton and modified cottons: Part I: Physical and crystalline modifications and oxidation. *Textile Res. J.,* **28:** 382-92.

PRAJÑĀ - **Journal of Pure and Applied Sciences**
Vol. 17: 099-103, 2009 ISSN 0975 - 2595

SKEW DETECTION AND TEXT LINE EXTRACTION FOR HAND WRITTEN GUJARATI TEXT

Chhaya N. Patel [*] and Apurva Desai [1]

Anand Institute of Information Science, Opp. Town Hall, Anand, Gujarat – 388 120
[1]Department of computer science, Veer Narmad South Gujarat University, Surat, Gujarat – 388 120

ABSTRACT

The area of Optical Character Recognition (OCR) has been addressed very well for many popular international languages like English, Chinese , Arabic , Japanese and some of the Indian languages like Oriya, Bengali, Tamil , Telugu etc. Gujarati language OCR has also been focused since last few years, but still there is a scope for developing new and innovative techniques. This paper describes two important and basic preprocessing tasks for OCR, the skew detection and text line extraction for handwritten Gujarati text. This paper also describes properties of Gujarati script, brief overview of the OCR process and problems related to Gujarati OCR. This paper describes various techniques of skew detection and correction. The results based on radon transform for skew detection and correction are discussed. Text line extraction is done using projection profile techniques. The radon transform based techniques are found quite satisfactory for detecting and correcting skew angle.

Keywords: **OCR, skew angle, skew detection, skew correction, text line extraction, document image analysis, radon transformation, projection profile.**

INTRODUCTION

India is a country where people use verity of languages. India has wide variety of knowledge base and this knowledge is stored in various forms and is in various languages. In the era of computerization, the e-versions of information are becoming popular for local languages. This in turn had boosted use of electronic representation, storage, and access of information in Indian languages. An Optical Character Reader is a critical tool in creating electronic content for Indian languages, as most of the literature is found either in the form of 'Hast Pratas', Handwritten form or in printed form in all popular languages. The rise in the development of Optical Character Recognizers (OCRs) for the scripts of Indian languages is been noticed since last few decades due to fast adoption of the information technology tools.

This paper describes briefly some of the stages that are part of the Optical Character Recognition system for off-line Gujarati text. Gujarati is a language spoken by millions of people in the state of Gujarat, India. Gujaraties dwell in most of the countries in the world hence, it becomes more important to have Gujarati OCR to digitize the rich heritage of Gujarati literature, documents and manuscripts. Many OCRs for Indian scripts have been reported [1, 2, 3, 4]. The development for the Gujarati OCR is in its initial stage. Very little work is found for printed Gujarati OCR [5] and there is no work available for the handwritten Gujarati text as compared to other Indian languages like Bengali, Devnagari, Tamil etc. This paper is an attempt to address few of the basic stages for Gujarati OCR namely skew detection and correction for the handwritten Gujarati text.

PROPERTIES AND PROBLEMS RELATED TO GUJARATI SCRIPT

In most Indian script alphabet system we found vowel and consonant characters, called basic characters [6]. Gujarati language also has similar characteristic as the other Indian scripts. Major reasons causing difficulties at various stages of OCR for Gujarati script can be described as follows: -

I. It has wide range of characters and modifiers - Gujarati script has character set has of 35 consonants, 13 vowels and 6 signs, 13 dependent vowel signs, 4 additional vowels for Sanskrit, 9 digits and 1 currency sign – (₹.) [7].

II. Some of the Gujarati characters when used with modifies get looks similar to the basic character e.g. KU (Ku) if not written properly may be identified as F. (pha) e.g.

* Corresponding author – chhayapatel@email.com

the word KUVao may be wrongly identified as Fvo which is not a Gujarati word.

III. There are many possibilities for the conjunct consonants that increase difficulties in identification of the character and at the segmentation stage. e.g.

શ્મ શ્લ ષ્ટ

śma śla ṣṭa

IV. The intra-word characters in the Devanagri are connected with an over stroke. This eases the problem identification of text line, skew detection and word separation from a text line. The same is not the case with Gujarati, as Gujarati characters within a word and words in a line are separated by white space, as shown in Fig. 1.

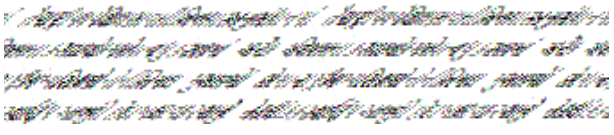

Figure 1: Sample text in Gujarati

CHARACTERISTICS OF GUJARATI TEXT

The concept of upper and lower case letters is absent in the languages of Indian origin. For Indian languages vowels are represented by a single symbol. Some vowels appear as the combination of one vowel and a dependent vowel sign and they may occur after, before, above or below the consonant.

A line of Gujarati text can be considered as being logically divided into three horizontal parallel lines :-

- The base line, the imaginary line separating the middle and lower zone on which consonants and independent vowels are written. (*Middle zone*)
- The line below the base line, used for writing dependent (lower) vowels.(*Lower Zone*)
- The line above the base line, used for writing dependent (upper) vowels.(*Upper zone*)

A typical example of zoning is shown in Fig. 2.

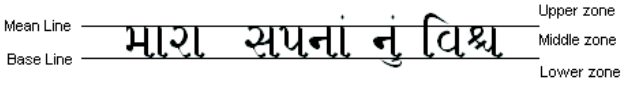

Figure 2: Zones in a Gujarati text line

The zone identification and modifier extraction is more difficult in case of handwritten text. It is found that projection profile based techniques gives good results for character and modifier extraction for printed text but the same is not the case for handwritten text. The same can be used for the handwritten text with a compromise of accuracy. To increase the accuracy we need to consider inter line skew, the writing style, spacing between the words and spacing between various zones.

BASIC STRUCTURE OF THE OCR SYSTEM

The basic process for Gujarati OCR system is more or less similar to other Indian language OCR systems, as shown in Fig. 3, except some extra care to be taken at the skew detection and segmentation stage. The document image is first captured using a flat-bed scanner and is digitized. The digitized document is then passed through different preprocessing modules like noise cleaning, skew detection and correction, line segmentation, zone detection, word and character segmentation, modifier extraction etc. Once the segmentation phase is over we have derived basic characters and modifier that can be feed to the recognition engine to identify individual token based on the predefined rules based on specific features. There are many feature extraction techniques available [8]. The classified individual characters and modifiers can be combined at a latter stage to form words and sentences which in turn is used to form an editable text as a final output.

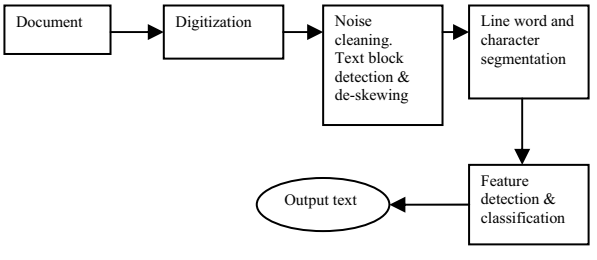

Figure 3: Diagrammatic structure of the OCR system

TEXT DIGITIZATION AND NOISE CLEANING

In our case text digitization is done using a flatbed scanner at a resolution varying from 200 to 300 dots per inch (dpi). It is often desirable to represent gray-scale or color images as binary images by picking a threshold value. Two

categories of thresholding exist: *global* and *local*. *Global thresholding* picks one threshold value for the entire document image which is often based on an estimation of the background level from the intensity histogram of the image [9]. *Local (adaptive) thresholding* use different values for each pixel according to the local area information [10]. We have used Global thresholding as we have restricted the application for pure text documents.

The Gray scale image is converted into two-tone image by applying Global thresholding. The threshold value is decided by testing various samples of text written by different persons using different thickness of pen point. The two-tone image is having 0 and 1 labels where 1 and 0 represent object and background respectively. The digitized image shows protrusions and dents in the characters, as well as isolated black pixels over the background, which can be cleaned by applying various morphological operations.

SKEW DETECTION AND CORRECTION

When a document is fed to the scanner either mechanically or by a human operator, a few degrees of skew (tilt) is unavoidable. The *skew angle* is the angle that the text lines in the digital image make with the horizontal direction. Skew detection and correction are important preprocessing steps of document layout analysis and OCR approaches. Skew correction can be achieved in two steps, namely (i) estimation of skew angle, and (ii) rotation of the image by the skew angle in the opposite direction.

One of the popular skew estimation technique is based on the projection profile of the document. The horizontal/vertical projection profile is a histogram of the number of black pixels along horizontal/vertical scan-lines. For a script with horizontal text lines, the horizontal projection profile will have peaks at text line positions and troughs at positions in between successive text lines. To determine the skew angle of a document, the projection profile is computed at a number of angles, and for each angle, the difference between peak and trough heights is measured. The maximum difference corresponds to the best alignment with the text line direction. This in turn determines the skew angle.

Other technique proposed by Chaudhuri & Pal [3] uses generalized clustering approach for skew detection of Indian script documents. This concept uses mean line of the script for skew estimation.

We also found references for some proven techniques based on the Hough transform and Fourier transform for skew estimation [8]. The application of radon transform based technique to detect the skew for the handwritten Gujarati text is found satisfactory in our case.

We have assumed that persons writing style remains uniform in most cases hence to speed up the image processing, we have extracted middle part of the text to use as input for the radon transform for skew detection purpose. The radon transform computes projections of an image matrix along specified directions. A projection of a two-dimensional function f (x, y) is a set of line integrals. The radon function computes the line integrals from multiple sources along parallel paths, or beams, in a certain direction. The beams are spaced 1 pixel unit apart. To represent an image, the radon function takes multiple, parallel-beam projections of the image from different angles by rotating the source around the center of the image. Projections can be computed along any angle.

The extracted middle portion of the text was considered as an input image for Radon function. To detect the skew the Radon transform for input image is computed at angles from 0° to 179°, in 1° increments of angles. We have used MATLAB – radon function to calculate Radon transform for input image. The maximum value of R provided by the function [R,xp] = radon(I,theta); where I is our input image and theta varies for 0 to 179, helps to detect the skew angle. The locations of strong peaks in the Radon transform matrix are detected in the next phase. The locations of these peaks correspond to the locations of straight lines in the original image. The actual skew angle is 90 – location of the peak value. Once the skew angle is detected the whole text is rotated by the skew angle to correct the skew. Our algorithm works perfectly for the skew angle in the range of -20 to +20 degree.

SEGMENTATION

The document achieved after the preprocessing stage is "clean" document. It has sufficient amount of shape information, high compression, and low noise on a normalized image. The next stage is segmenting the document into its subcomponents. Segmentation is an important stage because the extent one can reach in separation of lines, words, or characters directly affects the recognition rate of the script. There are two types of segmentation:

i. External segmentation: It is related to the isolation of various writing units, such as paragraphs, sentences, or words.

ii. Internal segmentation: It is related to the isolation of letters only for languages like English but for Languages for Indian origin it also includes isolation of modifiers and isolation of conjunct characters.

The first step for segmentation in our case is segmentation of lines. We have used a purely text information written in a normal form, on a plain paper in single column format. We need to apply additional document image analysis algorithms to determine text region and text location, to identify number of columns, to check presence of other type of information like figures, formulas etc, if we have been provided any general document like a teachers note or students answer sheet.

LINE EXTRACTION

Extracting lines for the text is a challenging job especially if the text is in handwritten form. A novel text line extraction technique for multi-skewed document images of handwritten English or Bengali text [11]. It assumes that hypothetical water flows, from both left and right sides of the image frame, face obstruction from characters of text lines. The stripes of areas left unwetted on the image frame are finally labelled for extraction of text lines.

Another approach is based on minimum spanning tree (MST) clustering with new distance measures, in which the connected components of the document image are grouped into a tree by MST clustering. The edges of the tree are then dynamically cut to form text lines by using an objective function for finding the number of clusters [12].

We have used horizontal projection profile to extract individual lines from the skew corrected document. The input text is thinned before determining horizontal profile. The histograms of horizontal profile indicates position of individual text line. We have implemented an algorithm to detect contiguous presence of black pixels, indicating a space between two text lines. The blank lines with contiguous 'off' pixels are ignored as they indicate non text or blank lines. The predefined value of threshold related to number of on pixels helps to determine whether a line is a part of text or is part of blank line – a non text part. A line with sufficient number of 'on' pixels is considered to be a part of text line. The next occurrence of contiguous "off" pixels indicates end of current text line. The extracted text line is stored as an individual line for further segmentation. The same process is repeated till we complete processing of all row in the input text image i.e. end of the document.

This technique is suitable for Gujarati handwritten text, as it provides reasonably good accuracy. The presence of modifiers (matras) of different shapes generates difficulty in some cases, as with other Indian Scripts [13]. We know that modifiers in Gujarati script can appear in four places namely left, right, upper and lower. There are chances that we may get two or three lines for a single text line if all or majority of matras, present in upper zone or lower zone are written without any connection with the consonants. In this case we may get three separate lines - one comprising of upper zone matras, another with middle zone characters and matras and the last one with lower zone matras. We have applied smoothing operation to reduce such negative effect of modifiers in lower and upper zone.

RESULTS

Input text with skew angle of 10 degree.

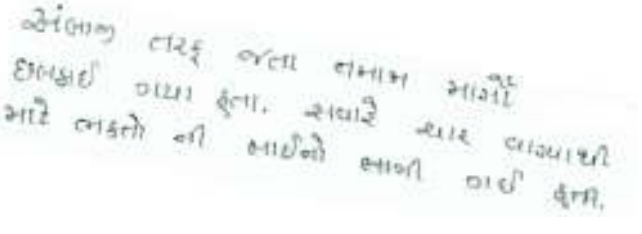

The skew angle was detected as 10 degree and the lines were extracted as

Line 1

Line 2

Line 3

CONCLUSIONS

As the Gujarati handwritten text OCR is in its initial stage, we need to apply and check various other proven techniques for the Indian origin language. The skew detection techniques mentioned in the paper has sufficient accuracy for a limited angle of skew, which can be enhanced for larger skew angles. The line segmentation works well for nicely written document. It can be improved to process badly written document.

REFERENCES

[1] Indian language document analysis and understanding (2002) Special Issue of Sadhana.

[2] Bansal, V. and Sinha, R. M. K. (2001) "A Devanagari OCR and a brief review of OCR research for Indian scripts", In: *Proceedings of STRANS* 01.

[3] Chaudhuri, B. and Pal, U. (1997) "An OCR system to read two Indian language scripts: Bangla and Devanagari (Hindi)" In: *Proceedings of ICDAR*, pp. 1011–1015.

[4] Jawahar, C. V., M. N. S., Pavan Kumar, S. K., Ravi Kiran, S. S. (2003) A Bilingual OCR for Hindi-Telugu Documents and its Applications. *Proceedings of the Seventh International Conference on Document Analysis and Recognition* 0-7695-1960-1/03.

[5] Antanani, S. and Agnihotri, L. (1999) Gujarati character recognition. *Proceedings ICDAR*, pp. 418–421.

[6] Pal, U., Sinha, S. and Chaudhuri, B. B. (2003) Multi-script line identification from Indian documents", *Proceedings of the Seventh International Conference on Document Analysis and Recognition*, 0-7695-1960-1/03

[7] Unicode character code for Gujarati.

[8] Nafiz Arica and Fatos T. and Yarman-Vural, (2001) An Overview of Character Recognition Focused on Off-Line Handwriting IEEE-Transactions on Systems, Man and Cybernetics - Part C, *Applications and Reviews* **31(2)**.

[9] Solihin, Y. and Leedham, C. G. (1999) Integral ratio: A new class of global thresholding techniques for handwriting images. *IEEE Transactions on Pattern Analysis & Machine Intelligence* **21**: 761–768.

[10] Saula, J. and Pietikainen, M. (2000) Adaptive document image binarization. *Pattern Recognit.* **33(2)**: 225–236.

[11] Basu, S., Chaudhuri, C., Kundu, M. and Basu, D. K. (2007) Text line extraction from multi-skewed handwritten documents. *Pattern Recognition*. **40(6)**: 1825 – 1839.

[12] Yin, Cheng-Lin Liu (2007) Handwritten text line extraction based on minimum spanning tree clustering", Wavelet Analysis and Pattern Recognition. *ICWAPR, Pattern Recognition*. **33(2)**: 225–236.

[13] Sanghamitra Mohanty and Hemanta Kumar Behera (2002) A complete OCR development system for Oriya script. *S¯adhan¯a.* **27(1)**: 23–34.

PRAJÑĀ - **Journal of Pure and Applied Sciences**
Vol. 17: 104-107, 2009 ISSN 0975 - 2595

SENSING IMAGE FORGERY USING MATLAB

Brijesh Jajal [*] and Vipul Desai [1]

Ashok & Rita Patel Biotechnology Institute (ARIBAS), New Vallabh Vidyanagar, Gujarat - 388 120
[1]Managment Advisor, Charutar Vidya Mandal, Vallabh Vidynagar, Gujarat – 388 120

ABSTRACT

Due to availability of immense number of image editing software, a layman can easily perform editing operations into a digital image. Among the major operations, Copy-paste of one image area into another is considered to be the common example of manipulating image. A digital image consists of storage representation of RGB (Red-Green-Blue) color format. Usually an image is assumed to be acquired in 24 bits Bitmap format. The procedure devised here senses the same regions within an image, assuming the test image to contain such forgery. The suggested procedure can be considered as a tool to image forensics. This paper discusses the procedure successfully implemented using Matlab.

Keywords: **Image forensic, image tampering, image doctoring, detection of copy-paste regions.**

INTRODUCTION

In July 2009, a picture essay in The New York Times (NYTimes) Sunday Magazine entitled "Ruins of the Second Gilded Age", by Edgar Martins, showed large housing construction projects that were halted due to the housing market collapse. After discovering the photo manipulations, the Times posted the following on their website. "After a reader discovered that the photos were digitally altered, Editors later confronted the photographer and determined that most of the images did not wholly reflect the reality they purported to show. Had the editors known that the photographs had been digitally manipulated, they would not have published the picture essay, which has been removed from their website."

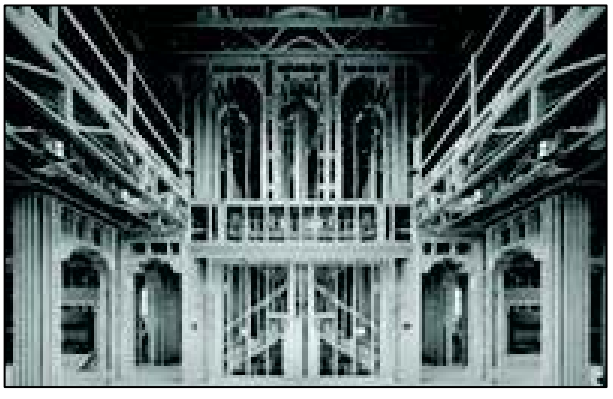

Figure 1: The image forgery by photographer of NYTimes.

The given photograph (Fig. 1.) is an example of forgery into the original image by pasting a specific area of another digital image. Since the image is represented in RGB format [2], such manipulations contain a clear partition line indicating the major changes into pixel values [3] of an image. The detection of such partitions can expose the forgery.

There are few methods available for the detection of such digital image forgery. The lighting condition of two separate photographs can detect the forgery with the help of estimation of a point light source [5]. However, this method might not work when the object does not have a compatible surface. The other detection methods are based on digital camera properties, like watermarking [4] and sensor pattern noise [8]. The Copy-Move detection methods [9], [7] are limited to one particular case of forgeries. This paper introduces the forgery detection with a general perspective, by using color data of an image.

We refer to a new approach for detecting the image portions which are copied from another image. This method can supplement to the CFA (Color Filter Array) interpolation technique [6]. This research paper illustrates a source code in Matlab, which senses the image forgery which is carried out using a Copy-Paste operation.

METHODOLOGY

A test image contains the image forgery, where the portion of a same image and copied and pasted into another part of an image. A raster scan [2] of an image senses the image points having the same color values. Since such forgery is assumed to contain a group of pixels instead of an individual

* Corresponding author – jajalbr@yahoo.com

value, the comparison of a left/right co-ordinate value is also done. The double comparison also reduces the false positive values. A 4-connected method for flood-filling a graphical object considers the neighbours on all 4 sides, while in a current study; 1-connected approach [3] is applied.

A Matlab Source Code for Sensing image forgery is as follows:
% Matlab code to sense the copy-paste regions into image file

The above algorithm executes to compare each and every pixel of an image with another one having exactly the same value. Once the same pixels are determined, they are also checked to have same value of neighbouring pixels. This check is with reference to the assumption that a wide area is copied, rather than a single pixel. On determination of such set of same pixels, they are assumed for forgery and an algorithm changes the pixel value to zero, representing black color.

The above algorithm executes to compare each and every pixel of an image with another one having exactly the same value. Once the same pixels are determined, they are also checked to have same value of neighbouring pixels. This check is with reference to the assumption that a wide area is copied, rather than a single pixel. On determination of such set of same pixels, they are assumed for forgery and an algorithm changes the pixel value to zero, representing black color.

```
i=imread('sample1.bmp');
z=zeros(100,100);  %   To check that pixel is already processed or not
for x=1:98
  for y=1:98
    for a=x:98
      for b=y:98
        if (z(a,b)==0)  % If not processed then ..
          if ( (i(x,y,1)==i(a,b,1)) && (i(x,y,2)==i(a,b,2))&&(i(x,y,3)==i(a,b,3))&&
          (i(x+1,y,1)==i(a+1,b,1)) && (i(x+1,y,2)==i(a+1,b,2))&&(i(x+1,y,3)==i(a+1,b,3))&&
                                        (~ ((x==a)&&(y==b))))
                                        % Check that pixel with its adjacent (x+1) is also same
                                              i(x,y,1)=0;  % Make all 3 values 0 for black.
                                              i(x,y,2)=0;
                                              i(x,y,3)=0;  % i(a,b) represents another set of copy.
        end  % inner if over
      end  % outer if over
    end  % b loop
  end  % a loop
  z(x,y)=1; % Now pixel checking is over with all other pixels of image.
 end % y loop – image width
end % x loop – image height
imshow(i)  % Displaying resultant sensed areas.
```

RESULTS

An image manipulation or forgery is assumed to be carried out with the two major intentions:

I. Copying the background portion to hide some information, considered as eliminate forgery.

II. Copying the portion to show it multiple times, considered as enhance forgery.

The Fig. 2. represents an original family photo, which is tampered to remove the unwanted person on left side (Fig. 3). The execution of a procedure considers the forgery image as an input and results into sensing the area which is tampered (Fig. 6). In order to verify the procedure for enhance forgery, another image (Fig. 4) is tampered by the user (Fig. 5), which also senses the forgery area successfully (Fig. 7).

ANALYSIS

From the above results, it can be easily predicted that a second run of the same algorithm may be carried out in order to reduce the false positives, which is found to be less than 10% in the results.

Figure 2: Family photo

Figure 3: Eliminate Forgery

Figure 4: River photo

Figure 5: Enhance Forgery

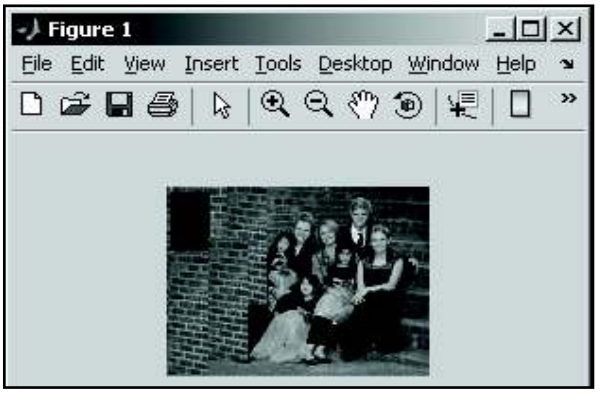

Figure 6: Sensing Eliminate Forgery

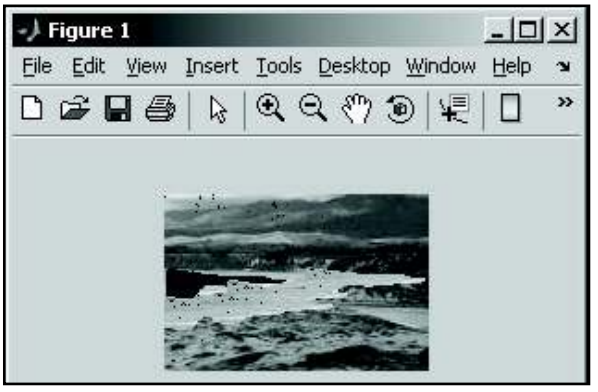

Figure 7: Sensing Enhance forgery

Table 1: Image samples with corresponding false positives

Image RGB Distribution	False positives	Percentage
Uniform 100x100 (Worst Case)	730	7.30
Normal 100x100	103	1.03
Random 100x100 (Best case)	12	0.12

Table-1 shows the results of using 1-connected approach. From the above results, it can be easily predicted that if the image comprises the similar areas within, the false positives are naturally ought to be more. However, the moderate images are found to be almost near to the normal distribution.

CONCLUSION

This paper is an effort to determine the image forgery at preliminary level, with a straight forward imperative. The method can be utilized in conjunction with the other existing techniques, for better results and cross verifications. The problem of detection of digital forgeries is a complex one with no universally applicable solution.

ACKNOWLEDGEMENT

The authors convey sincere gratitude to Dr. Darshan Chokshi, Professor and Head, P. G. Department of Computer Science for his helpful tips and guidance. The appreciation is also due to Dr. Paresh Virparia for being a source of inspiration to the research work.

REFERENCES

[1] *Website*: http://www.hackerfactor.com

[2] Gonzalez, R. C. and Wood, R. E. (2005) *Digital Image Processing*, 2nd edn. Addison Wesley Publishing Company.

[3] Hern, D. and Baker, M. P. (1996) *Computer Graphics*, 2nd edn. Prentice-Hall, India.

[4] Katzenbeisser, S. and Petitcolas, F. (2000) *Information Techniques for Steganography and Digital Watermarking*, Artec House.

[5] Johnson, M. K. and Farid, H. (2005) *Exposing Digital Forgeries by Detecting Inconsistencies in Lighting*, ACM Multimedia and Security Workshop, New York, USA.

[6] Popescu, A. C. and Farid, H. (2005) Exposing digital forgeries in dolor filter array interpolated images, IEEE *Transactions on Signal Processing*, **53(10)**: pp. 3948-3959.

[7] Popescu, A. C. and Farid, H. (2004) Exposing digital forgeries by detecting duplicated image regions, *Technical Report*, TR2004-515, Darmouth College, Computer Science 2004.

[8] Lukáš, J., Fridrich, J. and Goljan, M. (2006) Detecting digital image forgeries using sensor pattern noise, In: *Proceedings of the SPIE*, **6072**, pp. 362-372.

[9] Fridrich, J., Soukal, D. and Lukáš, J. (2003) Detection of copy-move forgery in digital images, In: *Proceedings of Digital Forensics Research Workshop*.

PRAJÑĀ - **Journal of Pure and Applied Sciences**
Vol. 17: 108-116, 2009 ISSN 0975 - 2595

CROSS LAYER MOBILITY MANAGEMENT IN HETEROGENEOUS WIRELESS SEAMLESS TECHNOLOGY USING IPV6

Krunalkumar C. Kamani and Dhaval R. Kathiriya [1*]

Information Technology Center, Anand Agricultural University, Anand, Gujarat – 388 001.
[1]MCA Department, L. D. R. P. Institute of Tech. and Research, Gandhinagar, Gujarat

ABSTRACT

The growing availability and ubiquity of different types of access networks is driving an evolution towards a "network of networks" consisting of heterogeneous but interconnected core and access network technologies that enable users to be always "best connected" anytime, anywhere, without much thought to the background technology used for maintaining and securing connectivity. However, before this vision is realized there are several technological barriers that must be overcome. It is widely anticipated that beyond 3G networks will be an IP-based integration of heterogeneous wireless access technologies. "Seamless Mobility" in such network is much more difficult to be achieved than in traditional wireless telecommunication networks because the B3G network environments are more complex, and various IP-based services presents various QoS requirements, and single handover strategy can not meet all the situations. An integrated mobility management solution is really needed instead of the one fold IP-layer solution such as Mobile IP. In fact, Mobile IP is a simple routing redirection mechanism and the handover performance of Mobile IP is very poor due to the inherent problems in IP such as no sensitivity on the requirements of QoS from application layer and the change of under layer service environments. This article tries to divide the task of "Seamless Mobility" into several subtasks including a well-defined mobility management framework, an IP-layer signaling protocol with good extensibility to support mobility, an set of typical IP-layer handover strategies, an adaptive Handover Control scheme and multi-mode support in Mobile Nodes. Obviously, Mobile IPv6 is perfect as IP-layer mobility protocol and all the handover strategies are designed based on Hierarchical Network-layer Mobility Management framework and implemented by extending of Mobile IPv6. The adaptive Handover Control scheme is proposed to improve IP-layer handover performance and optimize the utilization of multiple network resources based on accurate handover decision on target network, handover strategy and handover time according to cross-layer information. In addition, Mobile Nodes should be modified to support multiple available interfaces and the network-layer mobility management functions.

Keywords: **heterogeneous IP-based networks, cross-layer, handover control, hierarchical network-layer mobility management, mobile IPv6**

INTRODUCTION

The future of telecommunication network will be an IP-based integration of heterogeneous wireless and wired access networks. Such integration means not only the multiple access capability in mobile nodes, the dominant IP-based service across Mobile Internet but also the seamless mobility between the IP-based heterogeneous networks. Implementation of seamless traditional cellular wireless systems. The complexity of IP-based heterogeneous network environments implicate that Mobile Node must support multi-access capabilities which result in that different handover strategy should be adopted in different network scenario. As figure 1 show, handover may happen within an IP-subnet with homogeneous access technology. The article focuses on the handovers happen between IP-subnets. Such handover will introduce the change of IP-prefix and the network connectivity will be interrupted resultantly according to the IP-layer routing mechanism. IP-layer handover of Mobile IP defined by IETF is introduced to maintain continuous data connectivity in such situations. IP-layer handover scenarios should be identified by heterogeneous access technologies and movement direction. One fold IP-layer handover strategies can not meet all the handover scenarios.

IP as in 3GPP2, Mobile IP is also introduced in the core network. The IEEE recently approved a group called 802.21 to standardize cross-network handover mechanism based on Mobile IP. At the same time, the poor IP-layer handover performance has become the big trouble for the usability of Mobile IP and the inherent issues in IP/Mobile IP result in the obstacle to support seamless mobility in heterogeneous networks. IP layer provides upper layers "best-effort" packet transmission mechanism with no sensitivity on service QoS requirements and network service environments. However, such sensitivity is required to decide on appropriate target network,

* Corresponding author – drkathiriya@yahoo.com

handover strategy and handover time when an IP-layer handover is detected. Due to such inherent problems, Mobile IP cannot define an effective handover control scheme to schedule the activities of IP-layer handover and dispatch the data flows from different applications to appropriate network interfaces.

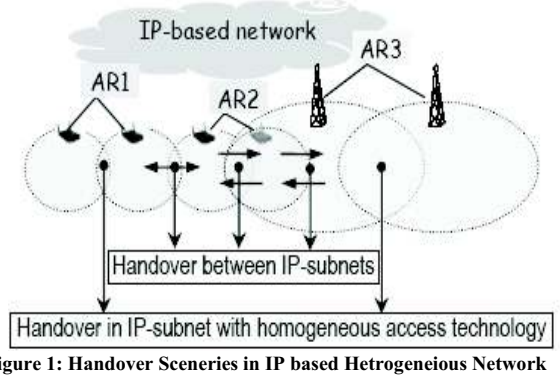

Figure 1: Handover Sceneries in IP based Hetrogeneious Network

Research Contributions

Paper focuses on seamless roaming of beyond 3G systems, tries to divide the task of "Seamless Mobility" into several subtasks as Fig. 2 shows.

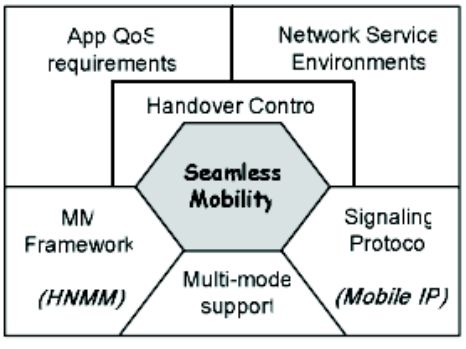

Figure 2: Key Components to Support Seamless Mobility

- ✓ Well-defined mobility management framework.
- ✓ An IP-layer signaling protocol with good extensibility to support mobility and a set of typical IP-layer handover strategies by extending such protocol.
- ✓ An adaptive Handover Control scheme.
- ✓ Multi-mode support in Mobile Nodes.

We define Mobile IPv6 as IP-layer mobility-support protocol with good extensibility and all the handover strategies can be implemented by extending Mobility Header in IPv6. In the paper, a Hierarchical Network-layer Mobility Management framework – HNMM is designed as research foundations. The adaptive Handover Control scheme is proposed to improve IP-layer handover performance and optimize the utilization of multiple network resources based on accurate handover decision on target network, handover strategy and handover time according to cross-layer information. Mobile Node is modified to support multiple available interfaces and the new mobility management functions. In addition, we analysis on the handover performance of the typical IP-layer handover strategies combined with different network overlapped scenarios in NS simulation environments.

OVERVIEW OF BASIC MOBILE IP

Basic Mobile IP Mechanism

Mobile IP attempts to solve the macro-mobility problem: when mobile users move between different IP subnets, network connections will be interrupted due to the change in point-of-attachment IP address. In Mobile IP, the Mobile Node (MN) is configured with a static Home Address and a temporary Care of Address (CoA) as the MN roams to a foreign network. The Home Agent (HA) on the MN's home link acts as a routing anchor for the roaming MN on its home network. It does so by intercepting all the packets bound to the MNs' Home Address and dispatching these packets to the MNs' CoA via dynamically created IP tunnels. When the MN roams between IP-subnets, the MN sends Binding Update (BU) messages with its CoA to the Home Agent in order to update the HA of its current point of attachment. All the Mobile IP signaling messages are formed by extending IP protocols with option headers. Therefore, the signaling and data traffic are all transmitted via a unified IP framework.

Handover Performance of Basic Mobile IP

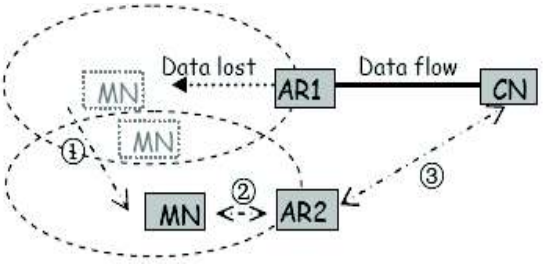

Figure 3: Analysis of IP - layer Handover Latency

In base Mobile IP, IP-layer handover latency is unacceptably long for real-time services with three aspects contributing to the latency as illustrated in figure 3.

IP-layer handover detection time (Td)
This is the time taken by a Mobile Node to detect the change of Access Router (AR) by processing a new Router Advertisement (RA) from the new AR. Td is determined by the RA interval (MinRtrAdvInterval). The Neighbor discovery protocol RFC2461 specifies a random RA interval between three and ten seconds; this interval will introduce the intolerant latency for IP-layer handover. The IETF specifies a much shorter interval of between 30ms to 70ms for ARs supporting MIPv6. However, shortening the interval will introduce additional signaling overhead and burden limited wireless bandwidth. The tradeoff between fast movement detection and cost of bandwidth is given in, which concludes that different RA intervals should be specified for different networks, i.e. the RA interval for GPRS is between 500 msec and 1 second based on experimental results from a GPRS-WLAN interworking test bed.

AR access admission time (Ta): This is the time taken by an MN to negotiate admission with a new AR, including MN Authentication time, CoA configuration time and IP connection becoming-effective time.

Binding Update time (Tb): This is the round-trip delay incurred by an MN sending a Binding Update to a Corresponding Node (CN) or Home Agent (HA) and receiving a BU Acknowledgement. When CN/HA receives BU from one MN, the packet to this MN's home address is redirected to the new CoA accordingly and the IP-layer handover ends.
In basic mobile IP, it is implicit that IP-layer handover is initiated after Layer-2 handover. As defined in, Layer-2 handover is a process by which an MN changes from one access point to another. Layer-2 handover time (TLayer-2) is a "built-in" value for a specified access technology. In basic Mobile IP, the total data interruption time is equal to amount of the four variables: "TLayer-2+Td+Ta+Tb" as figure 4 shows. IP-layer handover delay can be enhanced by improving Td, Ta and Tb respectively.

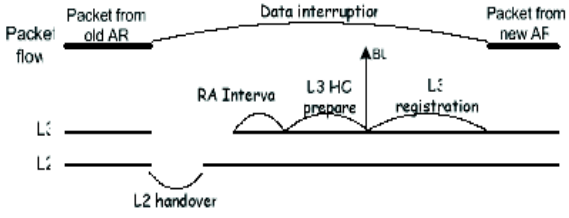

Figure 4 Data Interruption in Basic Mobile IP

In fact, IP-layer handover can be initiated ahead of Layer-2 handover if only MN can detect new AR at the time Layer-2 handover will happen by Link Layer triggers (Layer-2 trigger). The IETF has taken such proposals into consideration. The drafts "Fast Handovers for Mobile IPv6" and "Candidate Access Router Discovery" can be combined to provide fast handover functions. Layer-2 triggers provide a way to notify IP of the change on underlying network service environments. CARD protocol provides the network capability information to help decide on target network. Such mechanism can be looked as the rudiment of handover control scheme in IP-layer handover.

Problems in Mobile IP
The following problems in IP should be noticed when designing a seamless mobility mechanism based on Mobile IPv6.

1. Mobile IP is a simple routing redirection protocol instead of an integrated mobility management solution and mobility management framework should be well-defined to reduce the signaling cost and improve the handover performance.

2. IP/Mobile IP is not sensitive on the change of underlying network environments. Movement detection in basic Mobile IP is based on Router Advertisement in IP-layer, which introduces the primary latency in IP-layer handover.

3. IP/Mobile IP is not sensitive on the application QoS requirements and transmits packets in the "best-effort" way. Such insensitivity presents big trouble for seamless

mobility when vertical IP-layer handover happens.

4. IP/Mobile IP in Mobile Node can not support multiple working interfaces in overlapped network environments. However, some enhanced IP-layer handover strategies require multiple interfaces to transmit data and signaling synchronously. In IP/Mobile IP, it is implicated that there is only one default interface used to transmit the packets according to the Destination-Address-Routing principle even if there are multiple available interfaces in Mobile Node. Therefore, routing principle of Local Routing in Mobile Node should be different with Destination-Address-Routing in router. Therefore, it is necessary to design an integrated mobility management solution with well-defined mobility management framework and adaptive Handover Control scheme with awareness of cross-layer information.

Modeling of Mobility Management Framework

A well-defined Mobility Management framework is the foundation of seamless mobility. Mobility Management functions can be implemented as Mobility Management Agents (MMA) located in the routers, gateways or hosts. The mobility management signaling is exchanged between these MMAs to implement mobility management on Mobile Nodes. We introduce hierarchical structure to construct "Hierarchical Network-Layer Mobility Management [HNMM]" framework, because hierarchical structure is very efficient to reduce the signaling overhead and improve the handover performance The logical network structure of HNMM is shown in figure 5. HNMM is based on Mobile IPv6 and can be easily extended to support HMIPv6 . There are four function entities in HNMM: HMMA, RMMA, MMA and TMA.

- *HMMA* can be looked as Home Location Register (HLR) of Mobile Node (MN) and records all the basic information of every MN that belongs to the HMMA domain, such as current location and historical location and user profile information. HMMA cooperates with AAA system to manage the security of users and their services. Also the first-arrived packets sent to MN from CN will be intercepted at HMMA and be forward to RMMA that MN attaches to currently. So HMMA has two main functions, HLR and Home Agent for MN.

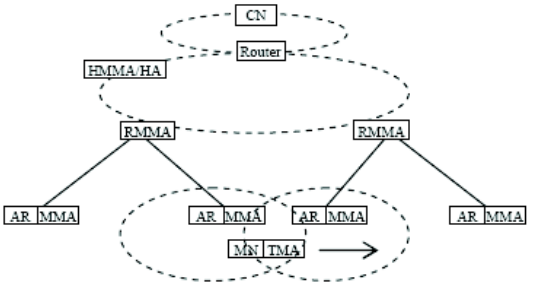

HMMA: Home Mobility Management Agent
RMMA: Region Mobility Management Agent
MMA: Mobility Management Agent
TMA: Terminal Mobility Agent

Figure 5: Hierarchical Network - Layer Mobility Management Framework

- *RMMA* can be looked as the Visit Location Register (VLR) and local mobility management functions including signaling analysis, location management and handoff management. RMMA also is responsible for initialization of paging.
- *MMA* is located in a radio access router on the hop between MN and RMMA. MMA is responsible for Configuring Care-of-Address for MN and collecting the mobility information of MN.
- *TMA* is located in MN and its location management functions include handoff control, signaling packet process, construction and firing, multiple interface management, etc.

Based on the hierarchical structure, mobility can be divided into Macro-mobility between RMMAs and Micro-mobility between MMAs attached to the same RMMA. Such structure distributes the location management information on different MMAs and minimizes macro-mobility management signaling and effectively improves IP-layer handoff performance by introducing micro-mobility concept.

Definition of Handover control scheme

Handover is the most important function of mobility management. In heterogeneous networks overlapping areas, seamless handover means not only the continuous data transmission but also the selection of the appropriate target access network and handover strategy at appropriate time. Therefore, the Handover Control function should be able to adapt itself to dynamic network environments and various QoS requirements. Handover (HO) can be controlled either by Network or Mobile Node. There are four types of handover scheme, Network Controlled, Mobile Controlled, Network Assisted and Mobile Assisted. Network Assisted Mobile Controlled (NAMC) scheme is adopted by considering that Mobile Node will become more powerful and intelligent. Comparing with network, Mobile Node is more sensitive on the change of multiple available interfaces. Network only provides the required information such as capability information of Candidate Access Router (CAR) as the criterion of handover decision, so NAMC can minimize the modification of network. The IP-layer Handover Control function is resident in Mobile Node as partial functions of Terminal Mobility Agent [TMA].

Modeling of Handover Control Scheme

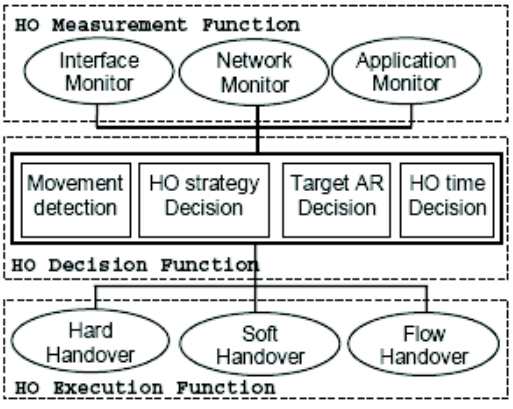

Figure 6: Functional Modeling of IP Layer handover

IP-layer handover control can be modeled as three functions as figure 6 shows: HO Measurement, HO Decision and HO Execution. HO Measurement is responsible for collecting the information from local interface, network and applications as the criterions for handover decisions. Handover Measurement function is alive all along. Some new-defined protocols can be used as the carriers of capability information of networks. For example, the Candidate Access Router set and their capability information can be confirmed and transported by CARD protocol. In the HO Decision function, IP-layer HO related issues are decided such as handover strategy, target AR and handover time according to dynamic and static parameters such as network load information, available interface, QoS requirements etc collected by HO Measurement. In HO Execution, the selected handover strategy is executed, and IP connectivity with the new AR is established and binding update is sent out to complete Mobile IP re-registration. In traditional cellular systems input parameters for handover decision algorithm is comparatively simple than in the heterogeneous network environments. Traditional cellular systems provide mobile users with a unified access technology and service environment. Handover is triggered primarily by decision on link quality and singling strength. While in heterogeneous wireless networks, HO decision is made according to more complex service environments with different access technologies and charging models. In our Handover Control Scheme, HO Decision algorithms are designed based on fuzzy logic because a fuzzy logic system is flexible and capable of operating with imprecise data, and can therefore be used to model nonlinear functions with arbitrary complexity.

The Handover Control framework is designed as a background control plane comparing with User Protocol Plane (typically TCP/IP protocol stack). The plane is divided into multiple sub-functions such as Handover Measurement and Handover Decision. In order to make accurate handover decisions, Handover Measurement should intercommunicate with multiple protocol layers to collect sufficient information for Handover Decision. Handover Execution is the process of IP-layer handover signaling in Mobile IP module in User Protocol Plane. Mobile IP module is responsible for processing, constructing and sending out the special IP signaling packets under the control of Handover Control. The relationship between Handover Control Plane (HC-P) and User Protocol Plane (UP-P) is described as Figure 7.

- ✓ HO Measurement in HC-P can collect the information from multiple layers of UP-P;
- ✓ HC-P makes Handover Decisions according to the information collected by HO Measurement;
- ✓ Mobile IP module located in UP-P is responsible for process, construction and firing of IP-layer signaling under the control of HC-P.
- ✓ UP-P dispatches its data flows from different applications to appropriate interfaces under the control of UC-P.
- ✓ HC-P proposes to provide the multiple interface control functions.

Some new functions should be extended base on current UP-P to meet the requirements of seamless mobility. Mobile IP protocol should be supported. IP-layer must be modified to support Local Routing among multiple working interfaces. Cross-layer interaction interfaces between UP-P and HC-P should be defined to transmit the HO Measurement information and HO control information. Trigger mechanism should be supported by under layers to promote the process of IP-layer handover.

Functional Entities in Handover Control Scheme

Figure 8 illustrates the functional entities in HC-P and their interaction with UP-P. There are four functional elements in HC including Handover Measurement, Handover Decision, Unified Trigger Mechanism and Interface Control. Every functional part has its sub-entities.

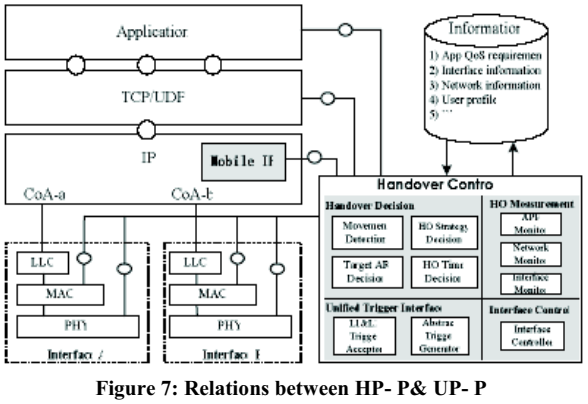

Figure 7: Relations between HP- P& UP- P

Handover Measurement Application Monitor collects the QoS requirements from applications *Network Monitor:* collects the network capability information from remote network. The entity can utilize the CARD protocol to perform the function or define its special mechanism to obtain the information.

Interface Monitor: collects the status and load information from local interfaces.

L1&L2 Trigger Accepter: is responsible for retransmit all registered the triggers from PHY layer (L1) and MAC layer (L2) to upper layer through a unified SAP.

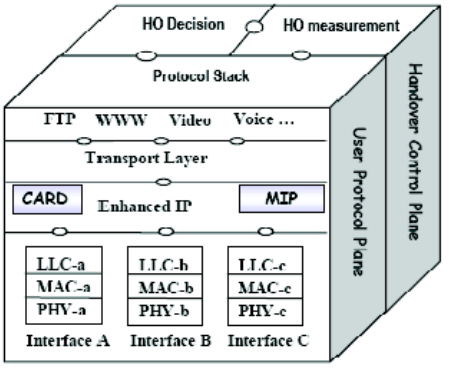

Figure 8: Hanover Control Function Entities

Abstract Trigger Generator: is responsible for generating abstract triggers (multi-dimension triggers) according to specific algorithms and multiple input parameters. The parameters can be information items stored in Information Base and be parameters in L1 and L2 trigger.

Handover Decision Movement Detection

Decision on Movement can be triggered by special trigger such as Link_going_down and the criterion can be the information provided byHO Measurement.

Target Access Router Decision: Decision on target AR is to decide which IP sub-network the Mobile Node (MN) intends to handover to. In the heterogeneous network environment, to make the decision on target network is complex for it needs more parameters such as network load, user profile, QoS requirements of MN's current services, candidate access routers and their capacity information, etc. Sometimes, the location information of MN can also be used as one of the parameters if it is available. These parameters are provided by HO Measurement. In order to schedule IP-layer handover effectively, decision on target AR can be fired by special triggers. When receiving the trigger, MN starts to make the

decision on target AR according to the information collected by HO Measurement.

Handover strategy decision: Decision on handover strategy is to decide the proper handover strategy which Mobile IP module will adopt the parameters which must be considered in this decision process are similar to those used in decision on target network. Handover strategy decision can be fired by trigger, too.

Handover timing Decision: Decision on handover time is to decide when to send out the IP-layer handover signaling. In generally, the decision may be simplified as receiving a special trigger. Once such trigger is received by HC-P, the IP-layer handover signaling should be sent out immediately.

Interface Control

It is responsible for providing the limited control functions on under layers. HC-P should not disturb the functional process and working status except consideration of power management, etc. HC-P can select appropriate interface to use according to cross layer information but can not determine when to initiate an attach process to a new access point (such as Scan process in WLAN) because it should be control by the specific access technologies and depends very much on different network devices and drivers.

Information Base

It is responsible for providing detailed dynamic and static information about various networks that can assist in handover decision. Static & dynamic information in Information Base is maintained by Handover Measurement and trigger mechanism.

Trigger Mechanism in Handover Control Scheme

In the general proposals, trigger performs as simple Handover Control mechanism. For example, in Fast handover proposal, movement detection and handover time are decided by information in L2 triggers. Such triggers are generally defined as the signaling strength exceeding the predefined thresholds. In fact, such trigger mechanism should be refined to support more accurate Handover Control scheme.

In our Handover Control scheme, the usage of trigger is extended. Not only the IP-layer handover signaling but also the handover decision can be fired by trigger. Triggers generated from different layers are transmitted to their client modules by the unified interface in HC-P. In addition, we propose new trigger concept to provide more accurate indication of abstract events such as Link_going_down.

- ✓ One-dimension trigger: means that the trigger should only indicate an event related to one parameter. For example, when signaling strength exceeds a predefined threshold, a one-dimension trigger will be generated.

- ✓ Multi-dimension trigger: It is also called "abstract trigger", means that the trigger reflects an abstract event related to multiple parameters. For example, Link_going_down trigger indicates an abstract event of "one link is going to down". More exact Link_going_down indication should be got by integrated decision based on multiple input parameters such as signaling strength, FER,Location etc, according to specific algorithm instead of only by signaling strength because signaling strength is affected by many factors and may change a great many in a very short time. The algorithm should be carefully designed to generate such indication more accurately.

In the Handover Control scheme, multi-dimension trigger is generated by Abstract Trigger Generator in HC-P and one-dimension trigger is generated by modification on current under layers in UP-P. L1 and L2 triggers are designed as one-dimension trigger because the design can be implemented easily with minimized modification of under layer in UP-P. It is appropriate to generate multi-dimension triggers in HC-P because multi-dimension trigger is got by integrated decision on multi-layer parameters from one interface or all interfaces in Mobile Node according to specific algorithm. HC-P provide the possibility of more exact decision on abstract event (such as Link_going_down) and executing corresponding algorithm to generate abstract triggers with minimized modification of UP-P. The various triggers introduce the disorder in registration and transmission of triggers between different

modules in protocol stacks. HC-P is proposed to provide a unified trigger interface of all these triggers from different modules. HC-P is endowed with the unified interface function for under layers triggers. L1 and L2 triggers are transmitted to HC-P firstly and repeated to upper layer or stored in the Information Base. HC-P provides a unified SAP to transmit the triggers and any module is asked to register their required triggers in HC-P trigger module.

Multiple interface support in local routing

It is necessary to transmit packets on multiple interfaces synchronously when considering seamless mobility requirements. For example, in a global network like 3G network, MN can provides the services like telephony, video and web browser through the 3G wireless interface. When the MN enters the hotspot covered by the technology with the higher rate (e.g. WLANs) and the WLAN interface is available, the MN maybe prefers to handover the high-rate service such as video to the WLAN interface while keep the others in 3G interface. Such handover is called "Flow-handover" and multiple working interfaces should be supported in Flow handover. In IP/Mobile IP, it is implicated that there is only one default interface used to transmit the packets according to the "Destination-Address-Routing" principle even if there are multiple available interfaces in Mobile Node. In fact, routing principle of Local Routing in host should be different with Destination-Address-Routing in router. Figure 9 illustrates the modification to support multiple working interfaces in Mobile Node. The main functions include Target AR selection in HC-P, Source Network Address Mapping and Source Address Local Routing in UP-P.

- Target AR Selection plays a key role in QoS guarantee because it is responsible for selecting the appropriate target Access Router and resultant selecting the network interface connected to the AR to transmit data flow from specific service when network serving environments changes or a new application begins to run.

- Source Network Address Mapping is introduced by Mobile IP. In Mobile IP, Home Address is looked as a static terminal identifier in global scale and Care of Address (CoA) configured on the network interface is looked as local routing identifier. When MN sends a packet out, Home Address is the only available source address in IP header from the transport layer point of view. The mapping of source address in IP header between Home address and CoAs is needed within Mobile IP module. One Home Address in MN can be mapped to one or several CoAs.

- Source Address Local Routing, which will dispatch the out-going packets to the specific interface according to Source Address (it is CoA now) in IP header instead of Destination Address. Because the CoAs are configured corresponding to certain interfaces respectively, selection of target interface is transformed into selection of CoA. Multiple working interface support should be designed combining with Target Access Router Selection in HC-P.

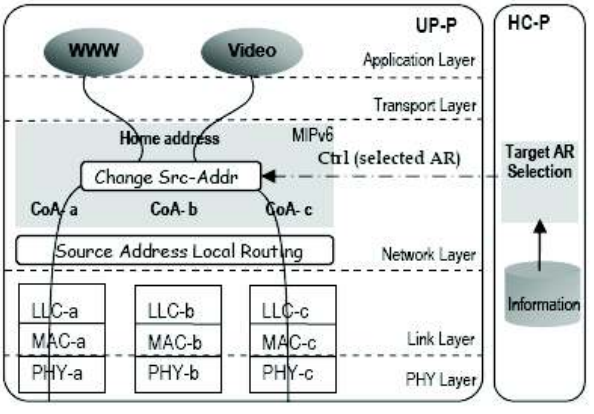

Figure 9: Multiple Working Interface Support in Local Routing

In mobile IP module, the home address will be replaced by one of the CoAs with the direction of Target AR Selection. In fact, decision on target Access Router means that the interface connected to the Access Router is selected and resultantly the corresponding CoA configured on the interface is confirmed. Once the Source Address in IP packet is overwritten by a certain CoA, the local routing can dispatch the packet to the corresponding interface according to the CoA. It is necessary to maintain two mapping tables in UP-P. One is AR-to-CoA mapping table and another is CoA-to-Interface mapping table.

CONCLUSION

Seamless mobility between heterogeneous IP-based networks is a cross-layer problem. If only IP-layer solution is considered, the performance enhancement of IP-layer handover is very limited. So under-layer trigger is proposed to assist Mobile IP to schedule IP-layer handover signaling in a more effective way. When considering seamless mobility from the point of view of services, QoS requirements from application layer should also be noticed. In such conditions, it is appropriate to reconsider Mobile IP only as a simple IP-layer signaling protocol. A cross-layer Handover Control scheme should be defined to enhance the IP-layer handover performance and optimize the utilization of redundant network resources. With the trend of IP-based convergence of heterogeneous networks and the development of intelligent terminals, the network functions such as Mobility Management will be transferred to mobile terminals gradually. The complex Handover Control in heterogeneous network environments presents big challenges on the hardware and software design of mobile devices. Therefore, Handover control functions may be distributed in network and terminal at the first implementation phase. In a word, implementing seamless mobility between heterogeneous networks is a road to hope with big challenges.

REFERENCES

[1] http://w3.antd.nist.gov/seamlessandsecure.shtml.

[2] Kamani, K. C., Kathiriya, D. R. and Virparia, P. V. (2009) "NFC: Essential for Successful Short Range Wireless Interoperable Communications" *IJCA-ETS-2009.*

[3] Kamani, K. C., Kathiriya, D. R. and Virparia, P. V. (2009) "NFC: Security Issues in the Context of Authentication using Mobile Coupons Scheme" *Processing of CSI national Seminar on Current Trends in ICT, Sardar Patel University, V.V.Nagar (CTICT-2009).*

[4] Kamani, K. C., Desai, R. S. and Gandhi, V. A. (2008) NFC: The Next Gen ISO Specification in Wireless Technology for Communication*, Proceedings of the International Conference on ETA -ETS, 2008.*

[5] Kathiriya, D. R., Kamani, K. C., Atkotiya, K. H. and Gondaliya A. K. (2008) Network based Authentication using Kerberos. *Proceeding of the National Conference on Evolving Communication Technologies and Knowledge Management (ECTKM-08).*

[6] Kamani, K. C. and Gandhi, V. A. (2006) Exploring Security in Near Field Communication. *9th National Conference of Indian Society of Statistics Saurashtra University- Rajkot, 11-13 November, 2006.*

[7] Johnson, D., Perkins, C. and Arkko, J. (2004) "Mobility Support in IPv6", RFC 3775, IETF, June 2004.

[8] IEEE 802.21 work group, http://www.ieee802.org.

[9] Yana Bi, Ruijun Feng, Prakash Iyer, Xiao Hu and Mei Song (2004) "HNMM: A Novel IP Layer Mobility Management Framework For Beyond 3G Networks", WWRF04, February 2004.

[10] Hsieh, R. Zhou, Z. and Seneviratne, A. (2003) "S-MIP: A Seamless Handoff Architecture for Mobile IP", IEEE INFOCOM 2003, March 2003.

[11] Rajeev Koodli (2003) "Fast Handovers for Mobile IPv6", Internet-draft, IETF, March 2003.

[12] Manner, J. and Kojo, M. (2002) "Mobility related terminology", draft-manner-seamoby-terms-04.txt.

[13] Narten, T. (1998) "Neighbor Discovery for IP Version 6 (IPv6)", RFC2461, IETF, December 1998.

[14] Chakravorty, R. Vidales, P. Patanapongpibul, L. and Subramanian, K. "On Inter-network Handover Performance using Mobile IPv6".

[15] http://www.cl.cam.ac.uk/users/rc277/handovers.pdf.

PRAJÑĀ - **Journal of Pure and Applied Sciences**
Vol. 17: 117-121 2009 ISSN 0975 - 2595

ROLE OF MTF IN ANALYSING THE CONTRAST AND THRESHOLD PERFORMANCE OF HUMAN VISUAL SYSTEM

Priti Srinivas Sajja [*] and Vishal Dahiya [1]

Department of Computer Science, Sardar Patel University, Vallabh Vidyanagar, Gujarat – 388 120
[1]Institute of Business Management & Research, Ahmedabad, Gujarat – 380 001

ABSTRACT

This research is focused on practical model of the contrast performance of the human visual system. The level of contrast required to achieve recognition of a given image or class of images projected onto the photon sensitive surface at a specific scale is discussed in this paper. The solution is derived from the signal to threshold condition for its mapping on the retina and from retina to brain. Different types of image exhibits different signals to the threshold requirement. The difference between them is small relative to the total instantaneous dynamic range of the visual system. The signal processing is also dependent on the Modulation Transfer Function (MTF) that impacts the threshold contrast performance of the Human Visual System (HVS). There are number of stages and pathways for processing an image by HVS, which are explored in this paper.

***Keywords*: modulation, visual, system, contrast.**

INTRODUCTION

Radiation space to which the eye responds is of complicated nature and hence, it has always been difficult to provide a meaningful but short description of this environment. This has usually been done by assuming that the eye exhibits a fixed or nearly fixed spectral response over a wide range of irradiant intensity almost regardless of the color temperature of the source. Unfortunately, the eye does not exhibit a constant spectral response over the two regions normally considered. These are imprecisely defined photopic and scotopic regions. In addition, the color temperature of the source of radiation is a crucial factor in determining the performance of the eye. Illuminance is primarily an application oriented engineering term. It attempts to provide a scalar value for the integral of the irradiance of a given source, at a normally unspecified color temperature, over a nominal spectral interval.

It is known that the density of photoreceptors in the retina is greatest in the central area (fovea) and decreases to the retinal periphery whereas the size of neuronal receptive fields in the retinal output and in the cortical map of the retina increases to the periphery [1]. As a result, the resolution of the image representation in the visual cortex is highest for the part of the image projected onto the fovea and decreases rapidly with distance from the fovea center. During visual perception and recognition, human eyes move and successively fixate at the most informative parts of the image which therefore are processed with the highest resolution. At the same time, the mechanism of visual attention uses information extracted from the retinal periphery for selection of the next eye position and control of eye movement. Thus, the eyes actively perform problem-oriented selection and processing of information from the visible world under the control of visual attention. A perceived color for a long wavelength trichromat is defined precisely by the pair of values, (P, Q), associated with the two chrominance channels of vision.

Models that predict human performance on narrow classes of visual stimuli abound in the vision science literature. However, the vision and the applied imaging communities need robust general-purpose, rather than narrow, computational human visual system (HVS) models to evaluate image fidelity and quality and ultimately improve imaging algorithms. Psychophysical measures of image quality are too costly and time consuming to gather to evaluate the impact each algorithm modification might have on image quality. Modulation Transfer Function (MTF) is an important factor for determining the relationship between number of variables such as perception criteria, level of threshold, signal luminance and contrast threshold. Acquiring the image consists not only of the optical capturing process occurring on the

* Corresponding author – priti_sajja@yahoo.com

retina of the eye, but also of the lighting that makes the objects in the scene visible.

The question of what features are detected from 2D retinal images at the preattentive stage to represent the shape of 3D objects is still open. Neurophysiologic studies have demonstrated that neurons in the primary visual cortex can detect elementary image features such as local orientations of line segments or edges. Therefore, most early theories based on neurophysiologic data assumed that the visual system detects relatively simple features at the preattentive stage and uses some attention mechanisms of a serial type to bind the simple features into more complex shape features [2]. Alternatively, recent psychological studies have shown that early visual processes are much more sophisticated than previously assumed. Certain relations among features are detected preattentively including some 2D feature combinations reflecting elements of 3D shapes [3]. The spatial patterns of edges may represent 2D projections of elementary 3D shapes (e.g. vertices) and more complex combinations of 3D angles. The detection of spatial patterns of edges at the preattentive stage may contribute to 3D scene perception in addition to other mechanisms [1] (stereopsis and binocular depth perception; color and texture analysis; analysis of occlusions during head or body movements, etc.). Stereopsis is the sense of depth derived from binocular disparities between the left and right retinal images. Several studies have shown that spatial frequency is one of crucial factors for determining the disparity threshold (or stereo acuity). Some researchers showed that the disparity threshold increased with the decrease of spatial frequency (size-disparity correlation) below 2 c/deg while approximately constant at frequencies higher than 2 c/deg [5]. Such a dependency of disparity threshold on spatial frequency is likely related to the spatial frequency channels with which the visual system analyzes the retinal images dividing several spatial frequency components [4, 6].

MODULATION TRANSFER FUNCTION

The signal information can be described by considering Modulation Transfer Function which is inversely proportional to the product of signal luminance and contrast threshold and directly proportional to perception and threshold level.

We can use this equation to find out the value of MTF:

Modulation Transfer Function = (PC * LT) / (CT*SL) --- ------ (1)

Where PC -> Perception Criteria
LT->Level of Threshold
CT->Contrast Threshold
SL->Signal Luminance

The threshold contrast performance of the human visual system can be described using a slightly more complex concept of modulation transfer functions. The approach is the same as that used in image transmission systems that involve a series of MTF's. This function describes the response of a given parameter as a function of spatial or temporal frequency. There are four primary elements in the visual system that exhibit MTF's [5]. The first is the lens group and the second is the Photoexcitation/De-excitation mechanism within the Outer Segments of the photoreceptors. The third is the adaptation amplifier and fourth is the integrator associated with the demodulator associated with the signal projection circuits. Typical delay associated with the Photoexcitation/De-excitation Equation at photopic levels 3.36 milliseconds. Typical transmission delays (latencies) from retina to midbrain 1.0 ms. [9]

The term spatial frequency, as applied herein, contemplates cycles per degree based on the number of gratings per degree of visual angle subtended when observing the grating from a distance of one meter. As defined, it is based on a small angular excursion. Clearly, the observation distance and grating size are inextricably linked when spatial frequency is presented in terms of cycles per degree.

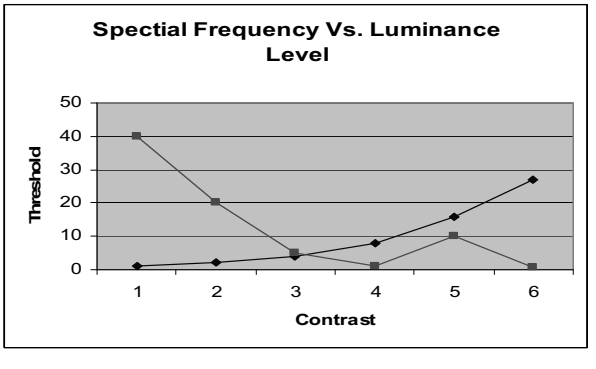

Figure 1: Effect of spatial frequency and luminance level on to the contrast and threshold

Figure 1 explains the relationship i.e. if spatial frequency increases then the contrast and threshold both are increasing, while Threshold is directly proportional to the luminance level while contrast is inversely proportional to luminance level [5].

The visual components of a scene such as color and light can be easily evaluated but it is very difficult to get the geometrical components of the image. In most cases it is obvious how to display the images, but geometrical information is needed for a correct synthesis of novel views [8].

Till now most of the work is done on physiological structure of eye, how human eye can perceive an object, evaluate it and recognize it. Number of models based on attention guided visual perception and visual recognition are proposed which work on eye movement, memorizing an image, recognizing an image [11]. However, limited work is done on how a 3D perceived image is to be mapped onto the 2D screen. Most of the models which are proposed do not describe the different processing which is to be done by the human eye and brain before mapping that object onto the 2D screen. This work attempts to find out how eye and brain collectively recognize an image and projects that image onto the 2D screen.

Most of the computer vision work is done on either 3D image mapping on to 2D screen (i.e. most of image processing applications) or the retinal analysis of image (image acquisition) [10]. However, limited research is done on the composite work of eye and brain and then its mapping on the computer screen.

The proposed model shows what are the different stages required to get an image and displaying that image on the monitor. This model is a new concept as the previous models or concepts are mainly based on the pattern recognition, image formation, image sensing, shape formation etc. This model describes all the major elements that are required to get the performance of the visual system. For getting the actual performance of the visual system, two most important situations are: The visual system relies upon the tremor of the eye during a gaze to convert spatial frequency information into temporal frequency information and the description of MTF's.

This model is very useful in many areas such as: finding out the problems that exist in an individual eye such as color disorder, not able to recognize the object, and not able to find the intensity of light while perceiving an image.

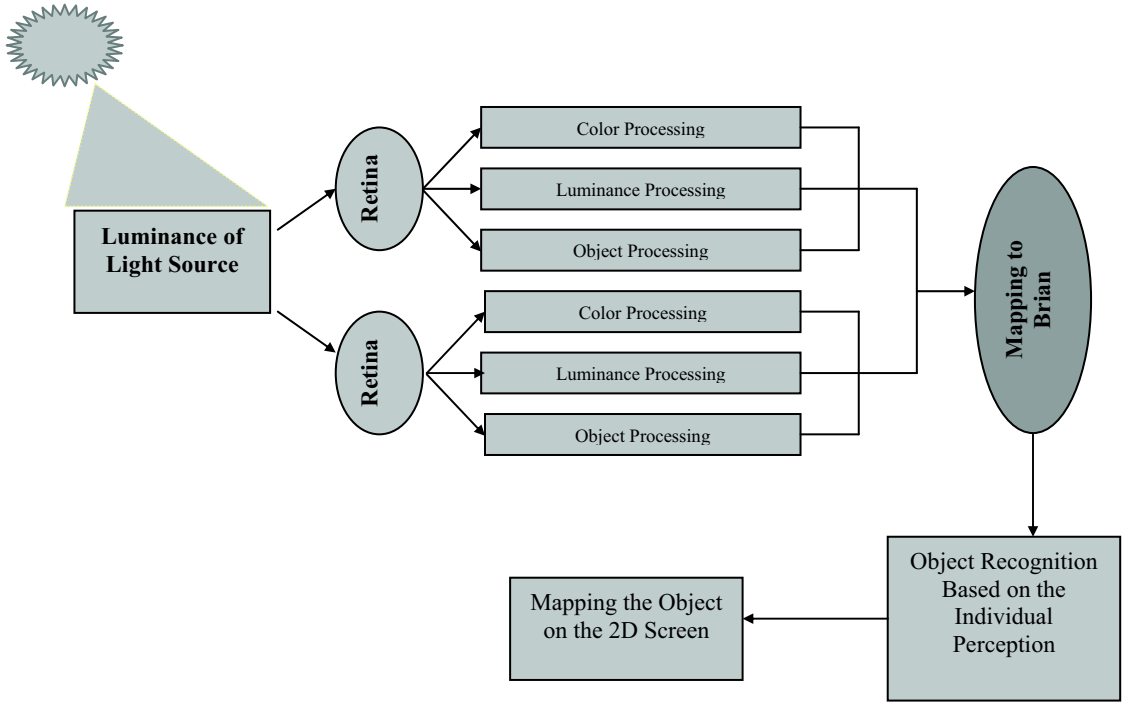

Figure 2: Proposed model for receiving an object by human visual system and its mapping to screen

PROPOSED MODEL

The stimulus comes from the light source or luminance, as it falls on the retina of the eye and three processing will start that is Color processing, Luminance Processing, and Object processing. Color Processing is to find out the different colors the image has, Luminance processing is to find out the different intensity of light the image has, Object processing is to find the shape, size, structure of the image. In this processing, the mapping is to be done on human brain and then the brain directs about the object i.e. its color, shape, contrast, depth cuing etc. All this process depends on the perception of the receiver. To get the information how a particular person is analyzing the object, we can map that particular object on to the 2D screen by digitizing the object. Now the object will be converted to the matrix representation which will be derived from the digitization process. After digitization of the image, image processing is to be done that is segmentation, shape information, interpretation, semantic analysis, etc.

The light source is shown explicitly in Figure 2 because it determines to a large extent the operating regime of the visual system. The image must be of sufficient luminance to establish the photopic visual range. It must also be free of any dynamic elements in the temporal or spatial frequency range that might interfere with the data collection and analysis program. This condition is a function of both the source (frequently a CRT monitor) and the brain. As an example, Watson has explored the phosphor decay characteristics of a particular monochrome monitor and how they impact the performance of the eye along the direction of the flying spot. A similar analysis of the visual system would demonstrate that it is important to hold the stimulus fixed in both space and time for the duration of the stimuli interval since the eye may perform minor saccades between gazes during that interval. This is particularly true with respect to complex spatial patterns. The spectral content of the source and scene play a major role in the contrast performance of the visual system. This performance can be impacted by the spectral content of the luminance.

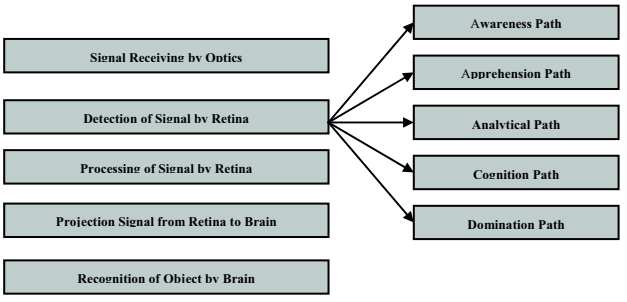

Figure 3: Process model for HVS

As shown in Figure 3, the signal receiving by the optics, the Optical stage is very important because how we receive is directly proportional to the optics property of the human eye. The pupil size is an important parameter in determining both the MTF of the system and the radiance applied to the photoreceptors. The square of the pupil diameter plays a major role in determining the actual illuminance achieved at the surface of the retina because it is a major determinant of the optical system. It is the illuminance of the retina, not the luminance of the source, which is the factor controlling visual performance. The signal detection stage of the visual system is different for different person. But considering the detection power we can consider two time constants and one of them is a variable as a function of the incident irradiation. This variable time constant is responsible for the primary *variation* in the contrast threshold. The second time constant is a function of the irradiance of the stimulus on the retina and is therefore proportional to the square of the pupil diameter. After receiving the signal on to the retina and detection of the signal, it will be projected to the brain because it is the responsibility of the brain to recognize that object.

SIGNAL PROCESSING PATHWAYS

The different pathways that can be taken by the signal while it is received by the retina and processed by the brain are:

- **The awareness path →** sometimes it happens that for the sake of knowledge collection, we will perceive the signal more attentively, so the processing of that signal is moderate.
- **The apprehension path →** the signal is received and processed because of anxiety or uneasiness. So the way taken by such signal is Apprehension path, processing of such signal is fast.

- **The analytical path** → more time is consumed in this path by the processing of luminous and proper mapping of the signal. So this path is quite slow as compared to others.
- **The cognition path** → the mental faculty or process of acquiring knowledge by the use of reasoning, intuition, or perception.
- **The domination path** → the signal processing is done for controlling the knowledge flow between retina and brain, so the path which we follow is the command path.

All the paths which are discussed in this paper are the different ways in which we perceive information about any signal and depending upon the situation we follow any one of the above paths. People examine the surroundings making a series of fixations and saccades. In this process, only the meaningful and informative parts of the images are observed, instead of looking around at random. The fact that path which a person will follow is highly influenced by the motivation.

CONCLUSION

In this research article, Modulation Transfer Function is described which plays an important role in the contrast assessment of the Human Visual System. The proposed model is very useful in finding out the defects in an individual's eye and solution can be found by analyzing those defects. Further work can be done by generating some experiments on retina analysis of different people which enables to get the information how different people actually perceive a signal and their brain recognizes it. Database can be created on the basis of the experiment done and then it becomes easy to find out the retinal properties of different people by case matching. The proposed model discussed in this paper can also be used in the photographic and image transmission fields.

REFERENCES

[1] Rybak, I. A., Gusakova, V. I., Golovan, A. V., Podladchikova, L. N. and Shevtsova, N. A. (1998) A model of attention-guided visual perception and recognition. *Vision Research*, **38**: 2387-2400.

[2] Julesz, B. (1984) A brief outline of the texton theory of human vision. *Trends Neurosci*, **7**: 41-45.

[3] Enns, J. T. and Rensink, R. A. (1990) Influence of scene-based properties on visual search. *Science*, **247**: 721-723.

[4] Lee, S., Shioiri, S. and Yaguch, H. (2003) Effects of temporal frequency and contrast on spatial frequency characteristics for disparity threshold. *Optical Review*, **10(2)**: 120-123.

[5] Fulton, J. T. (2003) Threshold contrast versus spatial frequency in human vision. Retrieved 31-08-2009 from http://neuronresearch.net/vision/files/contrastperf.htm

[6] Weidemann, C. T., Huber, D. E., and Shiffrin, R. M. (2005) Confusion and compensation in visual perception: Effects of spatiotemporal proximity and selective attention. *Journal of Experimental Psychology: Human Perception and Performance*, **31(1)**: 40-61.

[7] Dumont, R., Pellacini, F. and Ferwerda, J. A. (2003) Perceptually-driven decision theory for interactive realistic rendering. *ACM Transactions on Graphics*, **22(2)**: 152-181.

[8] Evers-Senne, J. F. and Koch, R. (2003) Image based interactive rendering with view dependent geometry. *EUROGRAPHICS*, **22(3)**: 573-583.

[9] Fulton, J. T. (2008) Processes in biological vision. Retrieved 06-08-2009 from http://neuronresearch.net/vision/

[10] Killing, J. (2007) Design and development of an intelligent neuro-fuzzy system for automated visual inspection, Ph.D Thesis, Queen's University, Canada.

[11] Rybak, I. A., Gusakova, V. I., Golovan, A. V., Podladchikova, L. N. and Shevtsova, N. A. (2005) Attention-guided recognition based on "what" and "where" representations: A behavioral model. In *Neurobiology of Attention* (Eds. Itti, L., Rees, G. and Tsotsos, J.), Elsevier Academic Press, pp. 663-670.

PRAJÑĀ - Journal of Pure and Applied Sciences
Vol. 17: 122-124, 2009 ISSN 0975 - 2595

BIOINFORMATICS APPROACH FOR DISCOVERING CODON BIAS

Pratik Raval, Harshika Shah and Hetalkumar Panchal *

G. H. Patel P. G. Department of Computer Science and Technology,
Sardar Patel University, Vallabh Vidhyanagar, Gujarat – 388 120.

ABSTRACT

A "book" has been written in form of genome for each and every organism. Now it is time to read the book by various means for getting crucial information form it. We outline one way of doing it with the help of computer in this paper. The genetic code has degeneracy i.e. a single amino acid is coded by different codons depending upon the employed codon usage for each organism. According to non-randomness of the codon usage, there are optimal and non-optimal codons for each organism. This is called the *codon bias* of the organism. *Codon bias* refers to the tendency for an organism to use certain codons more than others to encode a particular amino acid. Here we intend to put a bioinformatics approach for finding a codon bias in the selected organism. We have created one module in the Java programming language using which one can easily find out the particular codon bias for a specific organism. This tool accepts any file format as input and it can also take multiple files as input. It runs on any platform, as Java is a platform independent language. It produces output in Microsoft Excel file format so that the output can be used for certain statistical analyses.

Keywords: **genetic degeneracy, codon usage, codon bias, platform independent.**

INTRODUCTION

In recent years the usage of computers in solving biological problems has been increasing day by day. As a significant amount of biological data is available online, it is important to develop an application that can access the data and generate specific information. Several databases are there that give significant information about DNA, RNA and Protein sequences. There are also several tools available that give you an opportunity to obtain authenticated information from these databases. In this paper too we attempt to produce authenticated information from these databases. Here we have developed a utility, which uses the coding sequence of a gene and gives its codon usage table. Gene is a locatable region of genomic sequence, corresponding to a unit of inheritance, and is associated with regulatory regions, transcribed regions and/or other functional sequence regions. In cells, a gene is a portion of the DNA that contains both "coding" sequences that determine what the gene does, and "non-coding" sequences. We can differentiate between the two when the gene is active. When a gene is active, the coding and non-coding sequences are copied in a process called transcription, producing an RNA copy of the gene's information. This piece of RNA can then direct the synthesis of proteins via the genetic code. A codon is a series of three nucleotides (triplets) that encodes a specific amino acid residue in a polypeptide chain. Codon bias is the differences among organisms in the frequency of the usage of codons in protein-coding DNA sequences. There are several parameters that are taken into account when we look for a codon bias including gene expression level (reflecting selection for optimizing translation process by tRNA abundance), % G+C composition (reflecting horizontal gene transfer or mutational bias) [1] GC skew (reflecting strand-specific mutational bias), amino acid conservation, protein hydropathy, transcriptional selection, RNA stability, optimal growth temperature and hyper saline adaptation [1, 2].

The codon usage of different genes of one organism also relates to their specific rate of expression [3]. Currently, one of the central techniques used in biomedical research and biotechnological production processes is the heterologous gene expression. Several problems were experienced when trying to express genes outside their natural context. Codon usage, one major factor among others, has a significant impact on heterologous gene expression [1, 4]. Rarely employed codons of the host found in the target gene can lead to poorly translated mRNAs, decreased mRNA stability and sometimes to premature termination of translation [1, 5].

* Corresponding author – swamihetal@gmail.com

As per our knowledge, currently only few organism have been studied for the codon bias; so we have focused on the *Arabidobsis thaliana* for codon bias analysis by develpoing easy to use program in Java environment. Here we focused on the frequency of the particular codon that is used most by that organism in the translation method. The present tool can accept any file format as input and it can also accept multiple files as input. The tool will discover the prefered codon for the submitted CDS sequences of any selected organism. It runs on any platform, as Java is a platform independent language. It produces output in Microsoft excel format, so the can be used for certain statistical analyses. We have also removed the restriction on the length of the sequence found in exiting tools. Existing tools are developed using other programming languages, but here we have used the Java development environment that provides various advantages.

MATERIALS AND METHODS

The NetBeans IDE

This is an Integrated Development Environment (IDE) for creating Java applications. It is based on the open source NetBeans Platform and uses the Java Development Kit (JDK) for Java development.

Approach

In the field of bioinformatics and computational biology, many statistical methods have been proposed and used to analyze codon usage bias. Methods such as the "frequency of optimal codons" (FOP) and the "codon adaptation index" (CAI) are used to predict gene expression levels. Our tool is based on the "frequency of optimal codons" method.

Input

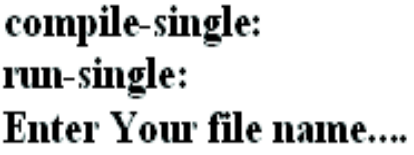

Figure 1: Input window

- Get protein sequences from the Swissprot home page(**http://www.expasy.ch/sprot/)**.
- Select a protein sequence from the list and visit its cross-reference section.
- After selecting "Genbank" from the combo box, click on the corresponding genomic DNA.
- Take coding segment CDS from the gene sequences and paste all the CDS sequences of the selected organism into the Notepad editor with single line space. Also add the greater than sign (>) at end of the set of sequences and save it.
- There is also an option of inputting the Genebank flat file and the tool will automatically extract the CDS regions for further processing.
- Now run the tool using Java and enter the input file name with appropriate path.

Reckonings

- From the input file, the tool will take all sequences and will remove spaces and sequence numbers from the raw coding segment sequences and will concate them into single line sequences.

Then the tool will generate triplet genetic codes from the sequences by taking 3 characters and matching them with the 61 genetic codons available. Simultaneously it will count the frequency of each triplet and finally it will calculate the maximum frequency out of the triplet codes for the same amino acid.

Output

```
compile-single:
run-single:
Enter Your file name....
C:\pratik\a1.txt
-----------------------------------
File Written...
BUILD SUCCESSFUL (total time: 2 minutes 14 seconds)
```

Figure 2: Shows successful run of the program.

- Output screen will be as shown above and an output file in the Microsoft Excel format will be automatically generated in the same folder with the name output.xls.

RESULTS

In basic biochemical research and also for various biotechnological applications, heterologous protein production is of central importance. However, there are only a limited number of

prokaryotic and eukaryotic production hosts for the wealth of organisms under investigation. The codon usage of the gene of interest and of its desired production host often differs significantly. Frequently, this results in low protein recoveries. In the age of commercially competitive gene synthesis, a synthetic target gene with perfect host codon usage offers an attractive alternative to rare tRNA-supplemented strains, which are currently only available for *E. coli*. So, in the investigation for the perfect alternate host, codon usage information plays a very important role in the area of the rDNA technology. If we know the codon bias of the various organisms than we can make prefect pairs of the donor and host organisms for high protein recoveries. Thus the easy-to-use analysis tool described here will help researchers working in the area of the biotechnology and bioinformatics.

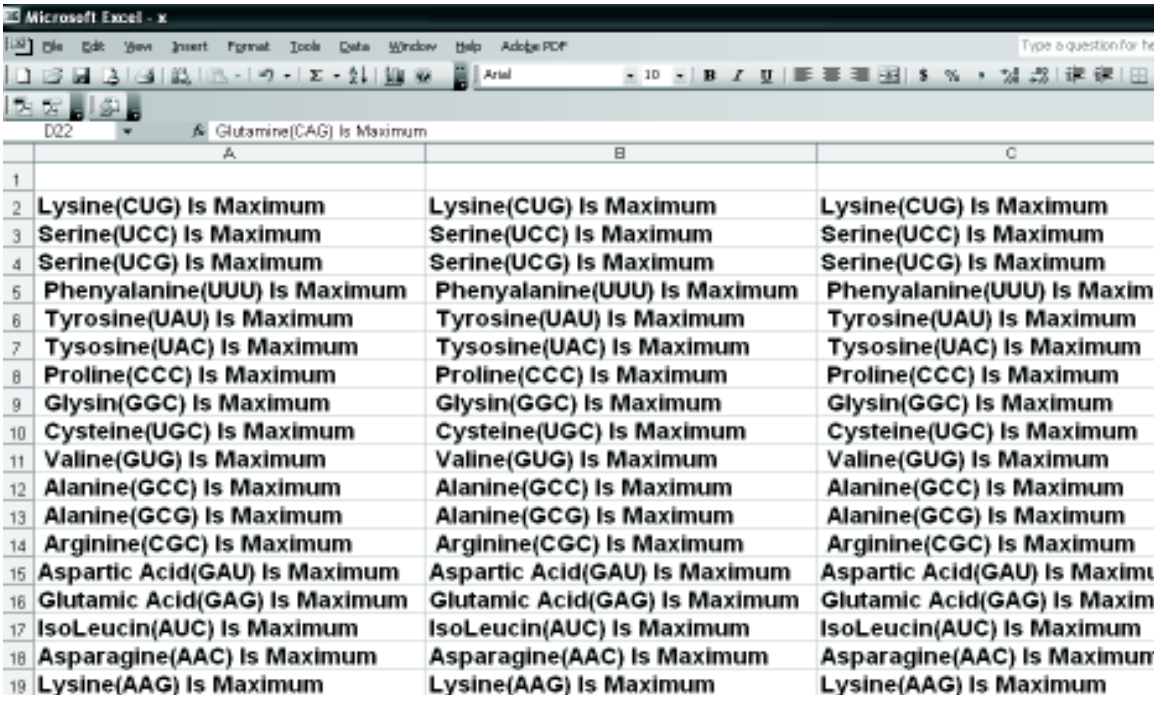

	A	B	C
1			
2	Lysine(CUG) Is Maximum	Lysine(CUG) Is Maximum	Lysine(CUG) Is Maximum
3	Serine(UCC) Is Maximum	Serine(UCC) Is Maximum	Serine(UCC) Is Maximum
4	Serine(UCG) Is Maximum	Serine(UCG) Is Maximum	Serine(UCG) Is Maximum
5	Phenyalanine(UUU) Is Maximum	Phenyalanine(UUU) Is Maximum	Phenyalanine(UUU) Is Maxim
6	Tyrosine(UAU) Is Maximum	Tyrosine(UAU) Is Maximum	Tyrosine(UAU) Is Maximum
7	Tysosine(UAC) Is Maximum	Tysosine(UAC) Is Maximum	Tysosine(UAC) Is Maximum
8	Proline(CCC) Is Maximum	Proline(CCC) Is Maximum	Proline(CCC) Is Maximum
9	Glysin(GGC) Is Maximum	Glysin(GGC) Is Maximum	Glysin(GGC) Is Maximum
10	Cysteine(UGC) Is Maximum	Cysteine(UGC) Is Maximum	Cysteine(UGC) Is Maximum
11	Valine(GUG) Is Maximum	Valine(GUG) Is Maximum	Valine(GUG) Is Maximum
12	Alanine(GCC) Is Maximum	Alanine(GCC) Is Maximum	Alanine(GCC) Is Maximum
13	Alanine(GCG) Is Maximum	Alanine(GCG) Is Maximum	Alanine(GCG) Is Maximum
14	Arginine(CGC) Is Maximum	Arginine(CGC) Is Maximum	Arginine(CGC) Is Maximum
15	Aspartic Acid(GAU) Is Maximum	Aspartic Acid(GAU) Is Maximum	Aspartic Acid(GAU) Is Maximu
16	Glutamic Acid(GAG) Is Maximum	Glutamic Acid(GAG) Is Maximum	Glutamic Acid(GAG) Is Maxim
17	IsoLeucin(AUC) Is Maximum	IsoLeucin(AUC) Is Maximum	IsoLeucin(AUC) Is Maximum
18	Asparagine(AAC) Is Maximum	Asparagine(AAC) Is Maximum	Asparagine(AAC) Is Maximum
19	Lysine(AAG) Is Maximum	Lysine(AAG) Is Maximum	Lysine(AAG) Is Maximum

Figure 3: Shows the maximum used codon by the all gene sequence individually.

CONCLUSION

With the help of the tool described here, one can discover frequency of the optimal codons used in the organism of interest. In this tool, the user only has to provide a raw data sequence and he/she will get the information about the codon bias of the gene coding segments.

This tool has several aspects that could be enhanced. We can add the calculation of Relative Synonymous Codon Usage Value (RSCU). We can also provide a GUI environment which offer more comfort to users.

REFERENCES

[1] David B. Carlini (2005) Context-Dependent Codon bias and Messenger RNA Longevity in the Yeast Transcriptome. Molecular Biology and Evolution (MBE), **22(6)**: 1403-1411.

[2] Suzuki, H., Brown, C. J., Forney, L. J. and E. M. (2008) Top comparison of correspondence analysis methods for synonymous codon usage in bacteria DNA Res, **15(6)**: 357 - 365.

[3] Sharp, P. M., and Li, W. H. (1987) The codon adaptation indexes a measure of directional synonymous codon usage bias, and its potential applications. Nucleic Acids Research 15: 1281-1295.

[4] Wright.F.(1990) The effective number of codon used in a gene. Gene 87: 23-29.

[5] Mclnerney James O. GCUA: General Codon Usage Analysis. Bioinformatics Vol. 14, No. 4 (1998): 372-373.

PRAJÑĀ - **Journal of Pure and Applied Sciences**
Vol. 17: 125-131, 2009 ISSN 0975 - 2595

COMPARATIVE STUDY OF QUERY RETRIEVAL METHODS IN DATABASE MANAGEMENT SYSTEM AND SEMANTIC WEB

Kamlesh Vaishnav, Priya Swaminarayan and P. V. Virparia [1*]

Institute of Science and Technology for Advanced Studies and Research, Vallabh Vidyanagar, Gujarat – 388 120
[1]Department of Computer Science, Sardar Patel University, Vallabh Vidyanagar, Gujarat – 388 120.

ABSTRACT

The main objective of the computer machine is to store the information in some structured format and to provide the right information to right person at right time. In history, several such systems were developed from flat files to DBMS to the latest framework such as Semantic Web, which is an evolving extension of the World Wide Web in which web content can be expressed not only in natural language, but also in a form that can be understood, interpreted and used by software agents, thus permitting them to find, share and integrate information more easily. This paper describes the query retrieval in database management system through SQL and query retrieval in Semantic Web through SPARQL. We have implemented an example sub schema in SQL server and Protégé to provide the comparison between the wide spread SQL query language and a new semantic query language SPARQL.

***Keywords*: semantic web, semantic retrieval, SPARQL, protégé.**

INTRODUCTION

A Database Management System is a collection of programs that enables users to create and maintain a database. The DBMS is a general-purpose software system that facilitates processes of defining, constructing, manipulating and sharing databases among various users and applications. Defining is a database involves specifying the data types, structures, and constraints of the data to be stored in the database. The database definition or descriptive information is also stored in the database catalog or dictionary; it is called meta-data. Constructing the database is the process of storing the data on some storage medium that is controlled by the DBMS. Manipulating a database includes functions such as querying the database to retrieval specific data, updating the database to reflect changes and generating reports from the data. Sharing a database allows multiple users and programs to access the database simultaneously. An application program accesses the database by sending queries or requests for data to the DBMS. A query typically causes some data to be retrieved [1].

Semantic web is evolving extension of the World Wide Web in which web content can be expressed not only in natural language, but also in a form that can be understood, interpreted and used by software agents, thus permitting them to find, share and integrate information more easily. In Semantic Web, an explicit specification of a conceptualization in any domain is represented through Ontology. Ontology defines concepts in a specific area and their relationships; however, ontology is more than an agreed-on term. It has a set of well-defined constructs that can be leveraged to build structured knowledge. Although taxonomy enhances the semantics of terms in a vocabulary, ontology includes richer relationships among terms (Smith, 2004). Ontology is the framework of the semantic web, and permits intelligent navigation (Information Intelligence, 2004). For humans, ontologies enable better access to information and promote reuse and shared understanding; for computers, ontologies facilitate comprehension of information and more extensive processing (Ontology Engineering, n.d.).

QUERY RETRIEVAL IN DBMS

The Database Management System can be broadly divided into the storage manager and the query processor components. The query processor helps in database system in query retrieval. It simplifies and facilitates access to data. It is used to translate and updates and queries written in non-procedural language, at the logical level, into an efficient sequence of operations, at the physical level. It includes following subcomponents: DDL-interpreter, DML-compiler and query evaluation engine. Most of the DBMS system supports the SQL language. SQL has clearly established itself

* Corresponding author – pvvirparia@yahoo.com

as the standard relational database management system through which all functions of query processor can be performed by user using non-procedural language [2].

QUERY RETRIEVAL IN SEMANTIC WEB

A number of techniques have been developed to facilitate powerful data retrieval on the Web and Semantic Web. Three categories of Web query languages can be distinguished, according to the format of the data they can retrieve: XML, RDF and Topic Maps. A wide range of query languages for the Semantic Web exist, ranging from pure "selection languages" with only limited expressivity, to full-fledged reasoning languages capable of expressing complicated programs, and from query languages restricted to a certain data representation format (e.g. XML or RDF), to general purpose languages supporting several different data representation formats and allowing one to query data on both the standard Web and the Semantic Web at once. SPARQL (SPARQL Protocol and RDF Query Language) is the W3C recommended query language for the Semantic Web. It lets us: pull values from structured and semi-structured data, explore data by querying unknown relationships, perform complex joins of disparate databases in a single, simple query, and transform RDF data from one vocabulary to another. There are several tools and APIs that already provide SPARQL functionality, and most of them are up to date with the latest specifications. A brief list includes: ARQ, Rasqal, RDF::query, twinql, Pellet, and KAON2 [3].

CASE STUDY

We have considered the following sub schema that describes partial entity sets with partial attributes from the schema of an academic institute system. In this sub schema there are three entity sets, viz., "Institute", "Dept", and "Program". There are two one-to-many relationships: "Has" (Institute Has Dept) and "Run" (Dept Run Program). The relationship "Has" has inverse relationship "Belongs_To" (Dept Belongs_To Institute) and the relationship "Run" has inverse relationship "Is_Run_By" (Program Is_Run_By Dept).

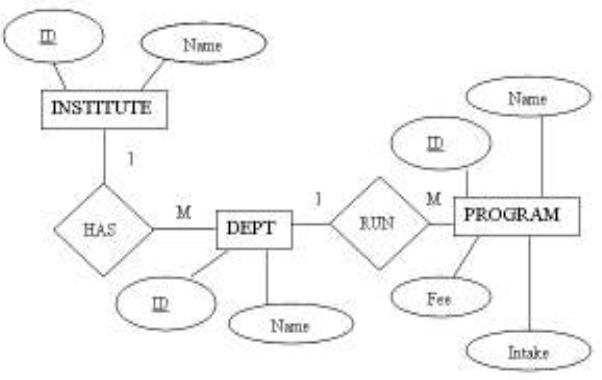

Figure 1: Sub schema from the Schema of an Academic Institute System

The physical schema is created for this sub schema in SQL Server database and in OWL DL format using the Protégé.

We expect to solve the following queries based on this schema in order to compare the process and result of both information retrieval processes: SQL data retrieval and semantic retrieval using SPARQL [4, 5, 6].

- Query – 1: List city where specific course (say, MCA) is running.
- Query – 2: List institutes along with city where specific course (say, MCA) is running.
- Query – 3: List Fee and Intake of various Dept along with college name and city name that runs given program (course).
- Query – 4: List all courses run in specific city.
- Query – 5: List institutes along with city where specific course (say, MCA) is running, and the fee of this course is between given two amounts.

COMPARATIVE STUDY OF QUERY RETRIEVAL PROCESS IN SQL SERVER (SQL) AND PROTÉGÉ (SPARQL)

The Fig. 2 and Fig. 3 shows the result of the query "List city where 'PGDCA' program is running" in SQL Server and in Protégé respectively.

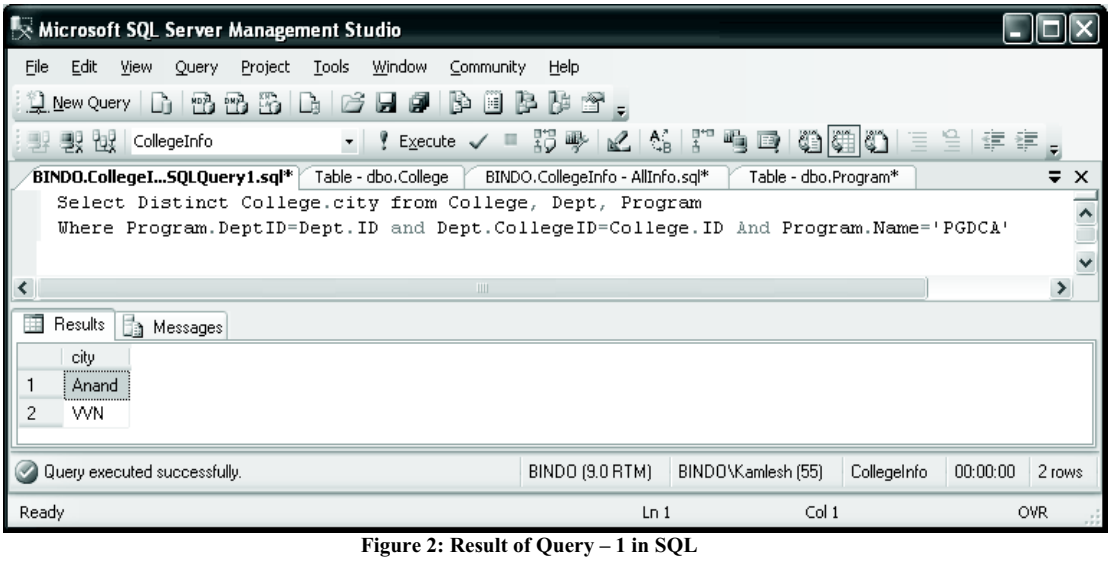

Figure 2: Result of Query – 1 in SQL

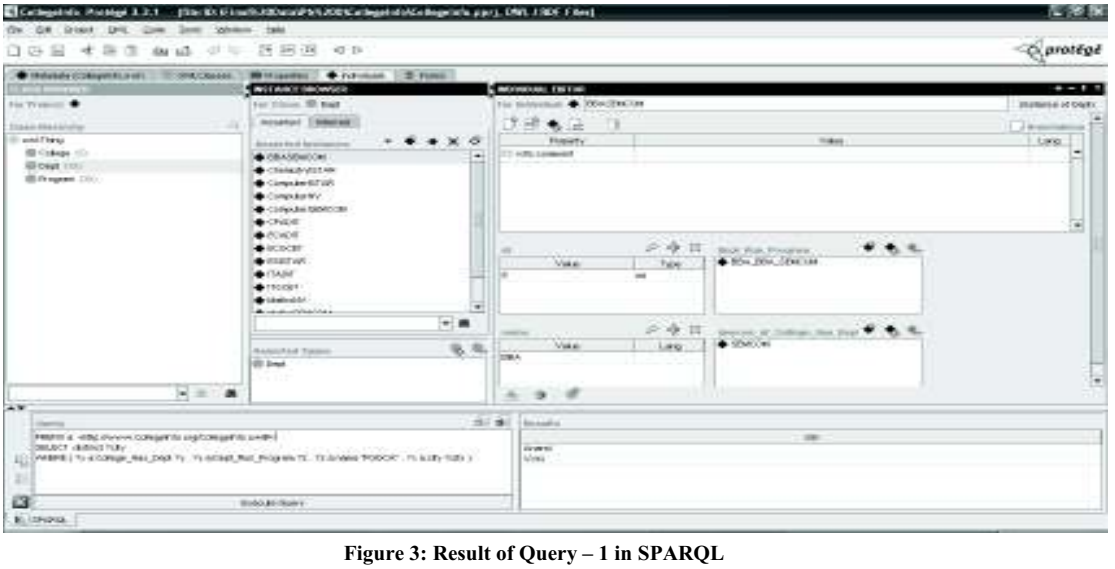

Figure 3: Result of Query – 1 in SPARQL

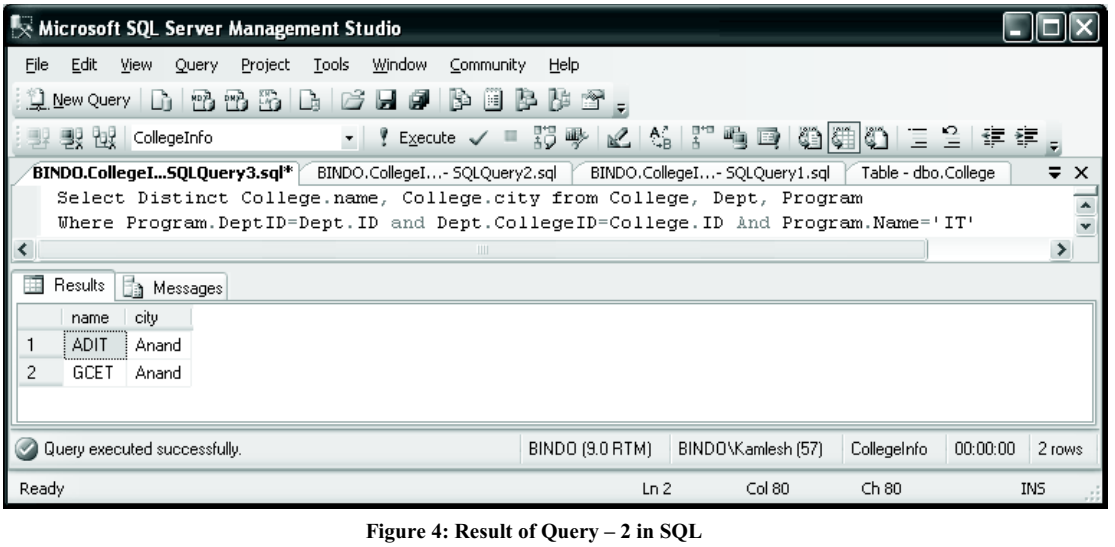

Figure 4: Result of Query – 2 in SQL

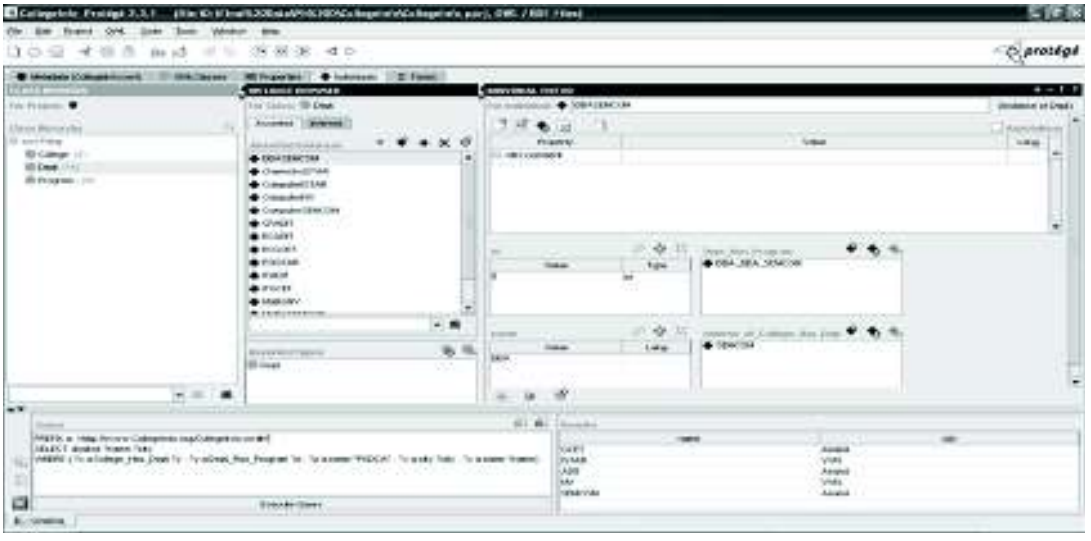

Figure 5: Result of Query – 2 in SPARQL

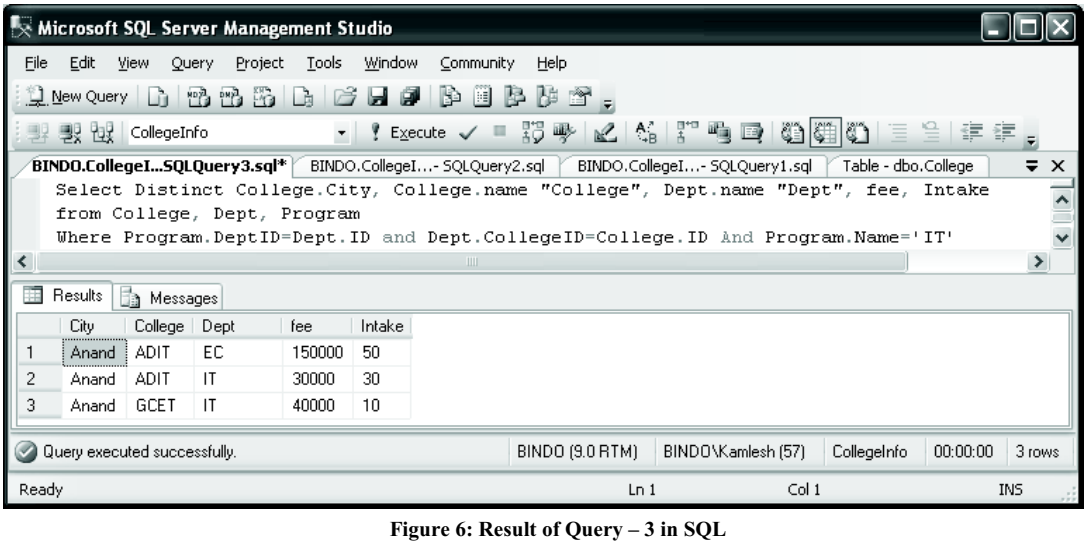

Figure 6: Result of Query – 3 in SQL

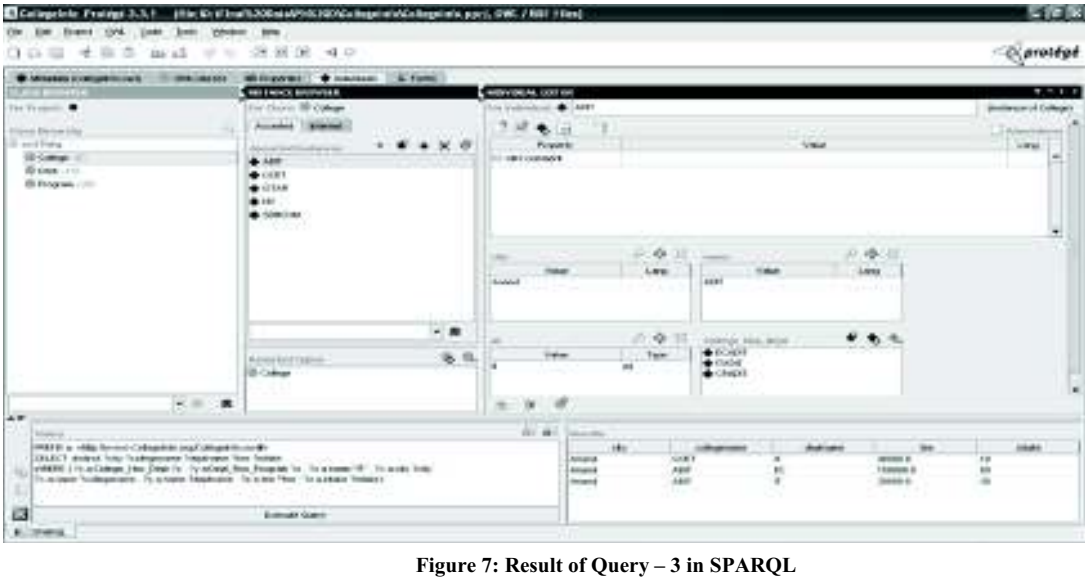

Figure 7: Result of Query – 3 in SPARQL

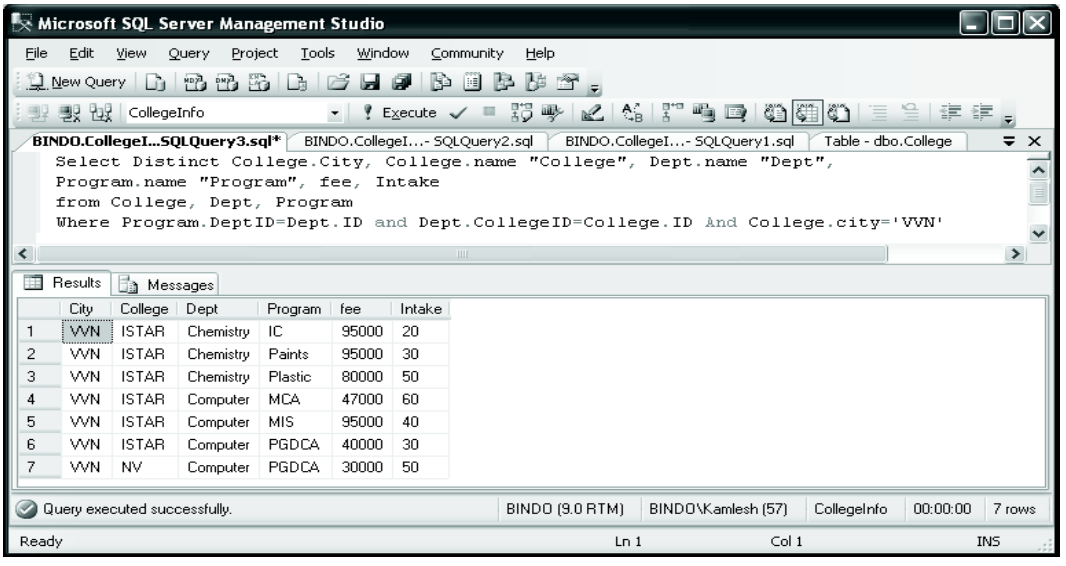

Figure 8: Result of Query – 4 in SQL

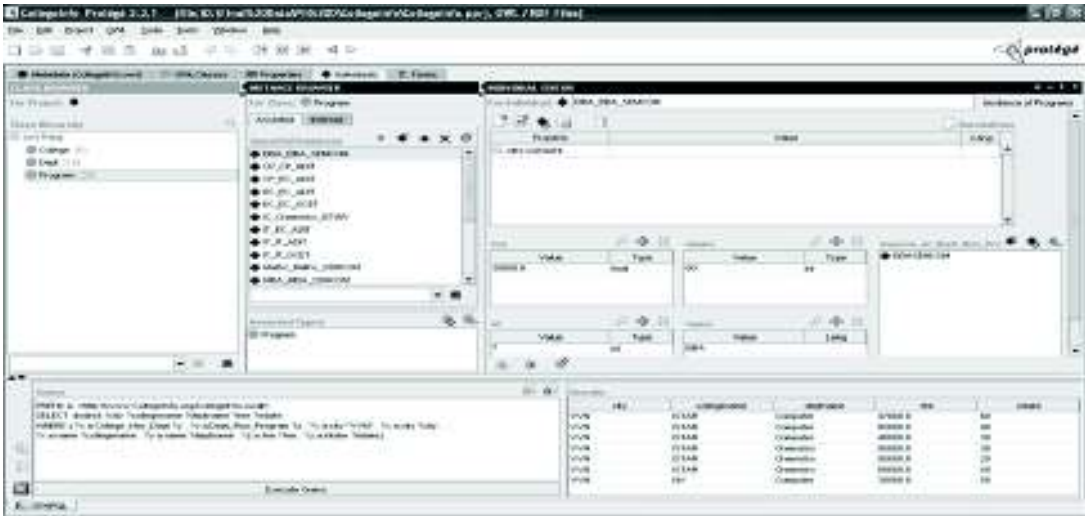

Figure 9: Result of Query – 4 in SPARQL

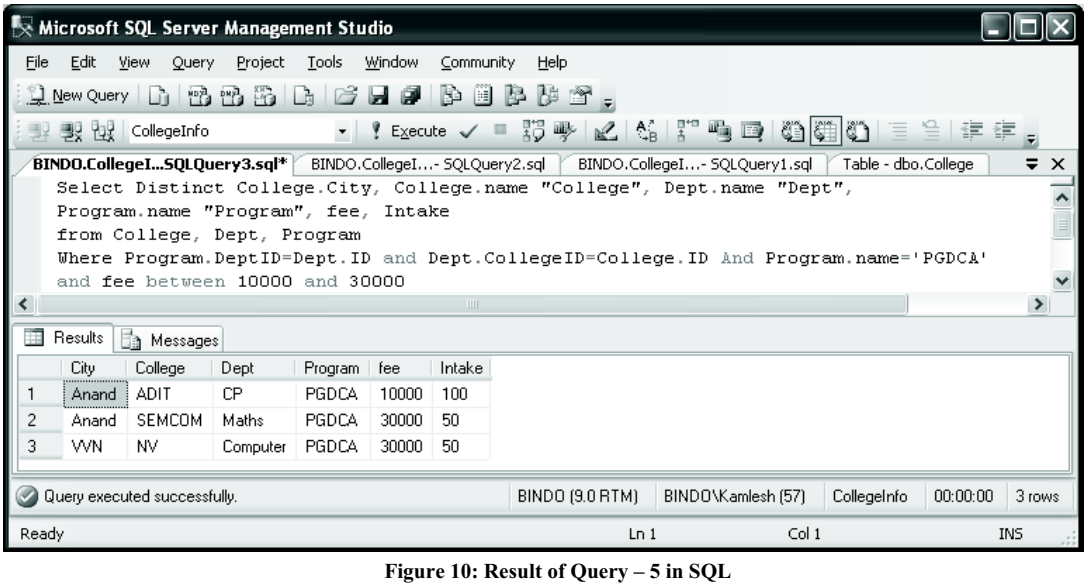

Figure 10: Result of Query – 5 in SQL

Figure 11: Result of Query – 5 in SPARQL

The Fig. 4 and Fig. 5 shows the result of the query "List institutes along with city where 'IT' course is running" in SQL Server and in Protégé respectively. The Fig. 6 and Fig. 7 shows the result of the query "List Fee and Intake of various Dept along with college name and city name that runs 'IT' program (course)" in SQL Server and in Protégé respectively. The Fig. 8 and Fig. 9 shows the result of the query "List detail information about all courses run in 'VVN' city" in SQL Server and in Protégé respectively. The Fig. 10 and Fig. 11 shows the result of the query "List institutes along with city where 'PGDCA' course is running and the fee of this course is between 10000 and 30000" in SQL Server and in Protégé respectively.

BENEFITS OF SEMANTIC RETRIEVAL OVER DATABASE RETRIEVAL

The benefits of semantic retrieval (SPARQL) over the database retrieval (SQL) are following: SPARQL can query RDF (Semantic) data natively. It supports implicit join syntax. It queries RDF graphs, which consist of various triples expressing binary relations between resources, by specifying a sub graph with certain resources replaced by variables. Because all relationships are of a fixed size and data lives in a single graph, it does not require explicit joins that specify the relationship between differently structured data. That is, SPARQL is a query language for pattern matching against RDF graphs, and the queries themselves *look and act* like RDF. This is one main point made by Oracle's Jim Melton in his analysis of SPARQL vis a vis SQL and XQuery.

SPARQL has strong support for querying semi structured and ragged data—i.e., data with an unpredictable and unreliable structure. Variables may occur in the predicate position to query unknown relationships, and the OPTIONAL keyword provides support for querying relationships that may or may not occur in the data (SQL left joins). SPARQL is often an appropriate query language for querying disparate data sources (not sharing a single native representation) in a single query. Because RDF represents all data as a collection of simple binary relations, most data can be easily mapped to RDF and then queried and joined using SPARQL. Often, these mappings can be performed on the fly, meaning that SPARQL can be used to join heterogeneous data at a higher level than that of the native structure of the data. It also supports queries in a networked, web environment. SPARQL introduces the notion of an RDF dataset, which is the pairing of a default graph and zero or more named graphs. As both the default graph and the named graphs are identified by URIs, it is common for SPARQL implementations to retrieve a graph by performing an HTTP GET on the graph's URI. This allows a single query to join information from multiple data sources accessible across different Web sites.

ISSUES AND CHALLENGES INVOLVED IN SEMANTIC RETRIEVAL

The major drawbacks of SPARQL are as follow: Lack of wide deployment - SPARQL is relatively young, and as such there are not many data stores which can be directly queried with SPARQL (as compared with SQL or XPath). Immaturity - As a young query language, SPARQL lacks the explicit processing model of XQuery or the decades of SQL-optimization research. As with the above point, this is likely to improve as current and new research and implementations contribute to a body of knowledge surrounding SPARQL. Lack of support for transitive/hierarchical queries - While SPARQL is designed to query RDF graphs, SPARQL has no facilities for easily querying transitive relations or hierarchical structures within a graph. There are some workarounds for this, but SPARQL does not approach the power of, for instance, XQuery's axes. There are a number of issues that SPARQL does not address yet; most notably, SPARQL is read-only and cannot modify an RDF dataset. [3]

CONCLUSION

From the case study implementation we can conclude that SPRQL, a query language for Semantic Web, can solve all the queries that are solvable in Database management System using SQL. We also came to the point that it is far easier to support the reusability and interoperability of the information base in Semantic Web than in DBMS. In future, we would like to import (reuse) the FOAF upper ontology in our case study ontology so that one more benefit of Semantic Retrieval can be tested, that is, for a given attribute value of some entity we can deduce in Semantic Web with the help of FOAF that this is a Person or Place; which is not possible in DBMS.

REFERENCE

[1] Elmasri, R. and Navathe, S. B. (2009) *Fundamentals of Database Systems*, Fifth Edition, Pearson Education. pp: 3-27

[2] Silberschatz, A., Korth, H., and Sudarshan, S. (2005) *Database System Concepts*, Fifth Edition, Mc Graw Hill. pp:1-30

[3] Dodds, L. (2005) Introducing SPARQL: Querying the Semantic Web, from http://www.xml.com/lpt/a/2005/11/16/introducing-sparql-querying-semantic-web-tutorial.html

[4] Feigenbaum, L. (2009) Cambridge Semantic Tutorial, retrieved 22-9-2009 from http://www.cambridgesemantics.com /2008/09 /sparql-by-example/

[5] Feigenbaum, L., The SPARQL FAQ retrieved 22-9-2009 from http://www.thefigtrees.net/lee/sw/sparql-faq

[6] Prudhommeaux, E. and Seaborne, A., (2008) "SPARQL Query Language for RDF" retrieved from http://www.w3.org/TR/rdf-sparql-query/ on 1/09/2009

[7] http://en.wikipedia.org/wiki/SPARQL

PRAJÑĀ - **Journal of Pure and Applied Sciences**
Vol. 17: 132 - 136, 2009 ISSN 0975 - 2595

FABRICATION OF ENZYME BASED AMPEROMETRIC SUCROSE BIOSENSOR

U. B. Trivedi and D. Lakshminarayana *

Department of Electronics, Sardar Patel University, Vallabh Vidyanagar, Gujarat – 388 120

ABSTRACT

An amperometric sucrose biosensor based on the immobilization of a multi enzyme system of Invertase (INV), Mutarotase and Glucose Oxidase (GOD) has been developed. A polymer matrix of Polyethylenemine (PEI) and Poly (carbamoylsulphonate) (PCS) hydrogel could successfully be implemented for the immobilization. A thick film screen printing technique was adopted for the fabrication of the basal conducting track of the amperometric working electrode and counter electrode. An Ag/AgCl reference electrode completed the amperometric sucrose biosensor system. The fabricated multi enzyme based Pt/PCS+PEI/(INV + Mutarotase + GOD) sucrose biosensor system was found to be able to detect the presence of sucrose in test samples and the results obtained are presented.

Keywords: **biosensor, sucrose, polymer matrix, enzyme immobilization, amperometry**

INTRODUCTION

Sucrose is one of the most important representations in many food and beverage products. Rapid measurement as well as an accuracy for measuring the sucrose is an advantage in food process and control. It is to be mentioned here, that many countries have for a long time used sucrose extensively in a variety of sweetened food stuffs. Sucrose is a disaccharide with the molecular formula of $C_{12}H_{22}O_{11}$. It is best known for its role in human nutrition and is formed by plants but not by higher organisms. Sucrose is available in a variety of forms and is extensively used in many different food products. Sucrose has a range of properties that, either individually or in combination with other ingredients, makes it further an important ingredient in modern food production. Its functions include sweetness, flavor, bulk, texture, viscosity control, aroma, shelf-life, fermentation, freezing point depression and color [1, 2]. In some diets, the energetic value of sucrose is its specific metabolism in the human digestive tract and is considered an undesirable feature. Substitution of sucrose by other sweeteners is also a common practice in the food and beverage industries [3]. The formulation of sweet gelled products, therefore implies an extensive knowledge of the properties and behavior of the sweetener used and of the factors that can affect the final characteristics of the sweet product. Due to the special functions of sucrose as a bulking agent and also as a texture modifier, the substitution of sucrose by another sweetener will affect both the mechanical properties and the perceived texture of the milk product. In some applications, particularly, in fermentation processes, the higher concentrations of sucrose at a particular stage of the industrial process may cause a significant and long term decrease in fermentation performance. It is surprising that, in spite of its significance, not much research work has been reported on sucrose detection [4-7].

In view of the importance of the sugars like glucose, fructose, sucrose etc. in food and beverage industries, a great deal of research is needed for developing a rapid detection and measuring of these sugars in food and beverages. It is rather important to have a detection method that is simple, fast and sensitive which could be effectively used in food industries. The authors have successfully developed enzyme based biosensor systems for the detection of glucose, fructose and urea for food and clinical analyses, and reported [8-11] the results duly. It is, thus, natural to extend our research investigation towards developing a low cost and disposable type of amperometric biosensor for the detection of sucrose too. In the present communication, the authors report the development of a low cost, portable and disposable type of sucrose biosensor system.

* Corresponding author – dlnvvn@yahoo.com

EXPERIMENTAL

Chemicals and Reagents

The various solutions utilized in the present investigation were all prepared with analytical reagent grade chemicals and double distilled water. The various enzymes, polymers, pastes and chemicals used in this investigation are listed below with their makes.

Enzymes

Invertase (INV) from baker's yeast (*S. cerevisiae*) , *BioChemika*, Powder, 100-200 units/mg, (E.C. 3.2.1.26) 57629 (Fluka, Switzerland),Mutarotase (E.C. 5.1.3.3), (Merck, Germany) ,Glucose Oxidase (GOD) from *Aspergillus niger* (10) Type II-S, 15,000-50,000 units/g solid (without added oxygen) (E.C.1.1.3.4) G-6641 (Sigma, St. Louis, USA)

Polymers

Polyethylenemine (50% w/v aqueous solution) (PEI) (Sigma, USA), Poly (carbamoylsulphonate) (PCS) hydrogel (Sens Lab, Germany0

Pastes for Screen Printed Fabrication of the Electrodes:

Platinum Paste R-474 (DPM-80) (Ercon, USA),Graphite Paste G-449 (Ercon, USA),Graphite Paste (Acheson, The Netherlands),Silver/Silver Chloride Paste R-414 (DPM-68)(Ag/AgCl)(Ercon, USA)

Chemicals

Disodium Hydrogen Phosphate 67mM (Merck, Darmstadt,Germany), Sodium dihydrogen Phosphate 67mM (Merck, Damstadt, Germany), Potassium Chloride 0.1M KCl, (Merck, Darmstadt, Germany), Sodium Chloride, (Merck, Darmstadt, Germany), Sodium Hydroxide (Merck, Darmstadt, Germany), Glutaraldehyde, 50% in H_2O (Fluka, Switzerland), Ascorbic Acid (Sigma, St. Louis, USA), Potassium hexacyanoferrate (III) and Potassium hexacyanoferrate (II) (Fluka, Switzerland),

Apparatus

- ✓ Micro Pipette (Eppendorf, Germany)
- ✓ Multi-Channel ISE/pH/mV/ORP/Temperature Benchtop Meter (Thermo Orion, USA)
- ✓ Ag/AgCl Reference Electrode (Thermo Orion, USA)

Electrode Fabrication

The fabrication of sucrose biosensor involved screen printing, lamination and enzyme immobilization. The base transducer used for the amperometric sucrose biosensor was a screen printed graphite electrode on a Melinex sheet of 150μm thickness. The graphite paste was screen printed using screens having a mesh of about 68μm. A transducing tip was formed of platinum (Pt) paste over the graphite conducting track and functioned as the working electrode for the amperometric sensor system. The working electrode along with a screen printed graphite counter electrode and an Ag/AgCl reference electrode completed the amperometric biosensor measuring system. The immobilization of the enzymes was carried out on the platinum (Pt) tip of the working electrode. The experimental procedure adopted for the fabrication of the amperometric electrodes in the present sucrose biosensor system was essentially the same as that was reported, in detail, earlier by the authors [8,10] for glucose and fructose. Hence, the detailed electrode fabrication procedure is not being repeated here.

Sucrose determination requires a multi enzyme system. Invertase in combination with glucose oxidase was used to produce a sucrose enzyme electrode. However, an additional third enzyme of mutarotase was also utilized in order to convert α-D-Glucose to its β-isomer on which glucose oxidase is specific. A multi enzyme electrode was obtained by a two step immobilization of the enzymes glucose oxidase, mutarotase and invertase for the determination of sucrose. The glucose oxidase was first entrapped in PCS hydrogel and PEI polymer matrix on the platinum tip of the graphite working electrode. A combination of mutarotase and invertase was then cross linked with glucose oxidase on the electrode.

Measurements

A four channel potentiostat (ICB, Munster, Germany) was used in the electrode configuration for the amperometric measurements of sucrose detection. The fabricated enzyme based sucrose biosensor was used as the working electrode with Ag/AgCl as the reference electrode. At the working electrode, a potential of +750mV with reference to the Ag/AgCl reference electrode was

applied for the sucrose analyte determination. Before starting the first measurement with the fabricated biosensor, a pre conditioning step was carried out by applying a potential of +1.2V at the working electrode (against Ag/AgCl) for about 240 sec.

Test Samples and Sensor Operation

A standard solution of 1000mg/L of sucrose was prepared. The solution was filtered using a cellulose 0.2µm filter and kept at 6ºC. A calibrating solution was prepared for diluting the standard solution to a concentration interval of 60/90, µg/mL for sucrose detection.

The sucrose determination was carried out through multi enzyme system. The sucrose is hydrolyzed enzymatically by the enzyme Invertase. The enzymatic reactions involved in this process are as follows:

$$\text{Sucrose} + H_2O \xrightarrow{\text{Invertase}} \alpha\text{-D-Glucose} + \text{Fructose} \quad (1)$$

$$\alpha\text{-D-Glucose} \xrightarrow{\text{Mutarotase}} \beta\text{-D-Glucose} \quad (2)$$

$$\beta\text{-D-Glucose} + O_2 \xrightarrow{\text{GOD}} \text{Gluconic Acid} + H_2 \quad (3)$$

The hydrogen peroxide (H_2O_2) generated in the above equation could easily be measured by oxidation at the platinum anode as shown below.

$$H_2O_2 \xrightarrow{+650\ \text{mV}} O_2 + 2H^+ + 2e^- \quad (4)$$

The electron current thus generated is an indicative of the sucrose concentration present in the amperometric cell.

RESULTS AND DISCUSSION

The effect of the working potential on the amperometric response of the sucrose enzyme electrode was examined in the potential range of 300–900mV against Ag/AgCl reference.

The highest amperometric responses for the sucrose bio-electrodes were obtained at the potential of 750mV for the sucrose (Figure. 1). Working potentials higher than 750mV were found to result in a decrease of response. It may be due to the oxidation of electro chemical interferents in the solutions and enzyme inactivity. Hence, a working potential of 750mV was utilized as the optimum value for further studies.

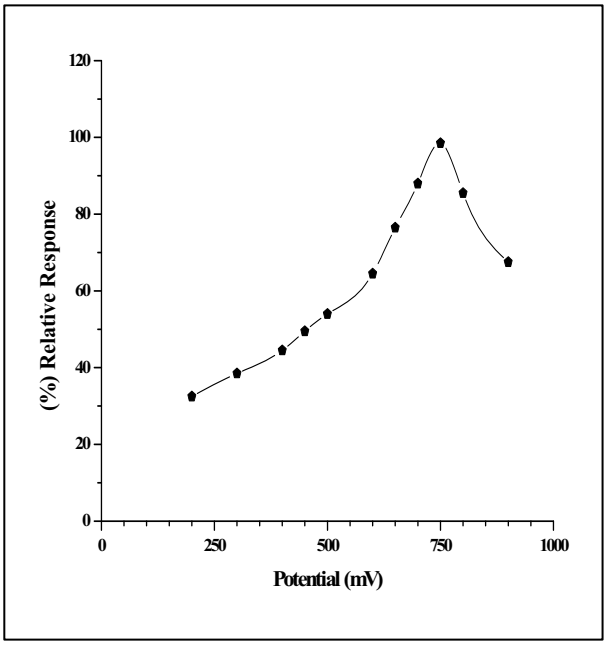

Figure 1: Effect of working potential on the amperometric response for sucrose bio electrode.

As mentioned earlier, the sucrose determination requires a multi enzyme system. The detection process is a highly complex one with a high degree of chemical cross talk, because real samples contain both glucose and sucrose in variably. With regard to sucrose detection, electrodes made up of invertase, mutarotase and glucose oxidase [12-14] and mediated tri-enzyme electrode based on sucrose phosphorylase and electrocatalytic oxidation of NADH, have been previously used [15]. The literature survey indicates that only a scanty research work has so far been carried out for the sucrose detection by way of biosensor route [16-19]. In the present work, the sucrose biosensor developed by the authors was based on the invertase, mutarotase and glucose oxidase reaction scheme shown above.

The amperometric response time of the multi enzyme (INV+ Mutarotase+ GOD) electrode to the additions of stock solutions of sucrose was found to be 20-30 seconds. The recovery time was in the range of 40-70 seconds. A typical response curve of the Pt/PCS+PEI/(INV + Mutarotase +GOD) sucrose biosensor system is shown in figure 2. The figure represents the response current (nA) to the additions of 100µM sucrose to the biosensor system.

The calibration curve shown in the inset of the figure 2 exhibits a good linearity with a correlation coefficient of 0.986 (n=7). The sucrose enzyme electrode produced a linear steady state amperometric response in the range of 3mM to 10mM. From the slope of the calibration curve, the sensitivity of the sucrose biosensor system has been found to be 0.54 ± 13nA/μM. In addition, the lower detection limit for the designed sucrose biosensor system has been observed to be about 0.4 to 0.6μM of sucrose.

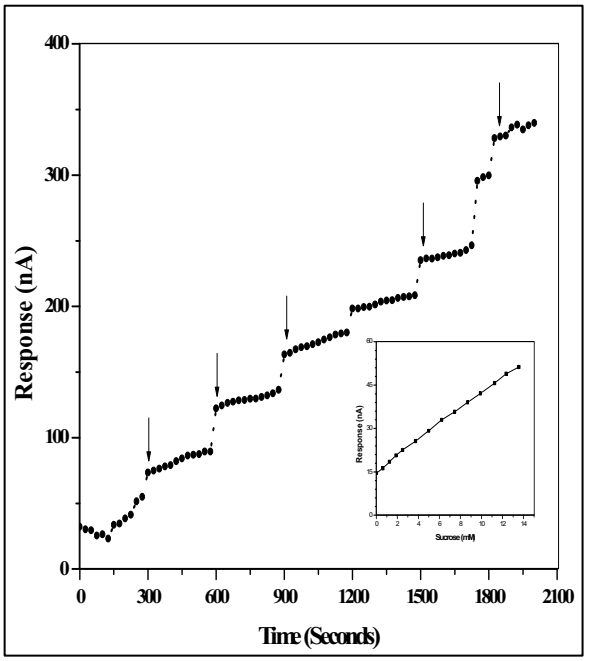

Figure 2: The amperometric response of the sucrose biosensor system to the additions (indicated by the arrows) of 100μM sucrose solution. The inset represents the calibration curve.

Known amounts of glucose stock solutions were added to the Pt/PCS+PEI/(INV + Mutarotase + GOD) sucrose biosensor system to test the chemical crosstalk due to glucose. The response did not show any significant variation up to about 5mM addition of glucose. Higher amounts of glucose addition were found to result in amperometric fluctuations. Hence, it can be concluded that the present biosensor system would effectively function as an exclusive sucrose sensor. Since the present sucrose sensing mechanism is based on GOD also, the system may show chemical crosstalk and interfering currents if the samples contain significant amounts of glucose. Even though, significant amperometric currents were observed for real samples of fruit juices and soft drinks, it may be difficult to attribute the currents to the sucrose concentrations only, at this stage. Hence, in order to minimize the chemical crosstalk, a selective enzyme based membrane technology needs to be developed further and incorporated in this system.

CONCLUSION

A unique multi enzyme based Pt/PCS+PEI/(INV + Mutarotase + GOD) sucrose biosensor system could be designed and fabricated successfully. The biosensor has been found to detect the presence of sucrose in test samples with a high degree of reproducibility. The sensitivity of the sucrose biosensor system has been found to be 0.54 ±13nA/μM and shows the potentiality for real sample testing in food and beverage industries.

REFERENCES

[1] Food and Beverage Trends (2007) www.preparedfoods.com

[2] Sugar and Sweeteners (2007) www.ext.colostate.edu/pubs/foodnut/09301.html.

[3] Sara, B., Luis, D., Luis, L. and Elvira C. (2005) Effect of substitution of aspartame for sucrose on instrumental texture profile of hydrocolloids gelled systems. *Eur. Food Res. Technol.,* **220:** 25-30.

[4] Salgado, M., Folly, R. O. M., Valdman, B. and Valero, F., (1998) Development of a sucrose enzymatic biosensor. *Biotechnology Technique* **12(4):** 305-307.

[5] William, G. M., Maria, T. B., Beatriz, Q and Steven, E. L., (2001) Biological sensor for sucrose availability: Relative sensitivities of various reporter genes. *Applied and Environmental Microbiology,* **67:** 1308-1317.

[6] Gouda, M. D., Thakur, M. S., and Karanth, N. G., (2001) Optimization of the multienzyme system for sucrose biosensor by response surface methodology. *World Journal of Microbiology and Biotechnology*, **17:** 595-600.

[7] Yuanhang, Xu and George, G. G., (1989) Sucrose enzyme electrode. *Anal. Chem.,* **61(7)**: 782-784.

[8] Trivedi, U. B., Lakshminarayana, D., Kothari, I. L., Makhija, K. K., and Kapse, H. N., (2007) Fabrication of enzyme based

glucose biosensor. 'Prajna", Sardar Patel University, *Journal of Pure and Applied Sciences*, **15:** 42-48.

[9] Trivedi, U. B., and Lakshminarayana, D., (2008) Perfomance comparison of glucose biosensor based upon different polymer materials. *'Prajna", Sardar Patel University, Journal of Pure and Applied Sciences*, **16:** 37-40.

[10] Trivedi, U. B., Lakshminarayana, D., Kothari, I. L., Patel, P. B. and Panchal, C. J., (2009) Amperometric fructose biosensor based on fructose dehydrogenase enzyme. *Sensors and Actuators B.,* **136:** 45-51.

[11] Trivedi, U. B., Lakshminarayana, D., Kothari, I. L., Patel, N. G., Kapse, H. N., Makhija, K. K., Patel, P. B. and Panchal, C. J., (2009) Potentiometric biosensor for urea determination in milk. *Sensors and Actuators B*., **140**: 260-266.

[12] Schwedt, G., and Stein, K., (1994) Immobilized enzyme as tools in food analysis. *Ziebensm Unters Forsch*, **199:** 171-182.

[13] Thomas, J. D. R., (1998) Enzyme electrode for carbohydrate analysis: Biosensor for Food Analysis, *The Royal Society of Chemistry*, **115.**

[14] Guemas, Y., Boujtita, M., and Murr, N., (2000) Biosensor determination of glucose and sucrose in fruit juices by flow injection analysis. *Applied Biochemistry and Biotechnology*, **89(2-3):** 171-181.

[15] Maester, E., Katakis, I., and Dominguez, E., (2001) Amperometric flow injection determination of sucrose with a mediated tri-enzyme electrode based on sucrose phosphorylase and electrocatalytic oxidation of NADH. *Biosensors and Bioelectronics*, **16:** 61.

[16] Klinchan, S., Chotiwongpipat, W., Suwannakum, T., Tanticharoen, M., and Kirtikara, K., (2002) Construction of sensor chip by electrochemical polymerization technique for sucrose determination. *The Journal of KMITNB*, **12(1):** 12-17.

[17] Scheller, F., and Renneberg, R., (1983) Glucose eliminating enzyme electrode for direct sucrose determination in glucose containing samples. *Analytical Chemica Acta*, **152:** 265-269

[18] Folly, R. O. M., Valdman, B., Valero, F., and Sola, C., (1996) Potentiometric sensor for on line glucose determination. *Biotech. Tech*., **10:** 867-870.

[19] Jawaheer, S., White, S. F., Rughooputh, S. D. D. V., and David. C. C, (2003) Development of a common biosensor formate for an enzyme based biosensor array to monitor fruit quality. *Biosensors and Bioelectronics*, **189(12):** 1429-1437.

PRAJÑĀ - **Journal of Pure and Applied Sciences**
Vol. 17: 137 - 139, 2009 ISSN 0975 - 2595

COMPACT 80 KV TRIGGER GENERATOR FOR TRIGGERED SPARK GAP

Surender Kumar Sharma,[*] R. Shukla, P. Banerjee, A. Shyam, Sourobh Rana [1] and Akash Shah [1]

Energetics & Electromagnetics Division, Institute for Plasma Research, Gandhinagar, Gujarat – 382 428
[1]Electronics Department, U.V. Patel College of Engineering, Mehsana, Gujarat – 382 711

ABSTRACT

A 80 kV trigger generator was designed and fabricated for triggering the field distortion type spark gap switch. The trigger generator can be operated in mode up to repetitive 10 Hz operation. The trigger generator consists of a compact power supply, transformer, bridge rectifier, capacitor, thyristor switch and a pulse transformer. The capacitor is charged with supply mains voltage stepped up to 800 V and then rectified using full bridge or by another 9 V battery operated compact power supply. The two power supplies are isolated and they charge a 2 µF capacitor to 1 kV. The capacitor is discharged into the input of 1 kV / 80 kV pulse transformer and produces 80 kV at the secondary of pulse transformer. The triggering circuit of thyristor consists of RC circuit and 555 timer producing 5V pulse for gate terminal of the thyristor. The 80 kV pulse is used to trigger the spark gap of high voltage capacitor bank.

***Keywords*: trigger generator, spark gap, capacitor, thyristor, compact power supply.**

INTRODUCTION

The increased interest in pulse power field applications has generated the need for development of compact and remotely operated chargers driven by rechargeable batteries [1]. With this objective, a compact and portable DC to DC converter has been developed which has an output rating of 1 kV and charges a capacitor for triggering system. Pulsed power technologies essentially refer to power sources providing a huge amount of energy during very short times. These technologies have applications in several fields of science and engineering for production of transient electrical discharges and plasmas, generation of radiation and ion beams, high density matter, production of pulsed high magnetic fields and shock waves. The achievements of these fields are relevant for several economical and industrial areas in electronics, microlithography, mining, medicine, agriculture, defense, materials, among others. A trigger generator is designed and fabricated for a triggered spark gap. A triggered spark gap switch requires some charge carriers (electron, ions etc) for changing from OFF state to ON state. These charge carriers are provided by secondary circuits which follow different mechanisms such as electric field distortion, irradiation by means of UV light, laser and over voltage. Triggered spark gaps are very popular as fast high current switches. A triggered spark gap can switch megawatts of power in a few microseconds, with jitters of less than a nanosecond. These devices make use of the very low impedance of an arc, once the arc is established.

* Corresponding author – surender@ipr.res.in

Trigger Generator

The trigger generator (Fig. 1) consists of two power supplies isolated with each other, a capacitor, a thyristor switch, triggering system for thyristor switch and a pulse transformer for increasing the voltage required for the triggered spark gap. The compact power supply charges the capacitor with 9 Volts battery and another power supply charges the capacitor with supply mains. The schematic diagram of trigger generator is shown in Fig. 2.

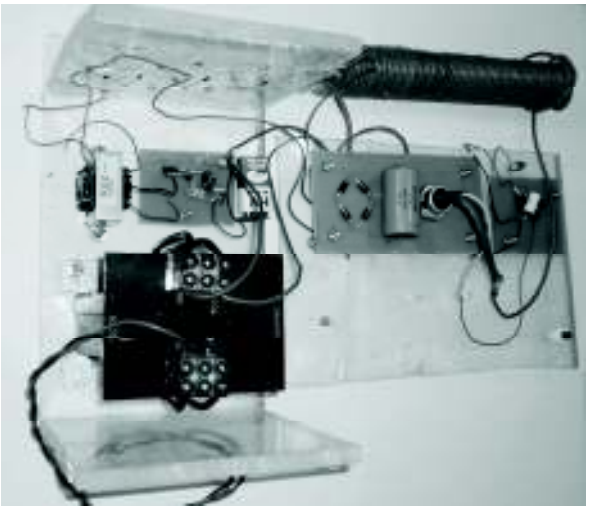

Figure 1: Trigger generator.

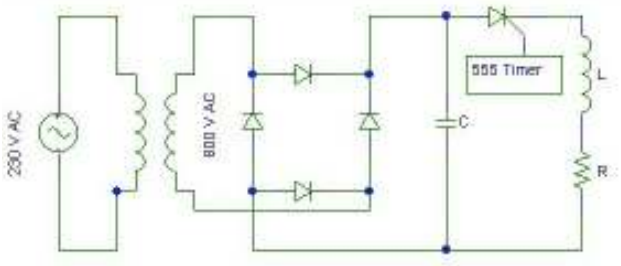

Figure 2: Schematic diagram of trigger generator.

Power Supply

Two power supplies are designed for charging the capacitor which is completely isolated. First power supply steps up the supply main voltage using transformer (220 V/ 800 V) to 800 V and then rectifying using a bridge rectifier. Four diodes IN504H (1.6 kV PIV, 1A) were used for rectification. The power supply charges a 2 µF El-Ci-R make capacitor. Second power supply uses a 9V battery and transistor circuit connected in flyback mode which will produce 8 Vp-p, 10 KHz. It is then given to ferrite core transformer which steps it from 8 V to 200V. A five stage cockroft multiplier is made with diode and capacitor. The output of multiplier gives 1kV and charges the 2 µF capacitor.

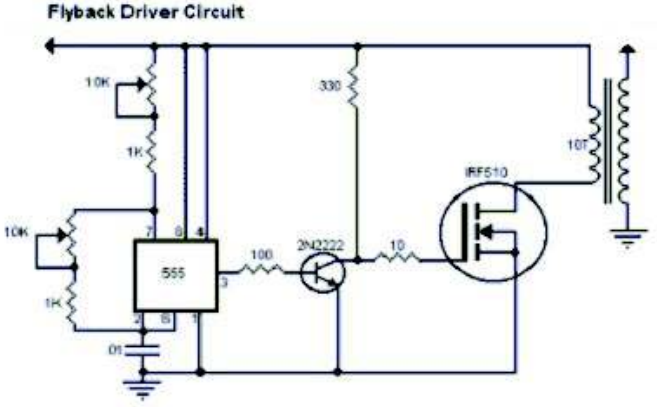

Figure 3: Flyback driver circuit.

The compact power supply has an efficient flyback driver circuit (Fig. 3) and its parts are easily available [1]. This circuit uses a 555 timer to pulse a 2N2222 with square wave at a frequency set by capacitor and the potentiometer. The 2N2222 then drives the gate of the MOSFET (IRF 510) and the MOSFET delivers the pulse to the input of the ferrite core transformer. It will produce 200 Vp-p, 10 KHz. The output of the transformer is given to a five stage cockroft voltage multiplier circuit. The cockroft multiplier (Fig. 4) is basically a voltage multiplier that converts AC or pulsing DC electrical power from a low voltage level to a higher DC voltage level. Voltage given to transformer (Vac) is stepped up to Voltage (Eac) and N stage mulitiplier produces Voltage (Eout) given by

$$Eout = 1.414\ Eout\ N \qquad (1)$$

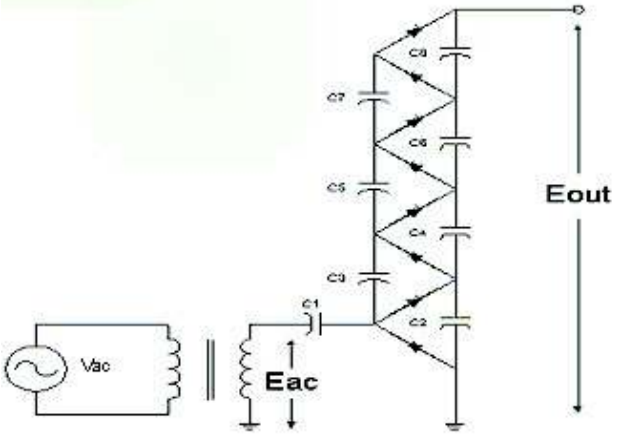

Figure 4: Cockroft multiplier circuit.

It is made up of a voltage multiplier ladder network of capacitors and diodes to generate high voltages. Unlike transformers, this method eliminates the requirement for the heavy core and the bulk of insulation/potting required. Using only capacitors and diodes, these voltage multipliers can step up relatively low voltages to extremely high values, while at the same time being far lighter and cheaper than transformers. The biggest advantage of such circuits is that the voltage across each stage of the cascade is equal to only twice the peak input voltage, so it has the advantage of requiring relatively low cost components and being easy to insulate.

Capacitor

El-Ci-R make 2µF capacitor is used for electrical energy storage. The capacitor is charged to 1 kV with either of the power supply. The power supply selection is done with an isolator switch. The charged capacitor is discharged into the primary of the pulse transformer through a thyristor switch.

Thristor Switch

Thyristor switch (70LS120) [2, 3] is used for switching the capacitor energy to pulse transformer. It has hold off voltage of 1200 Volts

and rms current rating of 120A. The thyristor is triggered with 5 Volts pulse generated with RC circuit and 555 timer.

Triggering of Thyristor

For reliable triggering the gate current must be greater than the minimum DC value specified by the thyristor manufacturer at the lowest possible operating temperature. To ensure reliable triggering, the gate current must never go below this value. A 555 timer in astable mode is used for gate triggering of thyristor [4, 5]. In astable mode, the 555 timer output is continuous stream of rectangular pulses having a frequency determined by the external RC circuit. A resistor (R1) is connected between Vcc and the discharge pin (pin 7) and another resistor (R2) is connected between the discharge pin (pin 7) and the trigger (pin 2). The trigger (pin 2) is shorted with threshold (pin 6). Hence the capacitor (C) is charged through R1 and R2, but discharged only through R2, since pin 7 has low impedance to ground during output low intervals of the cycle. The use of R2 is mandatory, since without it the high current spikes from the capacitor may damage the internal discharge transistor.
The frequency of oscillation is given by,

$$F = 1.44/(R1+2R2)C \quad (2)$$

By selecting R1 & R2, the duty cycle of the output can be adjusted. C charges through R1+R2 & discharges only through R2, duty cycle approaching a minimum of 50% can be achieved if, R2>>R1 so that the charging and discharging times are approx. equal.
The time that output is high (tH) is given by,

$$tH = 0.694(R1+R2)C \quad (3)$$

The time that the output is low (tL) is given by,

$$tL = 0.694R2C \quad (4)$$

The period T, the output waveform is the sum of tH & tL. The following formula for T is the reciprocal of f.

$$T = tH + tL = 0.694(R1+2R2)C \quad (5)$$

Percent duty cycle is,

$$\text{Duty cycle} = (tH/T)100\% = (tH/tH+tL)100\% = (R1+R2/R1+2R2)100\% \quad (6)$$

We have selected the value of R1, R2 & C; R1= 11.5 Kohm, R2= 1.5 Kohm, C= 10 μF, tH = 90 ms , tL = 10 ms

The output of the circuit is inverter with transistor switch so that thyristor is triggered with 10 ms, 5 Volts pulse. A repetitive 10 Hz trigger signal can be generated with this circuit.

Pulse Transformer

The Zeonics make pulse transformer is used to step up the 1 kV output of the trigger generator to 80 kV. The capacitor is discharged into the primary of pulse transformer and it step up to 80 kV which is given to the trigger point of the field distorted type triggered spark gap.

CONCLUSION

A compact trigger generator is fabricated which can be operated through a 9V battery to produce 80 kV pulse for triggering of field distorted spark gap for high energy capacitor bank for the production of peak power for a very short duration.

ACKNOWLEDGEMENT

This work was carried out as a part of final year project work of "B. E. (E & C) Programme of U. V. Patel College of Engineering" Programme at Institute for Plasma Research, Gandhinagar, Gujarat, India. The authors would like to acknowledge all members of E&E Division for their support and guidance.

REFERENCES

[1] Leopold, K.E. and Alcock, A J. (1976) Simple, fully isolated high voltage trigger generator. *Rev. Scientific Instru.* **47**: 254-255.
[2] Efficient flyback driver by IC 555 + IRF510, *Information website:* www.elecfree.com/ electronics/ efficeint-flyback-driver-circuit.
[3] Data sheet, *Information website*: www.alldatasheet.com.
[4] Singh, M. D. and Khanchandani, K. B. (2006) *Power Electronics*, Tata McGraw-Hill, pp 1 – 1096.
[5] Ramakant. A. G. (1995) *Op-Amps and Linear Integrated Circuits*, Prentice Hall of India, pp 1-640.

PRAJÑĀ - **Journal of Pure and Applied Sciences**
Vol. 17: 140 - 144, 2009 ISSN 0975 - 2595

EFFECT OF GERMINATION AND FERMENTATION ON PHENOLIC COMPOUNDS OF WHITE AND BLACK SOYBEAN

Nil Raval and Gayatree Jadeja *

Smt. K. P. Patel College of Home Science, Nr. Sardar Baug, Anand, Gujarat -388 001

ABSTRACT

In the present study, the phenolic compounds present in two different varieties of raw and processed, white and black soybean were evaluated. Total phenolics, tannin, flavonoid and proanthocyanidin content were assessed from raw white and black soybean. In addition, the germination and fermentation treatment were given to check out the changes occurred in phenolic content of processed soybeans. The highest phenolic content was found in black, *Bifidobacterium bifidum* fermented soybean. While, the lowest level of polyphenol were found in white, *Lactobacillus plantarum* fermented soybean. The results conclude that the changes occurred in phenolic content due to different processing conditions. The results suggested that the phenolic contents should also consider as an important characteristic feature of soybean seeds and as a potential selection criterion for antioxidant activity in soybean.

Keywords: **Soybean, total phenols, tannins, flavonoids, proanthocyanidin, antioxidant activity, germination, fermentation.**

INTRODUCTION

It is now well known that polyphenols present in the foods serve as antioxidants and preserve foods against oxidation damage. These polyphenols are most important not only because the diversity of their families is possible to find in the nature, but also in terms of their antioxidant activity [1].

Naturally occurring plant phenolics include several groups of compounds that have health promoting properties. Phenolics may act as antioxidants, thereby reducing the risk of atherosclerosis and coronary heart disease, which can be caused by oxidation of low-density lipoprotein [2]. Soybeans also contain the isoflavones, genistein and daidzein, types of phytoestrogen that are considered by some nutritionists and physicians to be useful in the prevention of cancer and by others to be carcinogenic and endocrine disruptive. Phenolic compounds play also an important role in plant resistance and defense against microbial infections which are intimately connected with reactive oxygen species (ROS) [3].

Many phenolic compounds found in plant tissues are potential antioxidants: flavonoids, tannins & lignin precursors may all work as ROS-scavenging compounds [4]. Antioxidants are compounds whose primary function is to protect our body from the molecules known as free radicals (among others) that cause oxidative stress. This oxidative damage is responsible for a major degenerative diseases of the circulatory system, cardiovascular disease, cataracts, premature ageing and cancer, all of which are now the main cause of death in our society [5].

To prevent oxidation of fats and oils, antioxidants are widely used in foods and cosmetics. Because of possible toxicity of the widely used butylated hydroxytoluene (BHT) and butylated hydroxyanisole (BHA), together with consumer's preference for "natural" products, much research on natural antioxidants has been undertaken in the recent past [6].

With the exception of isoflavonoid, few studies have been carried out on the other phenolic classes present in soybean. Thus the aim of this study was to assess the amount of phenolic compounds i.e. total polyphenol, tannin, flavonoid, proanthocyanidin etc. present in two different varieties of soybean (white & black) and to examine the effect of germination & fermentation on quantity of phenolic compounds.

MATERIALS AND METHODS

Experimental design

Polyphenolic compounds present in different foods and food products are of great interest. It was proposed to study different polyphenolic compounds, total phenol, tannin, flavonoid, proanthocyanidin etc. in varied processing conditions like germination & fermentation in

* Corresponding author –jadejagayatree@yahoo.com

order to determine the changes due to processing conditions.

Raw material preparation

Many foods like fruits, vegetables, legumes, tea etc. contain polyphenolic compounds among them soybean were procured from local market. Raw & processed white and black soybeans were selected for quantitative analysis of total polyphenolic content and other phenolic compounds like tannin, flavonoid & proanthocyanidin.

Soybean (Black and White) was purchased from local market of Anand city. Soybeans of both varieties were ground to a fine powder in a mill and were stored in Air tight container. 100 gm soybeans of both varieties were soaked separately in 200 ml of D/W for 14 to 18 hours. Then water was extracted from soaked soybeans and bound them in muslin cloth for germination. After completion of germination soybeans were dried into hot air oven at 60^0C for 1-2 hours. Again it was ground for getting fine powder. The germinated soy powder was used for assay.

Three different strains (*Sacharomyces cerevisiae, Lactobacillus plantarum, Bifidobecterium bifidum)* and mixture of these three cultures were used for fermentation of soybeans and checked out the changes occurred in polyphenolic content and other phenolic compounds content present in fermented samples.

Inoculum's preparation for fermentation process

First colony of each culture from master slant was picked up and transferred into 1 ml sterile distilled water under aseptic condition. Then 0.1 ml of each culture were transferred to 5 ml sterile luria broth under aseptic condition and incubated at room temperature for 24 hours (until becomes turbid). 2ml of culture was transferred from this inoculated luria broth to 100 ml flask contain sterile luria broth, under aseptic condition and again incubated at 24 hours, mixed well and check out O.D. (around 0.2 to 0.5 nm).

Fermentation process

From inoculums flask 2ml of inoculums was transferred under aseptic condition into 100 ml of flask contained 5 gm of soybean powder with 100 ml of sterile D/W. All the flasks were kept on shaker for 48 hours for continuous shaking (at 37^0C R.T.). The flasks were removed from shaker and centrifuged the whole content for 2-3 times at 10,000 rpm for 15 min. The filtrate was collected in 100 ml flasks by removing the supernatant using whatman no.1 filter paper. Filtrate was stored in refrigerator for quantification of polyphenol and other phenolic compounds.

Total polyphenolics

Total phenolics were determined by Folin-ciocalteu procedure [7]. 1 gm of soybean powder was taken into 100 ml of 70% aqueous acetone, mixed well at ambient temperature for 20 min and centrifuged at 8000 rpm for 15 min followed by filtration using whatman no. 2 filter paper. Filtrate was stored in refrigerator until assay.

Aliquots (0.1 ml) of aqueous acetone extracts were transferred in to test tubes and their volumes made up to 1 ml with distilled water. After addition of folin ciocalteu reagent (1ml) and 35% aqueous sodium carbonate solution (1ml). Tubes were vortexed and incubated at room temperature for 1 hour. After incubation 5 ml total volume was made up with distilled water and the absorbance of resulting blue colored mixtures was recorded at 620 nm against a blank containing D/W, instead of extraction solvent. The amount of total phenolics was expressed as Gallic acid g% dry plant material. Dilute samples with D/W (if needed). By using above method the determination of total phenolic compound from both raw and germinated soybean powder can be possible. In case of fermented samples filtrate was used directly instead of extracted solution.

Tannin

Tannin present in soybean was quantifying using Folin Denis method [8]. 2 gms of powder were taken into 75 ml D/W and heat it for 30 min in boiling water bath, centrifuged whole content at 2000 rpm for 20 min and filtered out using whatman no. 3 filter papers. Filtrate was collected and final volume made up to 100 ml with D/W.

0.1ml aliquot of extract was taken and volume made up 7.5 ml with D/W, followed by addition of Folin Denis reagent and 35% Na_2CO_3(W/V), 0.5 ml and 1 ml respectively, final volume was made up to 10 ml with D/W. Absorbance was read against blank at 700 nm in spectrophotometer.

The amount of Tannins was expressed as tannic acid g% dry plant material. In case of fermented samples filtrate used directly as a sample instead of extract for quantification of tannin.

Flavonoid

Flavonoid present in given sample could be quantified using reported method [9]. 1 gm of soybean powder was taken in to 50 ml of 80% methanol, mixed well and kept at room temperature for 20 min, centrifuged whole content for 10 min at 8000 rpm and filtered out using whatman no.2 filter paper. Filtrate was collected and stored for assay.

Aliquots of 1 ml & 2 ml of extracted solvent were taken & volume adjusted to 5 ml with D/W, 0.3 ml 5% NaNO2 (W/V) was added & incubated at room temperature for 5 min followed by addition of 10% AlCl3 (W/V) & 2 ml 1M NaOH, respectively. Final volume was made up to 10 ml by D/W & absorbance was measured at 510 nm against blank in spectrophotometer. The amount of flavonoid could be expressed as catechin g% dry plant material. In case of fermented samples, filtrate was used directly for quantification of flavonoid content instead of extracted solvent.

Proantocyanidin

Proantocyanidin present in given sample could be quantified using Julkunen-Titto method [10]. 2 gms of soybean powder were taken into 50 ml of 80% acetone and mixed well for 20 min, centrifuged whole content at 8000 rpm for 10 min, then filter out using whatman no. 2 filter paper. Filtrate could be stored in refrigerator for further assay.

Aliquots of 0.5 ml and 1 ml were taken and final volume was made up to 2 ml with D/W followed by addition of 3 ml 4% vanillin and 1.5 ml concentrated HCl. Read it out against blank at 500 nm after incubation of 30 minute at room temperature. The amount of proanthocyanidin was expressed as catechin g% dry plant material. In case of fermented samples, filtrate was used directly for quantification of proanthocyanidin content instead of extracted solvent.

All measurements were done in triplicate. Results were expressed as mean ± standard error. Statistical comparisons between samples were performed with student's t-test for independent observations. Differences were considered significant at $p<0.05$.

RESULTS AND DISCUSSION

With regards to total phenolics contents raw, germinated & fermented black soybean showed the highest levels of these compounds compared to white soybean (Table 1 and 2). These results are in accordance with the findings of other authors concerning phenolic contents and antioxidant activity in common beans (*Phaseolus vulgaris* L.), another *Leguminosae* species [11]. The total polyphenolic content were higher in white mix and *Sachharomyces cereviseae* fermented soybeans than black fermented soybean, however black fermented soybean with *Lactobacillus plantarum* & *Bifidobactarium bifidum* cultures contain higher amount of polyphenolic content than white fermented soybean.

The highest level of tannin was recorded in *Saccharomyces cereviseae* fermented white soybean, which also had highest level of total phenolics. Proanthocyanidin contents ranged from 0.16-1.16 Catechin g% of dry plant material. The highest content was observed in the *Saccharomyces cereviseae* fermented white soybean, although its total phenolic content was significantly lower, compared to black soybean. The amount of total flavonoid in the seed extracts of white & black soybean, only reached up to 0.63 Catechin g% of dry plant material.

This is considerably less than that observed in many wild growing plant species which are flavonoid rich [12].

Plants consumed by humans may contain thousands of different phenolic compounds. The effects of dietary phenolics are of great current interest, due to their antioxidative and possible anticarcinogenic activities. A popular belief is that dietary phenolics are anticarcinogens because they are antioxidants, but direct evidence supporting this supposition is lacking [13]. Phenolics may inhibit carcinogenesis by affecting the molecular events in the initiation, promotion and progression stages. Isoflavones from soybean may influence

TABLE 1: Phenolic content of raw and processed white soybean

Sample	Total Polyphenols[a]	Tannins[b]	Proantho Cyanidins[c]	Flavonoids[c]
Raw	0.54±0.03	0.16±0.01	0.34+0.04	0.08±0.02
Germinated	0.43±0.01	0.19±0.08	0.16+0.01	0.19±0.05
Fermented				
1.*Lactobacillus plantarum*	0.41±0.04	0.27±0.01	0.78+0.01	0.13±0.01
2. *Saccharomyces cereviseae*	1.41±0.02	1.93±0.01	1.16+0.03	0.32±0.01
3. *Bifidobacterium bifidum*	0.57±0.04	0.50±0.01	0.54+0.01	0.24±0.01
4. Mix culture	1.50±0.07	2.09±0.04	0.23+0.01	0.43±0.01

[a] Expressed as Gallic acid g% of dry plant material, [b] Expressed as Tannic acid g% of dry plant material, [c] Expressed as Catechin g% of dry plant material

TABLE 2: Phenolic content of raw and processed black soybean

Sample	Total Polyphenols[a]	Tannins[b]	Proantho Cyanidins[c]	Flavonoids[c]
Raw	0.99±0.04	0.26±0.01	0.55±0.02	0.09±0.03
Germinated	0.56±0.01	0.22±0.01	0.24±0.01	0.20±0.05
Fermented				
1. *Lactobacillus plantarum*	0.51±0.03	0.26±0.01	0.16±0.01	0.20±0.02
2. *Saccharomyces cereviseae*	0.70±0.16	0.22±0.01	0.10±0.01	0.15±0.01
3. *Bifidobacterium bifidum*	1.01±0.10	0.78±0.03	0.84±0.01	0.63±0.01
4. Mix culture	1.45±0.01	1.40±0.03	0.37±0.01	0.60±0.01

[a] Expressed as Gallic acid g% of dry plant material, [b] Expressed as Tannic acid g% of dry plant material, [c] Expressed as Catechin g% of dry plant material

tumor formation by affecting estrogen-related activities. They also modulate the growth of benign and malignant prostatic epithelial cells *in vitro* [14]. The bioavailability of the dietary phenolics has been discussed extensively, because the tissue levels of the effective compounds determine the biological activity. Epidemiological studies concerning consumption of phenolics and human cancer risk suggest the protective effects of certain food items and phenolics, but more studies are needed to reach clear cut conclusions [15].

SUMMERY AND CONCLUSION

Our results on soybean seed extracts suggest that phenolic content should be considered as an important feature of soybeans, besides protein and oil contents. Soybean is widely accepted as a "healthy food" and some of their pharmacological effects could be attributed to the presence of these valuable constituents. Results showed that black soybean were rich in total phenolics. White soybean fermented with *Saccharomyces cereviseae* were rich in total phenolics, tannin, proanthocyanidin and flavonoid compared to

black soybean. For this reason, we propose that the biological source of the plant material needs to more precisely defined, as observed phenolic contents were greatly dependent on plant material source.

REFERENCES

[1] Joshua, D., Lambert, S. Chung, Y. (2003) Cancer cehmopreventive activity and bioavailability of tea and tea polyphenols. *Mutation Research / Fundamental and Molecular Mechanisms of Mutagenesis*. **523–524**: 201-208.

[2] Emmons, C. L. and Peterson, D. M. (2001) Antioxidant activity and phenolic content of oat as affected by cultivar and location. *Crop Science*. **41**: 1676-1681.

[3] Grassmann, J., Hippeli, S., Elstner, E. F. (2002) Plant's defence and its benefits for animals and medicine: Role of phenolics and terpenoids in avoiding oxygen stress. *Plant Physiological Biochemistry*. **40**: 471-478.

[4] Blokhina, O., Virolainen, E., Fagerstedt, K. V. (2003) Antioxidants, oxidative damage and oxygen deprivation stress: a review. *Analytical Botany*. **91**: 179-194.

[5] Gottstein, N., Ewins, B. A., Eccleston, C. (2003) Effect of genistein and daiclzein on platelet aggregation and monocyte and endothelial function. *British Journal of Nutrition*. **89(5)**: 607-616.

[6] Cuvelier, M. E., Richard, H., Berset, C. (1996) Antioxidative activity and phenolic composition of pilot-plant and commercial extracts of sage and rosemary. *Journal of American Oil Chemical Society.* **73**: 645-652.

[7] Hagerman, A., Harvey M. I., Makkar, H. P. S. (2000) *Quantification of tannins in tree foliage. A laboratory Manual* FAO / IAEA: Vienna.

[8] Bajaj, K. L., Devsharma, A. K. (1977) A colorimetric method for the determination of tannins in tea. *Microchimica Act.* **68**: 249-253.

[9] Lamaison, J. L. C., Carnet, A. (1990) Teneurs en principaux flavonoids fleurs de crataegenus monogyna Jacq Crataegeus Laevigata (Poiret D.C) en function de la vegetation, *Pharmacology Acta.* **65**: 315-320.

[10] Julkunen, T., Cody, R. and Mark, H. (1985) Phenolic constituents in the leaves of Northern Willows: Methods for the analysis of certain phenolics. *Journal of Agricultural and Food Chemistry.* **33:** 213-217.

[11] Oomah, B. D., Cardador-M. A., Loarca, P. G. (2005) Phenolics and antioxidant activities in common beans. *Journal of Science and Food, Agriculture.* **85:** 935-942.

[12] Malencic, D. J., Gasic, O., Popovic, M. and Boza, P. (2000). Screening for antioxidant properties of salvia reflexa Hornem. *Phytotheraputic Research*. **14:** 546-548.

[13] Yang, C. S., Landau, J. M., Huang, M. T. and Newmark, H. L. (2001) Inhibition of carcinogenesis by dietary polyphenolic compounds. *Analytical Review of Nutrition*. **21:** 381-406.

[14] Hedlund, T. E., Johannes, W. U., Miller, G. J. (2003). Soy isoflavonoid equol modulates the growth of benign and malignant prostatic epithelial cells *in vitro. Prostate*. **54**: 68-78.

[15] Takahashi, R., Ohmori, R., Kiyose, C., Momiyama, Y., Ohsuza, F., Kondo, K. (2005). Antioxidant activities of black and yellow soybean against low density lipoprotein oxidation. *Journal of. Agricultural and Food Chemistry*. **53:** 4578-4582.

PRAJÑĀ - Journal of Pure and Applied Sciences
Vol. 17: 145 - 148, 2009 ISSN 0975 - 2595

ON SQUARE GENERALIZED PROJECTION

S. A. Alzuraiqi and A. B. Patel *

Department of Mathematics, Sardar Patel University, Vallabh Vidyanagar, Gujarat - 388 120

ABSTRACT

We investigate some characterizations and some properties of generalized projections (i.e., $T^2 = T^*$) on a Hilbert spaces. We introduce square generalized projections and discuss some of its properties.

***Keywords*: normal operator, projection, generalized projection.**

INTRODUCTION

Throughout this paper, $B(H)$ denotes the algebra of all bounded linear operators acting on a Hilbert space H. $P \in B(H)$ is called projection if $P^2 = P = P^*$ (where P^* is the adjoint of P). $T \in B(H)$ is called an 2-normal operator if $T^* T^2 = T^2 T^*$. In fact T is 2-normal if and only if T^2 is normal [3]. J. GroB, G.Trenkler have introduced generalized projections [1], $T \in B(H)$ is a generalized projection if $T^2 = T^*$. An orthogonal projection is a generalized projection. However if $T = \begin{pmatrix} \frac{-1+i\sqrt{3}}{2} & 0 \\ 0 & \frac{-1-i\sqrt{3}}{2} \end{pmatrix}$, then $T^2 = T^*$ but $T \neq T^*$. Thus a generalized projection may not be an orthogonal projection. A generalized projection is normal but if $T = \begin{pmatrix} 2 & 1 \\ 1 & 1 \end{pmatrix}$ is a normal operator but $T^2 = \begin{pmatrix} 5 & 3 \\ 3 & 2 \end{pmatrix} \neq T^*$.

We define that $T \in B(H)$ to be a square generalized projection if $T^4 = (T^*)^2$. A generalized projection is a square generalized projection. However if $T = \begin{pmatrix} 0 & 1 \\ 0 & 0 \end{pmatrix}$, then $T^2 = \begin{pmatrix} 0 & 0 \\ 0 & 0 \end{pmatrix}$. Hence $T^4 = (T^*)^2$, $T^2 \neq T^*$. Thus T is a square generalized projection but T is not a generalized projection. If T is a square generalized projection, then $T^6 = (T^*)^2 T^2 = T^2 (T^*)^2$ i.e., T is 2-normal. However if $T = \begin{pmatrix} 1 & -i \\ i & 2 \end{pmatrix}$, then T^2 is selfadjoint. Thus T is 2-normal but need not be a square generalized projection. If $T = \begin{pmatrix} 1 & 2 \\ 0 & -1 \end{pmatrix}$, then T^2 is a generalized projection but T is not normal.

* Corresponding author – abp1908@yahoo.com

Generalized Projections

Lemma 2.1.
Let $0 \neq T \in B(H)$ be a generalized projection. Then T is a partial isometry.

Proof. Since $T^2 = T^*$, T is normal, $TT^* = T^* T$. So we have $(T^* T)^2 = (T^* T)(T^* T) = (T^*)^2 T^2 = (T^2)^* T^* = (T^*)^* T^* = T T^* = T^* T$. Hence $T^* T$ is a projection. So T is a partial isometry.

We list the following basic properties without proof.

Proposition 2.1.
If $T \in B(H)$ is a generalized projection, then the following hold:
(1) T^* is a generalized projection.
(2) If T^{-1} exists, then T^{-1} is a generalized projection and T is unitary.
(3) If $T \neq 0$, then $\| T \| = 1$.
(4) If $T \neq 0$ and $(\alpha T)^2 = (\alpha T)^*$ for real α, then $\alpha \in \{0, 1\}$.
(5) If $S \in B(H)$ and S, T are unitary equivalent, then S is a generalized projection.
(6) If M a closed subspace of H such that M reduces T, then $S = T|M$ is a generalized projection.

Proposition 2.2. *The class of generalized projections is strongly closed in $B(H)$.*

Proof. Let $\{T_n\}$ be a sequence of generalized projections such that $\{T_n\}$ converges strongly to $T \in B(H)$. Now, since T_n's are normal, for $x \in H$, $\|T_n^* x - T_m^* x\| = \|T_n x - T_m x\|$. So $\{T_n x\}$ is a Cauchy sequence in H. Hence there is $y \in H$ such that $T_n^* x \to y$, as $n \to \infty$. Now, for $z \in H$, $\langle y, z\rangle = \lim_{n\to 0} \langle T_n^* x, z\rangle =$ $= \langle x, Tz\rangle = \langle T^* x, z\rangle = \langle x, Tz\rangle = \langle T^* x, z\rangle$. So $y = T^* x$. Thus $T_n^* x \to T^* x$ as n $\to \infty$ for each $x \in H$. Since $\{T_n\}$ converges to T strongly, T_n^k converges strongly to T^k by P. R. Halmos ([2], problem.93). Thus T_n^* converges strongly to T^k which implies that $T^k = T^*$. Thus T is a generalized projection, which implies that the class of generalized projections is strongly closed.

Proposition 2.3.
Let $T_1, \ldots, T_k \in B(H)$ be generalized projections. Then $(T_1 \oplus \ldots \oplus T_k)$ and $(T_1 \otimes \ldots \otimes T_k)$ are generalized projections.

Proof. Let $T_1, \ldots, T_k \in$ B(H) and $T_i^2 = T_i^*$ for $i = 1, \ldots, k$, and let $x = (x_1 \oplus \ldots \oplus x_k) \in (\oplus_1^k H)$. Then $(T_1, \oplus \ldots \oplus T_k)^2 x = (T_1, \oplus \ldots \oplus T_k)^2 (x_1 \oplus \ldots \oplus x_k) = T_1^2 x_1 \oplus \ldots \oplus T_k^2 x_k = T_1^* x_1 \oplus \ldots \oplus T_k^* x_k = (T_1^* \oplus \ldots \oplus T_k^*)(x_1 \oplus \ldots \oplus x_k) = (T_1, \oplus \ldots \oplus T_k)^* x$. Thus $(T_1, \oplus \ldots \oplus T_k)$ is a generalized projection.

Next, let $x = (x_1 \otimes \ldots \otimes x_k) \in (\otimes_1^k H)$. Then $(T_1 \otimes \ldots \otimes T_k)^2 x = (T_1 \otimes \ldots \otimes T_k)^2 (x_1 \otimes \ldots \otimes x_k) = T_1^2 x_1 \otimes \ldots \otimes T_k^2 x_k = T_1^* x_1 \otimes \ldots \otimes T_k^* x_k = (T_1^* \otimes \ldots \otimes T_k^*)(x_1 \otimes \ldots \otimes x_k) = (T_1 \otimes \ldots \otimes T_k)^* x$. Hence $(T_1 \otimes \ldots \otimes T_k)$ is a generalized projection.

Proposition 2.4. *Let $T \in B(H)$ be a generalized projection. Then the following hold.*

(1) If $(I - T)$ is a generalized projection, then T is an orthogonal projection.

(2) If $T = F + iG$ is the Cartesian decomposition of T such that $FG = -GF$, then T is an orthogonal projection.

(3) If $T = F + iG$ is the Cartesian decomposition of T such that F is an orthogonal projection, Then T is an orthogonal projection.

(4) If $T^3 = T$, then T is an orthogonal projection.

Proof.

(1) Since T and $I - T$ are generalized projections, $(I - T^*) = (I - T)^2 = I - 2T + T^2 = I - 2T + T^*$. Thus $2T = 2T^*$, which implies that $T = T^*$. Hence T is an orthogonal projection.

(2) Since $T = F + iG$ and $FG = -GF$, T^2 is selfadjoint. Since T is a generalized projection, $T^2 = T^*$. Hence T^* is selfadjoint, which implies that T is an orthogonal projection.

(3) Since T is a generalized projection, $T^2 = T^*$. Hence $(F^2 - G^2) + i(FG + GF) = F - iG$. So $(F^2 - G^2) = F$. Since F is an orthogonal projection, $G^2 = 0$. Thus T is an orthogonal projection.

(4) Since $T = T^3 = TT^2 = TT^*$, T is selfadjoint. Thus T is an orthogonal projection.

Square generalized projections

We list some simple results pertaining to square generalized projections in the following.

Lemma 3.1.
Let $T \in B(H)$ be a square generalized projection. Then the following hold.

(1) T^* is a square generalized projection.

(2) If T^{-1} exists, then T^{-1} is a square generalized projection.

(3) If $S \in B(H)$ be a square generalized projection, S, T are unitarily equivalent, then S is a square generalized projection.

(4) If M be a closed subspace of H such that reduces T, then $T|M$ is a square generalized projection.

Proposition 3.1. *The class of square generalized projections is strongly closed, hence uniformly closed in $B(H)$.*

Proof. Let $\{T_n\}$ be a sequence of square generalized projections such that $\{T_n\}$ converges strongly to $T \in B(H)$. Now, since T_n^2's are normal, for $x \in H$, $\|T_n^{*2} x - T_m^{*2} x\| = \|T_n^2 x -$

$T_m^2 x\|$. So $\{T_n^{*2}x\}$ is a Cauchy sequence in H. Hence there is $y \in H$ such that $T_n^{*2}x \to y$, as $n \to \infty$. Now, for $z \in H$, $\langle y, z\rangle = \lim_{n\to\infty} \langle T_n^{*2}x, z\rangle =$ $\lim_{n\to\infty} \langle x, T_n^2 z\rangle = \langle x, T^2 z\rangle = \langle T^{*2}x, z\rangle$. So $y = T^{*2}x$. Thus $T_n^{*2}x \to T^{*2}x$ as n $\to \infty$ for each $x \in H$. Since $\{T_n\}$converges to T strongly, T_n^4 converges strongly to T^4 by P. R. Halmos ([2], problem.93). Thus T_n^{*2} converges strongly to T^4 which implies that $T^4 = T^{*2}$. Thus T is a square generalized projection, which implies that the class of generalized projections is strongly closed.

Proposition 3.2. *Let $0 \neq T \in B(H)$ be a square generalized projection. Then the following hold.*

(1) If $(I - T)$ is a square generalized projection, then T is normal.

(2) If T^{-1} exists, then T^2 is unitary.

(3) If S is an idempotent such that S is similar to T, then T is a generalized projection

Proof.

(1) Since $(I - T)$ is a square generalized projection, $(I - T)^4 = (I - T^*)^2$. Hence $I - 4T + 6T^2 - 4T^3 + T^4 = I - 2T^* + T^{*2}$. Since T is a square generalized projection T, $T^* = T^2 = 2T - 3T^2 + 2T^3$. By premultipling and postmultipling the last equation by T, we get $TT^* = T^*T$. Thus T is normal.

(2) Since T is a invertible, T^2 is invertible. So by Proposition 2.1. (2), T^2 is unitary.

(3) Since S, T are similar, there is an invertible operator $V \in B(H)$ such that $S = V^{-1}TV$, $S^2 = V^{-1}T^2V$. Since $S^2 = S$, $V^{-1}T^2V = V^{-1}TV$, $T^2 = T$. Since T is a square generalized projection, $T^2 = T^4 = (T^2)^* = T^*$. Thus T is a generalized projection.

Proposition 3.3. *Let $S, T \in B(H)$ be commuting square generalized projections. Then the following hold.*

(1) ST is a square generalized projection.

(2) If $ST = 0$, then $(S + T)$ is a square generalized projection.

Proof.

(1) Since $(ST)^4 = S^4T^4 = S^{*2}T^{*2} = ((TS)^*)^2 = (ST)^{*2}$, ST is a square generalized projection.

(2) Since $(S + T)^4 = ((S + T)^2)^2 = (S^2 + ST + TS + T^2)^2 = (S^2 + T^2)^2 = S^4 + S^2T^2 + T^2S^2 + T^4 = S^4 + T^4 = S^{*2} + T^{*2} = (S^2 + T^2)^2 = (S + T)^{*2}$. Then $S + T$ is a square generalized projection.

From the last Proposition, it follows that if $0 \neq T \in B(H)$ is a square generalized projection, then T^m is a square generalized projection for any positive integer m.

Only commutativity in the above Proposition is not enough for the sum to be a square generalized projection. Let $0 \neq T \in B(H)$ be a square generalized projection. Then $(T + T)^4 = (2T)^4 = 16T^4$, while $((T + T)^*)^2 = 4T^{*2}$.

Proposition 3.4. *Let $T_1, \ldots, T_k \in B(H)$ be square generalized projections. Then $(T_1 \oplus \ldots \oplus T_k)$ and $(T_1 \otimes \ldots \otimes T_k)$ are square generalized projections.*

Proof. (1) Let $T_1, \ldots, T_k \in B(H)$ and $T_i^4 = T_i^{*2}$, for $i = 1, \ldots, k$, and $x = (x_1 \oplus \ldots \oplus x_k) \in (\oplus_1^k H)$. Then $(T_1 \oplus \ldots \oplus T_k)^4 x =$ $(T_1 \oplus \ldots \oplus T_k)^4 (x_1 \oplus \ldots \oplus x_k) = T_1^4 x_1 \oplus \ldots \oplus T_k^4 x_k = T_1^{*2} x_1 \oplus \ldots \oplus T_k^{*2} x_k = (T_1^{*2} \oplus \ldots \oplus T_k^{*2})(x_1 \oplus \ldots \oplus x_k) = (T_1^* \oplus \ldots \oplus T_k^*)^2 (x_1 \oplus \ldots \oplus x_k) = ((T_1 \oplus \ldots \oplus T_k)^*)^2 x$. Thus $(T_1 \oplus \ldots \oplus T_k)$ is a square generalized projection.

Next, let $x = (x_1 \otimes \ldots \otimes x_k) \in (\otimes_1^k H)$. Then $(T_1 \otimes \ldots \otimes T_k)^4 x = (T_1 \otimes \ldots \otimes T_k)^4 (x_1 \otimes \ldots \otimes x_k) = T_1^4 x_1 \otimes \ldots \otimes T_k^4 x_k = T_1^{*2} x_1 \otimes \ldots \otimes T_k^{*2} x_k = (T_1^{*2} \otimes \ldots \otimes T_k^{*2})(x_1 \otimes \ldots \otimes x_k) = (T_1^* \otimes \ldots \otimes T_k^*)^2 (x_1 \otimes \ldots \otimes x_k) = ((T_1 \otimes \ldots \otimes T_k)^*)^2 x$. Hence $(T_1 \otimes \ldots \otimes T_k)$ is a square generalized project.

Proposition 3.5. *If $T \in B(H)$ such that $T^{2^n} = T^{*2^{n-1}}$, then T is (2^{n-1})-normal.*

Proof.

Since $T^{2^n} = T^{*2^{n-1}}$, $T^{2^n}T^{2^{n-1}} = T^{2^{n-1}}T^{*2^{n-1}}$ and $T^{2^{n-1}}T^{2^n} = T^{*2^{n-1}}T^{2^{n-1}}$. Hence $T^{2^{n-1}}T^{*2^{n-1}} = T^{*2^{n-1}}T^{2^{n-1}}$. Hence T is (2^{n-1})normal.

But the converse in general need not be true.

If $T = \begin{pmatrix} 0 & 1 \\ 0 & 0 \end{pmatrix}$, Then $T^2 = \begin{pmatrix} 0 & 0 \\ 0 & 0 \end{pmatrix}$ is normal operator, T is 2-normal But $T^* \neq T^2$.

By similar arguments given in the proof of the last Proposition one can see that if $T \in B(H)$ such that $T^{3^n} = T^{*3^{n-1}}$, then T is (3^{n-1})-normal.

ACKNOWLEDGEMENTS

S. A. Alzuraiqi is thankful to the Ministry of Higher Education and Scientific Research, Republic of Yemen for scholarship to peruse his Ph.D. studies, and to Thamar University, Republic of Yemen for granting his study leave. The authors would like to thank Professor S.J. Bhatt for helpful discussions. The UGC-SAP-DRS support to the Department of Mathematics is gratefully acknowledged by both the authors.

REFERENCES

[1] J. GroB, G. Trenkler, (1997) Generalized and hypogeneralized Projectors. *Linear Algebra Appl.,* **264**: 463-474.

[2] P. R. Halmos, (1982) *A Hilbert space proplem book, Springer-Verlag, New York.*

[3] S. A. Al-Zuraiqi, A. B. Patel, On n-normal operators, communicated.

PRAJÑĀ - **Journal of Pure and Applied Sciences**
Vol. 17: 149 - 154, 2009 ISSN 0975 - 2595

MAXIMAL IDEAL SPACE AND SHILOV BOUNDARY FOR THE CARTESIAN PRODUCT OF COMMUTATIVE BANACH ALGEBRAS

R. D. Mehta [*] and Nirav H. Shah [1]

Department of Mathematics, Sardar Patel University, Vallabh Vidyanagar, Gujarat – 388 120
[1]V. V. P. Engineering College, Rajkot, Gujarat - 360 005

ABSTRACT

We characterize the Maximal ideal space and Shilov boundary for the cartesian product of two commutative banach algebras. We also discuss the Hull-kernel topology on the maximal ideal space and characterize it for the cartesian product of two commutative banach algebras.

***Keywords*: cartesian product of two commutative banach algebras, maximal ideal space, shilov boundary, Hull-kernel topology.**

INTRODUCTION

Let A and B be two commutative Banach algebras over $\mathbb{C}$ with identities e_A and e_B. Now, for $(a,b) \in A \times B$, define $\| (a,b) \| = \max \{ \| a \|_A, \| b \|_B \}$, where $\| . \|_A$ and $\| . \|_B$ respectively denotes the norms in A and B. With coordinate-wise operations and maximum norm defined above $A \times B$ is a commutative Banach algebra with identity (e_A, e_B).

For commutative banach algebra A, Δ_A is maximal ideal space of A, and ∂_A is the Shilov boundary for A. Here we characterize $\Delta_{A\times B}$ and $\partial_{A\times B}$ in terms of Δ_A, Δ_B and ∂_A, ∂_B.

We shall need some topological preliminaries for the characterization.

Sum of Topological Spaces:[1]

Let $\{ X_\lambda : \lambda \in M \}$ be an indexed family of topological spaces, and let $X = \bigcup_{\lambda \in M} X_\lambda$. Then the collection

$\tau = \{ U \subset X : U \cap X_\lambda$ is an open set of the space $X_\lambda, \forall \lambda \in M \}$

is a topology on X. τ is called the sum topology. The topological space (X, τ) is called the topological sum of the spaces $\{ X_\lambda \}_{\lambda \in M}$ and is denoted by $X = \sum X_\lambda$.

Usually, the spaces X_λ to be taken distinct and in that case X is called the disjoint sum.

Now we establish some results on sum topology, which will be useful in our development of the topic.

Theorem 2.1 Let (X, τ_1) and (Y, τ_2) be two compact-Hausdorff spaces. Then disjoint sum X+Y with the sum topology is also compact and Hausdorff.

Proof: To show that X+Y is compact, let $\{W_\alpha\}_{\alpha \in \lambda}$ be an open cover of X+Y in the sum topology. Then $\{ W_\alpha \cap X \}_{\alpha \in \lambda}$ and $\{ W_\alpha \cap Y \}_{\alpha \in \lambda}$ are open covers of X and Y respectively. Since X and Y both are compact spaces, there exist finite subcovers of $\{ W_\alpha \cap X \}_{\alpha \in \lambda}$ and $\{ W_\alpha \cap Y \}_{\alpha \in \lambda}$ that cover X and Y respectively.

Let $\{ W_{\alpha_i} \cap X \}_{i=1}^n$ be a finite subcover of $\{ W_\alpha \cap X \}_{\alpha \in \lambda}$ which covers X. Thus $X = \bigcup_{i=1}^n (W_{\alpha_i} \cap X)$. Similarly if $\{ W_{\beta_j} \cap Y \}_{j=1}^m$ is a finite subcover of $\{ W_\alpha \cap Y \}_{\alpha \in \lambda}$ which covers Y, then $Y = \bigcup_{j=1}^m (W_{\beta_j} \cap Y)$.

* Corresponding author – Hvvnspu@yahoo.co.in

Take the collection $\{\{W_{\alpha_i}\}_{i=1}^{n}, \{W_{\beta_j}\}_{j=1}^{m}\}$ then it is a finite subcover of $\{W_\alpha\}_{\alpha\in\lambda}$, which covers X+Y.

Since $\{W_\alpha\}_{\alpha\in\lambda}$ was arbitrary, X+Y is a compact space.

It can be easily proved that X+Y is Hausdorff space when X and Y both are Hausdorff spaces.

The following results can be checked.

Theorem 2.2 Let (X,τ_1) and (Y,τ_2) be two topologicals paces and τ be the sum topology on X+Y induced by τ_1 and τ_2. If $f\in C(X)$ and $g\in C(Y)$ then h on X+Y defined by

$$h(z)=\begin{cases} f(z) & \text{if } z\in X \\ g(z) & \text{if } z\in Y \end{cases}$$

is continuous. where C(X) denotes the space of all continuous functions on X.

Theorem 2.3 Let (X,τ_1) and (Y,τ_2) be two topological spaces and τ be the sum topology on X+Y induced by τ_1 and τ_2 and *h* is continuous on X+Y with respect to τ. Then $h|_X\in C(X)$ and $h|_Y\in C(Y)$.

Maximal Ideal Space of $A\times B$:

Next we show that $\Delta_{A\times B}$ with the Gelfand topology is the topological sum of Δ_A and Δ_B equipped with the Gelfand topologies.

First we show that $\Delta_{A\times B}\cong\Delta_A\cup\Delta_B$.

Theorem 3.1 $\Delta_{A\times B}=\Delta_A\cup\Delta_B$

Proof: Let $\varphi_A\in\Delta_A$. Define $\varphi: A\times B\to\mathbb{C}$ by,

$\varphi((a,b))=\varphi_A(a)\quad\forall(a,b)\in A\times B$.

First we show that $\varphi\in\Delta_{A\times B}$. Let $(a_1,b_1),(a_2,b_2)\in A\times B$ and $\alpha,\beta\in\mathbb{C}$.

So

$\varphi((a_1,b_1))=\varphi_A(a_1),\ \varphi((a_2,b_2))=\varphi_A(a_2)$.

$$\begin{aligned}\varphi(\alpha(a_1,b_1)+\beta(a_2,b_2)) &= \varphi(\alpha a_1+\beta a_2,\alpha b_1+\beta b_2)\\ &= \varphi_A(\alpha a_1+\beta a_2)\\ &= \alpha\varphi_A(a_1)+\beta\varphi_A(a_2)\\ &= \alpha\varphi((a_1,b_1))+\beta\varphi((a_2,b_2))\end{aligned}$$

$$\begin{aligned}\varphi((a_1,b_1)\cdot(a_2,b_2)) &= \varphi((a_1a_2,b_1b_2))\\ &= \varphi_A(a_1a_2)\\ &= \varphi_A(a_1)\cdot\varphi_A(a_2)\\ &= \varphi((a_1,b_1))\cdot\varphi((a_2,b_2))\end{aligned}$$

Now $\varphi(e)=\varphi((e_A,e_B))=\varphi_A(e_A)=1$.

Therefore φ is a complex homomorphism on $A\times B$, i.e. $\varphi\in\Delta_{A\times B}$.

So we identify φ_A with φ. Similarly if $\varphi_B\in\Delta_B$ then we can define

$\varphi((a,b))=\varphi_B(b)\quad\forall(a,b)\in A\times B$ and we can show that $\varphi\in\Delta_{A\times B}$. So we identify φ_B with φ. Thus

$$\Delta_A\cup\Delta_B\subset\Delta_{A\times B}. \qquad (1)$$

Conversely, let $\varphi\in\Delta_{A\times B}$ then

$0=\varphi((0,0))=\varphi((0,e_B)\cdot(e_A,0))=\varphi((0,e_B))\cdot\varphi((e_A,0))$

.

Hence either

$\varphi((e_A,0))=0$ or $\varphi((0,e_B))=0$.

But

1=

$\varphi(e)=\varphi((e_A,e_B))=\varphi((0,e_B))+\varphi((e_A,0))$

Hence one of them has to be nonzero.

Suppose $\varphi((0,e_B))=0$. So $\varphi((e_A,0))=1$.

Since $\varphi((0,e_B))=0$,

$$\begin{aligned}\varphi((0,b)) &= \varphi((0,e_B)\cdot(0,b))\\ &= \varphi((0,e_B))\cdot\varphi((0,b))\\ &= 0.\end{aligned}$$

$\therefore \varphi\big((0,b)\big) = 0 \quad \forall b \in \mathrm{B}.$

$$\text{Hence } \varphi\big((a,b)\big) = \varphi\big((a,0)\big) + \varphi\big((0,b)\big)$$
$$= \varphi\big((a,0)\big) + 0$$
$$= \varphi\big((a,0)\big).$$

$\therefore \varphi\big((a,b)\big) = \varphi\big((a,0)\big) \quad \forall (a,b) \in \mathrm{A} \times \mathrm{B}.$

Define $\varphi_{\mathrm{A}} : \mathrm{A} \to \square$ by $\varphi_{\mathrm{A}}(a) = \varphi\big((a,0)\big)$. Then it can be checked by using the definition of algebraic operations in $\mathrm{A} \times \mathrm{B}$ that φ_{A} is a complex homomorphism on A.

Therefore $\varphi_{\mathrm{A}} \in \Delta_{\mathrm{A}}$. We identify φ with φ_{A}. If $\varphi\big((e_{\mathrm{A}},0)\big) = 0$ then $\varphi\big((0,e_{\mathrm{B}})\big) = 1$ and we define $\varphi_{\mathrm{B}} : \mathrm{B} \to \square$ by, $\varphi_{\mathrm{B}}(b) = \varphi\big((0,b)\big) \quad \forall b \in \mathrm{B}$ and we can show that $\varphi_{\mathrm{B}} \in \Delta_{\mathrm{B}}$. So we identify φ with φ_{B}. Thus

$$\Delta_{\mathrm{A}\times\mathrm{B}} \subset \Delta_{\mathrm{A}} \cup \Delta_{\mathrm{B}}. \qquad (2)$$

Hence From (1) and (2) we have,

$$\Delta_{\mathrm{A}\times\mathrm{B}} = \Delta_{\mathrm{A}} \cup \Delta_{\mathrm{B}}$$

Theorem 3.2 Let τ_1 be the sum topology on $\Delta_{\mathrm{A}} \cup \Delta_{\mathrm{B}}$ induced by the Gelfand topologies on Δ_{A} and Δ_{B} respectively and τ_2 be the Gelfand topology on $\Delta_{\mathrm{A}\times\mathrm{B}}$. Then $\tau_1 = \tau_2$.

Proof: Since Δ_{A} and Δ_{B} are compact and Hausdorff spaces in their respective Gelfand topologies, τ_1 on $\Delta_{\mathrm{A}\times\mathrm{B}}$ is also compact and Hausdorff [by Theorem 2.1]. Now the Gelfand topology τ_2 on $\Delta_{\mathrm{A}\times\mathrm{B}}$ is also compact and Hausdorff. Gelfand topology τ_2 on $\Delta_{\mathrm{A}\times\mathrm{B}}$ is the weakest topology which makes every $\hat{(a,b)}$ continuous on $\Delta_{\mathrm{A}\times\mathrm{B}}$. So if we can show that $\hat{(a,b)}$ is continuous on $\Delta_{\mathrm{A}\times\mathrm{B}}$ under τ_1, then Gelfand topology τ_2 on $\Delta_{\mathrm{A}\times\mathrm{B}}$ is weaker than τ_1 on $\Delta_{\mathrm{A}\times\mathrm{B}}$. Since both topologies are compact and Hausdorff, they must coincide.

Claim: $\hat{(a,b)}$ is continuous on $\Delta_{\mathrm{A}\times\mathrm{B}}$ with respect to τ_1.

For any $\varphi \in \Delta_{\mathrm{A}\times\mathrm{B}}$,

$$\hat{(a,b)}(\varphi) = \begin{cases} \hat{a}(\varphi) & \text{if } \varphi \in \Delta_{\mathrm{A}} \\ \hat{b}(\varphi) & \text{if } \varphi \in \Delta_{\mathrm{B}} \end{cases}$$

Since $\hat{a}$ is continuous on Δ_{A} and $\hat{b}$ is continuous on Δ_{B} with respect to their Gelfand topologies, $\hat{(a,b)}$ is continuous on $\Delta_{\mathrm{A}\times\mathrm{B}}$ with respect to τ_1 [From theorem 2.2]. Hence $\tau_1 = \tau_2$.

Remark 3.3 $\hat{\mathrm{A} \times \mathrm{B}} = \hat{\mathrm{A}} \cup \hat{\mathrm{B}}$.

Shilov Boundary:

Definition 4.1.[2] A subset E of Δ_{A} is said to be a ***boundary*** for A if every $\hat{x} \in \hat{\mathrm{A}}$ assumes its maximum modulus on E.

Definition 4.2.[2] The smallest closed boundary for A is called the ***Shilov boundary*** for A. It is denoted by ∂_{A}.

Now we obtain relation between $\partial_{\mathrm{A}\times\mathrm{B}}$, the Shilov boundary for $\mathrm{A} \times \mathrm{B}$, and ∂_{A}, ∂_{B} as follows.

Theorem 4.3 $\partial_{\mathrm{A}\times\mathrm{B}} = \partial_{\mathrm{A}} \cup \partial_{\mathrm{B}}$.

Proof: Let $\hat{a} \in \hat{\mathrm{A}}$. Since $\hat{\mathrm{A}} \cup \hat{\mathrm{B}} = \hat{\mathrm{A} \times \mathrm{B}}$ [by Remark 3.3], $\hat{a} = \hat{(a,0)}$.

Hence $\max \left| \hat{a} \right| = \max \left| \hat{(a,b)} \right| \quad \forall \hat{a} \in \hat{\mathrm{A}}$.

But $\left| \hat{(a,0)} \right|$ assumes its maximum on $\partial_{\mathrm{A}\times\mathrm{B}}$.

Hence $\left| \hat{a} \right|$ assumes its maximum on $\partial_{\mathrm{A}\times\mathrm{B}}$,

which is true for every $\hat{a} \in \hat{A}$. So $\partial_{A\times B}$ is a boundary for A. Since, ∂_A is the smallest closed boundary for A,
$\partial_A \subset \partial_{A\times B}$.

Similarly we can show that $\partial_{A\times B}$ is a boundary for B, hence
$\partial_B \subset \partial_{A\times B}$.
Hence from (1) and (2) we have,
$\partial_A \cup \partial_B \subset \partial_{A\times B}$. (3)

Now for any $(\hat{a},\hat{b}) \in \hat{A}\times\hat{B}$, $(\hat{a},\hat{b}) = \hat{a}$ or $(\hat{a},\hat{b}) = \hat{b}$ [Remark 3.3].

If $(\hat{a},\hat{b}) = \hat{a}$ then $|(\hat{a},\hat{b})| = |\hat{a}|$. Hence
$\max |(\hat{a},\hat{b})| = \max |\hat{a}|$. (4)

Since $\hat{a}$ assumes its maximum on ∂_A $\forall \hat{a} \in \hat{A}$, $|(\hat{a},\hat{b})|$ assumes its maximum on ∂_A from (4).

If $(\hat{a},\hat{b}) = \hat{b}$ then $|(\hat{a},\hat{b})|$ assumes its maximum on ∂_B. Hence $\partial_A \cup \partial_B$ is a boundary for $A\times B$. Since $\partial_{A\times B}$ is the Shilov boundary, it is the smallest closed boundary for $A\times B$.
Hence we have $\partial_{A\times B} \subset \partial_A \cup \partial_B$. (5)
Therefore from (3) and (5) we have,
$\partial_{A\times B} = \partial_A \cup \partial_B$.

Hull-kernel Topology:

Definition 5.1.[2] Let $F \subset \Delta_A$. Then ***kernel of F***, denoted as k(F), is defined as
$k(F) = \{ x \in A : \varphi(x)=0 \quad \forall \varphi \in F \}$
$= \{ x \in A : \hat{x}(\varphi) = 0 \quad \forall \varphi \in F \}$
$= \bigcap_{\varphi\in F} \varphi^{-1}\{0\}$.
Clearly if $F=\phi$, then $k(\phi) = A$. Evidently k(F) is a closed ideal in A.

Let $I \subset A$ be an ideal. Then the ***hull of I***, denoted by h(I), is defined as
$h(I) = \{ \varphi \in \Delta_A : I \subset \ker(\varphi) \}$. Evidently the hull of I is a closed subset of Δ_A. For any $E \subset \Delta_A$, we have $E \subset h[k(E)]$. (1)

A subset E of Δ_A is a hull, if E is the hull of some ideal in A. If E is hull, then E is the hull of k(E). (2)

Definition 5.2. The topology on Δ_A determined by the closure operation
$E \to \overline{E} = h[k(E)]$, $E \subset \Delta_A$ is called the ***hull-kernel topology*** on Δ_A [2,3]. We denote hull-kernel topology on Δ_A by τ_{hk}^A.
i.e. $\tau_{hk}^A = \{ G \subset \Delta_A : G = E,\ E = h[k(E)] \}$.

Since $h[k(E)]$ ($E \subset \Delta_A$) is always closed in the Gelfand topology, the hull-kernel topology is weaker than the Gelfand topology. Also the hull-kernel topology is a T_1-topology. It is T_2 if and only if it coincides with the Gelfand topology **[2, p.13]**.

Now let τ_{hk}^B denotes hull-kernel topology on the commutative Banach algebra B. Next theorem shows that the hull-kernel topology on $\Delta_{A\times B}$ is the same as the sum topology on $\Delta_{A\times B}$ induced by τ_{hk}^A (on Δ_A) and τ_{hk}^B (on Δ_B).

Theorem 5.3. Let τ_{hk}^A and τ_{hk}^B be hull-kernel topologies on Δ_A and Δ_B respectively. Let τ_1 be hull-kernel topology on $\Delta_{A\times B}$, and τ_2 be sum topology on $\Delta_{A\times B} = \Delta_A + \Delta_B$ induced by τ_{hk}^A and τ_{hk}^B. Then $\tau_1 = \tau_2$.

Proof: Let $E \subset \Delta_{A\times B} = \Delta_A + \Delta_B$ be closed in τ_1. Then E= h[k(E)].
Let $E_A = E \cap \Delta_A$ and $E_B = E \cap \Delta_B$. We have to show that E is closed in τ_2. For that we have

to show that E_A is closed in τ_{hk}^A and E_B is closed in τ_{hk}^B, because τ_2 is the sum topology induced by τ_{hk}^A and τ_{hk}^B. That is, to show $h[k(E_A)] = E_A$ and $h[k(E_B)] = E_B$.

Claim 1: $k(E_A \cup E_B) = k(E_A) \times k(E_B)$.

Let $(a,b) \in k(E_A) \times k(E_B)$. Then $a \in k(E_A)$ and $b \in k(E_B)$.

So $\varphi(a) = \hat{a}(\varphi) = 0 \quad \forall \varphi \in E_A$ and $\varphi(b) = \hat{b}(\varphi) = 0 \quad \forall \varphi \in E_B$. (1)

For any

$\varphi \in E_A \cup E_B$, $(\hat{a,b})(\varphi) = \hat{a}(\varphi)$ or $(\hat{a,b})(\varphi) = \hat{b}(\varphi)$.

In any case, $(\hat{a,b})(\varphi) = 0 \quad \forall \varphi \in E_A \cup E_B = E$ [by (1)].

Therefore $(a,b) \in k(E_A \cup E_B) = k(E)$.

Hence $k(E_A) \times k(E_B) \subset k(E_A \cup E_B)$. (2)

Let $(a,b) \in k(E_A \cup E_B)$.

Then $(\hat{a,b})(\varphi) = 0 \quad \forall \varphi \in E_A \cup E_B$.

Hence $(\hat{a,b})(\varphi) = 0 \quad \forall \varphi \in E_A$ and

$(\hat{a,b})(\varphi) = 0 \quad \forall \varphi \in E_B$.

When $\varphi \in E_A$ then $(\hat{a,b})(\varphi) = \hat{a}(\varphi)$.

Since $(\hat{a,b})(\varphi) = 0 \quad \forall \varphi \in E_A, \hat{a}(\varphi) = 0 \quad \forall \varphi \in E_A$. So $a \in k(E_A)$.

Similarly when $\varphi \in E_B$ then $(\hat{a,b})(\varphi) = \hat{b}(\varphi)$ and $\hat{b}(\varphi) = 0 \quad \forall \varphi \in E_B$.

So $b \in k(E_B)$.

Therefore $(a,b) \in k(E_A) \times k(E_B)$.

Hence $k(E_A \cup E_B) \subset k(E_A) \times k(E_B)$. (3)

From (2) and (3) we have,

$k(E_A \cup E_B) = k(E_A) \times k(E_B)$. (4)

Claim 2: When I_1 and I_2 are proper ideals in A and B respectively then

$h(I_1 \times I_2) = h(I_1) \cup h(I_2)$.

Let $\varphi \in h(I_1) \cup h(I_2)$.

If $\varphi \in h(I_1)$ then $I_1 \subset \ker(\varphi) = M_A$.

Where M_A is a maximal ideal in A. By theorem 3.1. we can identify φ with $\varphi' \in \Delta_{A\times B}$ such that $\ker(\varphi') = M_A \times B$.

Clearly $I_1 \times I_2 \subset M_A \times B$ so $\varphi \in h(I_1 \times I_2)$.

Similarly we can show that if $\varphi \in h(I_2)$ then $\varphi \in h(I_1 \times I_2)$.

Hence $h(I_1) \cup h(I_2) \subset h(I_1 \times I_2)$. (5)

Let

$\varphi \in h(I_1 \times I_2)$. Then $\varphi((a,b)) = 0 \quad \forall (a,b) \in I_1 \times I_2$

If $\varphi \in \Delta_A$, then $\varphi \in h(I_1)$ and if $\varphi \in \Delta_B$, then $\varphi \in h(I_2)$.

So $\varphi \in h(I_1) \cup h(I_2)$.

Hence $h(I_1 \times I_2) \subset h(I_1) \cup h(I_2)$. (6)

Therefore from (5) and (6) we have,

$h(I_1 \times I_2) = h(I_1) \cup h(I_2)$. (7)

We have $E = E_A \cup E_B$ and E_A and E_B are disjoint.

Also $h[k(E)] = E$. So $h[k(E)] = E_A \cup E_B$. (8)

Now, $h[k(E)] = h[k(E_A \cup E_B)]$

$= h[k(E_A) \times k(E_B)]$ [From (3)] (9)

From (8) and (9) we have,

$E_A \cup E_B = h[(k(E_A))] \cup h[(k(E_B))]$.

Since we have disjoint union on both sides, $E_A = h[k(E_A)]$ and $E_B = h[k(E_B)]$.

Therefore E_A is closed in τ_{hk}^A and E_B is closed in τ_{hk}^B. So E is closed in τ_2, when it is closed in τ_1.

Hence

$$\tau_1 \geq \tau_2. \quad (10)$$

Let F be closed set in τ_2.

Here $F \subset \Delta_{A\times B} = \Delta_A + \Delta_B$.

Let $F_A = F \cap \Delta_A$ and $F_B = F \cap \Delta_B$. Since F is closed in τ_2,

F_A and F_B are closed in τ_{hk}^A and τ_{hk}^B respectively.

So $F_A = h[k(F_A)]$ and $F_B = h[k(F_B)]$.

We have to show that F is closed set in τ_1. That is to show that F = h[k(F)].

$$\begin{aligned} \text{Now, } F &= F_A \cup F_B \\ &= h[k(F_A)] \cup h[k(F_B)] \\ &= h[k(F_A) \times k(F_B)] \quad \text{[From (7)]} \\ &= h[k(F_A \cup F_B)] \quad \text{[From (3)]} \\ &= h[k(F)]. \end{aligned}$$

Hence F is closed in τ_1, when it is closed in τ_2.

Therefore $\tau_2 \geq \tau_1$. (11)

From (10) and (11) we have $\tau_1 = \tau_2$.

ACKNOWLEDGEMENT

The Research was supported by the SAP to the department by UGC.

REFRENCES

[1] Dugundji James, Topology, Prentice Hall of India, New Delhi, 1975.

[2] Gamelin T. W., Uniform Algebras, Prentice-Hall, Inc. 1969.

[3] Larsen Ronald, Banach algebras an Introduction, Marcel Dekker, Inc. 1973.

[4] Rudin Walter, Functional Analysis, Mc. Graw-Hill Book Company, Inc. 1973.

[5] Simmons G.F., Introduction to Topology and Modern Analysis, McGraw-Hill Book Company, Inc. 1963

PRAJÑĀ - **Journal of Pure and Applied Sciences**
Vol. 17: 155 - 156, 2009 ISSN 0975 - 2595

A NOTE ON DEFORMED OPERATORS

Arvind B. Patel *

Department of Mathematics, Sardar Patel University,Vallabh Vidyanagar, Gujarat - 388 120

ABSTRACT

For q>0, an operator in a Hilbert space is q-normal if TT* = qT*T. Sum and product of operators of these type are discussed.

Keywords: **unbounded operator, q-normal operator.**

INTRODUCTION

Consider a number q > 0. A densely defined closed operator T in a Hilbert space H is called (i) q-normal (or deformed normal with deforming parameter q) if TT* = qT*T. (ii) q-hyponormal if $D(T) \subset D(T^*)$ and $\|T^*x\| \leq \sqrt{q}\,\|Tx\|$ for all $x \in D(T)$. (iii) q-quasinormal if $U|T| \subset \sqrt{q}\,|T|U$, where T = U|T| is the polar decomposition of the operator T. Motivated from the theory of quantum group, Ota [1], [2], [3] has initialized the study of q-deformed operators. If T is bounded and q-normal, then $\|T^*\|^2 = \|TT^*\| = q\|T^*T\| = q\|T\|^2 = q\|T\|^2$

this shows q = 1. So if $q \neq 1$, T must be unbounded. If T is q-quasinormal and $0 < q < 1$, then T must be unbounded. Every q-normal operator is q-quasinormal; and every q-quasinormal operator is q-hyponormal.

For a closed densely defined operator T in H, Ota proved that T is a q-hyponormal if there is a unique contraction K_T associated with T such that For bounded normal operators S and T, S+T and ST are normal operators if S and T commute; and for unbounded normal operators S and T with same domain, S+T is normal if S and T are doubly commuting [4]. The following discusses sum and product of deformed normal operators.

Theorem (A): ***Let S and T be q-normal operators with D(S) = D(T), $qK_TS = SK_T$, ST = TS and $qK_ST = TK_S$. Then S + T is a q-normal operator.***

Proof:
$(S+T)(S+T)^* = (S+T)(S^*+T^*) = SS^*+TS^*+ST^*+TT^* = qS^*S + \sqrt{q}\,TK_SS + \sqrt{q}\,SK_TT + qT^*T = qS^*S + \sqrt{q}\,qK_STS + \sqrt{q}\,qK_TST + qT^*T = qS^*S + \sqrt{q}\,qK_SST + \sqrt{q}\,qK_TTS + qT^*T = qS^*S + qS^*T + qT^*S + qT^*T = q(S+T)^*(S+T)$. Thus (S+T) is a q-normal operator. //

Theorem (B): ***Suppose q, r > 0; A is a bounded normal operators and T is a q-normal operator such that $rAT = TA$, $AK_T = K_TA$.***

Then AT is $\frac{q}{r^2}$-normal.

Proof:
Since T is closed, $A^*T = A^*T^{**} \subset (T^*A)^*$. Now $rAT^* = r\sqrt{q}\,AK_T T = r\sqrt{q}\,K_TAT = \sqrt{q}\,K_TTA = T^*A$, Since A is bounded operator, [5, Theorem 4.19] implies that $(AT^*)^* = T^{**}A^* = TA^*$. Hence $A^*T \subset (T^*A)^* = r(AT^*)^* = rTA^*$. Now $(AT)(AT)^* = ATT^*A^* = q\,AT^*TA^* = \frac{q}{r}T^*ATA^* \supset \frac{q}{r^2}T^*AA^*T = \frac{q}{r^2}T^*A^*AT = \frac{q}{r^2}(AT)^*(AT)$. Since $(AT)^*(AT)$ and $(AT)(AT)^*$ are self-adjoint, the equality holds. Hence $(AT)(AT)^* = \frac{q}{r^2}(AT)^*(AT)$. Thus (AT) is $\frac{q}{r^2}$-normal.

Here is a Fuglede - Putnam phenomenon for deformed operators. For q-normal operators S and T in H and a bounded operator A on H such that $AK_S = K_TA$ and $rAS \subset TA$ (r>0)., $rAS^* \subset T^*A$.

* Corresponding author – abp1908@yahoo.com

Indeed $rAS^* = r\sqrt{q}\, AK_S S = r\sqrt{q}\ K_T AS \subset \sqrt{q}\, K_T TA = T^*A$.

ACKNOWLEDGEMENT

This work is supported by UGC-SAP DRS Grants to Department of Mathematics, Sardar Patel University.

REFERENCES

[1] Ota, S. (2002) some classes of q-deformed operators. *J. Operator Theory*, **48:** 151-186.

[2] Ota, S. (2003) On q-deformed hyponormal operators. *Math. Nachr.*, **248-249**: 144-150.

[3] Ota, S. (2004) A note on q-deformed operators. *Studia. Math*. **165**: 295-301.

[4] Patel, A. B. (1983) A joint spectral theorem for unbounded normal operators. *J. Aust. Math. Soc*. Series A, **34**: 203-213.

[5] Weidman, J. (1980) *Linear operators in Hilbert spaces*, Springer, Berlin.

PRAJÑĀ - **Journal of Pure and Applied Sciences**
Vol. 17: 157 - 161, 2009 ISSN 0975 - 2595

TWO-PHOTON DECAY WIDTHS OF η_C, χ_{CO} AND χ_{C2} CHARMONIUM STATES USING COULUMB PLUS POWER POTENTIAL (CPP_ν)

Arpit Parmar, Bhavin Patel [1] and P. C. Vinodkumar [*]

Department of Physics, Sardar Patel University, Vallabh Vidyanagar, Gujarat – 388 120
[1]L. D. R. P. Institute of Technology & Research, Gandhinagar, Gujarat – 382 015

ABSTRACT

The present paper deals with the two-photon decay widths of the different charmonium states based on coulomb plus power form of the inter-quark potential (CPP_ν). The masses of the $c\bar{c}$ states and their radial wave functions obtained from the study of the charmonium spectroscopy are employed for the present calculations. The Schrödinger equation is solved numerically for different choices of the power index ν. The decay widths are found to be in accordance with the experimental values for the choices of the inter-quark potential index in the range $0.7 < \nu \leq 1.1$.

***Keywords*: decay widths, charmonium, potential model.**

INTRODUCTION

There is a renaissance in the hadron spectroscopy during the last few years as large number of charmed and beauty states are reported experimentally [1, 2, 3]. Bound states of heavy quarks - the heavy quarkonia are expected to provide physicists with ideal means to study the features of QCD.

With the recent new CLEO measurements [4, 5] of the two-photon decay rates of the even-parity, P-wave 0^{++} (χ_{c0}) and 2^{++} (χ_{c2}) states and with renewed interest in radiative decays of heavy quarkonium states, it seems appropriate to have another look at the two-photon decay of heavy quarkonium from the view point of theoretical attempts [6, 7]. In the traditional non-relativistic bound state calculation, the two-photon widths for the P-wave quarkonium state depend on the l^{th} derivatives of the spatial wave function at the origin extracted from potential models [8]. To have a prediction for the two-photon width of P-wave quarkonia, one need to express the decay amplitude in terms of the matrix element of a heavy quark field local operator computed in an essentially model-independent manner, such as QCD sum rules technique or lattice simulations. Though the physics of quarkonium decay seems to be better understood within the conventional framework of QCD [9], unlike the two-photon width of S-wave (η_c) which can be predicted from the corresponding J/ψ leptonic widths, there is no similar prediction for the P-wave χ_c states and all the existing theoretical values for the decay rates are based on potential model calculations [8-20]. With similar determinations of other quarkonium decay constants, one would be able to study QCD radiative corrections and can estimate the strong coupling constant, α_s.

* Corresponding author – pc_vinodkumar@spu.edu

Two-Photon Decay Width of Charmonium States

In the traditional non-relativistic bound state calculation, the two-photon widths for the scalar quarkonium state depend on the behavior of the radial wave function at the origin. The width of $\eta_c \to \gamma\gamma$ has been observed to be 6-7 keV, comparable to the quark model predictions [5, 19, 21]. Two photon widths of orbitally excited charmonium states ($\chi_{cJ=0,2} \to \gamma\gamma$) are suppressed by the mass of the charm quark. Theoretical ratio of P-wave (L=1) $\gamma\gamma$ width of 15/4 in the large quark mass limit is found to differ by experimental observation [5] which indicates significant contribution from QCD radiative correction. The two-photon decay width of the pseudoscalar S-wave meson is represented using the Van-Royen-Weiss kopf formula at the finite quark-antiquark separation as [22, 23, 24, 25].

$$\Gamma_{\gamma\gamma}(\eta_c) = \frac{12 Q_e^{\,2} \alpha_{em}^{\,2}}{M_{\eta c}^2} |R_0(0)|^2 \left[1 - \frac{\alpha_s}{\pi}\frac{(20-\pi^2)}{3}\right] \quad (1)$$

The two-photon decay of the spin one state χ_{c1} is forbidden by the Landau-Yang theorem [26, 27]. With the one-loop QCD radiative corrections, the

decays of $^3P_0$ and $^3P_2$ states into two photons are given by [8, 24, 28, 29],

$$\Gamma_{\gamma\gamma}(\chi_{c0}) = \frac{27Q_e^{\,2}\alpha_{em}^{\,2}}{(M_c+b)^4} \mid R_1^{'}(0) \mid^2 [1+B_0(\alpha_s/\pi)] \tag{2}$$

$$\Gamma_{\gamma\gamma}(\chi_{c2}) = \frac{36Q_e^{\,2}\alpha_{em}^{\,2}}{5M_c^{\,4}} \mid R_1^{'}(0) \mid^2 [1+B_2(\alpha_s/\pi)] \tag{3}$$

where $B_0 = \pi^2/3 - 28/9$ and $B_2 = 16/3$ are the next to leading order (NLO) QCD radiative corrections as given by [25,30,31].

The value of the radial wave functions $\mid R^{(l)}_{c\bar{c}}(0) \mid^2$ of Eqn. (1-3) can be obtained from the potential model description of the $c\bar{c}$ bound states.

Columb Plus Power Potential (CPP_ν)

For the description of the charmonium bound states, we adopt the coulomb plus power potential (CPP_ν) expressed in terms of vector plus scalar part given by

$$V(r) = -\frac{4}{3}\frac{\alpha_s}{r} + Ar^\nu \tag{4}$$

Here the first term is the vector (Coulomb) part and second term denotes the scalar (or confinement) part. The first term dominates at the small distances and the second term dominates at the large distances. The α_s denotes the strong running coupling constant and A denotes the confinement strength of the potential. The choice of ν corresponds to different type of potential models. For example, ν=1 represents coulomb plus linear potential. This potential has been extensively employed for the study of hadron spectroscopy containing heavy flavour quark [22, 23].

The spectroscopic parameters obtained for the different choices of the potential index ν, including the predicted masses and the resultant radial wave functions are being used here to compute the decay rates. We consider the conventional nonrelativistic formalism for computations of these decay properties. As considered by many authors [22, 23, 32, 33, 34], the contribution from the radiative corrections to these decays is also incorporated in the present study.

Numerical Calculation

The numerical values of the radial wave functions are obtained from the mathematica notebook of the Runge Kutta method [24, 35]. The analytical form for the same is more desirable as we need to find the derivatives (l^{th} derivatives) of the orbitally excited wave functions at the origin. We have employed an orthogonal function that fits the numerical solutions of the radial wave function to a more general form given by

$$R_{nl}(r) = \left(\frac{pn!}{\alpha^{\frac{2lp-(2l+3)}{p}}(n+k)!} \right)^{\frac{1}{2}} (\alpha r)^l e^{\frac{\alpha r^p}{2}} L_n^k(\alpha r^p) \tag{5}$$

Where, $k = \frac{2l+3}{p} - 1$. Here, α and p are the wave function parameters that are obtained by fitting the numerical data to the expression given by Eqn. (5), and are listed in Table 1. The different values of p denote different forms of the wave function. In this case the wave function parameter p varies from p=1 to p=2, i.e. wave function changes from hydrogenic type to harmonic as the potential index ν varies from 0.1 to 2.0. Also $L_n^k(\alpha r^p)$ is the Laguerre polynomial which makes the wave function orthogonalised for the higher excited states.

Table 1: Fitted wave function parameters for the different choices of ν.

	1S		1P	
ν	α	p	α	p
0.1	0.58469	1.115	0.312	1.196
0.3	0.64632	1.220	0.386	1.317
0.5	0.68525	1.290	0.429	1.406
0.7	0.70765	1.350	0.466	1.470
0.8	0.72026	1.370	0.488	1.488
0.9	0.72646	1.395	0.498	1.519
1.0	0.73042	1.420	0.512	1.541
1.1	0.73580	1.440	0.522	1.565
1.3	0.74498	1.475	0.539	1.610
1.5	0.74915	1.510	0.550	1.655
1.7	0.74977	1.545	0.562	1.691
1.9	0.75064	1.575	0.569	1.730
2.0	0.75021	1.590	0.570	1.750

Here, the charm quark mass parameter $m_c = 1.28 GeV/c^2$ and the potential parameters are the same as used in the $c\bar{c}$ spectroscopy [22, 23, 24]. Accordingly, the resultant masses of the $c\bar{c}\left({}^{2s+1}L_J\right)$ states are listed in Table 2. The calculated value of the two-photon decay width for the χ_{co}, χ_{c1} and η_c states with respect to different potential index ν are given in Table 3.

Table 2: Potential strength and Mass spectra of charmonium system in GeV.

ν	A	$M_{\eta c}$	$M_{\chi c0}$	$M_{\chi c2}$
0.1	0.4967	3.045	3.167	3.174
0.5	0.3282	3.008	3.324	3.357
0.7	0.2745	2.994	3.386	3.430
0.8	0.2519	2.987	3.414	3.464
0.9	0.2315	2.981	3.441	3.495
1.0	0.2130	2.976	3.466	3.524
1.1	0.1962	2.971	3.489	3.552
1.3	0.1668	2.962	3.532	3.602
1.5	0.1420	2.955	3.570	3.647
2.0	0.0953	2.940	3.647	3.737
Expt. [5]		2.980	3.415	3.556

Table 3: Two-photon decay widths for different charmonium states in keV.

CPPν	$\Gamma_{\gamma\gamma}(\chi_{c0})$	$\Gamma_{\gamma\gamma}(\chi_{c2})$	$\Gamma_{\gamma\gamma}(\eta_c)$
ν = 0.1	0.07	0.01	1.92
0.5	0.96	0.13	5.05
0.7	1.7	0.23	6.26
0.8	2.12	0.29	6.79
0.9	2.55	0.35	7.28
1.0	3.00	0.41	7.73
1.1	3.45	0.48	8.14
1.3	4.38	0.6	8.88
1.5	5.29	0.73	9.50
2.0	7.42	1.02	10.70
Barbieri [8]	3.5	0.93	-
Godfrey [18]	1.29	0.46	-
Barnes [20]	1.56	0.56	-
Bodwin [10]	6.7	0.82	-
Gupta [11]	6.38	0.57	-
Munz [12]	1.39	0.44	-
Huang [13]	3.72	0.49	-
Ebert [8]	2.9	0.5	-
Schuler [14]	2.5	0.28	-
Crater [15]	3.34	0.43	-
Wang [16]	3.78	-	-
Laverty [17]	1.99	0.3	-
Expt. [5]	2.397	0.493	6.41
Ebert [19]	-	-	4.33

RESULTS AND DISCUSSION

Two-photon decay widths for the χ_{c0}, χ_{c2} and η_c states are calculated and the results are shown in Table 2 along with other theoretical model predictions and with the PDG average value reported by different experimental groups [5, 8, 10-20]. The observed trend lines against the interquark potential index ν are shown in the Figs. 1 to 3. From the presently obtained results, it is observed that the values of two-photon decay width of the charmonium states matches with the experimental values at around ν ≈0.7 for η_c states, ν ≈0.9 for χ_{co} state and at ν ≈1.1 for χ_{c2} state. The shifting of the interquark potential index ν from 0.7 to 1.1 for the excited charmonium states indicate the behavior of quark-antiquark interaction as expected from QCD.

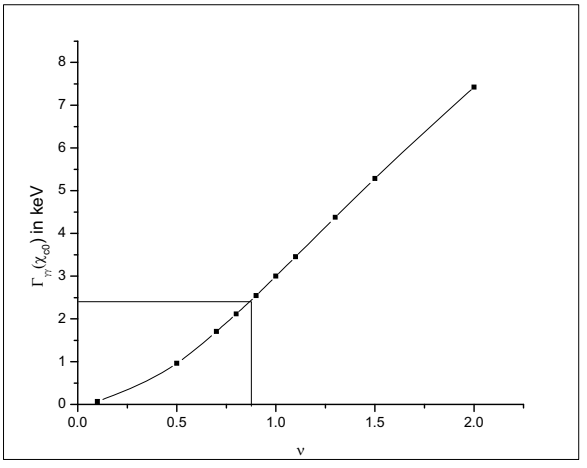

Figure 1: Two photon decay width for χ_{c0} state

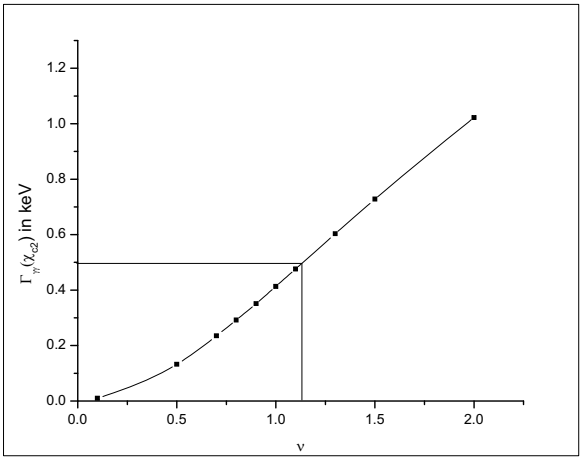

Figure 2: Two photon decay width for χ_{c2} state.

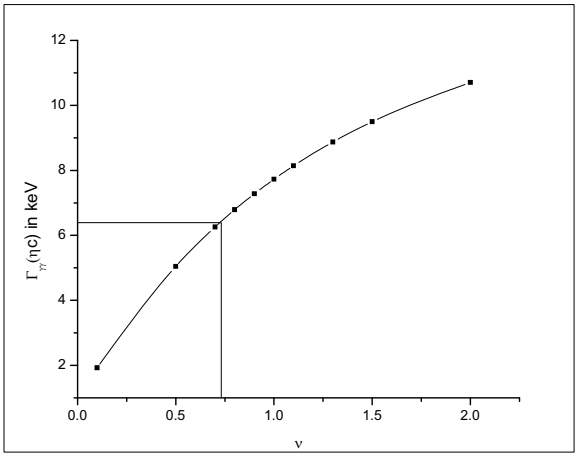

Figure 3: Two photon decay width for η_c state.

REFERENCES

[1] Aubert J J et al., (1974), "Experimental Observation of a Heavy Particle J" *Phys. Rev. Lett.* **33:** 1404.

[2] Wolfgang Lucha, F. F. Schoberl, "Solving the Schroedinger equation for bound states with Mathematica 3.0", *Int.J.Mod.Phys. C* **10** (1999) 607.

[3] Choi S K et al., "Observation of a Narrow Charmoniumlike State in Exclusive B±→K±π+π-J/ψ Decays", *Phys. Rev. Lett.* **91:** 262001.

[4] Ecklund K M, "Two-Photon Widths of the chi_cJ States of Charmonium", *Phys. Rev. D* **78**: 091501, (2008) and other recent results quoted therein.

[5] Amsler C et. Al., "Particle Data Group", *Phys. Lett.* **667**: 1 (2008).

[6] Lansberg J P and Pham T N, "J/psi, psi' and Upsilon Production at Hadron Colliders: a review", *Int.J.Mod.Phys.A* **21**:3857, (2006).

[7] Lansberg J P and Pham T N, "Two-photon width of ηb, ηb′ and ηb″ from heavy-quark spin symmetry", *Phys. Rev. D* **75**: 017501 (2007).

[8] Barbieri R, and kogerler R, "Calculation of the annihilation rate of P wave quark-antiquark bound states ", *Phys. OLett.* **60**: 183 (1976).

[9] Brambilla N et al (2005), Heavy quarkonium physics, CERN Yellow Report, CERN-2005- 005, Geneva : CERN, 487 pp arXiv:hep-ph/0412158

[10] Bodwin G et al., "Rigorous QCD predictions for decays of P-wave quarkonia" *Phys. Rev. D* **46**: R1914 (1992).

[11] Gupta S N and Johnson J M(1996) "Relativistic two-photon and two-gluon decay rates of heavy quarkonia" *Phys. Rev. D* **54**: 2075.

[12] Munz C R, (1996) "Two-photon decays of mesons in a relativistic quark model" *Nucl. Phys. A* 609 364.

[13] Huang H N and Ta-chao (1996), "QCD predictions for annihilation decays of P-wave quarkonia to next-to-leading order in αs" Phys. Rev. D 54: 6850.

[14] Schuler G A et al (1998), "Meson-photon transition form factors and resonance cross-sections in e+e− collisions" Nucl. Phys. B 523, 423.

[15] Crater H W, Won C Y and Alstine P V (2006), "Tests of two-body Dirac equation wave functions in the decays of quarkonium and positronium into two photons" Phys. Rev. D 74:054028.

[16] Wang G-Li (2007), "Annihilation Rate of Heavy 0^{++} P-wave Quarkonium in Relativistic Salpeter Method" Phys.Lett.B 653:206,.

[17] James T. Laverty, Stanley F. Radford, Wayne W. Repko, "\ga\ga and g g decay rates for equal mass heavy quarkonia", arXiv:0901.3917v3 [hep-ph].

[18] S Godfrey and N Isgur, "Mesons in a relativized quark model with chromodynamics", *Phys. Rev. D* **32**: 189 (1985).

[19] D Ebert , R N Faustov and V O Galkin, "Properties of heavy quarkonia and Bc mesons in the relativistic quark model",

Phys. Rev. D **67**: 014027 and references therein;

[20] Barnes T, Proceedings of IX InternationalWorkshop on Photon-Photon Collisions, edited by D. O. Caldwell and H.P.Paar(World Scientific, Singapore, p. 263 (1992).

[21] Zou B S and Chiang H C (2003), "One-pion-exchange final-state interaction and the pp□ near threshold enhancement in J/ψ→γpp□ decays", Phys. Rev. D 69: 034004.

[22] Rai A K, Pandya J N and Vinodkumar P C (2005), "Decay rates of quarkonia and potential models**"** *J. Phys. G.* **31:** 1453.

[23] A K Rai, J N Pandya and P C Vinodkumar (2008), "Decay Rates of Quarkonia with NRQCD Formalism Using Spectroscopic Parameters of Potential Models", *Eur. Phs. J.* **4:** 77.

[24] Bhavin Patel (2009), "Spectroscopy and decay properties of heavy flavor hadrons" Ph.D. Thesis, Sardar Patel University.

[25] Kwong W, Paul B, Mackenzie R R and Jonathan L R (1988), "Quarkonium annihilation rates", *Phys. Rev. D* **37:** 3210.

[26] Landau L *Phys. Abstracts* **52:** 125 (1950).

[27] Yang C N (1950)., "Selection Rules for the Dematerialization of a Particle into Two Photons", *Phys. Rev.* **77:** 2425.

[28] Huang H W and Kuang-Ta C (1996). "QCD predictions for annihilation decays of P-wave quarkonia to next-to-leading order in αs", *Phys. Rev. D* **54:** 6850

[29] Petrelli A, Cacciari M, Greco M, Maltoni F and Mangano M L (1998), "NLO production and decay of quarkonium" *Nucl. Phys. B*, **514:** 245.

[30] Barbieri R, Caffo M, Gatto R and Reiddi E (1981), "QCD corrections to P wave quarkonium decays" *Nucl. Phys.* **B** 192: 61.

[31] Mangano M. and Petrelli A., "An update on χc decays: perturbative QCD versus data" Phys. Lett. B 352: 445 (1995).

[32] Ebert D, Faustov R N and Galkin V O (2003), "Properties of heavy quarkonia and Bc mesons in the relativistic quark model" *Phys. Rev. D* **67:** 014027.

[33] Ebert D, Faustov R N and Galkin V (2003)., "Two-photon decay rates of heavy quarkonia in the relativistic quark model" *Mod. Phys. Lett. A* **18:** 601

[34] Kim C S, Lee T and Wang G L (2005), "Annihilation rate of heavy 0−+ quarkonium in relativistic Salpeter method" *Phys. Lett. B* **606:** 323.

[35] Lucha W and Schoberl F, "Solving the Schroedinger equation for bound states with Mathematica 3.0", arXiv: hep-ph/9811453.

PRAJÑĀ - **Journal of Pure and Applied Sciences**
Vol. 17: 162 - 169, 2009 ISSN 0975 - 2595

CALCULATIONS OF IONIZATION CROSS SECTIONS FOR ALKALI METAL ATOMS (Li, Na, K) AND HALOGEN ATOMS (F, Cl, Br, I) FROM THRESHOLD TO 2 kEV ON ELECTRON IMPACT

Harshad Bhutadia [*], Rucha Dave [1], Kirti Korot [2] and Minaxi Vinodkumar

V. P. & R. P. T. P. Science College, Vallabh Vidyanagar, Gujarat – 388 120
[1]Anand agricultural university, Anand, Gujarat - 388110
[2]Faculty of Engneering &Technology, CHARUSAT, Changa, Gujarat – 388 421

ABSTRACT

In this article we report calculations of the total ionization cross sections, Q_{ion}, for the alkali metal atoms (Li, Na, K) and also for halogen atoms (F, Cl, Br, I) upon electron impact for energies from circa threshold to 2 keV. We have employed the well-known spherical complex optical potential (SCOP) formalism, which provides total elastic cross section, Q_{el}, and its inelastic counterpart Q_{inel}. Q_{inel} includes Q_{ion} and we have used a semi-empirical method, called Complex Scattering Potential – ionization contribution (CSP-ic) to extract ionization cross sections, Q_{ion}, from the calculated total inelastic cross-sections, Q_{inel}. CSP-ic method has been employed for many systems (atomic, molecular, radicals etc) since decade and has been found very successful. Present calculations also provide information on the total excitation cross sections, ΣQ_{exc}, obtained as a byproduct of this calculation. The calculated cross sections are examined as functions of incident electron energy and are compared with available data and overall agreement is observed.

***Keywords*: spherical complex optical potential (SCOP), Complex Scattering Potential – ionization contribution (CSP-ic), total inelastic cross-sections, Q_{inel}, total ionization cross sections, Q_{ion}.**

INTRODUCTION

The alkali metals are highly reactive and as a consequence they are never found in elemental form in nature. Alkali atoms, having the electronic configuration of noble gas atoms with an *s*-electron added, are targets with very high polarizability [1]. Further, they have the lowest ionization potentials in their respective periods, as removing the single electron from the outermost shell give them the stable inert gas configuration. The low ionization potentials of the alkali metals make them useful candidate as sources of quiescent plasmas; their higher electrical polarizabilities result in large elastic, inelastic, ionization and reactive cross sections, ideal for many applications [2]. Moreover it is expected that electron atom scattering studies should provide a common meeting ground for experiment and theory as alkali metal atom-beams are relatively easy to produce and detect, and for theoreticians they are effectively one electron system. Due to the cited properties, alkali metals are of obvious interest for both theoreticians and experimentalists [3, 4].

The Halogen atoms are of particular importance in plasma processing technologies used by the microelectronics industry for etching of semiconductors and metals. The availability of cross section for halogen atoms also provides the opportunity for direct comparisons with those of rare gases, the neighboring group of the periodic table. Such comparison should help us to refine our ability to estimate unmeasured cross sections for other atoms [5].

Ionization, as an important inelastic channel at intermediate and high energies play important role in plasma-processing, aeronomy and in biological systems and other environmental sciences. Moreover, in order to develop understanding of the basic chemical behavior of above listed Alkali atoms (Li, Na, K) and Halogen atoms (F, Cl, Br, I), the data regarding to the total ionization cross-sections would prove crucial and therefore such study has attracted many theoreticians and experimentalists in last few decades. Here we are interested in the intermediate and high-energy region (from ionization threshold up to 2 keV) where almost all inelastic channels (electronic excitation, ionization etc) are open.

Apart for having strong applied interest of these atoms there is paucity of theoretical data. For

* Corresponding author – harshad_physics@yahoo.co.in

Lithium and Potassium, Q_{ion} is calculated by McFarland [6] by using classical theory and for Sodium, Q_{ion} is calculated by Haung *et al* [9] with the help of Binary-Encounter-Bethe (BEB) model. For all the three alkali metal atoms the experimental investigations are done by McFarland and Kinney [7] using modulated cross beam technique and also by Brink [8] using cross beam technique.

For all halogen atoms, total ionization cross sections is calculated by Margreiter *et al* [9] using Deutsch-Mark (DM) formalism and by Joshipura and Limbachiya [10] using complex scattering potential- ionization contribution (CSP-ic) method [11-16] and for Bromine and Iodine theoretical ionization cross sections are also reported by Ali and Kim [17] using BEB method. W. Huo [18] has calculated total ionization cross sections for Cl, Br and I using siBED method from threshold to 10 keV. The measured total ionization cross sections are reported by Hayes *et al* [5] by fast neutral atom beam method for all the halogen atoms.

THEORETICAL METHODOLOGY

We briefly describe the theoretical methodology employed here to determine various total cross sections for the impact of electrons on the targets studied. However, a more detailed description can be found in our earlier papers [11-16] and references therein. Our aim in this paper is to calculate Q_{ion} for the alkali and halogen atoms. The reason for choosing these targets is the difference in their electron configuration which results into many important properties and we wish to see how these properties have impact on the total ionization cross sections. Towards this goal, we have employed the well-known spherical complex optical potential (SCOP) formalism, through which the total elastic cross sections Q_{el} and its inelastic counterpart, Q_{inel} are obtained such that,

$$Q_T(E_i) = Q_{el}(E_i) + Q_{inel}(E_i) \qquad (1)$$

Present calculation for the TCS, vide equation (1) is based on a complex scattering potential, generated from electron charge density of the target which is derived from the wave functions of Bunge *et al* [19]. The key ingredient for all the interaction potentials is the charge density of the target. The complex potential, $V(E_i, r)$, thus constructed consists of real and imaginary parts, and is given by,

$$V(E_i, r) = V_R(E_i, r) + iV_I(E_i, r) \qquad (2)$$

Where the real part V_R comprises of static potential (V_{st}), exchange potential (V_{ex}), and polarization potential (V_p), expressed as follows,

$$V_R(E_i, r) = V_{st}(r) + V_{ex}(E_i, r) + V_P(E_i, r) \qquad (3)$$

For the exchange potential, we have used Hara's 'free electron gas exchange model' [20]. And for the polarization potential V_p, we have used parameter free model of correlation - polarization potential given by Zhang *et al* [21]. The present polarization model contains non-adiabatic corrections in the intermediate region and it smoothly approaches the correct asymptotic form at large 'r'. The imaginary part V_I in equation (2), also called the absorption potential V_{abs}, accounts for the total loss of scattered flux into all the allowed inelastic channels. For $V_{abs,}$ we have used the model potential given by Staszeweska *et al* [22], which is a non-empirical, quasifree, Pauli-blocking, dynamic potential. The form of the potential is given as

$$V_{abs}(r, E_i) = -\rho(r)\sqrt{\frac{T_{loc}}{2}} \cdot \left(\frac{8\pi}{10k_F^3 E_i}\right) \cdot \theta(p^2 - k_F^2 - 2\Delta) \cdot (A_1 + A_2 + A_3) \qquad (4)$$

The local kinetic energy of the incident electron is given by

$$T_{loc} = E_i - (V_{st} + V_{ex}) \qquad (5)$$

In equation (4), $p^2 = 2E_i$, $k_F = [3\pi^2 \rho(r)]^{1/3}$ is the Fermi wave vector and Δ is an energy parameter. Further $\theta(x)$ is the Heaviside unit step-function, such that $\theta(x) = 1$ for $x \geq 0$, and is zero otherwise. The dynamic functions A_1, A_2 and A_3 occurring in the equation (4) depend differently on $\rho(r)$, I, Δ and E_i. The energy parameter Δ determines a threshold below which $V_{abs} = 0$, and the ionization or excitation is prevented energetically. We have modified the original model, by considering Δ as a slowly varying function of E_i around I. Briefly, a preliminary calculation is done with a fixed value $\Delta = I$, but Δ as a variable accounts for the screening of the absorption potential in the target charge-cloud region. Further this is meaningful

since Δ fixed at I would not allow excitation at incident energy $E_i \leq I$. On the other hand, if parameter Δ is much less than the ionization threshold, then V_{abs} becomes unexpectedly high near the peak position. After generating the full complex potential given in equation (2) for a given electron - atom system, we solve the Schrödinger equation numerically and use partial wave analysis to get complex phase shifts which are employed to find the relevant cross sections.

The total inelastic cross sections, Q_{inel}, cannot be measured directly in experiment; however it can be estimated by subtracting total integral elastic cross section from the measured grand total cross sections. The measurable quantity of applied interest is the total ionization cross section, Q_{ion}, which is an important constituent of Q_{inel}. Accordingly Q_{inel} can be partitioned into discrete and continuum contributions, viz,

$$Q_{inel}(E_i) = \sum Q_{exc}(E_i) + Q_{ion}(E_i) \qquad (6)$$

Where the first term is the sum over total excitation cross sections for all accessible electronic transitions, the second term is the total cross section of all allowed ionization processes induced by the incident electrons. The first term in equation (6) arises mainly from the low-lying dipole allowed transitions.

$$Q_{inel}(E_i) \geq Q_{ion}(E_i) \qquad (7)$$

Q_{ion} cannot be rigorously derived from Q_{inel} but may be estimated by defining the energy dependent ratio of cross sections,

$$R(E_i) = \frac{Q_{ion}(E_i)}{Q_{inel}(E_i)} \qquad (8)$$

We require R=0 when $E_i \leq I$. For a number of stable atoms and molecules like Ne, O_2, CH_4, SiH_4 etc., for which the experimental cross sections, Q_{ion} are known accurately [23, 24] the ratio R rises steadily as the energy increases above the threshold, and approaches unity at high energies. Thus,

$$R(E_i)\begin{cases} = 0 \ for \ E_i \leq I \\ = R_p \ for \ E_i = E_p \\ \cong 1 \ for \ E_i > E_p \end{cases} \qquad (9)$$

Where 'E_p' stands for the incident energy at which the calculated Q_{inel} attains its maximum value. R_p is the value of R at E_i=E_p. The general observation is that, at energies close to peak of ionization, the contribution of Q_{ion} is about 70–80% of the total inelastic cross sections Q_{inel}. This behavior is attributed to the faster fall of the first term $\sum Q_{exc}$ in equation (6). Therefore we may choose $R_p \approx 0.7$. For calculating the Q_{ion} from Q_{inel} we need R as a continuous function of energy for $E_i > I$; hence we represent the ratio R in the following manner,

$$R(E_i) = 1 - f(U) \qquad (10)$$

Presently the above ratio has been determined using the following analytical form [13-18].

$$R(E_i) = 1 - C_1\left(\frac{C_2}{U+a} + \frac{\ln(U)}{U}\right) \qquad (11)$$

Where, U is the dimensionless variable defined by, $U = \frac{E_i}{I}$

The reason for adopting a particular functional form of $f(U)$ in equation (12) is the following. As E_i increases above I, the ratio R increases and approaches 1, since the ionization contribution rises and the discrete excitation term in equation (6) decreases. The discrete excitation cross sections, dominated by dipole transitions, fall off as ln(U)/U at high energies. Accordingly the decrease of the function $f(U)$ must also be proportional to ln(U)/U in the high range of energy. However, the two-term representation of $f(U)$ given in equation (12) is more appropriate since the first term in the brackets ensures a better energy dependence at low and intermediate E_i. The dimensionless parameters C_1, C_2, and a, involved in equation (12) reflect the properties of the target under investigation. The three conditions stated in equation (9) are used to determine these three parameters. Details are given in our recent publications.

Table 1: Total ionization cross sections for Li, Na, K, F, Cl, Br and I in Å^2

	Q_{ion}						
$E_i(eV)$	Li	Na	K	F	Cl	Br	I
6	8.00	0.82	1.92	---	---	---	---
8	**13.13**	4.04	5.50	---	---	---	---
10	10.63	6.08	7.33	---	---	---	---
15	7.35	**6.85**	8.82	---	0.23	0.41	1.84
20	6.01	6.72	**8.95**	0.02	1.09	1.62	4.08
25	5.44	6.38	8.72	0.11	1.91	2.76	5.37
30	4.78	6.01	8.38	0.23	2.53	3.62	5.86
40	4.19	5.37	7.64	0.46	3.27	4.56	6.16
50	3.84	4.86	6.94	0.63	3.61	4.92	**6.23**
60	3.53	4.46	6.26	0.76	3.75	**4.97**	6.10
70	3.32	4.13	5.80	0.85	3.83	4.90	5.91
80	2.93	3.86	5.29	0.91	3.87	4.87	5.72
90	2.74	3.62	4.84	0.96	**3.88**	4.76	5.52
100	2.52	3.42	4.48	0.99	3.87	4.62	5.35
150	1.89	2.68	3.56	**1.03**	3.60	4.00	4.64
200	1.42	2.21	3.00	1.01	3.26	3.56	4.14
300	1.01	1.59	2.41	0.91	2.71	3.03	3.47
400	0.75	1.17	2.03	0.80	2.31	2.66	3.03
500	0.60	0.99	1.82	0.70	2.02	2.39	2.70
600	0.56	0.91	1.65	0.63	1.79	2.17	2.50
700	0.51	0.84	1.52	0.58	1.61	1.99	2.31
800	0.45	0.80	1.41	0.53	1.46	1.84	2.14
900	0.40	0.75	1.36	0.49	1.34	1.71	1.99
1000	0.40	0.71	1.30	0.45	1.23	1.61	1.87
2000	0.35	0.56	0.96	0.26	0.69	0.99	1.46

RESULTS AND DISCUSSION

The theoretical approach of SCOP along with our CSP-ic method discussed is employed to determine Q_{ion} along with a useful estimate on electronic excitations in terms of the summed cross section, $\sum Q_{exc}$. The present results for the total ionization cross sections atoms (Li, Na, K, F, Cl, Br, I) are plotted in Figures 1-7and the sample results are also tabulated in Table 1. Total ionization cross sections are calculated using the CSP-ic method discussed in the earlier section. Figure 1 compares the present total ionization cross section for e – Li scattering with available data. The present results are in accord with theoretical values of McFarland [6] for entire energies except near the peak they are slightly lower. The experimental results of McFarland and Kinney (with 8 % experimental uncertainty) [7] and Brink (with 20% experimental uncertainty)[8] are also in accord with present data for the entire incident energy range.

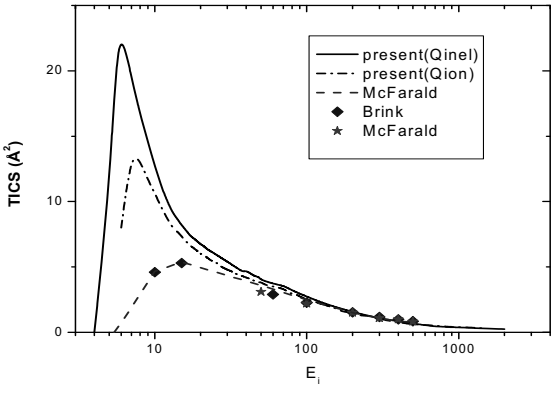

Figure 1: Total ionization cross sections for e – Li scattering in Å^2.
Solid line, Present Q_{inel}; Dash dot line, Present Q_{ion}; Dashed line, McFarland [6]; Stars, McFarland and Kinney [7]; Squares, Brink [8].

Now here in lithium ionization cross section we can see that the excitation cross section is very large compared with ionization cross section at low energy because in the case of lithium 2s→2p dipole allowed transition is strong. In other atoms, at energies close to peak of ionization, the contribution of Q_{ion} is about 70–80% of the total inelastic cross sections Q_{inel} but in the case of lithium it is not so, the contribution of Q_{ion} is much less than 70–80%. This behavior is attributed to the slower fall of the first term $\sum Q_{exc}$ in equation (6). Therefore we choose $R_p \approx 0.35$.

In all the alkali atoms electron impact excitation is quite strong compared to ionization. Figure 2 shows the total ionization cross sections for electron impact on Na with available comparisons. They are compared with theoretical data of McFarland [6] and experimental data of [7, 8]. The present results are in accord with theoretical values of Hwang *et al* [9] near the ionization threshold but beyond 5 eV they are quite low compared to all reported values. The experimental results of McFarland and Kinney [7] and Brink [8] are also accord with present data for entire energy range.

In Figure 3 we compare the total ionization cross section for e – K scattering with available data. The theoretical results of McFarland [6] are in good agreement with the present results for entire energies except near peak they are lower. The experimental results of McFarland and Kinney [7] and Brink [8] are in overall good accord with present data for entire energy range except peak region.

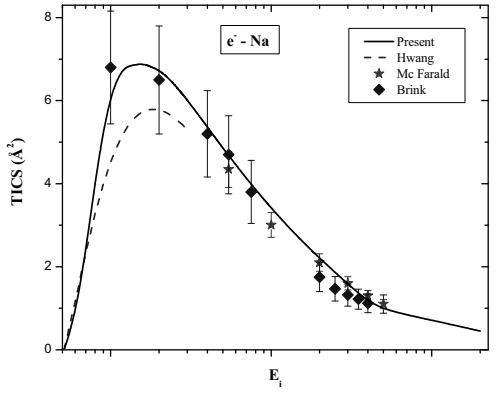

Figure 2: Total ionization cross sections for e – Na scattering in Å^{o2}. Solid line, Present Q_{ion}; Dashed line, Hwang *et al* [9]; Stars, McFarland and Kinney [7]; Squares, Brink [8].

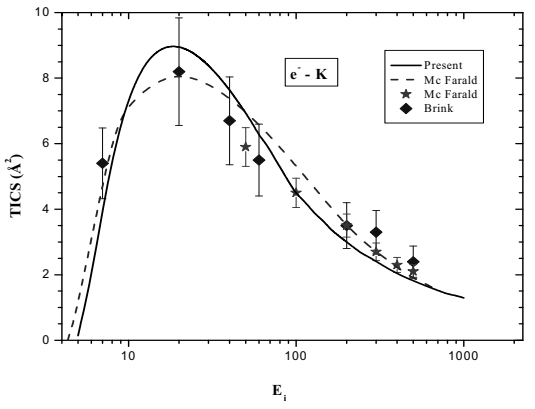

Figure 3: Total ionization cross sections for e – K scattering in Å^{o2}. Solid line, Present Q_{ion}; Dashed line, McFarald [6]; Stars, McFarland and Kinney [7]; Squares, Brink [8].

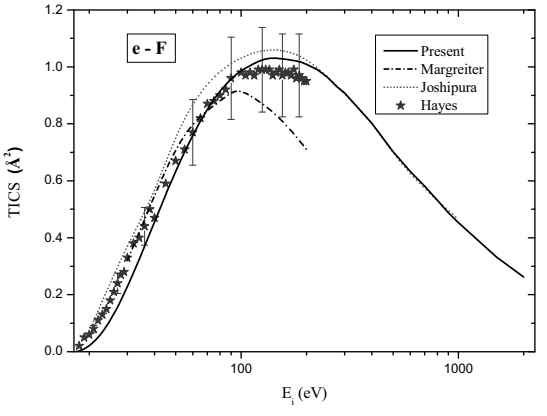

Figure 4: Total ionization cross sections for e – F scattering in Å^{o2}. Solid line, Present Q_{ion}; Short Dash Dot, Margreiter *et al* [10]; Short Dot, Joshipura and Limbachiya [26]; Stars, Hayes *et al* [5]

In halogen atoms the peak ratio is close to 70%. In Figure 4 we compare the total ionization cross section for e – F scattering. Here the theoretical results are due to Margreiter et al [9] and Joshipura and Limbachiya [10]. There is overall good agreement between all the theoretical data below 100 eV above which the data of Margreiter et al [9] are quite low compared to remaining data. The theoretical results of Joshipura and Limbachiya [10] are higher compared to the present results at low energies but they merge with the present results beyond the peak. The difference in the results is attributed to the fact that the present dynamic ratio R (E_i) is represented in different form. The experimental data of Hayes *et al* [5] are in good accord with the present results throughout the range of incident energy reported by them.

In Figure 5 we have shown the total ionization cross section for e – Cl scattering with available theoretical [9,10 18] and experimental investigations of Hayes et al [5]. The present results compare very well with all available data below 40 eV. Above 40 eV present results are higher compared to theoretical data of Margreiter et al [9] and Joshipura and Limbachiya [10] and also experimental data of Hayes et al [5]. However, the present data are within experimental uncertainty [5]. The present data matches very well with the calculated ionization cross sections of Huo et al [18] throughout the range of incident energy.

Figure 6 shows comparison for the ionization cross sections for e – Br scattering. Present data has overall good agreement with all theoretical results [9,10,17,18] and also with experimental measurements of Hayes at al [5] except at the peak where they are slightly higher. But still present data is within the error bar of the experimental data.

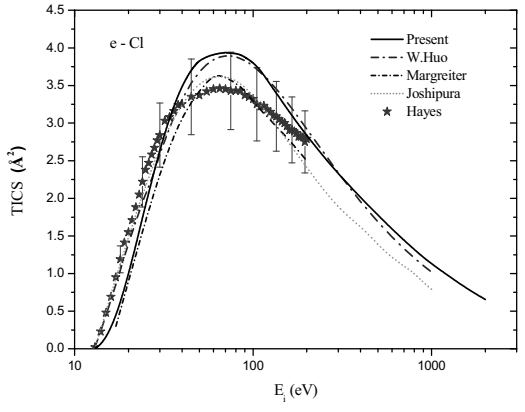

Figure 5: Total ionization cross sections for e – Cl scattering in Å°Å². Solid line, Present Q_{ion}; Dashed Dot line, W. Huo [18]; Short Dash Dot, Margreiter *et al* [9]; Short Dot, Joshipura and Limbachiya [10]; Stars, Hayes *et al* [5].

Figure 7 shows comparison for the total ionization cross sections for e – I scattering. The theoretical data are reported by [9,10,17,18] while the experimental investigation is done by Hayes et al [5]. Present results are in very good accord with theoretical data of Joshipura and Limbachiya [10] and Margreiter et al [9] throughout the range reported by them. Theoretical data of Huo et al [18] are shifted to the right compared to all reported values below 50 eV above which they are in good agreement with present results. The theoretical values of Ali et al [17] are in very good accord with present data till 80 eV beyond which they are lower compared to all reported data. Experimental data of Hayes et al (with 14% experimental uncertainty) [5] are in excellent agreement with present data throughout the energy reported by them.

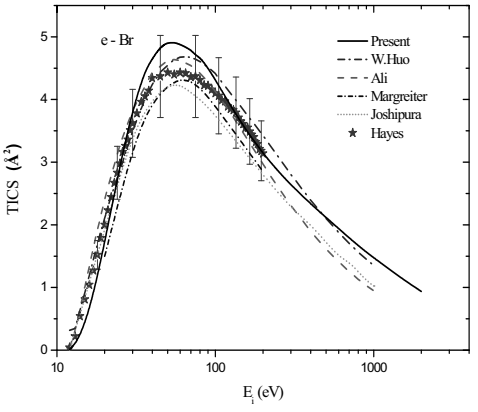

Figure 6: Total ionization cross sections for e – Br scattering in Å°². Solid line, Present Q_{ion}; Dashed Dot line, Huo [18]; Dashed line, Ali and Kim [17]; Short dashed dot line, Margreiter *et al* [9]; Short Dot, Joshipura and Limbachiya [10]; Stars, Hayes *et al* [5].

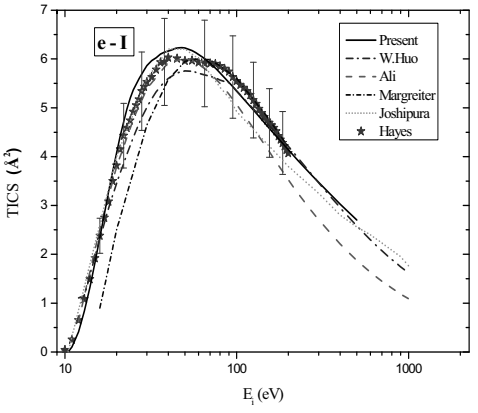

Figure 7: Total ionization cross sections for e – I scattering in Å°². Solid line, Present Q_{ion}; Dashed Dot line, Huo [18]; Dashed line, Ali and Kim [17]; Short dashed dot line, Margreiter *et al* [9]; Short Dot, Joshipura and Limbachiya [10]; Stars, Hayes *et al* [5].

Finally in Figure 8 we have made mutual comparison of present results of total ionization cross sections for all atoms studied in this paper. The two sets of atoms can be easily distinguished from the ionization curves itself. The alkali metal atoms having very low ionization threshold have very high ionization cross sections compared to all Halogen atoms. The highest cross section is about 8.95 **Å²** at 20 eV for Alkali metals while for Halogen atoms it is 6.23 **Å** at 60 eV**.** The other

important conclusion is that the cross section increases with increase in geometric size of the atom within the same group. At high energies all the curves tend to merge reflecting the fact that interaction time reduces as incident energy increases and as a result the cross sections also reduces.

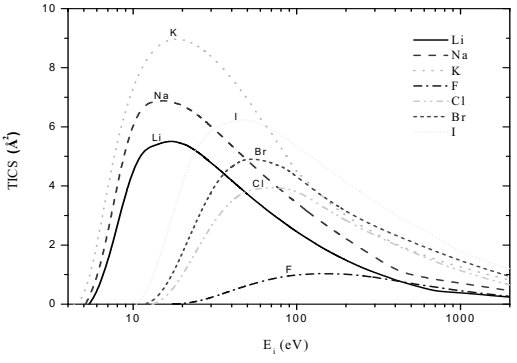

Figure 8: Comparisons of total ionization cross sections of present data in Å^{o2}. Solid line, **Li**; Dashed line, **Na**; Dot line, **K**; Dash dot line, **F**; Dash dot dot Line, **Cl**; Short dash line, **Br**; Short dot line, **I**;

CONCLUSIONS

Electron impact total ionization cross sections have been calculated for the Alkali atoms (Li, Na, K) and Halogen atoms (F, Cl, Br, I) using the well known spherical complex optical potential method. The CSP-ic formalism developed by the authors [13 - 18] was used to derive the total ionization cross section for these targets. This method has been tested successfully for a large number of atomic and molecular targets. The derived theoretical inelastic cross section serves as the upper limit and gives a useful estimate of the total ionization cross section. The alkali metal atoms are in excess of one electron in over the noble gas configuration while the halogen atoms are in deficit of just one electron correspondingly. Hence the ionization threshold of all Alkali metal atoms is very low. This guarantees two facts, one their ionization cross sections will be very high and other they will have peak of inelastic cross sections at very low energies. This is very much evident from our results. Moreover the excitations are very strong in alkali atoms. The cross section increases with increase in geometric size of the atom with in the same group. Finally, we note that in view of the approximations made here, no definitive values are claimed, but by and large our results fall well within the experimental error in most of the cases. The present theoretical ionization cross sections for halogens show good agreement with most other theoretical and experimental investigations.

ACKNOWLEGMENT

MVK is thankful to University Grants Commission New Delhi, for Major Research project under which part of this work is done.

REFERENCES

[1] Zecca, A., Karwasz, G. P. and Brusa, R. S. (1996) Cross sections for scattering- and excitation-processes in electron-molecule collisions. *Riv. Nuovo Cimento*, **19**(3): 1.

[2] Kasdan, A., Miller, T. M. and Bederson, B. (1973) Absolute Measurements of Total Cross Sections for Electron Scattering by Sodium Atoms (0.5-50 eV)**.** *Phys. Rev. A*, **8**: 1562.

[3] Miller, T. M. and Bederson, B. (1977) Electron scattering for the atomic targets. *Adv. At. Mol. Phys*, **13**: 1.

[4] McDaniel, E. W. (1989) *Atomic collisions: Electron and photon projectiles*, wiley, New York.

[5] Hayes, T. R., Wetzel, R. C. and Freund, R. S. (1987) Total ionization cross sections of Cl and Cl_2 by electron impact. *Phys. Rev. A*, **35**: 2.

[6] McFarland, R. H. (1965) Gryziński Electron - Impact Ionization Cross-Section Computations for the Alkali Metals. *Phys. Rev*, **139**: A40.

[7] McFarland R. H. and Kinney, J. D. (1965) Electron impact ionization cross sections for the alkali metals. *Phys. Rev*, **137**: A1058.\

[8] Brink, G. O. (1962) Ionization of Alkali Atoms by Electron Bombardment. *Phys. Rev*, **127**: 1204.

[9] Margreiter, D., Deutsch, H., Schmidt, M. and M¨ark T, D. (1990) Calculation of electron impact ionization cross sections for various atoms using DM formalisum. *Int. J. Mass Spectrom. Ion Process,* **100**: 157.

[10] Joshipura, K. N. and Limbachiya, C. G. (2002) Theoretical total ionization cross-sections for electron impact on atomic and molecular halogens. *Int. J. Mass Spectrom*, **216**: 239 – 247.

[11] Vinodkumar, M., Limbachiya, C., Antony, B., Joshipura, K. N. (2007) Calculations of elastic, ionization and total cross sections

for inert gases upon electron impact: threshold to 2 keV. *J. Phys. B: At. Mol. Opt. Phys*, **40**: 3259.

[12] Vinodkumar, M., Korot, K., Limbachiya, C., Antony, B. (2008) Screening-corrected electron impact total and ionization cross sections for boron trifluoride (BF3) and boron trichloride (BCl3). *J. Phys. B: At. Mol. Opt. Phys*, **41**: 245202.

[13] Vinodkumar, M., Joshipura, K. N., Limbachiya, C. and Mason, N. (2006) Theoretical calculations of the total and ionization cross sections for electron impact on some simple biomolecules. *Phys. Rev. A*, **74**: 022721.

[14] Vinodkumar, M., Joshipura, K. N., Limbachiya, C. G. and Antony, B. K. (2006) Electron impact total and ionization cross-sections for some hydrocarbon molecules and radicals. *Euro. Phys. J. D*, **37**: 67.

[15] Vinodkumar, M., Limbachiya, C., Korot, K. and Joshipura, K. N. (2008) Theoretical electron impact elastic, ionization and total cross sections for silicon hydrides, SiHx (x = 1, 2, 3, 4) and disilane, Si_2H_6 from threshold to 5 keV. *Euro. Phys. J. D*, **48**: 333.

[16] Vinodkumar, M., Limbachiya, C., Korot, K., Joshipura, K. N. and Mason, N. J. (2008) Electron impact calculations of total and ionization cross-sections for Germanium Hydrides (GeH_X; X = 1–4) and Digermane, Ge_2H_6. *Int. J. Mass Spectrom*, **273**: 145.

[17] Ali, M. A. and Kim, Y.-K. (2008) Ionization cross sections by electron impact on halogen atoms, diatomic halogen and hydrogen halide molecules. *J. Phys. B: At. Mol. Opt. Phys*, **41**: 145202.

[18] Huo W., Electron impact ionization cross sections data. From website: http://www.ipt.arc.nasa.gov/databasemenu.html.

[19] Bunge, C. F., Barrientos, J. A. and Bunge, A. V. (1993) Roothaan-Hartree-Fock ground state atomic wave functions Slater-type orbital expansions and expectation values for z=2-54. *At. Data Nucl. Data Tables*, **53**: 113.

[20] Hara, S. (1967) The Scattering of Slow Electrons by Hydrogen Molecules. *J. Phys. Soc. Jpn*, **22**: 710.

[21] Zhang, X., Sun, J. and Liu, Y. (1992) A new approach to the correlation polarization potential low energy electron elastic scattering by He atoms. *J. Phys. B: At. Mol. Opt. Phys*, **25**: 1893.

[22] Staszewska, G., Schwenke, D. W., Thirumalai, D. and Truhlar, D. G. (1983) Quasifree-scattering model for the imaginary part of the optical potential for electron scattering. *Phys. Rev. A*, **28**: 2740.

[23] Karwasz, G. P., Brusa, R. S. and Zecca, A. (2001) One century of experiments on electron – atoms and molecules scattering: A critical review of integral cross sections 1. – Atoms and diatomic molecules. *Riv. Nuovo Cimento*, **24**(1): 1.

[24] Krishna Kumar, E. and Srivastava, S. K. (1988) Ionization cross sections of rare gas atoms by electron impact. *J. Phys. B*, **21**: 1055.

PRAJÑĀ - **Journal of Pure and Applied Sciences**
Vol. 17: 170 - 175, 2009 ISSN 0975 - 2595

SINGLE CRYSTAL GROWTH, SURFACE MICROSTRUCTURE AND THERMAL STUDIES OF MoS_2

Sunil Chaki,* M. P. Deshpande, Pallavi N. Sakaria and Nilesh N. Pandya

Department of Physics, Sardar Patel University, Vallabh Vidyanagar, Gujarat -388 120

ABSTRACT

Direct vapour transport (DVT) technique was employed to grow large size single crystals of molybdenum disulphide (MoS_2). The Energy Dispersive Analysis of X-ray (EDAX) and X-ray diffraction (XRD) techniques were used to determine the stoichiometric composition and the lattice parameters of the as-grown DVT MoS_2 single crystals respectively. The detailed surface microstructure study reveals that the crystal growth is by spiral and lateral layer spreading mechanisms. The thermal stability of the as-grown DVT MoS_2 single crystals was studied using thermogravimetric analysis (TGA) technique. The thermal activation energy of the MoS_2 single crystal was determined using non-mechanistic equations for thermal decompositions.

Keywords: **MoS_2, single crystal, DVT technique, microstructure, TGA.**

INTRODUCTION

Transition metal dichalcogenides (TMDC) have a typical layered structure, which consists of covalently bound X–M–X (M = metal and X = chalcogen) tri-layers separated by van der Waals gap. One of the TMDC candidates, molybdenum disulphide, MoS_2, continues to generate considerable interest because of its potential applications as solid lubricants [1, 2], in electrochemical hydrogen storage [3], as industrial catalysts for hydrodesulfurization of crude oil catalysis [4], a promising electrode material for lithium and magnesium batteries [5. 6]. In addition, the semiconducting properties of the MoS_2 are determined by both intrinsic and extrinsic disorder in the crystal lattice. The intrinsic disorder depends on the electronic structure, mainly the width of the forbidden energy gap (bandgap), E_g. The extrinsic disorder is determined by both the departure from the non-stoichiometry and by the presence of foreign ions (impurities and dopants) in the crystal lattice. But unlike most transition metal sulphides, molybdenum disulphide, MoS_2 shows low departure from stoichiometric compositions during crystal growth [7, 8]. Chemical vapor transport has been reported as a reliable method of growing MoS_2 single crystals [9-11]. Good quality single crystals are needed for any type of device fabrication using MoS_2. Also, it is desirable to have information of its stability at high temperature. Realizing the significance of MoS_2, the present study has been undertaken to deal with its single crystal growth by direct vapour transport (DVT) technique. The growth mechanism was determined by studying the microstructure of the as-grown single crystal surface. The thermal stability was studied and activation energy was determined employing three standard relations using the thermogravimetric (TG) curve of the as-grown DVT MoS_2 single crystals.

MATERIALS AND METHODS

The single crystals of MoS_2 were grown by direct vapour transport (DVT) technique using constituent elements of 5N purity. For this, stoichiometric proportions of molybdenum and sulphur (Aldrich, USA) powder weighing in total to 10 gm was introduced into the quartz growth ampoule of dimension 24 cm (length) x 2.5 cm (I.D.) and evacuated to a pressure of about 10^{-5} Torr and sealed. This sealed ampoule was placed coaxially in a two-zone horizontal furnace with powder compound in the region of the hotter zone of the furnace. The direct vapour transport was carried out by maintaining the reaction zone (powder) at higher temperature of 960°C and growth zone at lower temperature of 910°C. In order to bring the ampoule to the growth temperature profile, the temperature was slowly increased at the rate of 20°C per hour from room temperature. After acquiring the final temperature profile, the ampoule was left in the furnace for 12 days; the cooling was carried out at the rate of 10°C per hour. The slow cooling rate was

* Corresponding author – sunilchaki@yahoo.co.in

employed to avoid any thermal strains on the as-grown single crystals.

The resulting single crystals were opaque and shining black in colour. The average dimensions of the large size single crystals thus grown were about 12 x 5 x 0.005 (mm x mm x mm)

The stoichiometric composition of the single crystals was studied through Energy Dispersive Analysis of X-rays (EDAX) attached to a Philips EM-400 electron microscope. The Figure 1 shows the obtained EDAX spectra. The EDAX data of weight % of DVT as-grown MoS_2 single crystals are Mo: 58.78 % and S: 41.22 %.

The crystallographic lattice parameters of the DVT as-grown MoS_2 single crystals were determined using X-ray diffraction (XRD) employing Philips X-ray powder diffractometer (X-pert-MPD) with CuK_α radiation. All the diffraction peaks of the pattern shown in Figure 2 are indexed as that of MoS_2 on a hexagonal unit cell basis. The determined lattice parameters are a = b = 3.16°A and c = 12.18°A.

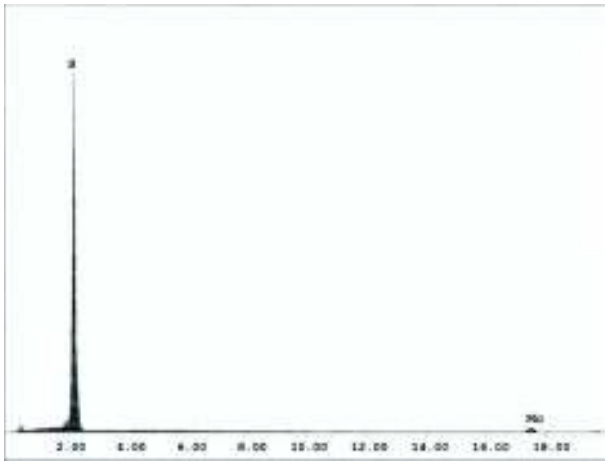

Figure 1: EDAX spectra of DVT grown MoS_2 single crystal.

The fresh as-grown faces of MoS_2 single crystals grown by DVT were examined under 'Epignost" optical microscope (Carl Zeiss Jena GmbH, Germany) for their surface microstructures. The Figures 3 & 4 show photographs of microstructures visible on the DVT as-grown basal faces of MoS_2 single crystals.

The DVT as-grown single crystals of MoS_2 were used for thermal analysis. Thermogravimetric (TG) curve, Figure 5, was obtained between temperature ranges of 40°C to 900°C at a heating rate of 10ºC/min. in inert nitrogen atmosphere, using 'Perkin-Elmer TGA-1'.

Evaluation of Kinetic Parameter Using TG Curve

The TGA curve (initial weight 8.739 mg) obtained for MoS_2 in inert nitrogen atmosphere is shown in Figure 5. The TG curve reveals that the material begins to decompose at around 213°C and continues up to 900 °C by weight loss. Between 40°C and 213°C temperature, MoS_2 is stable with very minor weight loss of 0.0343%. This weight loss is due to the loss of moisture by evaporation which might have been trapped between the lamellar layers of MoS_2.

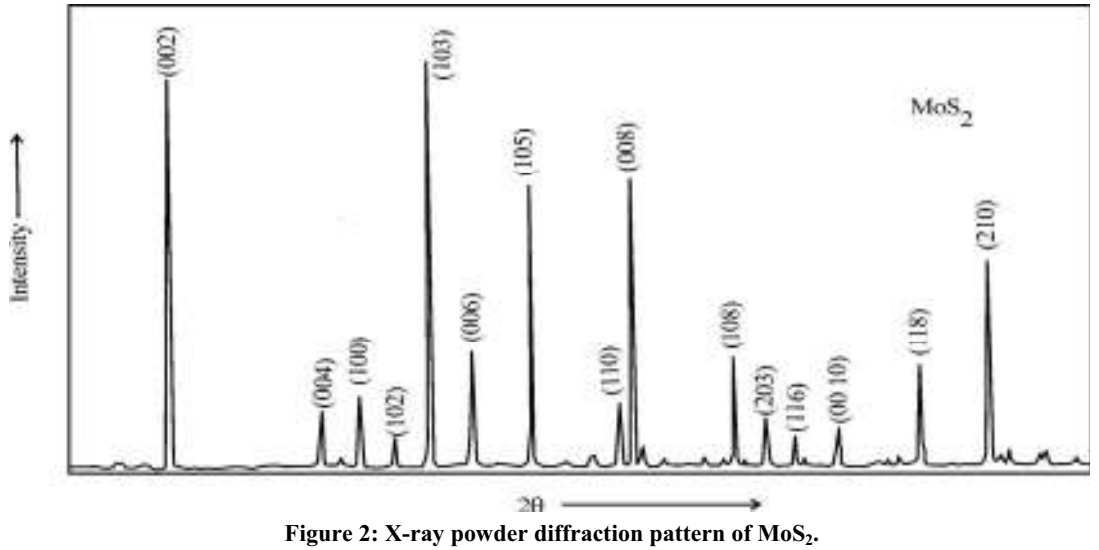

Figure 2: X-ray powder diffraction pattern of MoS_2.

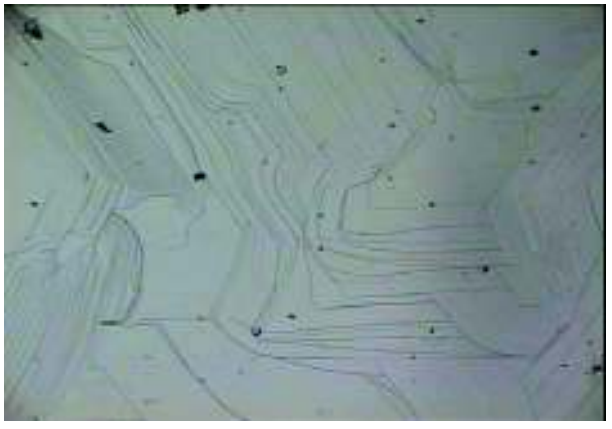

Figure 3: Lateral spreading of growth layers on the crystal surface (500X).

Figure 4: Spiral layer growth mechanism (500X).

The curve between the temperature ranges of 213°C to 900°C shows that the decomposition has three clear steps. The first step (Stage – I) of decomposition is from 213 – 287°C. The weight loss in this Stage – I is 2.5419%. This weight loss is due to the loss of excess sulphur in the form of gas. The second step (Stage – II) lies in the temperature range 440 – 700°C. The weight loss in this Stage – II is 9.4368%. This is followed by the third and the final step (Stage – III) of decomposition that lies in temperature range of 700 – 900°C. The weight loss in this Stage – III is 17.9565%. The activation energy was calculated for the DVT as-grown MoS_2 from the TG curve by the three standard relations.

Broido Relation [12]

The TG curve for a decomposition reaction is represented as

$$\ln(1/y) = \frac{k_o}{a}\int_{T_o}^{T} e^{-E/RT}\,dt \qquad (1)$$

Where a is the heating rate and y is the fraction of the initial materials not yet decomposed. Simplifying the expression to get,

$$\ln\left[\ln\frac{1}{y}\right] = \left[\frac{E}{RT}\right] + \text{constant} \qquad (2)$$

The straight-line plot of $\ln\left[\ln\frac{1}{y}\right]$ *vs*. 1/T for above equation (2) for MoS_2 between the temperatures range of 213°C to 900°C is shown in Figure 6. Using the slope of the plot and the total weight loss due to decomposition between temperature ranges of 213°C to 900°C, the activation energy value calculated by the Broido Relation comes out to be 0.368 eV.

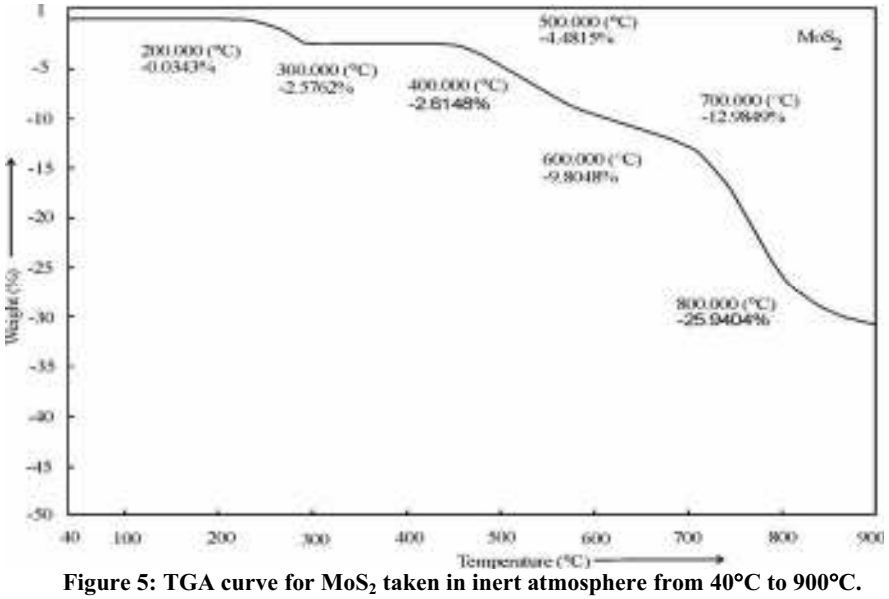

Figure 5: TGA curve for MoS_2 taken in inert atmosphere from 40°C to 900°C.

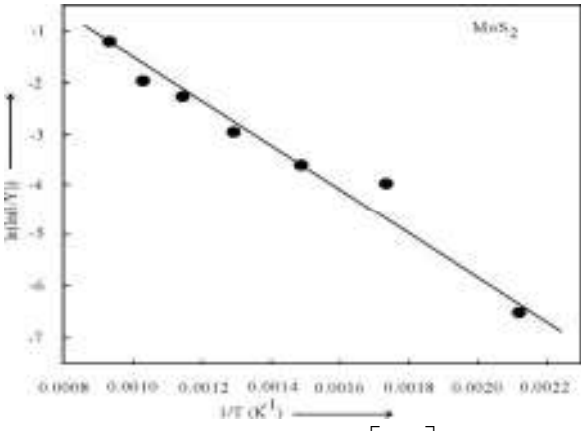

Figure 6: Broido Relation plot of $\ln\left[\ln\frac{1}{y}\right]$ *vs.* 1/T for as-grown MoS_2 single crystals.

Coats-Redfern (CR) Relation [13]

With the reaction: $aA_{(s)} \rightarrow bB_{(s)} + cC_{(g)}$, the rate of disappearance of A may be expressed as,

$$\log\left[\frac{-\log g(\alpha)}{T^2}\right] = \log\left[\frac{ZR}{E\beta}\right] - \frac{E}{2.303RT} \quad (3)$$

where $g(\alpha)$ = (W_∞ — W)/ W_∞, W_∞ = total mass loss in the reaction and W = mass loss at absolute temperature T. The straight-line plot of $\log\left[\frac{-\log(g(\alpha))}{T^2}\right]$ *vs.* $\frac{1}{T}$, Figure 7 for MoS_2, and using the total weight loss due to decomposition between 213°C to 900°C, the activation energy value determined by Coats-Redfern (CR) Relation comes out to be 0.296 eV.

Piloyan-Novikova (PN) Relation [14]

In P-N relation, the reaction order is not needed to be determined first. The rate of dissociation is given by the kinetic equation:

$$\log\left[\frac{\alpha}{T^2}\right] = \log\left[\frac{ZR}{E\beta}\right] - E/2.303RT \quad (4)$$

The activation energy has been calculated from the straight-line plot of $\log\left[\frac{\alpha}{T^2}\right]$ *vs.* $\frac{1}{T}$, (Fig. 8) for MoS_2. Using the total weight loss due to decomposition between temperature ranges of 213°C to 900°C, the activation energy value comes out to be 0.286 eV.

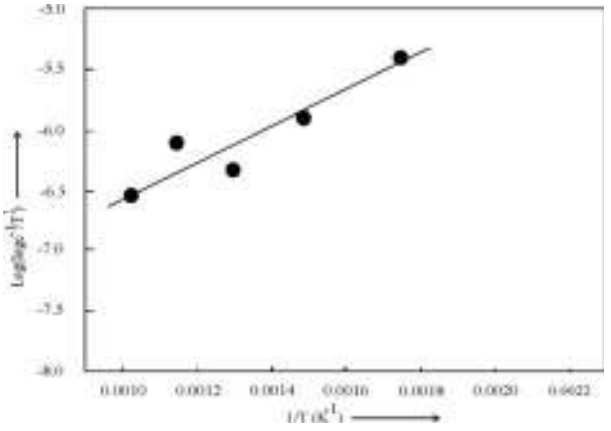

Figure 7: Plot of Coats-Redfern (CR) Relation, $\log\left[\frac{-\log(g(\alpha))}{T^2}\right]$ *vs.* $\frac{1}{T}$ for as-grown MoS_2 single crystals.

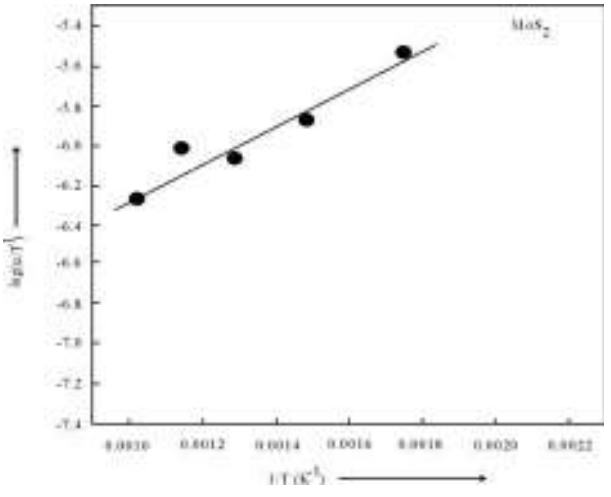

Figure 8: Plot of Piloyan-Novikova (PN) Relation, $\log\left[\frac{\alpha}{T^2}\right]$ *vs.* $\frac{1}{T}$ for as grown MoS_2 single crystals.

RESULTS AND DISCUSSION

Large size MoS_2 single crystals were successfully grown by direct vapour transport (DVT) technique. The chemical composition of the as-grown DVT MoS_2 single crystals determined using EDAX, Figure 1, showed that the crystals possessed near stoichiometry. The crystallographic lattice parameters of the DVT as-grown MoS_2 single crystals were determined using X-ray diffraction (XRD), Figure 2. All peaks as indexed manifest MoS_2 on a hexagonal unit cell basis (JCPDS Card No. 37-1492) with space group $P6_3/mmc$. The deduced lattice parameters were in good agreement with the reported data.

Table I: Thermal activation energy values determined by three standard models.

Models	Broido Relation	Coats-Redfern Relation	Piloyan-Novikova Relation
Activation Energy (eV)	0.368	0.296	0.286

The microstructures shown in Figure 3 & 4 are the common features that were visible on the surfaces of the as-grown DVT MoS_2 single crystals. The Figure 3 clearly shows that the growth is by lateral spreading of layers. Whereas Figure 4 demonstrates that spiral growth mechanism is also prevalent. The layer growth mechanism is further substantiated in Figure 4 where the spiral edges leads to the layer growth mechanism.

The thermogravimetric analysis (TGA) curve of MoS_2, Figure 5, showed that with increase of temperature the weight loss increases. The weight loss with increase in temperature is due to decomposition of MoS_2 single crystals at higher temperatures. The TG curve showed that the decomposition of MoS_2 has three clear steps indicated over here as Stage - I, II & III.

The temperature range of Stage – I is 213°C to 287 °C and the weight loss in this Stage is nearly 2.549%. The temperature range of Stage – II is 440°C to 700°C and the weight loss in this Stage is nearly 9.4368%, while the temperature range of Stage – III is 700 °C to 900°C and the weight loss is 17.9565%. The weight loss in Stage – I is due to the loss of excess volatile sulphur escaping from the compound. Whereas the weight loss in Stage – II & III is due to the solid state decomposition of MoS_2. Between Stages – I & II, i.e. between temperatures range of 287°C and 440°C the compound shows no weight loss, meaning that MoS_2, is stable between temperatures range from ambient temperature to 440°C. The minor weight loss in this temperature range (Stage –I) may be due to loss of excess sulphur. The solid state phase change of MoS_2 doesn't take place in this temperature range, confirmed by small weight loss (2.549%).

The values of thermal activation energy of MoS_2 calculated by three standard thermal relations in the decomposition temperature range of 213°C to 900 °C are given in Table – I as follows.

It is observed that the activation energy values determined from three standard models are nearly the same in the decomposition temperature range.

CONCLUSIONS

1. Large size single crystals of MoS_2 have been successfully grown by DVT technique.
2. The as-grown single crystals have been stoichiometrically and structurally characterized by EDAX and XRD respectively. Both the analyses showed good agreement.
3. The surface microstructure studies clearly suggest that the crystal growth is driven by spiral and lateral layer spreading mechanisms.
4. The TGA curve of MoS_2 single crystals in the temperature range of 40°C to 900°C showed that the compound is thermally stable between ambient temperature and 440°C. A minor weight loss in temperature range of 213 – 287°C is due to the loss of excess sulphur from the compound.
5. Above 440°C, the decomposition takes place in two steps stated here as Stage – II & III. The weight loss in Stage – II & III are due to the solid state phase transition of the MoS_2.
6. The thermal activation energy has been calculated by three models in the temperature range of 213 – 900°C, where the decomposition of MoS_2 is seen to occur. All the three values of the activation energy have been found to be nearly same.

ACKNOWLEDGMENTS

The authors are thankful to the Sophisticated Instrumentation Centre for Applied Research & Testing (SICART), Vallabh Vidyanagar, Gujarat for the EDAX, XRD and TGA characterization of the samples.

REFERENCES

[1] Chen, W. X., Xu, Z. D., Tenne, R., Rosenstveig, R., Chen, W. L., Gan, H. Y. and Tu, J. P. (2002) Wear and friction of Ni-P electroless composite coating

including inorganic fullerene-like WS_2 nanoparticles. *Adv. Eng. Mater*. **4**: 686-690.

[2] Rapoport, L., Bilik, Y., Feldman, Y., Homyonfer, M., Cohen, S. R. and Tenne, R. (1997) Hollow nanoparticles of WS_2 as potential solid-state lubricants. *Nature* **387:** 791-793.

[3] Chen, J., Kuriyama, N., Yuan, H. T., Takeshita, H. T. and Sakai, T. (2001) Electrochemical hydrogen storage in MoS_2 nanotubes. *J. Am. Chem. Soc.* **123**: 11813-11814.

[4] Chen, J., Li, S. L., Xu, Q. and Tanaka, K. (2002) Synthesis of open-ended MoS_2 nanotubes and the application as the catalyst of methanation. *Chem. Commun.* **16**: 1722-1723.

[5] Li, X. L. and Li, Y. D. (2004) MoS_2 nanostructures: Synthesis and electrochemical Mg^{2+} intercalation. *J. Phys. Chem*., B **108**: 13893-13900.

[6] Wang, Q. and Li, J. H., (2007) Facilitated Lithium storage in MoS_2 over layers supported on coaxial carbon nanotubes. *J. Phys. Chem. C.* **111**: 1675-1682.

[7] Rau, H., (1980) Estimation of the homogeneity range of MoS_2. *J. Phys. Chem. Solids* **41:** 765-767.

[8] Suzuki, Y., Uchida, T., Wakihara, M. and Taniguchi, M. (1981) Phase relationship on Mo-S system at high temperatures. *Mater. Res. Bull.***16**: 1085-1090.

[9] Nitsche, R., Bolsterli, H. U. and Lichtensteiger, M. J. (1961) Crystal growth by chemical transport reactions I: Binary, ternary, and mixed-crystal chalcogenides. *J. Phys. Chem. Solids* **21**: 199-205.

[10] Nitsche, R. (1961) The growth of single crystals of binary and ternary chalcogenides by chemical transport reactions. *J. Phys. Chem. Solids* **17**: 163-165.

[11] Vaidya, R., Dave, M., Patel, S. S., Patel, S. G. and Jani, A. R. (2004) Growth of molybdenum disulphide using iodine as transport material. *Pramana J. Phys.* **63**: 611-616.

[12] Broido, A. (1969) A simple sensitive graphical method of treating thermogravimetric analysis data. *Journal of Polymer Science Part A-2*, **7(10)**: 1761–1773.

[13] Coats, A. W. and Redfern, J. P. (1964) Kinetic parameters from thermogravimetric data. *Nature*, **201(4914)**: 68-69.

[14] Piloyan, G. O. and Novikova, O. S. (1967) DTA and TG Determination of the Activation Energy for Dissociation Processes. *Zh. Neorg. Khim.*, **12**: 602–604.

PRAJÑĀ - Journal of Pure and Applied Sciences
Vol. 17: 176 - 179, 2009 ISSN 0975 - 2595

STRUCTURAL AND OPTICAL CHARACTERIZATION OF CdTe THIN FILMS PREPARED BY THERMAL EVAPORATION PROCESS

K. D. Patel, H. S. Patel,* V. M. Pathak and R. Srivastava

Department of Physics, Sardar Patel University, Vallabh Vidyanagar, Gujarat – 388 120

ABSTRACT

Cadmium Telluride (CdTe), a member of group II-VI semiconductors is one of the promising materials from its applications point of view. The present investigations are about the preparation and optical characterization of CdTe thin films. Thin films of CdTe with thickness around 4.2kÅ have been deposited by thermal evaporation method. CdTe charge was used as starting material for preparation of the films. The structural characterization of this charge was carried out using XRD. The structure of CdTe before and after the deposition was found to be hexagonal. Also, the lattice parameters were evaluated from the XRD data. The chemical composition of the deposited CdTe thin films has been confirmed using EDAX technique. From TEM of CdTe thin films, the polycrystalline nature was confirmed. Optical characterization of CdTe thin films has been carried out using UV-VIS-IR spectroscopy and the results have been discussed here.

Keywords: **CdTe thin films, chemical composition, structural study, optical study.**

INTRODUCTION

In recent years, much attention has been shown in semiconducting II-VI compounds because of their interesting optoelectronic properties and applications. Cadmium telluride is an important member of this group. It has an indirect band gap of approximately 1.49eV at room temperature which makes it an interesting material for various applications. The CdTe thin films have been extensively studied for structural [1, 2] optical [3] and optoelectronic [2, 4] properties. The Schottky junction and heterojunction devices have also been investigated for understanding the charge transport mechanism [4], device parameters and solar energy conversion [1, 5]. The properties of the films generally depend on the structural parameters such as lattice constant, grain size etc. which are dependent on the deposition conditions e.g. rate of deposition, substrate temperature, vacuum conditions and the resultant film thickness. The optical absorption is known to arise through the interaction of the excited electrons with the lattice perturbed by the vibrations or imperfections. The experimental studies of the thermally evaporated CdTe thin films and the characterization using XRD, TEM and UV-VIS-IR have been presented in this paper.

MATERIALS AND METHODS

Thin films of 4200Å were deposited on chemically and ultrasonically cleaned glass substrates with the help of vacuum coating unit (12A4D, HHV). All the gadgets of the vacuum chamber were first cleaned by acetone. A clean evaporation source (molybdenum boat) was fixed in the filament holder inside the chamber. CdTe powder having purity 99.99% was kept in the molybdenum boat. The glass substrates were cleaned by acetone and ultrasonic vibrations. The substrates were kept on the substrate holder and crystal monitor was placed near it to measure the thickness in situ. The chamber was evacuated at a pressure better than 10^{-5} Torr by the combination of rotary and diffusion pump. When vacuum of 10^{-6} Torr was attained in the vacuum chamber, the temperature of the boat was gradually raised to heat CdTe to temperatures greater than the melting point. This allowed the evaporation of CdTe material. The chemical characterization was carried out with the help of EDAX. The X-ray diffraction analysis of CdTe starting material has been carried out at 300K using Philips X-ray diffrectomer, (model: X'PERT MPD Netherland) with CuKα radiation of wave length 1.54Å. For TEM studies, films were deposited simultaneously on freshly cleaved NaCl crystals also. The optical characterization of films were carried out using the UV-VIS-NIR spectrophotometer (Perkin Elmer-USA, Model: Lambda 19) in the range of 200nm to 2500nm wavelength.

* Corresponding author – haresh25884@gmail.com

RESULTS AND DISCUSSION

EDAX Studies

EDAX scan (Figure 1) confirmed that the charge used for the deposition of CdTe films comprised of only Cd and Te. No other elements were observed within the limits of sensitivity. (i.e. element with atomic number less than 11 or with concentration less than 1% would not be detected by EDAX scan)[6].

Table: 1 Chemical composition (Wt %) of CdTe charge.

Wt (%) of the Element	Cd	Te	Chemical formula
Expected stoichiometric proportion in CdTe	46.68	53.32	CdTe
Obtained stoichiometric proportion in CdTe charge	47.20	52.80	$Cd_{1.1}Te_{0.99}$

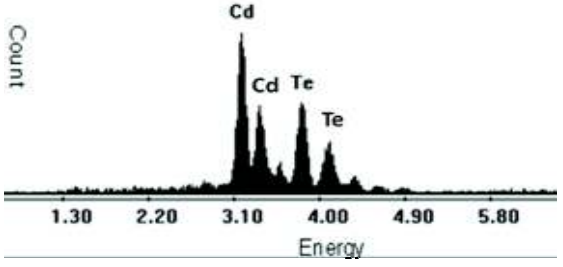

Figure 1: EDAX scan of CdTe charge.

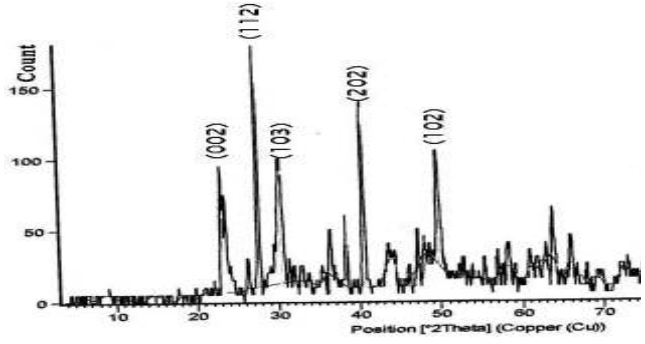

Figure 2: X – Ray Diffractogram of CdTe used for thin film deposition.

X – Ray Diffraction Studies

Fig. 2 shows the X-ray diffractogram of CdTe powder used in preparation of thin films.

The lattice parameters, a and c, were determined for hexagonal structure using the following equation.

$$\frac{1}{d^2} = \left[\left(\frac{4}{3}\right)\left(\frac{h^2 + hk + k^2}{a^2}\right)\right] + \left(\frac{l^2}{c^2}\right) \qquad (1)$$

where h, k and l represent the Miller indices and d is the inter planer spacing. The observed 'd' values and calculated values of the lattice constants 'a' and 'c' are in good agreement with the standard data file of JCPDS [7], and have been shown in Table 2.

Table 2: Calculated values of lattice parameters.

CdTe powder (Hexagonal structure)		
a = 4.66 Å	b = 4.66 Å	c = 7.11 Å
α = 90º	β = 90º	γ = 120 º

The particle size (D) of the charge used for evaporation of CdTe thin films was determined by using the Debye-Scherrer's formula,

$$D = \frac{k\lambda}{\beta \cos\theta} \qquad (2)$$

where λ is the wave length of X –rays used, β is the FWHM, k is a constant (taken as 1) and θ is the angle between the incident and scattered X-rays. The particle size found in the present investigations was around 9.4 nm [8].

TEM Studies

The electron diffraction pattern for CdTe thin film is shown in Fig. 3. The nature of this diffraction pattern confirms the polycrystalline structure of the deposited films.

The wavelength of incident electron beam λ was calculated using the equation

$$\lambda = \sqrt{\frac{150}{U(V)}} \qquad (3)$$

where U(v) is the acceleration potential in Volt.

The accelerating potential of the electron beam used for these measurements was 200 kV. Substitution of this value in equation (3) yields λ to be around 0.0274 Å. Using the value of L (3 m) and the value of λ , the product λL was calculated and it was found to be 822 x 10^{-10}cm^2 . The diameter of the ring patterns were measured using

a comparator. Substituting the values of the diameters of the rings and λL in equation (4) yields the value of inter planer spacing d as

$$d = \frac{2\lambda L}{diameter} \qquad (4)$$

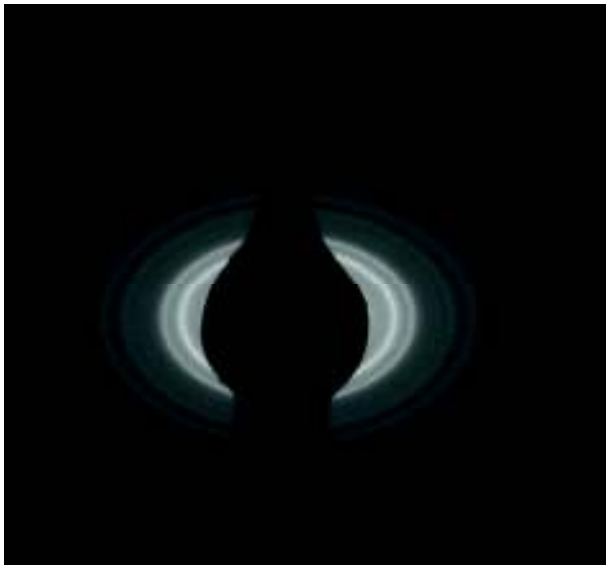

Figure 3: Electro diffraction pattern of CdTe thin film of thickness 4.2 kÅ.

The d – values corresponding to all these rings have been calculated and are given in Table – 3. This Table also contains the d values obtained from the JCPDS data [7]. The two values match and this confirms that the deposited CdTe films also possess the hexagonal structure [9].

Table 3: Results of TEM analysis for CdTe thin film for thickness 4.2 kÅ.

Ring No.	Ring diameter D cm	Interplaner spacing d = 2λL/D Å	JCPDS d-values Å	h k l
1	5.969	2.754	2.735	1 0 2
2	7.289	2.255	2.295	1 1 0
3	7.747	2.122	2.115	1 0 3
4	10.59	1.552	1.554	2 0 3

Optical Absorption Studies

The optical absorption and transmittance measurement of CdTe thin films have been carried out at room temperature. The optical spectra of thermally evaporated CdTe thin films have been recorded in the wavelength range 200nm to 2500nm. The results of these investigations have been used for the calculations of the absorption coefficient and other parameters.

To confirm the direct or indirect nature of the optical transitions of carriers in CdTe thin films, the above calculated absorption coefficient corresponding to each energy of incident radiation has been plotted with respect to the energy of the incident photons. The intercept of the straight line drawn from the linear portion of $(\alpha h\nu)^2$ vs. $(h\nu)$ and $(\alpha h\nu)^{1/2}$ vs. $(h\nu)$, are shown in Fig. 4 and Fig. 5 respectively and they have been used to evaluate the band gap energies. The values of direct and indirect band gaps were found to be 1.52 eV and 1.50 eV respectively for CdTe thin films which are in good agreement with the reported data [10].

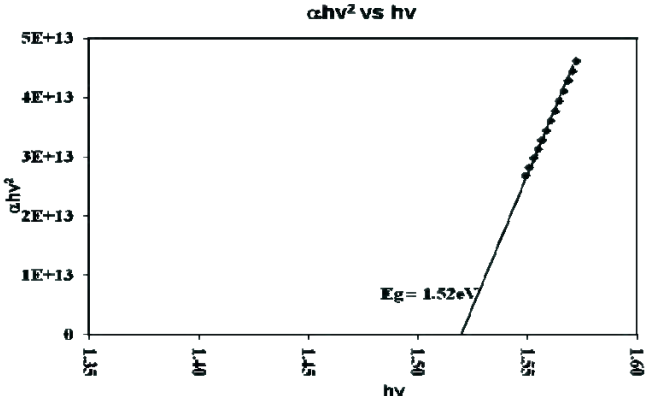

Figure 4: $(\alpha h\nu)^2$ vs. $(h\nu)$ Plot of CdTe thin film.

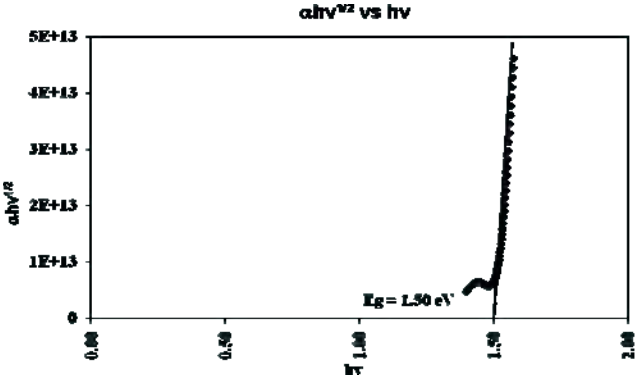

Figure 5: $(\alpha h\nu)^{1/2}$ vs. $(h\nu)$ Plot of CdTe thin film.

CONCLUSIONS

CdTe charge used as starting material for the thin film preparation possesses hexagonal structure. The deposited films also possess the same structure with polycrystalline nature. The optical characterization reveals that CdTe possesses both direct and indirect allowed band gaps of 1.52 eV and 1.50 eV respectively.

REFERENCES

[1] Basol, B. M. (1989) Electrodeposited CdTe and HgCdTe solar cells. *Solar Cells*, **23**: 69-88.

[2] Methaw, X., Sebastai, P.J., Sachez, A and Campos, J. (1999) Structural and opto-electronic properties of electrodeposited CdTe on stainless steel foil. *Solar Energy Mater and Solar Cells* **59**: 99-114.

[3] Methaw, X. and Sebastai, P. J. (1999) Optical properties of electrodeposited CdTe thin films. *Solar Energy Mater and Solar Cells* **59**: 85-89.

[4] Kidi, D. and Touskova. (1988) Charge transport study in thin film Au-CdTe schottky diodes. *J. Phys. Stat, Sol.* **106**: 297-304.

[5] Macandless, B. E. and Birkmine, R. W. (1921) Analysis of post deposition processing for CdTe/CdS thin film solar cells. *Solar Cells* **31**: 527-535.

[6] Murat Bayhan (1998) Structural and optical characterisation of vacuum deposited CdTe thin films. *Tr. J. Physics* **22**: 929-937.

[7] JCPDS International centre for Different Data, (1998) USA Card No. **19**: 0193.

[8] Moustafa, S. M. (2008) Effect of layer sequence on formation of CdTe thin film prepared by stacked elemental layers. *Egypt J. solids*, **31**: 1-10.

[9] Spinulescu, I. C. (1966) Growth of hexagonal crystallites in CdTe thin films. *Physica Status Solidi* **15(2)**: 761-765.

[10] Alejo-Armenta, L. N., Espinoza-Beltra, F. J., Aleja-Armenta, C. A., Vazque-Lopez, C. Arizpe-Chavez H., Ramirez-Bon, R., Zelanya-Angel O. and Gonzalez-Hermandez. J. (1922) Strain effects on the energy band-gap in oxygenated CdTe thin films studied by photoreflectance. *J. Phys. Chem. Solid* **6**: 807-811.

PRAJÑĀ - **Journal of Pure and Applied Sciences**
Vol. 17: 180 - 184, 2009 ISSN 0975 - 2595

STRUCTURAL AND OPTICAL PROPERTIES OF ZnTe THIN FILMS

K. D. Patel, J. R. Rathod *, V. M. Pathak and R. Srivastava

Department of Physics, Sardar Patel University, Vallabh Vidyanagar, Gujarat – 388 120

ABSTRACT

The present investigation deals with the structural and optical properties of ZnTe thin films. Thin films of ZnTe with thicknesses around 4.kÅ and 6.kÅ have been deposited by thermal evaporation method on the ultrasonically cleaned glass substrates kept at 373K under the pressures of 5×10^{-6} Torr. The thicknesses of the films were measured by quartz crystal thickness monitor. The structural and optical characterizations of the films were carried out by using X-ray diffraction (XRD) and UV-VIS-IR spectroscopy respectively. The lattice constant (a), grain size (D), strain (ε) and dislocation density (ρ) have been calculated. The optical band gap (E_g) which was evaluated from the optical absorption spectra indicates direct band to band transitions. Spectral distribution of transmission coefficient *T*, refractive index *n*, extinction coefficient *k* of ZnTe thin films have also been investigated and discussed in light of the structure of ZnTe.

***Keywords*: ZnTe thin films, thermal evaporation, structural study, optical study.**

INTRODUCTION

Among the wide band gap II-VI semiconductors, ZnTe with direct gap of 2.26eV at room temperature is a promising material for a variety of optoelectronic devices [1, 2]. ZnTe has been widely used as a substrate for the growth of CdTe. Heterostructure devices based on ZnTe and HgTe have been used for infrared optics [3]. When doped with vanadium, ZnTe becomes a photorefractive semiconducting material [2, 4] and has good potential for optical power limiting applications. The other applications as opto refractive materials for which it has been used are optical data processing [2], non-polarized memory switching [5] and γ-ray detectors. Moreover, ZnTe has particularly been used as terahertz (THz) detector at liquid nitrogen temperature [6, 7]. A variety of thin film growth techniques have been used for the preparation of ZnTe thin films. Some of them are: thermal evaporation , vapour phase epitaxy, molecular beam epitaxy , hot wall epitaxy, metallorganic vapour phase epitaxy, r.f. sputtering, solution growth, spray pyrolysis, electro synthesis etc.[8-10]. Pal *et al.* [11] made a detailed study of the crystal structure in ZnTe thin films and they concluded that these films deposited on well cleaned glass substrates kept at room temperature have cubic zinc blende type structure. The present paper deals with the determination of different microstructural parameters like grain size, microstrain, dislocation density etc. evaluated for thermally evaporated ZnTe thin films. The variation in optical band gap (E_g) with respect to thickness has also been studied from the optical absorption spectra and the results have been presented here.

MATERIALS AND METHOD

Zinc Telluride powder (99.99% pure, sigma Aldrich Chemicals Company) was evaporated from a tantalum boat under a vacuum of 5×10^{-6} Torr. The ZnTe films were deposited onto ultrasonically-cleaned glass substrates maintained at 373K during evaporation. The rate of evaporation, in the range of 2-5 Å/sec, was maintained to grow films of good quality and uniform thickness. Thickness of the films was measured by quartz crystal thickness monitor ('Hind Hivac' Digital Thickness Monitor Model–DTM–101). The structural parameters of ZnTe thin films were investigated using Philips X-ray diffractometer, (model: X'PERT MPD Netherland) with filtered CuKα radiation (λ = 1.5405 Å). The optical absorption spectra of these films were recorded using a UV–VIS-NIR spectrophotometer (Perkin Elmer USA, Model: Lambda 19).

RESULTS AND DISCUSSION

Structural characterization

The XRD patterns of ZnTe films having thicknesses around 4kÅ and 6kÅ deposited at substrate temperature of 373K are shown in Fig. 1(a, b). In this figure a strong peak is observed at

* Corresponding author – jrrathod84@gmail.com

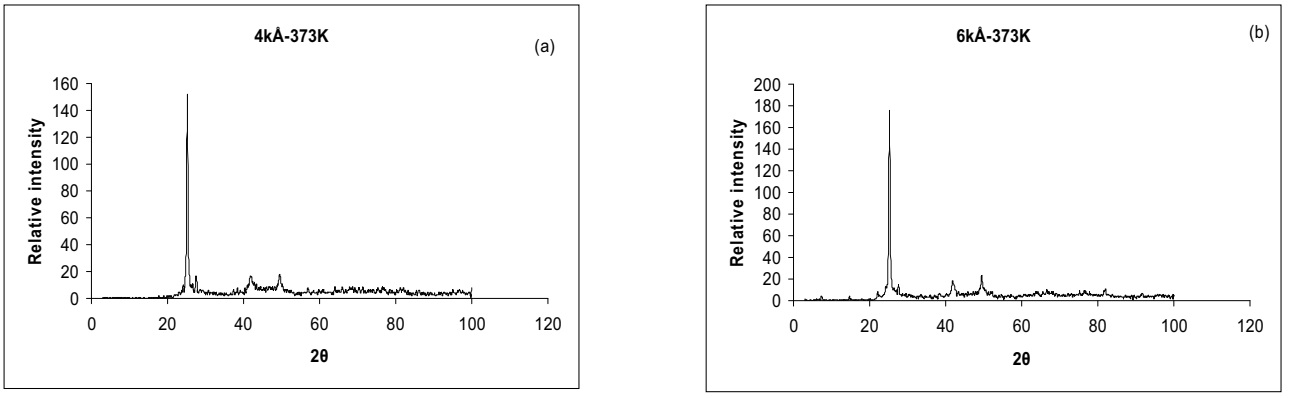

Figure 1: X-ray diffractrogram of ZnTe film.

2θ value of 25.223 which corresponds to the preferred orientation along (111) plane of the cubic phase. It is found to be in good agreement with the standard JCPDS (15-0746) data of cubic ZnTe. This confirms that the prepared films are well formed polycrystalline films and possess cubic phase zinc blend structure.

The value of the lattice constant (a) has been calculated using the following formula [12].

$$\frac{1}{d^2} = \frac{h^2 + k^2 + l^2}{a^2} \qquad (1)$$

Where h, k, l are the Miller indices and d is the inter planner spacing.

The average grain size in the polycrystalline films was calculated from the XRD data using Debye-Scherrer's relation [12].

$$D = \frac{k\lambda}{\beta \cos\theta} \qquad (2)$$

Where, k is a constant (taken as 1), λ is the wavelength of radiation (1.5405Å), β is the full width at half maximum and θ is the diffraction angle.

The micro strain (ε) and the dislocation density (ρ) were evaluated using the equations [13]

$$\varepsilon = \frac{\beta \cos\theta}{4} \qquad (3)$$

and

$$\rho = \frac{1}{D^2} \qquad (4)$$

The lattice constant (a), the particle size (D), the micro strain (ε) and the dislocation density (ρ) were evaluated using above equations and the results are given in Table 1.

From the table it can be seen that there is a slight upward change in 2θ value which gives little decrease in the lattice constant (a) and the inter planer spacing (d) values at higher thickness. It can also be noted that parameters like average grain size, micro strain and dislocation density show no significant change with thickness.

Optical Characterization

The transmittance spectra for ZnTe thin films have been shown in Fig. 2. From this spectra it can be clearly observed that the thin films have very low transmittance in the visible region. Further the transmittance in both films increases to higher values at higher wavelengths. However

Table 1: Structural parameter of ZnTe film.

Thickness (Å)	h k l	Lattice Constant a (Å)	2θ		Grain size D (Å)	Micro strain ε 10^{-3} (lines-m^2)	Dislocation density ρ 10^{15} (lines/m^2)	Lattice spacing d (Å)
			XRD	JCPDS				
4000	1 1 1	6.1193	25.207	25.279	246.97	1.4658	1.44	3.533
6000	1 1 1	6.1115	25.240	25.279	246.99	1.4657	1.44	3.528

in the near infrared region it increases sharply and then it again decreases.

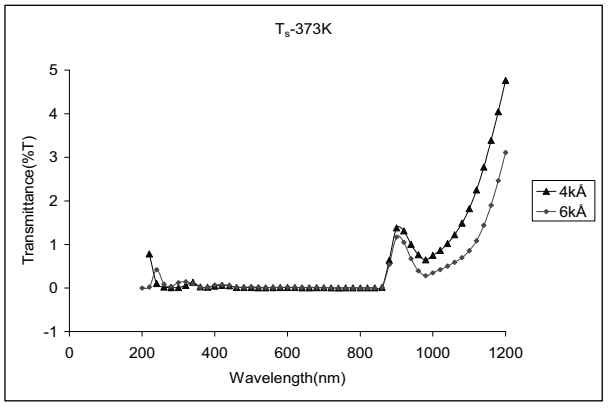

Figure 2: Transmittance spectra of ZnTe film at substrate temperature 373K.

After the wavelength of around 980nm a continuous increase in transmittance is observed. Fig. 2 also shows that the transmittance decreases with increase in film thickness. Therefore, it can be concluded that both films possess highly absorbing nature in the visible region (400nm-800nm) and are relatively transparent in the infrared region. This is in good agreement with the investigations reported in literature [14].

The extinction coefficient of the films was calculated by using the formula

$$K = \frac{\alpha\lambda}{4\pi} \qquad (5)$$

Where α is the absorption coefficient calculated as 2.303A/t. Here A is absorbance and t is the thickness of the film.

The refractive index (*n*) of the film was calculated from the formula

$$n = \frac{1+R}{1-R} \qquad (6)$$

Where R is the reflectance determined from the absorption data.

Using equation (5) and (6) extinction coefficient K and refractive index *n* were calculated as a function of wavelength and are plotted in Fig. (3) and (4). From Fig. 3, it is quite apparent that as one moves from ultraviolet to visible region, regular increase in extinction coefficient *k* is observed. This increase is followed by sudden decrease in the near infra red region. However, with increase in film thickness it is observed that extinction coefficient relatively decreases at all wavelengths.

From Fig. 3, it is quite apparent that as one moves from ultraviolet to visible region, regular increase in extinction coefficient *k* is observed.

This increase is followed by sudden decrease in the near infra red region. However, with increase in film thickness it is observed that extinction coefficient relatively decreases at all wavelengths.

A reverse trend is observed in the refractive index variation with wavelength as is evident from Fig. 4. Refractive index *n* only slightly decreases in the visible region and in near infrared region sharp increase in refractive index is observed accompanied with a hump.

In the domain of fundamental absorption edge, the absorption coefficient, α for allowed direct transitions, is given by the expression [15]

$$\alpha h\nu = A_\alpha (h\nu - Eg)^{1/2} \qquad (7)$$

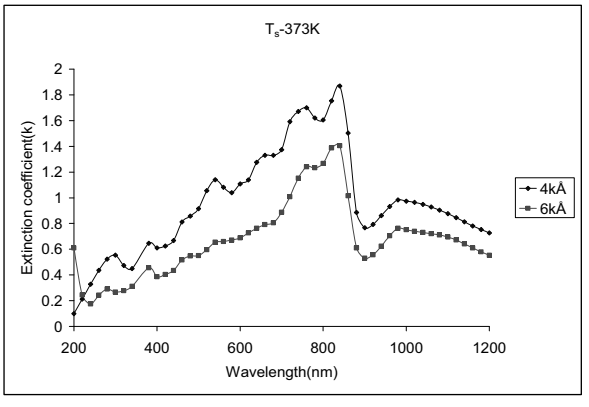

Figure 3: The variation of k with wavelength for ZnTe thin film.

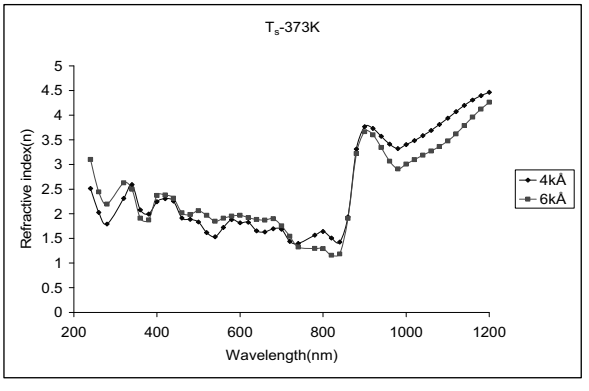

Figure 4: The variation of refractive index n with respect to wavelength.

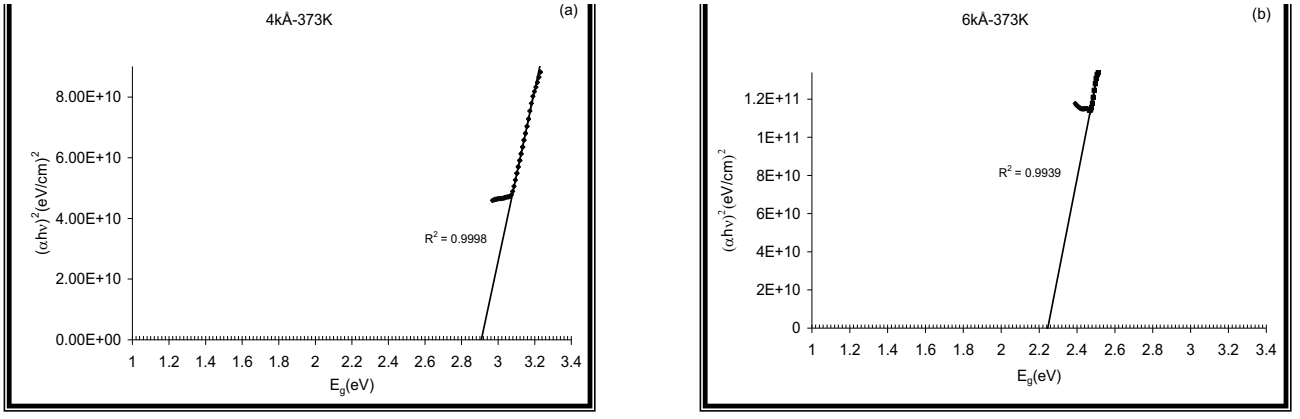

Figure 5 (a, b): Depicts the variation of square of $(\alpha h\nu)$ versus photon energy $(h\nu)$ for ZnTe films of the thicknesses 4kÅ and 6kÅ for substrate temperature 373K.

Where hν is the photon energy, E_g is the energy bandgap and A_α is the characteristic parameter, independent of photon energy, for respective transitions.

According to equation-7, in the vicinity of fundamental absorption edge, the dependence $((\alpha h\nu)^2 \rightarrow (\mathrm{h}\nu)$ is linear.

Fig. 5 (a, b) shows this dependence in present case. The values of bandgap Eg, can be determined by extrapolating the linear portion of the respective curve to $(\alpha h\nu)^2$=0. The value of energy gap, calculated in this manner is 2.90 eV and 2.24 eV for the films having thickness 4kÅ and 6kÅ respectively which are direct in nature.

CONCLUSIONS

ZnTe thin films were deposited onto well-cleaned glass substrates by vacuum evaporation at substrate temperature of 373K. The X-ray diffraction analysis indicates that the films are polycrystalline in nature and ZnTe exhibits a zinc blende structure. The optical transitions in ZnTe films are direct and allowed type. The spectral distribution of *T, n,* and *k* with respect to wavelength shows that material is of highly absorbing nature in the visible region while it is transparent in the near infrared region.

REFERENCES

[1] Nam, S., Rhee, B. O. J., Lee, K., Choi, Y. D. (1997) Optimum Growth conditions and near band-edge photoluminescence of high quality ZnS/GaAs(100) epilayers, *J. Crystal Growth*, **180:** 47.

[2] Zhou, H., Zebib, A., Trivedi, S., Duval, W. M. B. (1996) Physical vapor transport of ZnTe by dissociative sublimation, *J. Crystal Growth*, **16: 7**813.

[3] Jain, M., Godlevsky, V. V., Derby, J. J. and Chelikowsky, J. R. (2001) First-principles simulation of liquid ZnTe, *Phys. Rev. B*, **65:** 35212.

[4] Taike, A., Momose, M., Gotoh, J. and Mochizuki, K., (1996) Influence of convection on zinc selenide single crystal growth by chemical vapour transport *J. Crystal Growth,* 159271.

[5] Barshilia, H. C., Selvakumar, N., Rajam, K. S. and Biswas, A. (2008) Optical properties and thermal stability of tialn/alon tandem absorber prepared by reactive dc/rf magnetron sputtering. *Solar Energy Materials and Solar Cells* **92**: 1425-1433.

[6] Spisak, D. and Hafner, J. (2001) Growth of face-centered-cubic Fe films on Cu. 100: Interdiffusion, surfactant effects and island formation. *Phys. Rev. B*. **64,** 205422: 1-11.

[7] Schall, M., Walther, M. and Uhd Epsen P., (2000) Fundamental and second-order phonon processes in CdTe and ZnTe. *Phys. Rev. B.* **64**, 094301: 1-8.

[8] Mahalingam, T., John, V. S., Ravi, G. and Sebastian, P. J. (2002) Microstructural characterization of electrosynthesized ZnTe thin films. *Cryst. Res. Technol*. **37(4):** 329-339.

[9] Mahalingam, T., John, V. S., Rajendran, S. and Sebastian, P. J., (2002) Electrochemical

deposition of ZnTe thin films. *Semicond. Sci. Technol*, **17:** 465-470.

[10] Bhargava, R. (1997) *Properties of Wide Bandgap II-IV Semiconductors, Inspec*. London.

[11] Pal, U., Saha, S., Samantaray, B. K., Banerjee, H. D. and Chaudhuri, A. K., (1989) X-Ray line broadening and electron microscopic studies on ZnTe thin films. *Phys. Stat. Sol*. **111:** 515-522.

[12] Cullity, B. D. and Stock, S. R. (2001) *Elements of X-Ray diffraction*, 3rd Ed. Ney Jersey: Prentice Hall

[13] Senthilkumar, V., Venkatachalam, S., Viswanathan, C., Gopal, S., Narayandass, S. K., Mangalaraj, D., Wilson, K. C. and Vijaykumar, K. P. (2005) Influence of substrate temperature on the properties of vacuum evaporated InSb films. *Cryst. Res. Technol.,* **40**: 573-578.

[14] Lopez-Otero A., (1977) CdTe thin films grown by hot wall epitaxy. *J. Cryst. Growth* **45**: 214-217.

[15] Molin, A. N., and Dikusar, A. I. (1995) Electrochemical deposition of PbSe thin films from aqueous solutions. *Thin Solid Films,* **265:** 3-9.

PRAJÑĀ - **Journal of Pure and Applied Sciences**
Vol. 17: 185-190, 2009 ISSN 0975 - 2595

IONIZATION CROSS SECTIONS OF HELIUM AND NEON BY POSITRON IMPACT - THEORETICAL INVESTIGATIONS

Harshit N. Kothari * **and K. N. Joshipura**

Department of Physics, Sardar Patel University, Vallabh Vidyanagar, Gujarat – 388 120

ABSTRACT

In this paper we have calculated various total cross sections of positron interactions and scattering with helium and neon atoms. We have calculated total elastic cross sections (Q_{el}) and inelastic cross sections (Q_{inel}) from partial wave analysis of complex spherical e^+ - atom potentials. In positron atom scattering it is difficult to separate out ionization and excitation cross sections from inelastic cross sections because the positronium formation is another inelastic channel taking off prior to excitation threshold in noble gas atoms. Our goal in this paper is to find out the contribution of ionization cross sections in the inelastic cross sections (Q_{inel}) along the lines of 'complex scattering potential-ionization contribution' (*CSP-ic*) method of electron – atom scattering.

***Keywords*: ionization cross sections, positron scattering, complex potential, inelastic cross sections.**

INTRODUCTION

Investigations of the scattering of positrons by atomic and molecular gases and beams have gained significant importance because the positron offers a more sensitive test than the electron, in our ability to understand atomic interactions. Positron (e^+- antiparticle of the electron) interactions with matter play important roles in many physical processes of interest in laboratory and nature. Examples include the origin of astrophysical sources of annihilation radiation, the use of positrons in medicine, the characterization of materials, and the formation of anti-hydrogen which is the simplest form of stable, neutral antimatter. The noble gas targets are chosen in the present investigation, because of their relatively simple atomic structure and the fact that they are naturally mono-atomic gases. Two phenomena that can only occur for positron collisions are annihilation (appreciable only for energies much less than 1 eV) and positronium (e^+e^- or Ps) formation, which has been found to be an important factor in positron – gas scattering processes. It is of interest to compare the positron scattering from a target with the scattering of electrons, for which extensive theoretical and experimental data are available.

* Corresponding author – harshitkothari_85@yahoo.co.in

Total cross sections for the scattering of positrons by both helium and neon were measured by Coleman *et al* [1], Stein *et al* [2], Griffith *et al* [3] and Kauppila *et al* [4]. The ionization cross sections of helium by positron impact have been measured by Fromme *et al* [5] and also by Mori and Sueoka [6]. Basu *et al* [7] calculated ionization cross sections of helium atom by positron impact by various theoretical methods. The ionization cross sections of neon by positron impact have been measured by Kara *et al* [8] and by Knudsen *et al* [9]. Positron scattering by atomic and molecular oxygen were calculated by Joshipura [10].

To understand how the positronium formation is dominated in various scattering channels we have shown in figure 1 the contribution of positronium formation in inelastic channels for helium. The inelastic thresholds which determine the energy regions where positronium is formed, according to the Ore model [11], are shown in figure 1. The fractions of the positrons $(E_{ex} - E_{Ps})/E_i$ which initially enter the region $E_{ex} > E > E_{Ps}$ (the Ore gap) all form positronium, whereas for the fraction $(E_i - E_{ex})/E_i$ which initially enter the region $E_i > E > E_{Ps}$, positronium formation competes with the excitation to an extent which depends on the relative cross sections for these processes. The remaining fractions of the positrons E_{Ps}/E_i which initially enter the region $E_{Ps} > E > 0$ cannot form positronium.

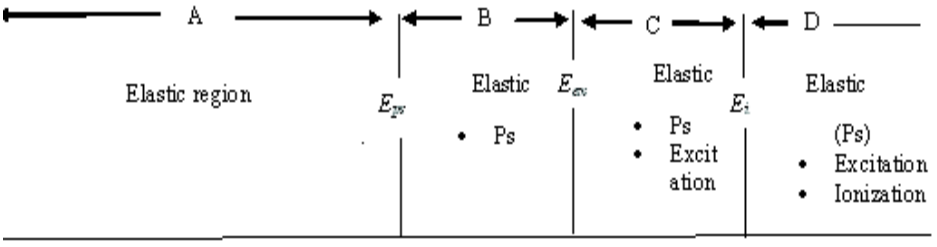

Figure 1: Contribution of positronium formation in inelastic channels for helium. Ref. [11]

Theory

Since the positron is distinguishable from the electrons in the target, there is no exchange interaction in positron- atom scattering. Further, the static (coulombian) interaction is repulsive for positrons, while it is attractive for electrons. The polarization interaction is attractive for both these particles. At lower energies the static and polarization interactions will tend to cancel each other for positron scattering, while these interactions add for electron impact. At sufficiently high energies, only the static interactions will remain, with the result that the total scattering cross sections will tend to be the same for positrons and electrons. In the present calculations we model the positron-target system by a complex interaction potential $V(r)$ which accounts for conservation of particle flux as well as energy. The total complex potential consists of only three terms, viz., the static potential V_{st} (r), the correlation-polarization potential $V_{cp}(r)$, and the absorption potential $V_{abs}(r)$ as follows.

$$V(r) = V_{st}(r) + V_{cp}(r) + iV_{abs}(r) \qquad (1)$$

The static potential is determined by the radial part of the electron charge density of the target atom ρ(r) for all present atomic targets. The polarization potential for positron scattering is given as under. The detailed expression of this potential is given in [12].

$$V_{corr}(r) = V_{corr}(r), \quad r \leq r_c \qquad (2)$$

$$= -\frac{\alpha_d}{2r^4}, \quad r \geq r_c$$

Where r_c is the radial distance of the first crossing of the $V_{corr}(r)$ and $-\alpha_d/2r^4$ terms. After generating the full complex potential of equation (1) for a given positron – atom system, we treat it exactly in a partial wave analysis by solving the first order differential equations for the real (δ_R) and imaginary (δ_I) parts of the complex phase shift function $\delta(r)$. This is done in the variable phase approach of [13] as done in electron –target atom scattering. The TCS Q_T obtained from the complex spherical potential is such that

$$Q_T(E_i) = Q_{el}(E_i) + Q_{inel}(E_i) \qquad (3)$$

Where, Q_{el} is total elastic cross section and Q_{inel} is the total (cumulative) inelastic cross section at a given incident energy E_i. The total inelastic contribution comprises of positronium formation, electronic excitation and ionization of the target atom, so that

$$Q_{inel}(E_i) = Q_{Ps} + \sum Q_{exc} + \sum Q_{ion} \qquad (4)$$

Here the first term on right hand side of equation (4) is positronium formation cross section, second term is the sum over total discrete-excitation cross sections for all accessible electronic transitions in the atom, while the third term indicates the sum of the total cross sections of all allowed (single, double etc.) ionization processes. The imaginary absorption term V_{abs} in the complex potential is an energy dependant potential that accounts for all possible inelastic scattering channels cumulatively, and has the generic

form, developed by Reid and Wadehra [14]. The form of absorption potential V_{abs} depends on incident positron energy (E_i), target charge density ($\rho(r)$), and energy gap Δ as given by [14]. This form differs from that of the electron-atom scattering [15].

The energy gap Δ is introduced here to account for the fact that the excitations of the target atom are possible only when the energy is lost by the projectile is larger than first inelastic threshold. For electron scattering the inelastic channels are open as soon as the energy of projectile is larger than the first excitation energy of the target atom, so we should set value of energy gap Δ at first excitation energy. In the case of positron scattering, the positronium formation is often the first inelastic channel to open. The binding energy of positronium is ~ 6.8 eV. Therefore the noble atoms whose ionization potential I is larger than positronium binding energy, the threshold of positronium formation is $E_{Ps} = I - 6.8$ eV. For atoms with threshold $I < 6.8$ eV, positronium formation is possible at all energies, i.e. E_{Ps}= 0.Hence for positron scattering we should set $\Delta = E_{Ps}$. The Q_{inel} contains Q_{Ps}, $\sum Q_{exc}$ and Q_{ion} vide equation (4). To find out the contribution of Q_{ion} first we have to subtract Q_{Ps} from the Q_{inel} thus giving Q_{inel} in the form of $Q_{ion}+ \sum Q_{exc}$. Next, we introduce the method called 'Complex scattering potential–ionization contribution' (*CSP-ic*) to ascertain the contribution of Q_{ion} from Q_{inel}. The *CSP-ic* method for e^--atom system rests on bifurcating the Q_{inel} into discrete and continuum contributions, at incident energies above I. So far the method has been employed for electron impact [15] with various atomic molecular targets. Along these lines, this is perhaps the first attempt to apply the CSP-ic to positron scattering. Thus, we introduce a break-up ratio function,

$$R(E_i) = \frac{Q_{ion}(E_i)}{Q_{inel}(E_i)} \qquad (5)$$

Obviously $R = 0$ when $E_i \leq I$. The ratio should increase as the energies increase above the threshold, and it can approach unity at high energies, such that

$$R(E_i) = 0, \quad E_i \leq I \qquad (6a)$$

$$R(E_i) = R_p, \quad E_i = E_p \qquad (6b)$$

$$R(E_i) = R', \quad E_i \gg E_p \qquad (6c)$$

Where E_p is the incident energy value at which the Q_{inel} achieves its maximum. The above equation expresses a correct quantum mechanical behavior since ionization offers continuously many many open channels of scattering. But to ascertain the values of the parameters R_p and R' in equations (6), we rely on the wealth of experimental data available on the well-known He atom target. This point is elaborated in section 3, on results and discussion.

Now, for the actual calculation of Q_{ion} from our Q_{inel} we need R (E_i) as a continuous function of energy E_i. Therefore, as in the case of electron projectiles let us have

$$R(E_i) = 1 - f(U) = 1 - C_1\left[\frac{c_2}{(U+a)} + \frac{\ln U}{U}\right] \qquad (7)$$

With,

$$U = \frac{E_i}{I} \qquad (8)$$

The reason for adopting a particular functional form of f (U) i.e. second term of the right hand side of equation (8) is as follows. As E_i increases above I, the ratio R increases from zero and approaches value 1, since the ionization contribution rises and the discrete excitation term in equation (4) decreases. The discrete excitation cross sections, dominated by dipole transitions, fall off as $ln\ (U)/U$ at high energies. Accordingly the decrease of the function f (U) must also be proportional to $ln\ (U)/U$ in the high range of energy. However, the two term representation

of f (U) given in equation (7) is more appropriate since the 1st term in the square bracket ensures a better energy dependence at low and intermediate E_i. Equation (7) involves dimensionless parameters C_1, C_2, and a, that reflect the target properties. The three conditions stated in equation (6a-c) are used to determine these three parameters, in an iterative manner. Thus we first assume a = 0 and consider a two-parameter expression in equation (7). We employ therein the two conditions (6a) and (6b) to obtain C_1 and C_2. The two-parameter equation is then used to determine the value of R at a high energy E_i =10 E_p, and the same value is employed in equation (6c) to obtain the new set of three parameters C_1, C_2 and a. Having thus obtained the parameters we calculate Q_{ion} from equation (6), and therefore generate R_p value from these Q_{ion}. The resulting R_p value is used next as an input to the equation (6b) iteratively to finally calculate Q_{ion}. The properties of interest, viz., ionization potential, polarizability, energy at the peak E_p and energy gap Δ of the present targets are listed in table 1.

RESULTS AND DISCUSSION

For positron scattering it is meaningful to calculate the important cross section Q_{ion} from Q_{inel} which is complicated by the presence of positronium formation. The present work is also important in view of in the energy range of incident energy from ionization threshold to 2000 eV. We have organized the discussion of our present results along with comparisons in two sub-sections as follows.

e^+ - Helium scattering

First of all, we address the question of determining the values of the parameters R_p and R' in equations (7) for the well-known He target. This requires the values of ratio R (E_i) at appropriate energies, in equation (7). For this in turn, we need experimental Q_{inel} which we can get in two alternative ways. The first way is to add experimental measurements of Q_{ion} and $\sum Q_{exc}$ and the second way is to subtract measurements of Q_{el} and Q_{Ps} from measurements of Q_T. These data are available in the case of He, but there are uncertainties in the experimental results of Q_T so the better option is to add experimental measurements of Q_{ion} and $\sum Q_{exc}$. These data have been published by Mori and Sueoka [6] up to 90 eV and by Basu *et al* [7] for Q_{ion} up to 150 eV. We have extrapolated that data up to about 800 eV. We got the $\sum Q_{exc}$ from measurements of Campeanu *et al* [17] which are up to 300 eV extrapolated by us up to 800 eV. Finally these data were employed to get experimental Q_{inel}. We find from the analysis of these data that, for He the ratio R (E_i) is around 0.7 at peak position of Q_{inel} and it approaches 1 at high energies as in electron scattering. To get the presently calculated Q_{inel} without the Ps cross sections (Q_{Ps}) we subtracted the Q_{Ps} of Fornari *et al* [18] from our Q_{inel} results. Next, the Q_{ion} is calculated from the present Q_{inel} by the CSP-ic method i. e. from equations (7) and (8).

Our focus in this paper is on ionization by positron impact. Our calculated cross sections along with compared data on e^+ -Helium system are as shown in figure 1. Here we can see that our present Q_{ion} results are within the error bars of experimental results of Mori and Sueoka [6]. At high energy our results are closer to Fromme *et al.* [5]. The theoretical results of Basu *et al.* [7] using first born approximation are lower than experimental results. It is interesting to note that the ionization cross sections of electron impact are lower than those of positron impact. But at high energy they tend to merge each other as expected. The ionization cross sections of electron impact of present results have been compared with measurements of Rejoub *et al* [19].

Table 1: **Properties of the present targets used in the calculations**

Target	Ionization potential(I_p)[a]	Polarizability[a] α_d Å^3	Energy at the peak E_p (eV)	Energy gap Δ For positrons (eV)
He	24.58	0.20	100	17.78
Ne	21.56	0.39	90	14.76

(a) Ref. [16]

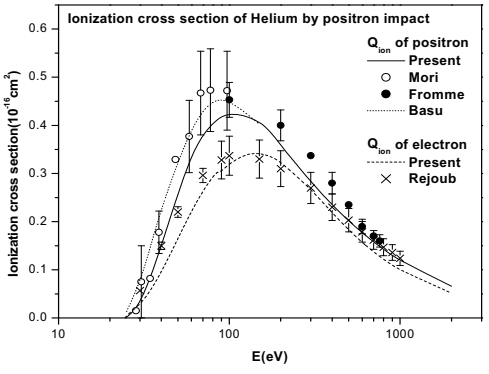

Figure 1: Ionization cross sections for e^+ and e^- Helium scattering.

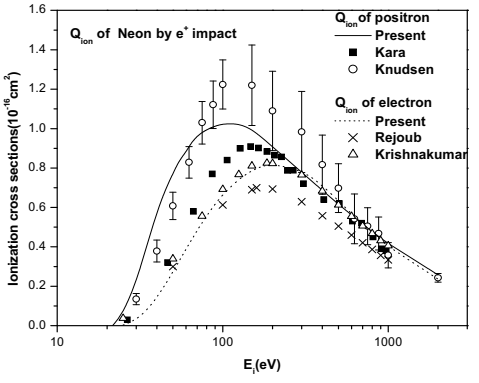

Figure 2: Ionization cross sections for e^+-Neon scattering.

e^+-Neon scattering

In positron neon scattering, to calculate the Q_{inel} without the positronium formation cross sections (Q_{Ps}) we subtracted Q_{Ps} of Marler *et al* [20] from our present Q_{inel} results. We have calculated ionization cross sections using '*CSP-ic'* method using the same ratio *R* (equations 7-9) as used in helium case. As shown in figure 2, the presently calculated results are within error bars in most of experimental measurements [9] of neon after the peak of Q_{ion}. The measurements of single ionization cross sections of Knudsen *et al* [9] are well matched with our results. At high energies double and multiple ionization becomes important. However our results are not well matched with experimental results of [8, 9] below peak of Q_{ion} and peak position is also not matched. The ionization cross sections of electron impact are lower than positron impact up to about 300 eV, and at high energy they tend to merge each other as in helium. The ionization cross sections of electron impact of present results have been compared with measurements of Rejoub *et al* [19] and also with Krishnakumar and Shrivastava [21].

CONCLUSION

We conclude that in positron scattering with any atom the positronium formation has important contribution at lower energy up to ~150 eV. At high energy the ionization cross sections will be more dominated as in electron – atom scattering. Also at high energy the electron and positron scattering cross sections are merging with each other.

The important conclusion of the present work is that the *CSP-ic* method of electron atom/molecule scattering is also applicable and valid for positron atom scattering.

ACKNOWLEDGEMENT

Author KNJ is thankful to ISRO Bangalore – India for a research Project grant and HNK is thankful to UGC, New Delhi for meritorious research fellowship through Sardar Patel University, Vallabh Vidyanagar India.

REFERENCES

[1.] Coleman P. G., Griffith T.C., Heyland G.R. and Twomey T.R. (1976) Measurements of positron –rare gas total cross sections at intermediate energies. *Appl. Phys*.,**11**: 321-325

[2.] Stein T.S., Kauppila W.E., Pol V., Smart J.H. and Jesion G. (1978) Measurements of total scattering cross sections for low-energy positrons and electrons colliding with helium and neon atoms. *Phys. Rev. A*, **17**:1600-1608

[3.] Griffith T.C. , Heyland G.R., Lines K.S. and Twomey T.R.,(1979) Total cross-sections for the scattering of positrons by helium, neon, and argon at intermediate energies, *Appl. Phys.,* **19**:431-437

[4.] Kauppila W.E., Stein T.S., Smart J.H., Dababneh M.S., Ho Y.K., Downinig J.P. and Pol V.,(1981) Measurements of total scattering cross sections for intermediate-energy positrons and electrons colliding with helium, neon, and argon, *Phys.Rev.A,* **24**:725-742

[5.] Fromme D., Kruse G., Raith W. and Sinapius G., (1986) Partial-Cross-Section Measurements for Ionization of Helium by Positron Impact. *Phys.Rev.Lett,* **57**:3031-3034

[6.] Mori S., Sueoka O. (1994) Excitation and ionization cross sections of He, Ne and Ar by positron impact. *J.Phys.B,* **27**: 4349-4364

[7.] Basu M., Mazumdar P. S. and Ghosh A. S. (1985) Ionization cross sections in positron-helium scattering. *J.Phys.B*, **18**:369-377

[8.] Kara V., Paludan K., Moxom J., Ashley P. and Laricchia G.,(1997)Single and double ionization of neon, krypton and xenon by positron impact. *J. Phys. B,* **30**:3933-3949

[9.] Knudsen H, Brun-Nielsen L, Charlton M and Poulsen M. R.,(1990) Single ionization of H2, He, Ne and Ar by positron impact. *J. Phys. B,* **23**:3955-3976

[10.] Joshipura K.N. and Mohanan S, (1990) High energy elastic e+ − O2 scattering, *Pramana J.Phys.,***34**:87-90

[11.] Charlton M., Griffith T.C., Heyland G.R. and Lines K.S.,(1979) Cross sections for positronium formation in gases, *J. Phys. B*, **12**: L633-639

[12.] Baluja K.L. and Jain A., (1992) Positron scattering from rare gases (He, Ne, Ar, Kr, Xe, and Rn): Total cross sections at intermediate and high energies, *Phys.Rev.A*, **46**:1279-1290

[13.] Gangopadhyay S., Vinodkumar P.C. and Joshipura K.N.,(2006)Variable phase calculations on e-H2 and e-CO scattering processes, *Prajna- J. Pure and Applied Sciences,***14**:108-116

[14.] Reid David D. and Wadehra J.M.,(1996) A quasifree model for the absorption effects in positron scattering by atoms, *J.Phys.B,* **29**: L127-L133

[15.] Vinodkumar M., Limbachiya C., Antony B. and Joshipura K. N., (2007) Calculations of elastic, ionization and total cross sections for inert gases upon electron impact: threshold to 2 keV, *J. Phys. B,* **40**:3259-3271

[16.] Lide R., (2003) CRC Handbook of Chemistry and Physics, CRC Press LLC, Boca Raton FL.

[17.] Campeanu R.I., Fromme D., Kruse G., McEachran R.P., Parcell L.A., Raith W., Sinapius G. and Stauffer, (1987) Partitioning of the positron-helium total scattering cross section A.D., *J.Phys.B*, **20**: 3557-3570

[18.] Fornari L.S., Diana L.M. and Coleman P.G.,(1985) Positronium Formation in Collisions of Positrons with He, Ar, and H2, *Phys.Rev.Lett.,* **51**: 2276-2279

[19.] Rejoub R., Lindsay B.G., Stebbings R.F.,(2002) Determination of the absolute partial and total cross sections for electron-impact ionization of the rare gases, *Phys.Rev.A*, **65**: 042713-08

[20.] Marler J.P., Sullivan J.P. and Surko C.M.,(2005) Ionization and positronium formation in noble gases, *Phys.Rev.A,* **71**:022701-10

[21.] Krishnakumar E. and Shrivastava K.S.,(1988) Ionization cross sections of rare-gas atoms by electron impact. *J.Phys.B,* **21**:1055-1082

PRAJÑĀ - Journal of Pure and Applied Sciences
Vol. 17: 191-197, 2009 ISSN 0975 - 2595

ESTIMATION FOLLOWING SELECTION IN THE POWER SERIES DISTRIBUTIONS

A. Shanubhogue * **and Riyadh R. Al-Mosawi**

Department of Statistics, Sardar Patel University, Vallabh Vidyanagar, Gujarat – 388 120

ABSTRACT

Let $\pi_1, ..., \pi_p$ be p ($p \geq 2$) independent power series populations with parameters $\theta_1, ..., \theta_p$, respectively. Let Z_i denotes the sum of n independent observations from the population $\pi_i, i = 1, ..., p$. For selecting the best population which is the one associated with the largest (smallest) θ_i, we consider the natural selection rule which selects the population having the largest (smallest) Z_i. Since our problem is in the discrete case, there is a high probability of existing ties in the values of Z_i, so, we break these ties by ordering the tied Z_i from the smallest to the largest index. In this paper, we consider the problem of estimating the parameter of the selected population under the k-normalized squared error loss function for $k = 0, 1, 2$. We have proved that the natural estimator of the parameter for the selected population is risk-biased. Some applications are presented for the selected Poisson, negative binomial and logarithmic series distributions.

Keywords: **estimation following selection, k-normalized squared error loss function, power series distribution, Lehmann's risk-unbiased.**

INTRODUCTION

Let $\pi_1,...,\pi_p$ be $p(p \geq 2)$ independent populations with densities (with respect to counting measure)

$$f(x,\theta_i) = \frac{a(x)\theta_i}{c(\theta_i)}, \quad x = 0,1,...;\theta_i > 0, a(x) > 0 \; \forall x$$

for $i = 1,2,..., p$, where $c(\theta_i) = \sum_{x=0}^{\infty} a(x)\theta_i^x$. Assume $\theta_i, i = 1,2,..., p$, are the unknown parameters. Suppose from each population π_i we have a random sample $(X_{i1},...,X_{in})$ and define $Z_i = \sum_{j=1}^{n} X_{ij}$. It is well-known that Z_i represents the sufficient and complete statistic for θ_i, with density

$$g(Z_i,\theta_i) = \frac{b(\theta_i,n)\theta_i^{Z_i}}{c^n(\theta_i)}, \; Z_i = 0,1,... \qquad (1)$$

where $b(Z_i,n)$ is the coefficient of $\theta_i^{Z_i}$ in the power series expansion of $c^n(\theta_i)$ i.e

$$c^n(\theta_i) = \sum_{Z_i=0}^{\infty} b(Z_i,n)\theta_i^{Z_i}.$$

From Roy and Mitra [1], the UMVUE of θ_i^t is given by

$$\delta(Z_i) = \begin{cases} b(Z_i - t,n)/b(Z_i,n) & \text{if } Z_i \geq t \\ 0 & \text{otherwise} \end{cases} \cdots (2)$$

where $t = 1,2,...$. Let $Z_{(1)} \geq ... \geq Z_{(p)}$ and $\theta_{[1]} \geq ... \geq \theta_{[p]}$ denote the ordered values of $Z_1,...,Z_p$ and $\theta_1,...,\theta_p$, respectively and let $Z = (Z_1,...,Z_p)$ and $\theta = (\theta_1,...,\theta_p,)$. Assume that $\theta_{(i)}$ represents the parameter of the population associate with $Z_{(i)}$. The population having the largest (smallest) parameter $\theta_{[1]}(\theta_{(p]})$ is called the best population and our aim is to select this population. We adopt the natural selection rule which selects the population with largest (smallest) Z_i. Since our problem is in the discrete case, there is a high probability of existing ties in the values of Z_i and our solution should consider this case especially when the ties are in the first (last) position. In this paper, the ties are broken by selecting the population with the smallest index among the tied populations in the first (last) position. The problem of estimation following selection has many real life applications. For example, a doctor not only likes to select the type of drug from a choice of p different drugs, that he quantifies the effectiveness and chooses the most effective one, but he wants to estimate the effectiveness of the chosen drug, based on the same data. This problem has received considerable attention from

* Corresponding author – a_shanubhogue@yahoo.com

many researchers. For the case of the populations dominated by Lebesgue measure see for example, Kumar and Gangopadhyay [2], Gangopadhyay and Kumar [3], Misra, Meulen and Branden [4, 5] Sill and Sampson [6] and Nematollahi and Motamed-Shariati [7]. In the populations dominated by counting measure, the problem has not been received enough attention due to the complexities involved. Sarkadi [8] derived an unbiased estimator of the mean for the selected population(s) for the case of two independent Poisson populations. Tappin [9] considered the problem of estimating the parameter of the best binomial population by using a two-stage sampling scheme. Vellaisamy and Jain [10] constructed explicit estimators which dominate the natural estimators for $\theta_{(1)}$ and $\theta_{(p)}$ by solving certain difference inequalities for the power series distributions. Al-Mosawi and Shanubhogue [11, 12] considered the problem of estimating function of parameter of the selected left-truncated modified power series population under asymmetric loss functions.

The loss function considered here is k-normalized squared error loss function (hereafter k-nsel) defined as $L_k(t,\theta) = (t-\theta)^2/\theta^k$, where t is an estimate of θ and $k = 0,1,2$.

Lemma 1. (Chou [13]) Let g be a real-valued function defined on $p-$fold the Cartesian product of ***I***, the set of all integers such that

1. $E_\theta|g(Z)| < \infty$,
2. $g(Z) = 0$ if $Z_i < k$ for some i.

Then,

$$E_\theta\left(\frac{g(Z)}{\theta^k}\right) = E_\theta\left(\frac{g(Z+ke_i)b(Z_i+k,n)}{b(Z_i,n)}\right),$$

where e_i represents the $p-$dimensional vector with i-th component equal to 1 and zero for others.

Now, similar to Vellaisamy and Jain [10], define the random variables M and N as

$$M = \sum iI(Z_i > Z_j, j < i; Z_i \geq Z_j, j > i)$$

and

$$N = \sum iI(Z_i < Z_j, j < i; Z_i \leq Z_j, j > i)$$

It follows that our estimand is $\theta_M(\theta_N)$ and the selected population is $\pi_M(\pi_N)$. From (2), the natural estimators of θ_M and θ_N can be defined, respectively, as

$$\delta(Z_M) = \begin{cases} b(Z_M-1,n)/b(Z_M,n) & Z_M \geq 1 \\ 0 & otherwise, \end{cases}$$

and

$$\delta(Z_N) = \begin{cases} b(Z_N-1,n)/b(Z_N,n) & Z_N \geq 1 \\ 0 & otherwise. \end{cases}$$

In this paper, we consider the Lehmann's risk-biased property of the natural estimators of θ_M and θ_N under k-nsel for $k = 0,1,2$. Hereafter, the symbols $\wedge$ and $\vee$ stand for the logical AND, OR, respectively.

ESTIMATING THE PARAMETERS θ_M And θ_N.

In this section, the natural estimators of θ_M and θ_N are shown to be biased with respect to k-nsel (risk -biased). First of all we need to impose a condition on estimator δ of θ to be unbiased under k-nsel using the following definition of the risk-unbiased of Lehmann [14].

Definition 1. (Lehmann [15] page 157)
An estimator $\delta(X)$ of $g(\theta)$ is said to be risk-unbiased if it satisfies

$$E_\theta L(\theta,\delta(X)) \leq E_\theta L(\theta',\delta(X)) \forall\, \theta' \neq \theta.$$

Now define

$$B_k(Z,\theta) = E_\theta(2(1-k)\delta(Z)\theta + k\delta^2(Z) + (k-2)\theta^2) \quad \cdots(3)$$

Using Definition 1, the estimator $\delta(Z)$ is said to be unbiased with respect to k-nsel if $B_k(Z,\theta) = 0, \forall\, \theta \in \Omega$, otherwise it is risk-biased and its bias is $B_k(Z,\theta)$, where Ω is the parameter space. The above condition of the risk-unbiased is of the component problem which is the problem of estimation without selection and the natural analogue of the condition to the problem of estimation following selection is in the following definition.

Definition 2. The estimator $\delta(Z_M)$ of θ_M is called unbiased estimator with respect to k-nsel if $B_k(Z_M,\theta_M)=0, \forall\,\theta\in\Omega$, otherwise it is risk-biased with bias $B_k(Z_M,\theta_M)$. If $B_k(Z_M,\theta_M) > (<)0, \forall\,\theta\in\Omega$, then we call $\delta(Z_M)$ is positively (negatively) risk-biased.

The three important special cases of $B_k(Z_M,\theta_M)$ are:

1. $B_0(Z_M,\theta_M)=E_\theta(\delta(Z_M)-\theta_M)$, under squared error loss function (usual unbiasedness).
2. $B_1(Z_M,\theta_M)=E_\theta(\delta^2(Z_M)-\theta_M^2)$, under normalized squared error loss function.
3. $B_2(Z_M,\theta_M)=E_\theta(\delta^2(Z_M)-\delta(Z_M)\theta_M)$, under scale-invariant loss function.

The definition of unbiasedness under k-nsel for the problem of estimating θ_N can be obtained from Definition 2 and after replacing $\delta(Z_M)$ and θ_M with $\delta(Z_N)$ and θ_N, respectively. It can be seen that $B_0(Z_M,\theta_M)$ is not directly a special case from (3), so that we shall use two different procedures to prove that the natural estimators $\delta(Z_M)$ and $\delta(Z_N)$ are risk-biased. The first procedure is for the case $k=0$ and the second one is for the cases $k=1,2$.

Now, we start with the problem of estimating θ_M.

Theorem 1. The natural estimator $\delta(Z_M)$ of θ_M is positively biased with respect to squared error loss function.

Proof. Without loss of generality, consider $p=2$. Now,

$$\begin{aligned}B_0(Z_M,\theta_M)&=E_\theta(\delta(Z_M)-\theta_M)\\&=E_\theta(\delta(Z_1)-\theta_1)I(Z_1\ge Z_2)\\&\quad+E_\theta(\delta(Z_2)-\theta_2)I(Z_2>Z_1)\\&=\eta_1(\theta)+\eta_2(\theta)(say).\end{aligned}$$

Consider first the term $\eta_1(\theta)$.

$$\begin{aligned}\eta_1(\theta)&=E_\theta(\delta(Z_1)-\theta_1)I(Z_1\ge Z_2)\\&=\sum\sum_{Z_1\ge Z_2}\left(\frac{b(Z_1-1,n)}{b(Z_1,n)}-\theta_1\right)\frac{b(Z_1,n)b(Z_2,n)\theta_1^{Z_1}\theta_2^{Z_2}}{c^n(\theta_1)c^n(\theta_2)}\\&=\sum_{Z_2=0}^{\infty}\frac{b(Z_2,n)\theta_2^{Z_2}}{c^n(\theta_2)}\left(\sum_{Z_1=Z_2}^{\infty}\frac{b(Z_1-1,n)\theta_1^{Z_1}}{c^n(\theta_1)}-\sum_{Z_1=Z_2}^{\infty}\frac{b(Z_1,n)\theta_1^{Z_1+1}}{c^n(\theta_1)}\right)\\&=\sum_{Z_2=0}^{\infty}\frac{b(Z_2,n)\theta_2^{Z_2}}{c^n(\theta_2)}\left(\frac{b(Z_2-1,n)\theta_1^{Z_2}}{c^n(\theta_1)}+\sum_{Z_1=Z_2+1}^{\infty}\frac{b(Z_1-1,n)\theta_1^{Z_1}}{c^n(\theta_1)}\right.\\&\qquad\left.-\sum_{Z_1=Z_2+1}^{\infty}\frac{b(Z_1-1,n)\theta_1^{Z_1}}{c^n(\theta_1)}\right)\\&=\sum_{Z_2=0}^{\infty}\frac{b(Z_2,n)b(Z_2-1,n)\theta_2^{Z_2}\theta_1^{Z_2}}{c^n(\theta_2)c^n(\theta_1)}\\&\ge 0\ \ \forall(\theta_1,\theta_2)\in\Omega.\end{aligned}$$

Next, consider the term $\eta_2(\theta)$. In similar way, we have

$$\begin{aligned}\eta_2(\theta)&=E_\theta(\delta(Z_2)-\theta_2)I(Z_2>Z_1)\\&=\sum\sum_{Z_2>Z_1}\left(\frac{b(Z_2-1,n)}{b(Z_2,n)}-\theta_2\right)\frac{b(Z_1,n)b(Z_2,n)\theta_1^{Z_1}\theta_2^{Z_2}}{c^n(\theta_1)c^n(\theta_2)}\\&=\sum_{Z_1=0}^{\infty}\frac{b(Z_1,n)\theta_1^{Z_1}}{c^n(\theta_1)}\left(\sum_{Z_2=Z_1+1}^{\infty}\frac{b(Z_2-1,n)\theta_2^{Z_1}}{c^n(\theta_2)}-\sum_{Z_2=Z_1+1}^{\infty}\frac{b(Z_2,n)\theta_2^{Z_2+1}}{c^n(\theta_2)}\right)\\&=\sum_{Z_1=0}^{\infty}\frac{b(Z_1,n)\theta_1^{Z_1}}{c^n(\theta_1)}\left(\frac{b(Z_1,n)\theta_2^{Z_1+1}}{c^n(\theta_2)}+\sum_{Z_2=Z_1+2}^{\infty}\frac{b(Z_2-1,n)\theta_2^{Z_2}}{c^n(\theta_2)}\right.\\&\qquad\left.-\sum_{Z_2=Z_1+2}^{\infty}\frac{b(Z_2,n)\theta_2^{Z_2}}{c^n(\theta_2)}\right)\\&=\sum_{Z_1=0}^{\infty}\frac{b(Z_1,n)b(Z_1,n)\theta_2^{Z_1+1}\theta_1^{Z_1}}{c^n(\theta_2)c^n(\theta_1)}\\&>0\ \ \forall(\theta_1,\theta_2)\in\Omega.\end{aligned}$$

This completes the proof.

Theorem 2. Consider the natural estimator $\delta(Z_M)$ of the parameter θ_M is an increasing function of Z_M. The estimator $\delta(Z_M)$ is positively biased with respect to k-nsel for $k=1,2$.

Proof. From (3), we have

$$\begin{aligned}B_k(Z_M,\theta_M)&=E_\theta\big(2(1-k)\delta(Z_M)\theta_M+k\delta^2(Z_M)\\&\qquad+(k-2)\theta_M^2\big)\\&=2(1-k)\textstyle\sum_{j=1}^{p}E_\theta\delta(Z_j)\theta_j I_1(Z_j)\\&\quad+(k-2)\textstyle\sum_{j=1}^{p}E_\theta\theta_j^2 I_1(Z_j)+kE_\theta\delta^2(Z_M),\end{aligned}$$

where

$$I_1 = I(Z_j > Z_t, j > t; Z_j \geq Z_t, j < t).$$

From Lemma 1, we get

$$\begin{aligned} B_k(Z_M,\theta_M) &= 2(1-k)\sum_{j=1}^{p} E_\theta\left(\frac{\delta(Z_j-1)b(Z_j-1,n)I_1(Z_j-1)}{b(Z_j,n)}\right) \\ &\quad +(k-2)\sum_{j=1}^{p} E_\theta\left(\frac{b(Z_j-2,n)I_1(Z_j-2)}{b(Z_j,n)}\right) \\ &\quad +kE_\theta\delta^2(Z_M) \\ &= 2(1-k)\sum_{j=1}^{p} E_\theta\delta(Z_j)\delta(Z_j-1)I_1(Z_j-1) \\ &\quad +(k-2)\sum_{j=1}^{p} E_\theta\delta(Z_j)\delta(Z_j-1)I_1(Z_j-2) \\ &\quad +kE_\theta\delta^2(Z_M) \qquad \cdots(4) \end{aligned}$$

It can be easily seen that

$$\begin{aligned} I_1(Z_j-1) &= I(Z_j-1 > Z_t, j > t; Z_j-1 \geq Z_t, j < t) \\ &= \begin{cases} 1 & if\ (j = M) \wedge J_2 \\ 0 & otherwise \end{cases} \end{aligned}$$

where J_t is a logical statement defined as

$$J_t \equiv \{(Z_M - Z_{(2)} > t) \vee ((Z_M - Z_{(2)} = t) \wedge (M < q_2))\}$$

and q_2 is the antirank of $Z_{(2)}$ that is $Z_{(2)} = Z_{q_2}$.

Then (4) becomes

$$B_k(Z_M,\theta_M) = E_\theta\delta(Z_M)D_1(Z_M),$$

where

$$\begin{aligned} D_1(Z_M) &= k\delta(Z_M) + \delta(Z_M-1)\big(2(1-k)I(J_1) \\ &\quad + (k-2)I(J_2)\big) \qquad ...(5) \end{aligned}$$

Clearly, the sign of $B_k(Z_M,\theta_M)$ depends on the sign of $D_1(Z_M)$. For the sign of $D_1(Z_M)$, we have the following cases:

Case $k = 1$. From (5) with $k = 1$ we get

$$\begin{aligned} D_1(Z_M) &= \delta(Z_M) - I(J_2)\delta(Z_M-1) \\ &\geq \delta(Z_M) - \delta(Z_M-1) \\ &> 0, \end{aligned}$$

since $\delta(Z_M)$ is an increasing function of Z_M.

Case $k = 2$. Similarly, from (5) with $k = 2$ we get

$$\begin{aligned} D_1(Z_M) &= 2(\delta(Z_M) - I(J_1)\delta(Z_M-1)) \\ &\geq 2(\delta(Z_M) - \delta(Z_M-1) \\ &> 0. \end{aligned}$$

This completes the proof.

Consider next the problem of estimating θ_N.

Theorem 3. The natural estimator $\delta(Z_N)$ of θ_N is negatively biased with respect to squared error loss function.

Proof. Similar to Theorem 1, consider $p = 2$:

$$\begin{aligned} B_0(Z_N,\theta_N) &= E_\theta(\delta(Z_N) - \theta_N \\ &= E_\theta(\delta(Z_1) - \theta_1)I(Z_1 \leq Z_2) \\ &\quad + E_\theta(\delta(Z_2) - \theta_2)I(Z_2 < Z_1) \\ &= \xi_1(\theta) + \xi_2(\theta)(say). \end{aligned}$$

Consider first the term $\xi_1(\theta)$.

$$\begin{aligned} \xi_1(\theta) &= E_\theta(\delta(Z_1) - \theta_1)I(Z_1 \leq Z_2) \\ &= \sum\sum_{Z_1 \leq Z_2}\left(\frac{b(Z_1-1,n)}{b(Z_1,n)} - \theta_1\right)\frac{b(Z_1,n)b(Z_2,n)\theta_1^{Z_1}\theta_2^{Z_2}}{c^n(\theta_1)c^n(\theta_2)} \\ &= \sum_{Z_2=0}^{\infty}\frac{b(Z_2,n)\theta_2^{Z_2}}{c^n(\theta_2)}\left(\sum_{Z_1=0}^{Z_2}\frac{b(Z_1-1,n)\theta_1^{Z_1}}{c^n(\theta_1)} - \sum_{Z_1=0}^{Z_2}\frac{b(Z_1,n)\theta_1^{Z_1+1}}{c^n(\theta_1)}\right) \\ &= \sum_{Z_2=0}^{\infty}\frac{b(Z_2,n)\theta_2^{Z_2}}{c^n(\theta_2)}\left(-\frac{b(Z_2,n)\theta_1^{Z_2+1}}{c^n(\theta_1)} + \sum_{Z_1=1}^{Z_2}\frac{b(Z_1-1,n)\theta_1^{Z_1}}{c^n(\theta_1)}\right. \\ &\quad \left. - \sum_{Z_1=1}^{Z_2}\frac{b(Z_1-1,n)\theta_1^{Z_1}}{c^n(\theta_1)}\right) \\ &= -\sum_{Z_2=0}^{\infty}\frac{b(Z_2,n)b(Z_2,n)\theta_2^{Z_2}\theta_1^{Z_2+1}}{c^n(\theta_2)c^n(\theta_1)} \\ &< 0 \ \ \forall(\theta_1,\theta_2) \in \Omega. \end{aligned}$$

Next, consider the term $\xi_2(\theta)$. In similar way, we have

$$\begin{aligned} \xi_2(\theta) &= E_\theta(\delta(Z_2) - \theta_2)I(Z_2 < Z_1) \\ &= \sum\sum_{Z_2 < Z_1}\left(\frac{b(Z_2-1,n)}{b(Z_2,n)} - \theta_2\right)\frac{b(Z_1,n)b(Z_2,n)\theta_1^{Z_1}\theta_2^{Z_2}}{c^n(\theta_1)c^n(\theta_2)} \\ &= \sum_{Z_1=0}^{\infty}\frac{b(Z_1,n)\theta_1^{Z_1}}{c^n(\theta_1)}\left(-\frac{b(Z_1-1,n)\theta_2^{Z_1}}{c^n(\theta_2)} + \sum_{Z_2=1}^{Z_1-1}\frac{b(Z_2-1,n)\theta_2^{Z_2}}{c^n(\theta_2)}\right. \\ &\quad \left. - \sum_{Z_2=1}^{Z_1-1}\frac{b(Z_2-1,n)\theta_2^{Z_2}}{c^n(\theta_2)}\right) \\ &= -\sum_{Z_1=1}^{\infty}\frac{b(Z_1,n)b(Z_1-1,n)\theta_2^{Z_1}\theta_1^{Z_1}}{c^n(\theta_2)c^n(\theta_1)} \\ &\leq 0 \ \ \forall(\theta_1,\theta_2) \in \Omega. \end{aligned}$$

This completes the proof.

Theorem 4. Consider the natural estimator $\delta(Z_N)$ of the parameter θ_N is an increasing function of Z_N and

$$\delta(Z_N) \le 2\delta(Z_N - 1)\ \forall Z_N \ge 2.$$

The estimator $\delta(Z_N)$ has the following cases:

(i) For $k = 1$. If $\big((n_0 = 1) \vee (Z_N = 1)\big) \wedge (n_1 = 0) \wedge (n_2{*} = 0)$ then $\delta(Z_N)$ is positively risk-biased, otherwise it is negatively risk-biased.

(ii) For $k = 2$. If $\big((n_0 = 1) \vee (Z_N = 1)\big) \wedge (n_1{*} = 0)$ then $\delta(Z_N)$ is positively risk-biased, otherwise it is negatively risk-biased.

where

$$n_0 = \#\{i : Z_i = Z_N\}$$
$$n_1 = \#\{i : Z_i = Z_N + 1\}$$
$$n_1{*} = \#\{i : Z_i = Z_N + 1, i < N\}$$
$$n_2{*} = \#\{i : Z_i = Z_N + 2, i < N\}$$

Proof. Similar to Theorem 2, we have

$$B_k(Z_N, \theta_N) = E_\theta\big(2(1-k)\delta(Z_N)\theta_N + k\delta^2(Z_N) + (k-2)\theta_N^2\big)$$
$$= 2(1-k)\sum_{j=1}^{p} E_\theta \delta(Z_j)\theta_j I_2(Z_j) + (k-2)\sum_{j=1}^{p} E_\theta \theta_j^2 I_2(Z_j) + kE_\theta\delta^2(Z_N),$$

where $I_2(Z_j) = I(Z_j < Z_t, j > t; Z_j \le Z_t, j < t)$.

From Lemma 1, we get

$$B_k(Z_N, \theta_N) = 2(1-k)\sum_{j=1}^{p} E_\theta \delta(Z_j)\delta(Z_j - 1) I_2(Z_j - 1) + (k-2)\sum_{j=1}^{p} E_\theta \delta(Z_j)\delta(Z_j - 1) I_2(Z_j - 2) + kE_\theta\delta^2(Z_N) \quad \ldots (6)$$

It can be easily seen that

$$I_2(Z_j - 1) = I(Z_j - 1 < Z_t, j > t; Z_j - 1 \le Z_t, j < t) = \begin{cases} 1 & \text{if } Z_j = Z_N, (Z_N + 1) \wedge (j < N) \\ 0 & \text{otherwise} \end{cases}$$

and

$$I_2(Z_j - 2) = I(Z_j - 2 < Z_t, j > t; Z_j - 2 \le Z_t, j < t) = \begin{cases} 1 & \text{if } Z_j = Z_N, Z_N + 1, (Z_N + 2) \wedge (j < N) \\ 0 & \text{otherwise} \end{cases}$$

Then (6) becomes

$$B_k(Z_N, \theta_N) = E_\theta\big(2(1-k)n_0\delta(Z_N)\delta(Z_N - 1) + 2(1-k)n_1{*}\delta(Z_N)\delta(Z_N + 1) + (k-2)n_0\delta(Z_N)\delta(Z_N - 1) + (k-2)n_1\delta(Z_N)\delta(Z_N + 1) + (k-2)n_2{*}\delta(Z_N + 1)\delta(Z_N + 2) + k\delta^2(Z_N)\big)$$
$$= E_\theta\big(-kn_0\delta(Z_N)\delta(Z_N - 1) + (k-2)n_2{*}\delta(Z_N + 1)\delta(Z_N + 2) + ((k-2)n_1 + 2(1-k)n_1{*})\delta(Z_N)\delta(Z_N + 1) + k\delta^2(Z_N)\big)$$
$$= E_\theta D_2(Z_N),$$

where

$$D_2(Z_N) = -kn_0\delta(Z_N)\delta(Z_N - 1) + (k-2)n_2{*}\delta(Z_N + 1)\delta(Z_N + 2) + ((k-2)n_1 + 2(1-k)n_1{*})\delta(Z_N)\delta(Z_N + 1) + k\delta^2(Z_N) \quad \ldots (7)$$

For the sign of $D_2(Z_N)$ in (7), we have the following cases:

Case $k = 1$. Putting $k = 1$ in (7), we obtain

$$D_2(Z_N) = -n_0\delta(Z_N)\delta(Z_N - 1) - n_2{*}\delta(Z_N + 1)\delta(Z_N + 2) - n_1\delta(Z_N)\delta(Z_N + 1) + \delta^2(Z_N).$$

Clearly, $D_2(Z_N)$ is positive if $\big((n_0 = 1) \vee (Z_N = 1)\big) \wedge (n_1 = 0) \wedge (n_2{*} = 0)$.

For the case $(Z_N \ge 2) \wedge (n_0 \ge 2)$, from the condition $\delta(Z_N) \le 2\delta(Z_N - 1)$ we get $\delta(Z_N) - n_0\delta(Z_N - 1) < 0$ which implies that $D_2(Z_N)$ is negative. For the remaining cases, $D_2(Z_N)$ is negative because of monotonicity of $\delta(Z_N)$.

Case $k = 2$. Putting $k = 2$ in (7), we obtain

$$D_2(Z_N) = -2n_0\delta(Z_N)\delta(Z_N - 1) - 2n_1{*}\delta(Z_N)\delta(Z_N + 1) + 2\delta^2(Z_N).$$

Obviously, $D_2(Z_N)$ is positive if $\big((n_0 = 1) \vee (Z_N = 1)\big) \wedge (n_1{*} = 0)$.

If $(n_0 \ge 2) \wedge (Z_N \ge 2)$ then

$$\delta(Z_N) - n_0\delta(Z_N - 1) < 0$$

follows from the condition $\delta(Z_N) \le 2\delta(Z_N - 1)$ and hence $D_2(Z_N)$ is negative. For all other cases, $D_2(Z_N)$ is negative.

This completes the proof.

SOME APPLICATIONS

In this section, we apply the results of Section 2 and show that the natural estimators of the parameter for the selected Poisson, negative binomial and logarithmic series populations are risk-biased.

Example 1. Let

$$X_{i1}, \cdots, X_{in}\ iid\ Poisson(\theta_i), i = 1, \cdots, p,$$

then $Z_i = \sum_{j=1}^{n} X_{ij}$ has Poisson distribution with parameter $n\theta_i$. It follows that $b(Z_i, n) = n^{Z_i}/Z_i!$ and $\delta(Z_i) = Z_i/n$. Clearly $\delta(Z_i)$ is an increasing function of Z_i. Hence the natural estimators of θ_M and θ_N are, respectively $\delta(Z_M) = Z_M/n$ and $\delta(Z_N) = Z_N/n$. Also, it can be seen that $\delta(Z_N) \le 2\delta(Z_N - 1)$. Then from Theorems 1-4, the estimators $\delta(Z_M)$ and $\delta(Z_N)$ are biased with respect to k-nsel.

Example 2. Let $X_{i1}, \cdots, X_{in}$ *iid* $NB(r, \theta_i), i = 1, \cdots, p,$ with r is known. Then $Z_i = \sum_{j=1}^{n} X_{ij}$ has negative inomial distribution with nr and θ_i. It follows that

$$b(Z_i, n) = (Z_i + nr - 1)!/Z_i!(nr - 1)!$$

and $\delta(Z_i) = Z_i/(Z_i + nr - 1)$. Clearly $\delta(Z_i)$ is an increasing function of Z_i. Hence the natural estimators of θ_M and θ_N are, respectively

$$\delta(Z_M) = Z_M/(Z_M + nr - 1)$$

and

$$\delta(Z_N) = Z_N/(Z_N + nr - 1).$$

It can be seen that $\delta(Z_N) \le 2\delta(Z_N - 1)$ Then from Theorems 1-4, the estimators $\delta(Z_M)$ and $\delta(Z_N)$ are biased with respect to k-nsel.

Example 3. Let $X_{i1}, \cdots, X_{in}$ *iid Logarithmi.*(θ_i), $i = 1, \cdots, p.$

Then $Z_i = \sum_{j=1}^{n} X_{ij}$ has the following density

$$f(Z_i, \theta_i) = \begin{cases} \dfrac{n!\left|S_{Z_i}^{n}\right|\theta_i^{Z_i}}{Z_i!(-\log(1-\theta_i))^n}, & Z_i = n, n+1, \cdots \\ 0, & otherwise, \end{cases}$$

where $\left|S_{Z_i}^{n}\right|$ is the Stirling's number of the first kind. Hence

$$\delta(Z_i) = \begin{cases} Z_i\left|S_{Z_i-1}^{n}\right|\Big/\left|S_{Z_i}^{n}\right|, & if\ Z_i > n, \\ 0, & otherwise, \end{cases}$$

which implies that the natural estimators of θ_M and θ_N are, respectively

$$\delta(Z_M) = \begin{cases} Z_M\left|S_{Z_M-1}^{n}\right|\Big/\left|S_{Z_M}^{n}\right|, & if\ Z_M > n, \\ 0, & otherwise, \end{cases}$$

and $$\delta(Z_N) = \begin{cases} Z_N\left|S_{Z_N-1}^{n}\right|\Big/\left|S_{Z_N}^{n}\right|, & if\ Z_N > n, \\ 0, & otherwise. \end{cases}$$

From Patil [16], it can be seen that $\delta(Z_i)$ is an increasing function of Z_i and $\delta(Z_N) \le 2\delta(Z_N - 1)$. Then Theorems 1-4 hold for the case of logarithmic series distribution.

ACKNOWLEDGMENT: The paper is a part of Ph.D. work of the second author. He is thankful to ICCR for providing scholarship to continue his study for Ph.D.

REFERNCES

[1] Roy, J. and Mitra, S. K. (1957) Unbiased minimum variance estimation in a class of discrete distribution, *Sankhya*, 18: 371-378.

[2] Kumar, S. and Gangopadhyay, A. K. (2005) Estimating parameters of a selected Pareto population, *Statist. Methodology*, **2**: 121-130.

[3] Gangopadhyay, A. K. and Kumar, S. (2005) Estimating average worth of the selected subset from two-parameter exponential populations, *Commun. Statist.-Theory Meth.*, **34**: 2257-2267.

[4] Misra, N., Meulen, E. C. and Branden, V. K. (2006) On estimating the scale parameter of selected gamma population under the scale invariant squared error loss function, *J. Comp. Appl. Math.,* **186(1)**: 268-282.

[5] Misra, N., Meulen, E. C. and Branden, V. K. (2006) On some inadmissibility results for the scale parameters of selected gamma populations, *J. Statist. Planning Inference*., **136(7)**: 2340-2351.

[6] Sill, M. W. and Sampson, A. R. (2007) Extension of a two-stage conditionally unbiased estimator of the selected population to the bivariate normal case, Commun. *Statist.-Theory Meth.,* **36**: 801-813.

[7] Nematollahi, N. and Motamed-Shariati, F. (2009) Estimation of the Scale Parameter of the Selected Gamma Population Under the Entropy Loss Function, *Commun. Statist.-Theory Meth.*, **38(2)**: 208-221.

[8] Sarkadi, K. (1967) Estimation after selection, Studia. *Scientarium Mathematicarum Hungaruica,* **2**: 341-350.

[9] Tappin, L. (1992) Unbiased Estimation of the parameter of a selected binomial population, *Commun. Statist.- Theory and Meth.,* **21**: 1067-1083.

[10] Vellaisamy, P. and Jain, S. (2008) Estimating the parameter of the population selected from discrete exponential family, *Statist. Probab. Lett.,* **78(9)**: 1076-1087.

[11] Al-Mosawi, R. and Shanubhogue, A. (2009) Inadmissibility results for the selected truncated modified power series distribution under entropy loss function, *Far East Journal of Theoretical Statistics,* **28(1)**: 21-34.

[12] Al-Mosawi, R. and Shanubhogue, A. (2009) Estimation after Selection in the Modified Power Series Distributions under Stein's Loss Function, *Journal of Probability and Statistical Science*, **7(1)**: 43-56.

[13] Chou, J. P. (1991) Simultaneous estimation in discrete multivariate exponential families, *Ann. Statist.,* **19**: 314-328.

[14] Lehmann, E. L. (1951) A general concept of unbiasedness, *Ann. Math. Statist*., **22**: 578-592.

[15] Lehmann E. L. and Casella G. (1998) Theory of point estimation, Second Edition, Springer.

[16] Patil, G. P. and Bildikar, S. (1966) On minimum variance estimation for the logarithmic series distribution, *Sankhya*, A, **28(2&3)**: 239-250.

PRAJÑĀ - **Journal of Pure and Applied Sciences**
Vol. 17: 198-202, 2009 ISSN 0975 - 2595

A STATISTICAL STUDY OF ATM OF A NATIONALIZED BANK BRANCH

A. Shanubhogue * **and D. P. Raykundaliya**

Department of Statistics, Sardar Patel University, Vallabh Vidyanagar, Gujarat – 388 120

ABSTRACT

In this paper we study statistical behavior of newly installed ATM (Automated Teller Machine) at a business center in the town. The data are from a branch of a nationalized branch. We consider total number of transactions per day at ATM (day is counted from midnight to midnight) and total volume of transaction per day as variables for study. We make detail study of the number of transaction at ATM per day and calculate mode of transaction, the seasonal indices for average volume of transaction. Further, through statistically modeling we obtain average amount of money per transaction per day. In the end we obtain percentiles of amount of transaction. Also we obtain confidence interval for average volume per transaction.

Keywords: **number of transactions, volume of transactions, three parameter Weibull distribution, confidence interval, chi-square goodness of fit test.**

INTRODUCTION

Banking is fastest growing service industry in financial sector. Every individual who earns money by means of agriculture, business or job uses as a part of it for ones need and comfort and saves the other part for future. Under the influence of many random factors, all kinds of bank transactions exhibit stochastic behavior. Therefore, it is essential to study such behavior statistically for the better understanding of the operation of schemes and give suggestions, if any, for improvement or modification of the schemes. Thanks to development in Electronic and Communication and advances in IT, banks have introduced ATM for customers to conduct their banking transactions from all over the world at any time. These advanced machines have replaced work being carriedout at a branch of a bank. However, it is necessary to study their cost effectiveness for the given levels of transactions.

The objectives of study of automated teller machine

The purpose of the study is to investigate popularity of ATM usages among the customers through detail study of the number of transactions per day, volume of transaction per day, average amount per transaction at the ATM center and about the seasonal variations of ATM transactions with weeks as seasons. Further, our study suggests the total amount of money to be kept in ATM for smooth transactions.

* Corresponding author – a_shanubhogue@yahoo.com

METHODOLOGY

In the era of information technology and cut neck competitions among different banking organizations, one who gives quick and better services can capture high portion of the market. With this idea banks have implemented ATM, but their cost effectiveness was not studied. For our study, we collect the data on the total number of transactions per day as it indirectly speaks about the popularity of ATM. We also collect data on amount per transaction for about 10 months. We use Weibull distribution for modeling average volume per transaction. The necessary computational methods for three parameter Weibull distribution are given in Appendix.

MATERIALS

We use the statistical techniques like mean, mode and variance to study the behavior of number of transactions per day at ATM as the number of transactions per day at ATM is discrete. For average volume per transaction, we try to build suitable probability models through which further study of behavior can be done. From the histogram of average volume per transaction, we infer that the three parameter Weibull distribution may give good fit to the data. With the help of fitted distribution we obtain percentiles of volume of transactions which help us to draw certain interesting conclusions. Further using the estimates of mean and mode of the distribution we obtain 95% confidence interval for average volume of transactions and average maximum amount of transaction per day. We also carryout

time series analysis by calculating seasonal indices using weeks of a month as season.

RESULTS

Number of Transactions per day

The Fig. 1 suggests that one can look for suitable skewed discrete distribution as statistical model for modeling 'number of transactions'. From the data the average number of transactions per day is 39 and standard deviation of number of transactions per day is 29 approximately while the model value of number of transactions per day is 40.

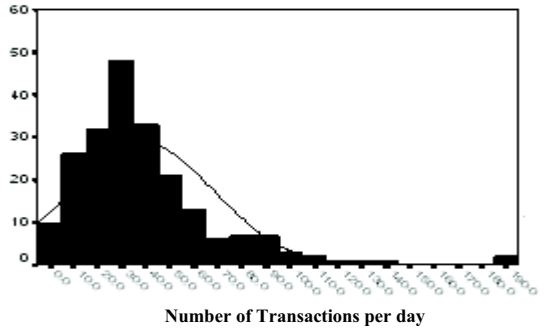

Figure 1: Histogram of number of transactions per day

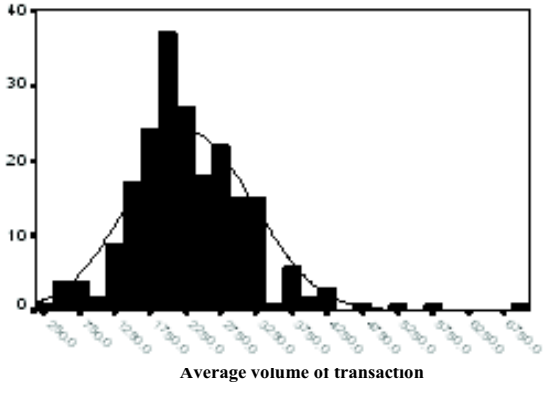

Figure 2: Histogram of average volume per transaction

The Fig. 2 suggests that one can try Weibull distribution for the variable 'average volume per transaction'. The fitting of this distribution is done and details are given below.

From Fig.3 we can see that the observed frequency and model frequency are close to each other. Also the chi-square value is 8.925604 and the corresponding p-value is 0.030297 which suggests that the Weibull distribution fits well to the data. With 95% confidence level the average volume per transaction lies between Rs.1900 and Rs.2700. Therefore, minimum withdrawal from ATM per day with 95% surety is Rs.74100. The average amount of transaction per transaction is approximately Rs.2300. The total average volume of transaction per day is Rs.89700. Percentiles of transaction provide us the information about the amount of money withdrawn with certain surety form the ATM per transaction. For example, from our calculation we can say that with 0.1 probability at least Rs.3302 would be withdrawn and with 0.95 probability Rs.1016 would be withdrawn from ATM. This suggests that with 95% confidence the withdrawal is at least Rs.39600 from ATM per day. The modal value of the data is Rs.2200. The average maximum amount of transaction per day is Rs.85800.

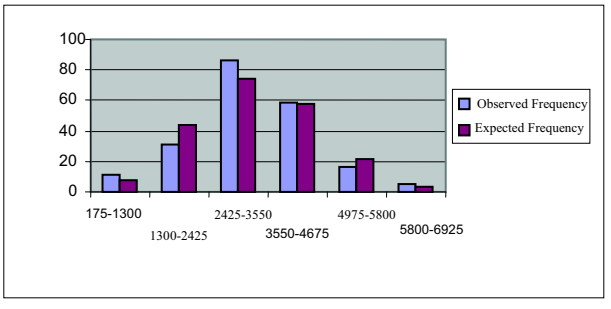

Figure 3: Bar chart of observed frequency and Expected Frequency of Volume of transactions

From the seasonal indices we see that the respective average number of withdrawals in the first and the third weeks of any month are 61 and 60 which are more than the overall average i.e. 51. Also the respective average number of withdrawals in second and the forth weeks of any month are 43 and 40 which are less than overall average. The trend continues to be same for all the months we study. This clearly indicates the presence of seasonal variation in the data.

CONCLUSION AND RECOMMENDATION

Number of transactions

From the modal value we find that most often repeated number of transactions is 40 transactions per day. At the same time mean number of transactions is 39 per day. Suppose that there are x numbers of card holders, who avail the facility of ATM. Further suppose that on the average, each individual will be using ATM 4 times a month. Then, the total number of transactions in a month is expected to be $4x$; if all of them are regularly using ATM facility. Therefore, we are

expecting $\frac{4x}{30}$ transactions per day. If this is going to be smaller than 40, the machine is underutilized. i.e., $x < 300$ the machine is underutilized. Suppose that C_a is the per day cost of an ATM. If a clerk is appointed instead, the cost per day will be, say C_c. Further if he is supposed to process M_H transactions per day, the cost per transaction will be $\frac{C_c}{M_H}$. At the same time cost per transaction at ATM is $\frac{C_a}{39}$. Therefore, ATM will be cost effective if $\frac{C_a}{39} < \frac{C_c}{M_H}$, i.e. $\frac{M_H}{39} < \frac{C_c}{C_a}$.

Average Volume of Transaction

From the percentile of volume of transaction we conclude that with 0.1 probability, at least Rs.3302 will be withdrawn per transaction and with probability 0.95, at least Rs.1016 will be withdrawn per transaction. The mode of the data being Rs.2200 per transaction suggests that often people would be withdrawing about Rs.2200. Total amount of money withdrawn often would be Rs.89700 per day. This suggests that at least Rs.90000 must be kept per day in the ATM so that there will be smooth transactions. If we keep Rs.100000 amount of money in ATM, we can assure smooth transaction with 95% confidence. The study also reveals that if numbers of card holders are less than 300 than the ATM becomes underutilized.

REFERENCES

[1] Deshpande J.V., Gore A.P. and Shahnubhogue A. (1995). "Statistical Analysis of Nonnormal Data", *New Age International Publishers Limited*, *Wiley Eastern Limited*, *New Delhi.*

[2] Gorden E. and Natarajank K. (2002). "Banking Theory, Law, and Practice", Sixth Edition ,*Himalaya Publishing House, Delhi*

[3] Gujarati Damodar(1998). "Basic Econometrics", Third Edition, *McGRAW-HILL International Editions Singapore.*

[4] Kale B.K. (1999). "A First Course on Parametric Inference", *Narosa Publishing House*, *New Delhi*

[5] Medhi J. (1982). "Stochastic Process", *Wiley Eastern Limited*, *New Delhi.*

[6] Sinha S. K. and Kale B. K. (1980). "Life Testing and Reliability Estimation", *Wiley Eastern Limited*, *New Delhi.*

APPENDIX

Three parameters Weibull distribution:

The random variable X having three parameter Weibull distributions is characterized by

$$f(x,\mu,\beta,\theta)=\frac{\beta}{\theta}(x-\mu)^{\beta-1}\exp\{\frac{-(x-\mu)^{\beta}}{\theta}\}$$
$$x>\mu,\beta>0 \text{ and } \theta>0$$
$$=0, \text{ otherwise}$$

Where μ: Location parameter, β:Shape parameter and θ: Scale parameter

Maximum likelihood estimation

The maximum Likelihood estimate of μ is:

$$\hat{\mu} = x_{(1)}$$
$$x_{(1)} = \min(x_1, x_2, \ldots, x_n)$$

The initial solution of the shape parameter is obtained by graphical method. We have

$$\hat{\beta} = \frac{\sum (s_i - \bar{s}_i)(t_i - \bar{t}_i)}{\sum (t_i - \bar{t})^2}$$

where

$$s_i = \log(\log(\frac{n+1}{n-i+1})), t_i = \log(x_i)\ i=1,2,\ldots,n$$

and

Maximum likelihood estimates of β and θ can be obtained by means of iterative procedure.

Let $X_1, X_2, ..., X_n$ be a random sample of size n from $w(0,\beta,\theta)$ distribution. The likelihood function of this sample is

$$L(x_1, x_2, \ldots, x_n; \beta, \theta) = \prod_{i=1}^{n} \frac{\beta}{\theta} x^{\beta-1} \exp\{\frac{-x^{\beta}}{\theta}\}$$

Taking logarithm we get

$$\ln L = n\ln\beta - n\ln\theta + (\beta-1)\sum_{i=1}^{n}\ln x_i - \frac{\sum_{i=1}^{n} x_i^{\beta}}{\theta}$$

Differentiating log-likelihood with respect to the parameters β and θ and equating to zero we obtain

$$\frac{\partial \ln L}{\partial \beta} = \frac{n}{\beta} + \sum_{i=1}^{n}\ln x_i - \frac{\sum_{i=1}^{n} x_i^{\beta}\ln x_i}{\sum_{i=1}^{n}\theta\, x^{\beta}} = 0$$

$$\frac{\partial \ln L}{\partial \theta} = -\frac{n}{\beta} + \frac{\sum_{i=1}^{n} x_i^{\beta}}{\theta^2} = 0,$$

$$\frac{\partial^2 \ln L}{\partial \beta^2} = \frac{-n}{\beta^2} - \frac{n(\sum_{i=1}^{n} x_i^{\beta}(\log x_i)^2)}{(\sum_{i=1}^{n} x_i^{\beta})}$$

$$\frac{\partial^2 \ln L}{\partial \theta^2} = \frac{n}{\theta^2} - \frac{2}{\theta^3}\sum_{i=1}^{n}(x_i^{\beta})$$

$$\frac{\partial^2 \ln L}{\partial \beta \partial \theta} = \frac{\partial^2 \ln L}{\partial \theta \partial \beta} = \frac{1}{\theta^2}\sum_{i=1}^{n}(x_i^{\beta}\log(x_i))$$

$$I(\theta) = E\begin{bmatrix} -\frac{\partial^2 \ln L}{\partial \beta^2} & -\frac{\partial^2 \ln L}{\partial \beta \partial \theta} \\ -\frac{\partial^2 \ln L}{\partial \theta \partial \beta} & -\frac{\partial^2 \ln L}{\partial \theta^2} \end{bmatrix}$$

$$\Sigma = E(I(\theta))^{-1}$$

$$K = E(-\frac{\partial^2 \ln L}{\partial \hat{\beta}^2})E(-\frac{\partial^2 \ln L}{\partial \hat{\theta}^2}) - E(-\frac{\partial^2 \ln L}{\partial \hat{\beta}\partial \hat{\theta}})E(-\frac{\partial^2 \ln L}{\partial \hat{\theta}\partial \hat{\beta}})$$

$$\Sigma = \frac{1}{K}\begin{pmatrix} E(-\frac{\partial^2 \ln L}{\partial \theta^2}) & E(\frac{\partial^2 \ln L}{\partial \beta \partial \theta}) \\ E(\frac{\partial^2 \ln L}{\partial \theta \partial \beta}) & E(-\frac{\partial^2 \ln L}{\partial \beta^2}) \end{pmatrix}_{(\hat{\beta},\hat{\theta})}$$

The elements of Σ cannot be evaluated. Therefore, we consider the score functions of elements and evaluate them at mles of β and θ to get the estimated values of $V(\hat{\theta})$, $V(\hat{\beta})$ and $cov(\hat{\beta}, \hat{\theta})$.

Confidence interval

To construct confidence interval for mean of the Weibull distribution, we need the distribution of the mles of mean of Weibull distribution. Since mles of mean of Weibull distribution depends upon the mles of θ and β, whose joint distribution is difficult to obtain, we use their asymptotic distribution. Then it is used for obtaining confidence interval for the mean.

We know that the joint distribution of $\hat{\theta}$ and $\hat{\beta}$ is asymptotic normal. By applying δ-method we can obtain variance of the maximum likelihood estimator of the mean.

We have

$$\hat{E}(X) = \Gamma(1+\frac{1}{\hat{\beta}})\hat{\theta}^{\frac{1}{\hat{\beta}}}$$

$$V(\hat{E}(X)) = V(\Gamma(1+\frac{1}{\hat{\beta}})\hat{\theta}^{\frac{1}{\hat{\beta}}})$$

$$f(\beta,\theta) = \Gamma(1+\frac{1}{\beta})\theta^{\frac{1}{\beta}}$$

$$\frac{\partial f(\beta,\theta)}{\partial \beta} = (\frac{-1}{\beta^2})\Gamma(1+\frac{1}{\beta})\{\log(1+\frac{1}{\beta}) - \frac{1}{2(1+\frac{1}{\beta})}\}\theta^{\frac{1}{\beta}} + \Gamma(1+\frac{1}{\beta})\theta^{\frac{1}{\beta}}\ln\theta$$

$$V(\hat{E}(X)) = \left(\frac{\partial f(\beta,\theta)}{\partial \beta}\right)^2_{(\hat{\beta},\hat{\theta})} V(\hat{\beta}) + \left(\frac{\partial f(\beta,\theta)}{\partial \theta}\right)^2_{(\hat{\beta},\hat{\theta})} V(\hat{\theta}) + 2\left(\frac{\partial f(\beta,\theta)}{\partial \beta}\right)_{(\hat{\beta},\hat{\theta})}\left(\frac{\partial f(\beta,\theta)}{\partial \theta}\right)_{(\hat{\beta},\hat{\theta})} COV(\hat{\beta},\hat{\theta})$$

$$\frac{\partial f(\beta,\theta)}{\partial \theta} = \Gamma\left(1+\frac{1}{\beta}\right)\frac{1}{\beta}\theta^{\frac{1}{\beta}-1}$$

$$s.e.(\hat{E}(X)) = (V(\hat{E}(X))/n)^{1/2}$$

The $100(1-\alpha)\%$ confidence interval for the mean of the Weibull distribution is

$$\hat{E}(X) \pm t_{\frac{\alpha}{2}}\, s.e(\hat{E}(X))$$

Mode:

The p.d.f. of Weibull distribution with parameters μ, β, θ is given by

$$f(x,\mu,\beta,\theta)=\frac{\beta}{\theta}(x-x_0)^{\beta-1}\exp\{\frac{-(x-x_0)^{\beta}}{\theta}\}$$

Set ($\mu = x_0$)

$$\therefore \ln(f(x))=\ln\beta-\ln\theta-\frac{(x-x_0)^{\beta}}{\theta}+(\beta-1)\ln(x-x_0)$$

$$\therefore \frac{\partial \log f(x)}{\partial x}=-\frac{\hat{\beta}}{\hat{\theta}}(x-x_0)^{\hat{\beta}-1}+\frac{\hat{\beta}-1}{(x-x_0)}=0$$

$$\therefore \frac{\hat{\beta}}{\hat{\theta}}(x-x_0)^{\hat{\beta}-1}=\frac{\hat{\beta}-1}{(x-x_0)}$$

$$\therefore\ x-x_0=((\hat{\beta}-1)\frac{\hat{\theta}}{\hat{\beta}})^{\frac{1}{\hat{\beta}}}$$

$$\therefore\ x=x_0+((\hat{\beta}-1)\frac{\hat{\theta}}{\hat{\beta}})^{\frac{1}{\hat{\beta}}}$$

This gives the mode of Weibull distribution.

Probability of Transaction beyond a specified value x:

$$P[X>x]=\overline{F}(x)=e^{\frac{-(x-x_0)^{\hat{\beta}}}{\theta}}$$

$$\therefore\ \log\ \overline{F}(x)=e^{\frac{-(x-x_0)^{\hat{\beta}}}{\theta}}$$

$$(x-x_0)=(-\hat{\theta}\ln P)^{\frac{1}{\hat{\beta}}}$$

$$x=x_0+(-\hat{\theta}\log p)^{\frac{1}{\hat{\beta}}}$$

This gives, with certain probability, the amount of average money that would be transacted from ATM machine per transaction.

GUIDELINES FOR CONTRIBUTORS

The Editorial Board of 'PRAJNA' invites Original Research Papers in the field of Basic and Applied Sciences from Scientists, Engineers, Industrialists, Colleges of Universities and Research Laboratories in Gujarat for the Next Volume of PRAJNA (December 2010), published by Sardar Patel University, Vallabh Vidyanagar.

The papers intended for publication (not exceeding 15 typed pages), accompanied by the declaration of not submitted the same for publication elsewhere, may be submitted in duplicate to Prof. T. V. Ramana Rao, Managing Editor, PRAJNA, B. R. Doshi School of Biosciences, Sardar Patel University, Satellite Campus, Vadtal Road, Vallabh Vidyanagar – 388 120 OR to a Member of the Editorial Board who represents the author's broad research area with a copy of the paper to the Managing Editor latest by September 30, 2010. Submission of the soft copies of the papers (as per the file format shown below) through e-mail OR on a PC compatible CD along with the hard copies of papers would be most appreciated. The font for MS should be Times New Roman with 9 point for Abstract and 11 point for other matter.

Short Communications and Announcement for forthcoming seminars/ conferences/ symposia/ workshops to be held by the institutions in Gujarat will be also considered for publication.

Preparation of manuscripts:

1. **The paper should be written in English and neatly typed with double spacing on one side of the bond paper.**
2. **File format for soft copies: text and tables must be saved in *.doc (word) or *.rtf (rich text) format.**
3. **The title of the paper and name(s) of the author(s) be in capital letters. The name of the Institution be given in small letters below the name(s) of the author(s).**
4. **The Abstract of the paper should not exceed more than 150 words and must be provided on a separate sheet along with 4-6 keywords.**
5. **The sub-titles e.g. INTRODUCTION, should be written in capital letters.**
6. **Photographs/ Figures should be original provided in Black and White with good contrast so as to be in a from suitable for direct reproduction/ scanning. Original tracing of line drawing should be provided where necessary. Graphs should be prepared in MS Excel (*.xls) and for illustrations (diagrams, maps, drawings, etc.) the *.TIF or *.JPEG format (minimum resolution of 300 dpi) should be provided on a separate sheet(s). All figures/ tables/ graphs must be numbered serially as they appear in the text and their legends / captions should be necessarily provided.**
7. **Displayed formulae, mathematical equations and expressions should be numbered serially.**
8. **Footnotes are not normally allowed, except to identify the author for correspondence.**
9. **References should be numbered in brackets [ ] in the order of appearance in the text. All the references in the bibliographic list must correspond to in-text references and vice versa. Abbreviated periodical titles should follow standard subject Abstracts. Names which are not listed by any standard subject indexing organizations should be spelled out in full.**
10. **All the references should be clear and follow the example below;**

Periodical articles

[2] Sadqui, M., Fushman, D. and Munoz, V. (2006) Atom by – atom analysis of global downhill protein folding. *Nature*, **442**: 317-321.

Books

[16] Stebbins, G. L. (1974) *Flowering plants: Evolution above the species level*. Arnold Press, London, pp. 1-399.

Chapters from a book

[19] Schafer, H. and Muyzer, G. (2001) Denaturing gradient gel electrophoresis in marine microbial ecology. In *Methods in Microbiology* (Ed. Paul, J. H.) Academic Press, London, Vol. 30, pp. 425-468.

Thesis or other diplomas

[21] Nayaka, S. (2004) *The visionary studies on the lichen genus Lecanora sensu lato in India*. Ph. D. Thesis, Dr. R. M. L. Avadh University, Faziabad, India.

Conferences proceedings

[4] Mohapatra, G. C. (1981) Environment and culture of early man in the valley of rivers Chenab and Ravi, western sub-Himalayas. In *Proceedigns X Congress of IUPPS*, Mexico, pp. 90-123.

Online Documentation

[9] Koning, R. E. (1994) Home page for Ross Koning. Retrived 26-06-2009 from *Plant Physiology Information* Website: http://plantphys.info/index.html.

CHEMISTRY

COMPUTER SCIENCE

ELECTRONICS

PRAJÑĀ – Journal of Pure and Applied Sciences

Volume 17 **December 2009**

CONTENTS

BIOSCIENCES

Sardar Patel University Press, Vallabh Vidyanagar, Gujarat – 388 120, INDIA